NASA CONTRACTOR REPORT

NASA CR-380

NASA CR-380

ELECTROMAGNETIC ALKALI METAL PUMP RESEARCH PROGRAM

by J. P. Verkamp and R. G. Rhudy

Prepared under Contract No. NAS 3-2543 *by*
GENERAL ELECTRIC COMPANY
Cincinnati, Ohio
for Lewis Research Center

NATIONAL AERONAUTICS AND SPACE ADMINISTRATION • WASHINGTON, D. C. • FEBRUARY 1966

NASA CR-380

ELECTROMAGNETIC ALKALI METAL PUMP RESEARCH PROGRAM

By J. P. Verkamp and R. G. Rhudy

Prepared under Contract No. NAS 3-2543 by
GENERAL ELECTRIC COMPANY
Cincinnati, Ohio

for Lewis Research Center

NATIONAL AERONAUTICS AND SPACE ADMINISTRATION

For sale by the Clearinghouse for Federal Scientific and Technical Information
Springfield, Virginia 22151 – Price $6.00

FOREWORD

The work described herein was performed under the sponsorship of the National Aeronautics and Space Administration under contract NAS 3-2543. The purpose was to determine the feasibility of applying electromagnetic pumps to large electric power plants to be used aboard spacecraft. Suitable pump configurations were selected, design parameters were established, and optimum designs were recommended for the specified applications.

This final report covers the initial phase of the Electromagnetic Alkali Metal Research Program, extending from June 27, 1963 through August 3, 1964.

J. P. Verkamp, Space Power and Propulsion Section, administered the program for the General Electric Company. Contributors to the program include: Electrical Power Equipment Consultation, J. P. Hanna, Advanced Technology Laboratories; Power Conditioning Systems, G. Vaughn, Space Power and Propulsion Section; Pump Analysis and Design, R. G. Rhudy, Large Generator and Motor Department; Materials and Processes, W. G. Hoehn, Space Power and Propulsion Section; Reliability Analysis, G. L. Hilbrich, Space Power and Propulsion Section; Power Plant Integration, A. Schnacke, Space Power and Propulsion Section.

R. T. Wainwright of the National Aeronautics and Space Administration was the technical project manager for this research study. His assistance and guidance are gratefully acknowledged.

The efforts of J. P. Couch of the National Aeronautics and Space Administration in reviewing this final report are also gratefully acknowledged.

CONTENTS

Section Page

start

ABSTRACT

A study program, initiated by NASA, to select EM pumps for six applications in space power systems using alkali metal coolants and working fluids, is described. Applications to both turboelectric and thermionic systems are considered for potassium, lithium, and NaK up to 2000 °F. The study covers flow rates to 3300 gpm and developed heads to 100 psi. Results indicate that a tenfold improvement over the weights of conventional EM pumps is attainable.

All basic pump types, plus the significant variants of each, are described relative to operating principles, general configurations, performance features, reliability, and advantages and disadvantages. Design considerations are developed mathematically and are presented graphically.

Five different kinds of pumps are selected for detailed study. For these, conceptual designs, calculations, and performance prediction methods are presented. Preliminary designs are shown for pumps satisfying the six specific applications. All materials selected are within present technology. Pump weights, efficiencies, and other power plant application data are determined. Also considered are power supply, power conditioning, and heat dissipation. Other conclusions reached during the study are discussed.

to p. 78

to p. 78

NOMENCLATURE

Letter symbols have been assigned, insofar as practical, in accordance with American Standards. Where the same symbol is indicated as applying to different quantities, precedence has usually been given to the symbol assigned in American Standard Z10.5-1949, Letter Symbols for Electrical Quantities.

Mathematical symbols for trigonometric and hyperbolic functions and for the operations of calculus are in general accord with American Standard Z10f-1928, Mathematical Symbols.

Subscripts, principally numeric, which are not enumerated here are defined where they are used in the text.

Units are not indicated in the nomenclature as the relationships expressed in this report are valid in any consistent system of units. Where numerical values for quantities are given in the report, the units are indicated.

Roman Letter Symbols:

a height of fluid in duct
A sheet current density
b width of fluid in duct
B magnetic induction
c length of duct
C constant (as defined)
d diameter
D hydraulic diameter
d_s depth of slot
e base of natural logarithms, 2.718 ----
E electric field intensity
f frequency
F force
g length of magnetic gap, gravitational acceleration
G performance parameter (as defined)
h number of velocity heads
H magnetic field intensity
i $\sqrt{-1}$, instantaneous linear current density
I current
j instantaneous current density
J current density
k constant
K constants (as defined)
k_1 winding factor
L inductance, length

Roman Letter Symbols:

m	number of phases
M	magnetomotive force
N	number of turns
N_H	Hartmann number
N_R	Reynolds number
P	pressure
PF	power factor
q	heat flow
Q	volume flow rate
r	specific resistance (electrical)
R	resistance (electrical)
s	slip
t	thickness of duct wall, time
T	temperature
U	energy
v	velocity of fluid
V	voltage
w	specific power
W, KW	power
W_q, KW_q	reactive power
x, y, z	rectangular coordinate axes
X	reactance
Y	duct parameter (as defined)
Z	performance parameter (as defined)

Greek Letter Symbols:

α, β, γ	constants, exponents (as defined)
δ	friction factor
η	efficiency
λ	pole pitch, wavelength $\div 2$
Λ	permeance
μ	magnetic permeability, fluid viscosity
π	constant, 3.141 ----
ρ	mass density of fluid
ρ_f	electrical resistivity of fluid
ρ_d	electrical resistivity of duct walls
σ	cavitation number
τ	ratio of slot width to slot pitch
ϕ	instantaneous magnetic flux
Φ	magnetic flux
ω	angular frequency, $2\pi f$

Subscripts:

b	body
B	pertaining to magnetic induction
d	pertaining to duct walls
f	pertaining to fluid
g	pertaining to magnetic gap
i	pertaining to input
m	pertaining to magnetic path
o	pertaining to output
s	synchronous
t	pertaining to one turn
T	total
w	pertaining to winding
x, y, z	components in respective axes
μ	viscous or pertaining to viscosity

General:

Re $\{A\}$	the real part of the phasor quantity A
Im $\{A\}$	the imaginary part of the phasor quantity A
$\|A\|$	the magnitude of the phasor quantity A
$\underline{A}^*$	the complex conjugate of the phasor quantity A
$\overline{A}$	the space average value of A

I. SUMMARY

The Space Power and Propulsion Section of the General Electric Company, under contract to the National Aeronautics and Space Administration, has completed the initial phase of a research program to study the applicability of electromagnetic pumps to space electric power plants. This is the final report for that initial phase.

Electromagnetic pumping provides a means of circulating fluids of high electrical conductivity within a hermetically sealed system. No seals, bearings or moving parts are required. Since the power systems under consideration utilize molten alkali metals as working fluids, the use of electromagnetic pumps is particularly attractive.

The objectives of the Electromagnetic Alkali Metal Pump Research Program were to 1) determine the feasibility of using electromagnetic (EM) pumps in space electric power plants, 2) establish the basis for selecting pumps for specific applications, and 3) develop concepts and design methods for EM pumps applicable to space power plants. Accomplishing these objectives required broad consideration of power systems integration and over-all requirements of electric power plants for spacecraft.

The study program began with a literature survey which identified ten basic pump types. Consideration of the fundamental characteristics of the ten, with reliability as a primary criterion, reduced to three the pump types worthy of more detailed study. These were the polyphase induction pump, the single phase induction pump and the direct current conduction pump. Analytical design procedures and performance prediction methods were developed in the detailed study of the three selected pump types. Computor programs were written for the design procedures allowing the examination of a large number of possible designs in selecting the optimum for each application.

In the final selection the polyphase induction pumps were the first choice for all applications. The single phase induction pump was an alternate choice for the highest temperature application. The dc conduction pump was eliminated at this final step primarily because of lower reliability.

For applications requiring high developed head at relatively low flow the helical induction pump was chosen. Where high flow was required the annular induction pump was the choice.

Specific weights or weight criteria were determined for all pumps reported out of the analytical procedures. Specific weights or weight criteria in lb. per KW hydraulic power output were determined on two bases: for the pump only and in terms of overall weight contribution to the power plant including all auxiliaries and weight penalties. The dc conduction pumps showed the lowest weight penalties. The dc conduction pumps also

showed the lowest specific weight in all cases. The selected polyphase induction pumps ranged from 130 lb / kw for the smallest to 94 lb/kw for the largest on the basis of the pump alone. The corresponding overall weight criteria were 290 lb/kw and 190 lb/kw.

Other conclusions of particular interest reached during the course of the study program were:

1) EM pumps for space power application with specific weights 1/10 that of conventional EM pumps appear to be readily attainable using presently available materials.

2) EM pumps, particularly the induction type, are expected to exhibit excellent cavitation characteristics because the pumping action is the result of "body forces" generated within the fluid itself.

3) It is expected that flow control can be obtained over the full range of flow capability with no tendency to stall at very low flow. This would be particularly valuable in startup and standby operations. Also, the need for high temperature throttling valves for flow control would be eliminated.

II. INTRODUCTION

A. History of Electromagnetic Pumps

Electromagnetic pumps have moved from the laboratory to the power plant within the last fifteen years. The basic principle, however, is precisely that of the electric motor established by Michael Faraday in the early nineteenth century. The precept of applying force to a fluid conductor rather than a solid wire by the interaction of a magnetic field and an electric current is not new. Faraday implied this application in his Bakerian Lecture of January 12, 1832, (Ref. 1).

Apparently little practical application of the Faraday idea was found until F. Holden (Ref. 2) used it in a watt-hour meter. Holden's patent, dated May 14, 1907, describes the determination of electric energy flow by measuring the quantity of mercury moved by what was basically an electromagnetic pump. About this same time, E. F. Northrup (Ref. 3) presented a discussion of the electromagnetic pumping forces in a fluid conductor. Still, the spur of practical applications was missing and little activity is recorded in this field until 1919 when a British patent was issued to Hartmann for a dc conduction EM pump (Ref. 4). Subsequently, sporadic traces of effort can be found from approximately 1920 to 1945 (Refs. 5 through 12). Of these, Hartmann's investigation of the effect of a magnetic field on the viscosity of a fluid conductor is particularly pertinent to the fundamentals of EM pump design.

About 1945, interest developed in the application of EM pumps for the metallurgical industry. The first such commercial application, devised to pump molten aluminum (Ref. 13), was effected in 1948 by Ajax Engineering Company. Here, eliminating the impeller, the shaft, and the seal of mechanical pumps was the primary objective. Concurrently, but of greater importance, was the new interest in EM pumps generated by the coming nuclear technology. Again, the need for a seal-less pump was the overriding consideration, but, in this case, absolute containment of the radioactive molten metal working fluids was the problem. Since 1945, half a dozen manufacturers in this country and several more in England have produced EM pumps on a commercial or experimental basis. Three domestic manufacturers recognized active in the field today are Atomics International, General Electric Company, and Mine Safety Appliances Research Corporation.

The General Electric Company became active in EM pump work about 1947. The earliest units, produced about 1948, were ac conduction pumps intended for laboratory use. Work on induction pumps also started in 1948 and, by 1950, a 400 gpm helical induction unit and a 1200 gpm flat induction unit had been produced and tested. When the Submarine Intermediate Reactor Project was initiated in 1948, with the objective of producing a sodium cooled nuclear power plant for submarines, considerable impetus was added to induction pump development work. The earlier work had proved sufficiently encouraging to warrant a greatly accelerated program. Between 1953 and 1956, seventeen large flat induction pumps were produced and tested. The four units installed in the Seawolf Submarine were rated at 3300 gpm developing 85 psi pressure with an over-all efficiency of 43%.

Closely following the Seawolf units, a 5000 gpm pump was produced in 1956 for the sodium cooled Experimental Breeder Reactor Program at Argonne National Laboratory. Then, in 1959, a 6500 gpm unit, also a flat induction pump, was delivered to Argonne to be used at the National Reactor Test Station in Idaho. During the 1950-1960 decade, considerable EM pump development work performed in England culminated in the delivery of forty-eight linear induction pumps for the large power breeder reactor at Dounreay.

About 1960 new activity, related to space power systems, began in the field of alkali metals technology. At that time there were only two well established producers of small pumps suited to laboratory work. Mine Safety Appliances Research Corporation has for many years offered a line of ac conduction pumps noted for good versatility at low cost. Since 1960 MSAR has added dc conduction pumps to its line primarily to meet the need for a design well suited to high vacuum environment.

The other producer in the laboratory EM pump field was Liquid Metals Inc. who had long carried a line of rotating magnet EM pumps that found favor in many small and medium size alkali metal test facilities.

A recent arrival to the EM pump business is Atomics International who now produce a line based on a helical rotor moving magnet design. The basic design is adaptable to a wide range of flow requirements. Even more recently AI has added thermoelectromagnetic pumps to their line.

The General Electric Company provides a line of induction pumps for alkali metal test facilities' applications. Because of the high temperatures, relatively high pressures, and low flows, the helical induction pump was selected for these applications. Between 1960 and 1964 over a dozen helical pumps for various ratings for liquid metal temperatures up to 2200 ^{o}F were put in service, some of which were designed for high vacuum environment.

In the design of the various classes of induction pumps, it is interesting to note the effect of differences in emphasis on the various design criteria. In the shipboard units, mentioned above, reliability and efficiency were emphasized. Both objectives were realized in the 43% efficiency attained and the successful 10,000-hour, maintenance free operation. Conversely, test facility units are usually designed for reliability and low cost. Here, the same high reliability is realized, but efficiency is usually ignored in favor of low cost materials and fabrication processes. Consequently, efficiencies of 5% or lower are not uncommon in test facility pumps. In pumps designed for space applications, reliability and weight become prime criteria. As indicated in the examples in Table 1, the space design obtains a much lower weight than the conventional EM pumps of comparable size. As a result of optimization to obtain the best design balance from the over-all space power plant standpoint, efficiency falls between the high of the shipboard types and the low of the facility types.

TABLE 1. SOME INDUCTION EM PUMPS
DESIGNED, PRODUCED, AND OPERATED BY GENERAL ELECTRIC

Flow, gpm	Press., psi	Temp., °F	Fluid	Eff., %	Wt., lbs	Sp. Wt.,[a] lbs/kw	Pump Type	Service and Delivery Date
400	40	500	Na	15	1,000	1,420	Helical Induction	Development Test 1948
3	75	2200	K	1	570	5,800	Helical Induction	100 KW Facility, G.E., Evendale 1962
200	20	1850	K	6	1,500	860	Helical Induction	300 KW Facility, G.E., Evendale 1961
15	100	1200	K	14	105	164[b]	Helical Induction	- - -
3300	85	600	Na	43	11,400	93[c]	Flat Induction	SSN Seawolf 1956

[a] Specific weight on the basis of pump weight (lbs)/pump hydraulic output (kw).

[b] Based on preliminary design only but typical of the study results. Listed here for comparison purposes.

[c] As a general rule, larger pumps have lower specific weights.

B. Need for EM Pumps in Space Power Systems

As presently conceived, large space power plants, exceeding 100 kw output, must operate unattended on space missions of two years' duration. The energy source for the power is a nuclear reactor cooled by alkali metal and the power cycles are based on alkali metals as heat transfer and working fluids. Because of their low electrical resistivities, the molten alkali metals can be circulated readily by electromagnetic pumping. Numerous advantages are foreseeable in such an application:

- High reliability since there are no moving parts.
- The ability to obtain hermetically sealed systems.
- Smooth flow control down to zero flow.
- Eliminating the need for high temperature throttle valves.
- Simplified startup and standby operations.
- Greater freedom of choice of those materials contacting or containing the pumped fluid.

As cited in Table 1, the weight of conventional EM pumps in sizes of interest here has commonly run in the order of 1000 lb/kw power output. Similarly, the canned motor pumps widely used in nuclear power plants show comparable specific weights. This merely reflects the fact that weight per se is of minor importance in a land based power plant. Information in subsequent chapters will demonstrate that weight improvement by an order of magnitude can be obtained in EM pumps.

C. The Study Program

Until recently, the use of EM pumps in space power plants employing liquid metal working fluids had been generally considered unacceptable from a weight penalty standpoint. In evaluating the reliability problems associated with other pumping methods, however, it appeared that a larger weight penalty might be accepted to gain the high reliability attainable with EM pumps.

To appraise thoroughly the use of EM pumps in space power applications, NASA established the present program. In its initial phase, the program was purely analytical and comprised:

- An evaluation of EM pumps suitable for space power systems.
- The development of analytical methods to predict performance and to define optimum design.

- o The development of analytical methods for scaling EM pumps to meet future requirements.

- o Recommendations on the selection of one or more EM pumps for test.

- o The definition of an EM pump test program.

Under the contract stipulations, evaluation, selection, and analysis were guided by six particular pump applications. The design objectives stated for the selection of these pumps were quite specific and were based on the best estimates from existing space power plant studies at the one megawatt output level. The pumps were intended for use in space electric power generating systems of the turboelectric and thermionic types using certain alkali metals as the working fluids. The energy source was a nuclear reactor; the heat sink, a radiator in space. The design objectives for the six applications are summarized in Table 2. Figure 1 locates the pumps schematically, by bold outline, in their respective power plants.

Figure 1.a is based on a typical turbogenerator space power plant (Ref. 14). A three-loop system is presented using a nuclear reactor as the energy source. The primary coolant pump, although indicated, was not a part of the study. Reactor heat, transported to the boiler by the primary coolant, vaporizes potassium to drive the turbine-generator unit, producing 2000 cycle ac power. Spent vapor from the turbine is condensed and the liquid is recycled by a boiler feed pump. One study application was a boost pump to increase pressure at the boiler feed pump suction to avoid cavitation problems. From the condenser, heat is rejected to space by a radiator using lithium or NaK as the transport fluid. The pumps prescribed here constituted the second and third study applications.

Figure 1.b is a schematic of a thermionic power plant (Ref. 14). In this case, the electric power is generated within the reactor by thermionic elements heated directly by the nuclear fuel. Heat is rejected from the thermionic elements to the primary coolant lithium; this pump was the fourth study application. Heat is transferred from primary to radiator coolant through a heat exchanger. The radiator system is similar to the turboelectric plant counterpart described above and requires lithium or NaK pumps for which the fifth and sixth applications are included in the study.

The schematics shown in Figure 1 are simplified for brevity and clarity. Details, which are not shown but which were considered in the study work, included:

1) Multiple pumps. All applications, except the primary coolant pump, required multiple parallel systems to gain reliability through redundancy.

2) Auxiliary cooling systems.

TABLE 2. SPACE POWER PLANT EM PUMP APPLICATIONS

	Application	Fluid	Fluid Temp., °F			Flow, lb/sec / gpm			Press. Rise, psi / ft.			Net Positive Suction Press., psi / ft.			No. Pumps in Parallel	Developed Hydraulic Power, kw		
			Design Point	Study Range	Test Range	Design Point	Study Range	Test Range	Design Point	Study Range	Test Range	Design Point	Study Range	Test Range		Design Point	Study Range	Test Range
I	Turboelectric Condensate Boost	K	1200	1000 to 1400	1000 to 1400	1.5 ... 16	1-12 10-130	1-10 10-110	30 ... 100	2.9-62 10-200	2.9-47 10-150	3.0 ... 10	0-16 0-50	0-16 0-50	4	0.21	0.01-3.5	0.01-2.2
II	Turboelectric Radiator Coolant	NaK	1200	1000 to 1300	1000 to 1300	6.0 ... 60	3-36 29-370	3-24 29-250	25 .. 80	10-100 30-320	10-100 30-320	30 .. 97	20-40 60-120	20-40 60-120	16	0.65	0.13-16	0.13-11
III	Turboelectric Radiator Coolant	Li	1200	1000 to 1500	1000 to 1500	2.0 ... 31	1-12 15-190	1-8 15-130	20 .. 98	10-60 48-300	10-40 48-200	30 ... 150	20-40 100-200	20-40 100-200	16	0.26	0.06-5	0.06-2.3
IV	Thermionic Primary Coolant	Li	1700	1200 to 2000	1200 to 1500	40 ... 640	35-200 540-3300	35-100 540-1600	6 .. 31	3-50 15-270	3-10 15-50	10 .. 52	5-20 25-110	5-20 25-100	1	1.7	0.20-12	0.70-7.0
V	Thermionic Radiator Coolant	NaK	1200	1000 to 1300	1000 to 1300	6.0 ... 60	3-36 29-370	3-24 29-250	25 .. 80	10-100 30-320	10-100 30-320	30 .. 97	20-40 60-120	20-40 60-120	16	0.65	0.13-16	0.13-11
VI	Thermionic Radiator Coolant	Li	1200	1000 to 1500	1000 to 1500	2.0 ... 30	1-12 15-190	1-8 15-130	20 .. 98	10-60 48-300	10-40 48-200	30 ... 150	20-40 100-200	20-40 100-200	16	0.26	0.06-5	0.06-2.3

3) Power conditioning systems to provide electricity to the pumps in a suitable form.

4) Shaft power at the turbine, if useful, to drive the EM pumps.

5) Thermoelectric elements as a power source.

As a further guide to selection and design, a set of general requirements were specified.

1) Reliability: The major design consideration is reliability, i.e., the EM pump configuration shall be designed for two years of continuous, maintenance-free life.

2) Weight: Consistent with other requirements, the over-all pumping system weight shall be as low as possible.

3) Efficiency: The over-all pumping system shall be designed for the optimum efficiency compatible with maximum reliability and low weight.

4) Leakage: External leakage of the working fluid from the system shall be zero.

5) Materials: Applications and methods of fabrication shall be considered in the design and be within present state-of-the-art.

III. EM PUMP TECHNOLOGY

A. Survey of EM Pump Types

A rational choice of those EM pump configurations best suited to space power applications required a complete appraisal of the principal features and characteristics of the various possible types and configurations of EM pumps. Accordingly, the intention here is to describe and illustrate basic EM pump types to facilitate visualizing their possible variations and to indicate their principal features and characteristics. To attain comprehensive coverage of EM pump types, the accumulation and organization of the material presented entailed the following steps:

1) The available literature was surveyed. Section VI, Bibliography, lists the most important sources which were consulted.

2) Principles and configurations analogous to electromagnetic devices in advanced stages of development, principally motors and generators, were sought.

1. Definition and Principle of Operation

For this study, the term EM pump is applied to any device in which the body force on a conducting fluid results from the interaction between an electric current and a magnetic field in the fluid and produces a pressure rise in the fluid as it passes from the inlet to the outlet of the device. This body force is completely analogous to the familiar force on a current carrying conductor in a magnetic field, i.e., the operating principle of dc motors, induction motors, and many other common electromagnetic devices.

Quantitatively, assuming an electric current and a magnetic field in a fluid, the pressure gradient is proportional to the product of the magnetic field strength and the component of current density perpendicular to the magnetic field strength. The pressure gradient is a maximum in the direction mutually orthogonal to field strength and current density. Thus, in the elementary duct section of the sketch below, assuming

$$B_x = j_y = 0,$$

$$dP_z = j_x B_y dz \qquad 1$$

where j_x and B_y are current density and flux density in the axes indicated by the subscripts; dz is an incremental length in the z axis; dP_z is the incremental pressure rise imparted to the fluid over the distance dz.

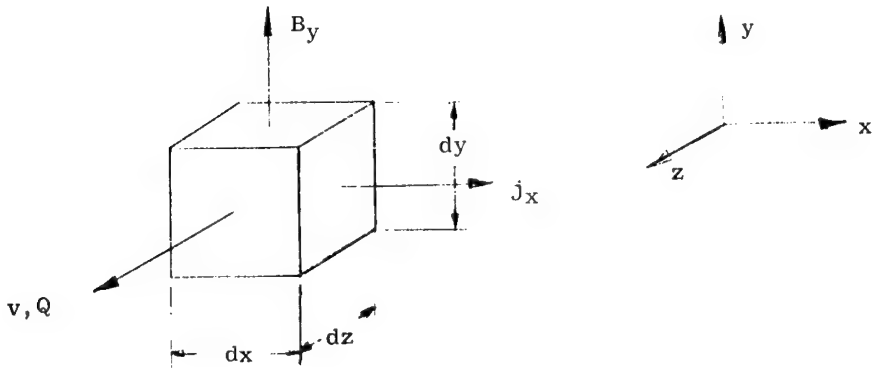

Elementary Duct Section.

The pressure rise developed by an EM pump is the integral of equation 1 over the axial length of flow passages of the pump. The total flow is the surface integral of the fluid velocity over the cross section of the pump duct. In most EM pump configurations, the local fluid velocity in the pump duct is directly proportional to the pump flow. In one exception, which has been called a centrifugal EM pump, the electromagnetic body force is used to accelerate the fluid to a high velocity in a closed path (as in a cylinder or disc), and a pressure increase is obtained by centrifugal force (as in a mechanical centrifugal pump). A second exception will be cited later in this section.

Because the method by which an electric current is established in the fluid provides a convenient classification system, EM pumps may be classified as either conduction or induction pumps. In conduction pumps, the current in the fluid is supplied from an external source and is conducted into the fluid by electrodes. In induction pumps, the current flows in the fluid because of voltages induced in the fluid by a time varying or moving magnetic field.

In addition to current in the fluid, a magnetic field perpendicular to the direction of current flow is essential for electromagnetic pumping. The method by which the magnetic field is established in the fluid, therefore,

affords a convenient subclassification system. For example, the field may be established by static or moving permanent magnets, by static or moving electromagnets excited by direct current, by electromagnets energized by single phase alternating current, or by distributed windings energized by polyphase alternating current.

A further subclassification is based on the duct shape and the geometric path followed by the fluid in traversing the duct. Several different configurations have been developed for various purposes in electromechanical devices; analogous configurations may also be employed in EM pumps. Examples are the familiar cylindrical rotor used in most dc and induction motors, the rotating disc used in axial gap induction motors, and the linearly moving slab used in electromagnetic catapults. In comparison with electromechanical devices, the absence of a fixed shape of the fluid in EM pumps provides an additional degree of freedom.

2. Duct Shapes

A consideration of the basic duct shapes which are adaptable to electromagnetic pumping of conducting fluids is pertinent. The fundamental requirements are that the duct contain the fluid and that a magnetic field and an electric current, with mutually perpendicular components, be established in the fluid. In the following discussion, a duct with a rectangular cross section is taken as the elementary duct, and the various duct shapes are generated from it.

a. Flat. This duct, illustrated in Figure 2, is straight and of rectangular cross section. As indicated earlier, a fluid in such a duct experiences a force in the z axis when mutually perpendicular components of flux density and current density are established in the x-y plane. Thus, B_y and j_x (and B_x and j_y) will produce a force on the fluid in the z direction. In practice, both pump design and power supply considerations make it preferable to minimize the exciting magnetomotive force (m.m.f.) and current.

Figure 2 shows clearly that, for b>a, the combination of B_y and j_x requires both lower exciting m.m.f. and fluid current than the combination of B_x and j_y, for the same values of flux density and of current density. Then, for B_y and j_x, only, and for fluid velocity v_z, the developed pressure, P_z, is

$$P_z = B_y j_x c \qquad 2$$

$$Q = v_z ab \qquad 3$$

where P and Q are pressure developed and flow rate, respectively, for the elementary pump. With the limitations imposed on the maximum values of B_y, j_x, and v_z by material properties, cooling considerations, and hydraulic losses, it is apparent that pumps developing relatively high pressure require relatively long pumping sections (large c); whereas pumps handling relatively high flows require relatively large cross-sectional areas a b . Compared with duct shapes to be described later, in reasonably well proportioned designs, the flat duct is best suited for low to moderate developed pressure and for moderate to high flow.

b. Annular. The elementary duct of rectangular cross section can be reshaped to form three basic annular configurations, which may be designated axial flow, tangential flow, and helical flow.

1. Axial Flow. The axial flow annular duct results from bending the rectangular duct in Figure 2 about the z axis to form an annulus. Figure 3 illustrates this duct configuration. Effective use of the configuration requires a radial component of flux density and a circumferential component of current density in the fluid, which produce a pressure rise along the z axis. A circumferential component of flux density and a radial component of current density also produce such a pressure rise, but this combination is not readily achieved. This duct shape is best suited to low to moderate developed pressure and moderate to high flow.

2. Tangential Flow. The tangential flow annular configuration results when the rectangular duct in Figure 2 is bent around the x axis to form the duct shape as illustrated in Figure 4. A radial component of flux density and an axial component of current density in the fluid interact to produce a pressure rise in the fluid passing through the duct. In reasonable proportions, this duct shape is best suited for moderate pressure and moderate flow.

3. Helical Flow. The helical flow annular duct configuration is formed by bending the rectangular duct in Figure 2 around the x axis into a helix with closely spaced turns. Figure 5 illustrates such a duct. Again, a radial component of flux density and an axial component of current density interact to produce a tangential force on the fluid. The helical passages direct the flow so that it proceeds axially along the duct through the helical passages. This duct shape affords great freedom of design because the pitch of the helix and the number of parallel helical passages may be varied over a wide range. Also, helical passages may be used in concentric annuli with one set of passages having a right hand thread and the other, a left hand thread. In this arrangement, fluid entry and exit are at the same end of the duct with one annulus connected to the other at the opposite end. The helical flow annular duct is best suited to low flow, high pressure applications.

c. Disc. Disc configurations analogous to each of the annular configurations exist and may also be generated from the flat duct of rectangular cross section.

1. Radial Flow. The radial flow disc configuration may be derived from the flat configuration by maintaining the b dimension of one end of the flat duct while expanding the b dimension at the other end in a circle in the x-z plane until it closes on itself. The disc shown in Figure 6 is formed. Flow in this configuration is radial with fluid entry and exit at inner and outer peripheries, respectively, or vice versa. The flux density is normally in the x axis. The usual application of the electromagnetic pumping principle would use circumferential current density in the y-z plane. In the centrifugal EM pump, however, the current density in the fluid is radial, interacting with B_x to produce a circumferential body force on the fluids. The fluid is thus accelerated to a relatively high tangential speed. A pressure rise is developed by centrifugal force between the "eye" of the duct and the outside diameter. Using a suitable diffuser at the outer periphery of the duct permits converting some of the velocity head of the fluid at the periphery into static pressure as it leaves the duct. This type duct is best suited to low pressure and low to moderate flow.

2. Tangential Flow. The tangential flow disc configuration results when the rectangular duct in Figure 2 is bent around the y axis to form the shape illustrated in Figure 7. Except for the proportions, this shape is identical to the tangential flow annular duct. In this arrangement, a component of flux density in the y axis and a radial component of current density produce a pressure rise on fluid passing peripherally through the duct. This duct shape is best suited to moderate pressure and flow.

3. Spiral Flow. The spiral flow disc configuration, analogous to the helical flow annular configuration, is produced by bending the rectangular duct in Figure 2 in a spiral form around the y axis. Figure 8 illustrates this duct shape. Normally, this configuration will be supplied with flux density in the y axis and radial current density to produce a circumferential force on the fluid in the spiral duct passages. This duct has some of the design flexibility of the helical flow annular duct and, similarly, is best suited to high pressure and low flow. The basic shape, however, is not as efficient a pressure vessel as the cylindrical helical annular shape.

3. Conduction Pumps

Conduction pumps may be designed incorporating any of the duct configurations described in the preceding paragraphs. Most conduction pumps, however, have been built with flat ducts of approximately rectangular cross section because of their simplicity and relative ease of manufacture and their adaptability to a wide range of pressure and flow. In the following general discussion of conduction pumps, a flat duct is used for illustration. Unless otherwise indicated, the comments and conclusions apply to conduction pumps having any duct configuration. Figure 9 illustrates a conduction pump with a flat duct. The current density and flux density in the fluid may be either direct or alternating.

Generally, this is true for all conduction pumps. Considerations unique to direct current and alternating current conduction pumps will be discussed later in this section.

If I is that part of the total current passing through the liquid under the magnet poles and if the flux density B is assumed uniform over the region covered by the poles, it follows from equation 1 that the developed pressure is given by

$$P_z = j_x B_y c = \frac{IB}{a} \qquad 4$$

The flow Q is given by equation 3:

$$Q = vab \qquad 3$$

where v is the velocity of the liquid metal. In conventional engineering units,

$$P = \frac{8.85}{a} \left(\frac{B}{10^3}\right) \left(\frac{I}{10^5}\right) \text{ psi} \qquad 5$$

$$Q = 3.12\ vab \text{ gpm} \qquad 6$$

where B is in lines/in.^{2}, I is in amperes, v is in ft/sec, and a and b are in inches. The total flux $\emptyset$, in lines, is given by

$$\emptyset = Bbc \qquad 7$$

The flux density in the fluid is limited by saturation of the magnet material to approximately 10^5 lines/in.^{2}. (In practice, much lower densities are used.) The value of a is variable, but it will seldom be less than 1/4 inch. Thus, it is apparent from equation 5 that conduction pumps with flat ducts producing pressures in the order of tens of psi require currents in the fluid in the order of thousands of amperes. When flows in the order of hundreds of gpm are required, the current required is typically tens of thousands of amperes at voltages in the order of one volt.

Variations in the elementary flat duct conduction pump configuration are possible and may offer advantages for certain applications. For example, Figure 10 illustrates two flat duct configurations which permit a greater developed pressure per ampere of current in the fluid than that of Fig 9. Assuming that the duct sections in the configurations shown in Figures 9, 10a and 10b are of equal size. for equal fluid current, flux density, and fluid velocity, the two configurations in Figure 10 develop twice the pressure at the same flow as that shown in Figure 9. In Figure 10a, the m.m.f. required to develop a given flux density

in the fluid is twice that required in Figures 9 and 10b, whereas the total flux required in Figure 10b is twice that required in Figures 9 and 10a. The configuration in Figure 10a has the additional advantage of armature reaction compensation which is described below.

Conducting materials are generally used for the duct structure with the electrodes solidly connected to the duct sides. The voltage applied across the fluid pumped, therefore, is also applied across the duct structure; the resulting duct wall current is both a source of considerable loss and a significant addition to the current in the fluid. The electrodes and their attachment to the duct sides constitute a difficult mechanical design problem for conduction pumps. The duct walls must be kept relatively thin to limit the duct wall loss; hence, the sections adjacent to the electrodes are subjected to thermally induced stresses caused by the different rates of change in temperature of the thin duct sections and the heavy electrode sections during changes in temperature of the pumped fluid. Furthermore, the ohmic losses in the electrodes themselves are often sufficiently great to require auxiliary cooling of the electrodes.

The current flowing in the fluid and the duct walls produces an air gap m.m.f. analogous to the armature reaction of rotating electric machinery. This distorts the m.m.f. across the duct and tends to produce a higher m.m.f. at the inlet than at the outlet of the duct. Decreased pump efficiency and hydraulic output result. As in the case of dc rotating machinery, this m.m.f. distortion may be compensated by returning the current passing through the fluid and the duct walls through the gap between the magnetic poles in the opposite direction. Figure 11 illustrates this compensation. The two-stage pump illustrated in Figure 10a is similarly compensated.

At the ends of the electrodes, current tends to fringe upstream and downstream in the fluid. Since the magnetic field beyond the ends of the magnetic structure is weak, little back electromotive force is developed in this region so that the fringing current is greater relative to the total current at high flow velocities and flux densities. This fringing current contributes little to the pressure developed by the pump; rather, it is a source of additional loss and it also increases the current required. Figure 12 illustrates the fringing current density field in the fluid at the ends of a conduction pump.

Figure 12a depicts the general nature of the fringing current when no insulating barrier is used; Figure 12b shows how the field is modified using one insulating barrier. It is apparent that the effects of current fringing at the duct ends on pump performance are strongly related to the ratio of the length of the pump (in the flow axis) to the width of the duct (in the current axis) and that these effects are less for large values of (c/b). Insulating barriers may be used to reduce the current fringing effects.

Figure 13 illustrated the flux fringing field. The effects on pump performance are strongly related to the ratio of the length of the pump c, to the length of the nonmagnetic gap, g ; i.e., these effects are less for large values of c/g.

a. DC Conduction Pumps. When direct current is supplied to duct and field circuits in Figure 9 and 11, these pumps become uncompensated and compensated direct current conduction pumps, respectively. They may be excited by direct current in the field windings, as illustrated in Figures 9 and 11, or by permanently magnetized hard magnetic material used for all or part of the magnetic structure. Using both direct current field excitation and permanent magnet excitation in the same pump is possible, although this is not a common design arrangement. Direct current excited conduction pumps may be series or shunt excited. In series excited pumps, the duct circuit and the field circuit are connected in series so that the field winding consists of a few turns of large conductors. In shunt excited pumps, the conductor size and number of turns may be adjusted for compatibility with the excitation power supply. Series excitation is particularly well suited to pumps subject to high radiation or high temperature since the field voltage is normally very low. Thus, materials which have relatively poor dielectric properties but good resistance to radiation and high temperature may be used for insulating the field winding.

As indicated previously, the fluid circuit of conduction pumps of useful capacity normally required very high current at very low voltage, typically thousands of amperes at a fraction of one volt. Special power supply equipment, therefore, is necessary. Conversion schemes starting with electrical, mechanical, and thermal power are possible. In the more conventional power conversion schemes, current may be supplied from an alternating current source by rectification or from a mechanical power source by a dc generator. When rectification is used, the voltage drop in the rectifiers approximates the output voltage required and, hence, the efficiency is poor. Also, many rectifier cells in parallel are required to develop the necessary high values of current. Because of the poor efficiency associated with brush voltage drop and the very large brush contact area required for conducting thousands of amperes, using dc generators of conventional design for supplying dc conduction pumps is quite impractical. Although acyclic (homopolar) machines, using liquid metal collectors, are well suited for supplying such pumps, they are not developed in small sizes. Direct conversion processes, particularly thermoelectric and thermionic, are attractive in that their characteristic output of high current, low voltage is admirably suited to dc conduction pump requirements. Negative features are temperature limitations, poor efficiency, and high specific weight. Although probably useful for auxiliary applications or in smaller power plants, the thermoelectromagnetic pump, in which thermoelectric elements become a part of the pump structure, is noncompetitive for the applications in this study.

To reduce the over-all size and weight of pump and power conversion equipment, several configurations have been conceived in which both power conversion and pumping are accomplished. One of the most promising of these is the thermoelectric heat exchanger pump. Here, thermoelectric materials are used in the heat exchanger in such a manner that electric power is generated when heat flows from the fluid at the higher temperature to the fluid at the lower temperature. The electric current thus available excites the pump field and passes through either one or both of the fluids involved to produce pressure and flow.

b. AC Conduction Pumps. When the pump configurations shown in Figures 9, 10, and 11 are supplied with alternating rather than direct current, they become ac conduction pumps. For effective operation, flux density and current density in the fluid must be in phase. The pressure developed is proportional to the product of field strength and current in the fluid and, hence, is a fully displaced sinusoid going from zero to twice its average value at twice the frequency of the power supply. Alternating current conduction pumps cannot be excited by permanent magnets. Although they may be either series or shunt excited, they are usually series excited to insure that flux density and current density are in phase.

The phenomenon of field distortion by current in the fluid and duct walls in uncompensated ac conduction pumps is similar to that in dc conduction pumps, except that the time variation of the magnetic field introduces an additional component of induced voltage in the fluid and the duct walls. The qualitative effect of the time variation of the field may be deduced as follows.

Consider the configuration in Figure 9. The sinusoidal variation of the exciting flux in the y axis induces voltages in duct walls and fluid that cause circulating currents (eddy currents) to flow in the x-z plane in a manner to oppose the change of the flux in the y axis. If the effect of the motion of the fluid is ignored, this situation is identical to the classical current and flux distribution problem in a lamination of finite length. As in the lamination problem, the eddy currents distort the flux density and reduce its value everywhere except at the edges of the duct. The eddy currents contribute nothing to the pump output but rather constitute an additional loss. The effects of the eddy currents are strongly dependent upon the b and c dimensions of the duct and the frequency of the power supply. In any event, conduction pumps, per se, can never perform as efficiently when operated on ac power as when operated on dc power.

Alternating current conduction pumps have the advantage, however, of easier adaptability to common power supplies; i.e., they require only a transformer to convert ac power from normal utilization voltage to the low voltage, high current power necessary. The transformer and pump are usually incorporated into a compact unit designed to minimize weight.

4. Induction Pumps

In induction pumps, the high duct currents demanded are induced within the duct itself and flow in closed loops contained within the duct. Thus, neither an external source of high current nor heavy electrode connections to the duct are necessary. These are significant advantages, permitting a symmetrical duct free of the stress concentrations caused by temperature gradients and physical restraints associated with the electrode-duct region in conduction pumps.

Induction pumps, however, have certain inherent disadvantages and limitations. Since the current in the fluid must be induced by a time rate of change of magnetic flux in the fluid, it is difficult to produce compact pump designs for liquid metals having high electrical resistivity. Also, because of eddy current losses as discussed under ac conduction pumps, high frequency power is not suitable for induction pumps. Furthermore, the optimum frequency decreases with increasing pump capacity. Induction pumps may be designed for either single phase or polyphase power supplies. Most of the induction pumps built to date have been designed for polyphase power.

a. Single Phase Induction Pumps. The consideration of ac conduction pumps in part A.3, tacitly assumed that the duct and the magnetic structure were symmetrical, so that the eddy current pattern and the flux density distribution were also symmetrical. If the fluid velocity is assumed to be zero, the resulting eddy current and flux density distribution are illustrated in Figure 14.

In the EM pump configurations examined earlier, the magnitude and direction of the force on each element of fluid was determined from the product of the flux density and current density in each element. In the configuration in Figure 14, in addition to the space variation in both flux density and current density across the duct, the phase relationships also vary across the duct. Accordingly, a different viewpoint is desirable to provide insight into operation and a guide in appraising the usefulness of various possible pumping configurations.

A suitable viewpoint, which can be developed from energy considerations, may be summarized by the statement that the forces exerted will tend to maximize the effective permeance of the system. That is, motion of the fluid will tend to maximize the flux passing between the poles in the pumping configuration. Before this principle can be applied to determine the direction of the forces in any configuration, the flux density distribution must be known. The flux density distribution may be ascertained by applying Lenz's law which states that the voltage induced causes current to flow in a direction opposing the change in the magnetic flux.

Thus, in the EM pump configuration in Figure 14, the symmetry is such that, assuming zero fluid velocity, the eddy currents in the fluid and the duct flow in closed paths in the general pattern illustrated. Now, if all fluid and duct

elements could move toward the low flux density region, the high flux density region would become larger and the total flux would increase. Accordingly, the forces are toward the center. The symmetry is such that the net force in any direction would be zero.

If, as illustrated in Figure 15, very low resistance bars are attached to one end of the duct structure, the symmetry is destroyed, and fluid (and duct) currents flow in the paths indicated. The m.m.f. caused by these eddy currents opposes the exciting m.m.f. and distorts the flux density so that the maximum occurs at the top of the duct in Figure 15. Current carrying fluid and duct elements tend to move toward the region of lower flux density and, hence, the force is directed toward the end of the pump where the low resistance bar is attached.

Figure 16 is an annular version of the pump illustrated in Figure 15. The duct is an annulus and the exciting coil is a toroid. The pump is symmetrical around the axial center line. The magnetic structure is laminated, and the major dimensions of the laminations, ideally, at least, lie in planes which contain the axial center line of the pump. The symmetry is such that the induced currents in the fluid and the duct flow in closed circles about the center line. The m.m.f. produced by these currents opposes the exciting m.m.f. and, therefore, flux density in the fluid concentrates at the left side of the duct in Figure 16. The current carrying fluid and duct elements then tend to move toward the region of lower flux density and, hence the fluid is pumped to the right.

Another version of the annular duct, single phase, ac induction pump is shown in Figure 17. The principle of operation and the general flux and current relationships for this pump are the same as those for the pump in Figure 16. It requires more "magnetizing current" and is less efficient in both power and space utilization but has a simpler and possibly lighter magnetic structure. Other variations of the configurations illustrated utilize a second exciting coil located at the end of the duct opposite the coil illustrated. Performance is similar to those of the configurations shown in Figures 16 and 17.

Annular duct, single phase, induction pumps have many attractive features. The exciting coils are compact and relatively easy to form, insulate, and cool. The duct is symmetrical and, hence, is relatively free of stress concentrations. The developed pressure is pulsating, however, with an ac component of the order of the average component (cf. ac conduction pumps). There are few references to single phase induction pumps in the literature (Ref. 15). The analysis is complex. A comprehensive analysis of single phase induction pumps is presented later in this report. Here, a limiting case analysis of developed pressure is made, assuming zero flow and neglecting duct wall current.

The current I_f in the fluid annulus, the radial flux density B in the nonmagnetic gap at the point marked 1 in Figure 16 and the radial length g of the nonmagnetic gap are related by the following expression:

$$B = \mu \frac{I_f}{g}$$

where μ is the magnetic permeability of the nonmagnetic gap. Assuming that power supply frequency, fluid resistivity, and annulus length are such that the flux passing through the pump core at point 2 approaches zero, the flux density in the nonmagnetic gap at point 3 also approaches zero. Then, the pressure developed becomes

$$P = \frac{1}{2} \frac{g}{t} \frac{B^2}{\mu} \qquad 9$$

where B is in lines per square inch, μ is the permeability of free space and g and t are the indicated distances in inches

$$P = 1.39 \frac{g}{t} \left(\frac{B}{10^4}\right)^2 \quad \text{psi} \qquad 10$$

From a limiting condition standpoint, the effective value of flux density in magnetic steel may approach 80,000 to 90,000 lines/in.^{2} and, hence, this type pump is capable ideally of pressures exceeding 100 psi.

b. Polyphase Induction Pumps. Polyphase induction pumps are excited by polyphase alternating current supplied to static windings distributed on one or both sides of a pump duct and supplied with power in a manner producing a sinusoidally distributed m.m.f. across the pump duct. This m.m.f. wave travels along the pump duct and induces voltages in the fluid and duct walls. The resulting currents in the fluid interact with the traveling magnetic field to produce force on the fluid in the direction of motion of the field. The principle of operation is identical to that of the polyphase induction motor, which is used widely in industry and utilities for motor applications in the 1 to 1,000 hp range. The polyphase induction motor owes its favorable acceptance and extensive usage primarily to the simplicity of its rotor and the absence of electrical connections to the rotor. Similarly, the attractiveness of the polyphase induction EM pump is due to duct simplicity, the absence of electrical connections to the duct, and its adaptability to widely available power sources.

Polyphase induction pumps may be built using any of the basic duct configurations described earlier. Flat duct pumps generally have been preferred for high flow applications and have received considerable development effort here and abroad. Helical flow annular pumps generally have been preferred for low flow applications and have operated quite satisfactorily in various applications.

1. Flat Linear. Two views of a flat linear induction pump in Figure 18 illustrate this basic arrangement. Distributed windings are arranged in the slots and supplied with polyphase power, producing a sinusoidally distributed traveling m.m.f. wave that moves linearly at

a velocity dependent upon the pole pitch of the windings and the frequency of the power supply. The duct, rectangular in cross section, is located in the magnetic field between the two stators. Normally the length of the pump is several pole pitches.

Figure 19 illustrates the relationship between the magnetic field and the current density in the fluid. Flux density and current density are sinusoidally distributed and are in phase, the condition required for maximum developed pressure. Pump output pressure is essentially constant, free from the twice power frequency pulsation characteristic of ac conduction pumps and single phase ac induction pumps.

Because of side and end effects, the flat linear induction EM pump is subject to a reduction in output. The current loops shown at both sides of the conducting fluid sheet in Figure 19 illustrate the side effects. A voltage drop occurs in these loops, reducing the x component of current density in the fluid sheet and, thereby, the developed pressure. It is apparent that the magnitude of the pressure reduction caused by side effects is related to the ratio of the width of the pump duct b to the pole pitch λ. The end effects are caused by discontinuities in permeance and in the traveling wave of exciting m.m.f. at each end of the pump. These discontinuities lead to ineffective utilization of the end poles particularly and, hence, to reduced output and efficiency. This effect is related to the number of poles employed and the winding arrangement in the end poles.

2. Annular Linear. The polyphase induction pump using an axial flow annular duct configuration is usually called the annular linear induction pump. It is illustrated in Figure 20. The windings consist of toroidal coils whose axes are concentric with the axis of the annular duct. As in the flat linear induction pump, when the windings are properly energized, a traveling wave of m.m.f. moves linearly along the axis of the pump. The effective component of the flux density in the annular duct is radial. The magnetic steel in both stator and core should have the principal planes of the laminations in radial planes passing through the axis of the pump. Because of the inaccessibility of the core, windings are normally located in the stator (outside the annular duct) only.

The annular pump is identical, in principle, to the flat pump. The ranges of application of the two pumps are similar; both are best suited to moderate and high flow, low pressure applications. The annular pump is not subject to the side effects present in flat pumps, since the circumferential component of current density is continuous in the fluid in the annulus. The end effects, however, are similar, although annular designs may permit greater freedom to control the field in the end poles by using special coils.

3. Helical Polyphase. Figure 21 illustrates the basic helical induction EM pump configuration. The flow passages consist of one or more helical passages within the annular duct. The stator is identical in principle and arrangement to the stator of a polyphase induction, or

synchronous, motor. When polyphase alternating voltage is supplied to the distributed windings, a rotating m.m.f. wave is established radially across the duct. The central magnetic core serves as a low reluctance flux path for transmitting the air gap flux between poles. The rotating magnetic field induces axial voltages in the fluid and the duct walls, and the resulting axial currents in the fluid interact with the field to produce a tangential force on the fluid. The length of path over which pressure is developed in the fluid is the developed length of a helical passage.

Many variations in the duct arrangement illustrated in Figure 21 have been developed recently. In Figure 22 a, two concentric helical ducts are shown. Obviously more concentric passes may be used if desired. In Figure 22 b, a central fluid return is shown inside the pump core. Both these variations in arrangement permit suction and discharge to be immediately adjacent at one end of the pump. This is quite advantageous considering ease of assembly and freedom from stresses arising from pipe reactions, thermal transients, etc. For extremely high temperature applications, the magnetic core may be omited from these configurations. The resulting construction is exceptionally rugged and reliable, but performance is adversely affected both in pump efficiency and weight.

Although the helical induction pump experiences a loss in output because of side effects similar to those described for flat pumps, it has no end effects analogous to those of flat and annular pumps. The axial component of fluid velocity, however, results in additional loss and reduction in output. This effect, insignificant in pumps having a small helix angle, becomes limiting when large angles (near 45°) are used.

The foregoing statements assume that the stator slots are axial. Some improvement in performance may be achieved by skewing the slots. In the optimum relationship, the skewed slots are perpendicular to the helical flow passages. It is also possible to achieve pumping in a helical induction pump configuration with skewed slots and an annular duct without helical flow passage separators. Such an arrangement is electromagnetically and hydraulically inferior to designs with helical flow passage separators, but the duct construction is simpler and better adapted for use with nonmetallic duct materials.

4. Spiral Polyphase. Figure 23 illustrates the spiral induction pump configuration. The pumped fluid passes through the duct through one or more involute passages which lie in a plane. The duct lies in the axial air gap, which is excited by stators on either side of the duct. The polyphase stator windings are distributed with the individual coil sides lying in slots, which may be radial or may spiral outward from the stator inside diameter to the stator outside diameter. Fluid suction is normally at the inside diameter of the duct; the discharge, at the outside diameter. Stator laminations are oriented in such a manner that a radial line is perpendicular to the principal surface of the laminations.

Like its helical counterpart, the spiral induction EM pump is best suited to relatively low flow and moderate to high pressure applications. Electromagnetically, it has an advantage over the helical pump because its design permits symmetrical stators on both sides of the fluid duct. This leads to lower leakage reactance of the windings and, hence, a tendency to better power factor. In most other comparisons, however, it is inferior to the helical pump. If the air gap is constant, it utilizes magnetic material poorly since, with uniform slots, flux densities in the stator teeth will be much lower at the outside diameter than at the inside diameter. Thus, efficient utilization of material leads to an air gap that varies inversely (approximately) with radius. The linear velocity of the revolving field obviously is greater at the outside diameter than at the inside diameter. It is desirable, therefore, that the linear velocity of the fluid be greater at the outside diameter than at the inside diameter to maintain the optimum slip throughout the pump. With a constant radial passage width, constant slip will be approximated if the axial dimension of the duct varies inversely with radius.

When the involute flow passage separators are omitted, the fluid in the duct will be spun around the pump center line by the interaction of the revolving field and the induced currents in the field. Thus, by centrifugal force, a pressure rise will occur between the fluid at the pump inside diameter and that at the pump outside diameter. The pumping phenomenon is essentially identical to that of the conventional mechanical centrifugal pump.

Just as in the case of axial air gap motors compared with radial air gap motors, the spiral induction pump is more complex physically and electromagnetically than its helical counterpart. It has, consequently, received very little attention and development effort.

c. Moving Magnet Induction Pumps. In principle, moving magnet induction pumps differ from polyphase induction pumps only in the means of excitation. Where polyphase induction pumps are excited by a traveling wave of m.m.f. generated by the flow of alternating current through stationary windings, moving magnet induction pumps are excited by the physical motion of permanent magnets or electromagnets. The field windings may be either stationary or wound around the poles of the rotating structure.

In the concept employing rotating field windings, field current may be supplied via slip rings, or alternating power may be supplied to the rotating element by induction and to the field by rectifiers mounted on the rotating structure. These excitation systems are commonly used in conventional synchronous motors and generators. Configurations employing stationary field windings are similar to those used in homopolar induction alternators. The field windings are toroidal in shape. The field current produces a constant m.m.f. across the duct. A traveling wave of field strength is produced by rotating a rotor structure with a number of magnetic salients in the region across which the exciting m.m.f. is applied. The

annular and disc pump configurations are well adapted to excitation by moving, or rotating, magnets.

1. Annular Helical Duct. In the annular helical configuration, the rotating magnets may be either external or internal to the duct cylinder with the opposite member a stationary laminated flux return structure. The duct configurations illustrated in Figures 5 and 8 appear well suited to excitation using a rotating electromagnetic structure. When the rotor poles are skewed, the helical flow passage separators may be omitted, although their omission will obviously modify the performance. Such a pump has been studied extensively and the results are reported in reference 16.

The inductor version of the annular helical rotating magnetic induction pump electromagnetically similar to the inductor alternator, is illustrated in Figure 24. The duct may or may not have helical flow passage separators. Considering the severe skew possible with the inductor configuration, an annular duct without helical separators appears feasible. In this design, excitation is provided by dc current in the centrally located, stationary, toroidal exciting coil. Rotating the wormlike magnetic rotor structure produces motion of the magnetic field in a helical path with a relatively small axial component. A visual analogue is the familiar revolving barber pole. This configuration is mechanically driven and was originally conceived as direct connected to a high speed turbine shaft.

2. Spiral Duct. In the disc spiral configuration, a set of rotating magnets may be located on both sides of the duct, or one set of rotating magnets and one stationary laminated magnetic flux return structure may be used. Spiral flow passage separators may or may not be used. Excitation may be by permanent magnets, dc excitation of rotating windings, or dc excitation of a stationary winding. Figure 25 illustrates one concept in which the rotating field structure is driven by an integral ac motor.

Advantages and disadvantages of the moving magnet pumps as compared to polyphase induction pumps are presented in Table 3:

TABLE 3. COMPARISON OF MOVING MAGNET AND POLYPHASE INDUCTION PUMPS

Advantages	Disadvantages
1. Much lower volt-ampere input because of the low power factor of polyphase induction pumps.	1. Inherently lower reliability, because of the additional failure mechanisms associated with rotation, bearings, etc.
2. Less volume of active material required, because stronger fields can be attained by more effective field windings.	2. Inability to use magnet structures to support duct walls.
3. Less stringent requirements for electrical insulation, ignoring rotation, because of lower voltages needed for windings.	

B. Basic Characteristics

1. Efficiency

a. Duct Efficiency. In the following development, the efficiency of an elementary EM pump duct section, shown in Figure 26, is related to the pertinent design parameters. Hydraulic power output, fluid I^2R loss, and duct wall I^2R loss are considered and the following assumptions are made:

1) The applied magnetic field has a y component only and does not vary with x and y.

2) The fluid velocity has a z component only and does not vary with x and y.

3) The current density in the fluid has an x component only and does not vary with x and y.

4) Entrance and exit irregularities are neglected.

In a consistent system of units,

$$P = Bjc \tag{11}$$

$$Q = v_f ab \tag{12}$$

$$V = (\rho_f j + v_f B)b \tag{13}$$

$$W_o = PQ = Bjv_f(abc) \tag{14}$$

Let synchronous velocity v_s be defined as the fluid velocity at which the fluid current density becomes zero. Then,

$$v_s = \frac{V}{Bb} \tag{15}$$

$$s = \frac{v_s - v_f}{v_s} \tag{16}$$

where s is defined as slip.

It follows that

$$j = \frac{B\, v_s\, s}{\rho_f} \tag{17}$$

$$V = B\, v_s\, b \tag{18}$$

$$W_o = \frac{B^2\, v_s^2\, s(1-s)\ (abc)}{\rho_f} \tag{19}$$

The I^2R loss in the fluid is clearly

$$W_f = j^2 \rho_f \text{ (abc)}$$

or

$$W_f = \frac{B^2 v_s^2 s^2}{\rho_f} \text{ (abc)} \qquad 20$$

The I^2R loss in the duct walls is

$$W_d = \left(\frac{V}{b}\right)^2 \frac{2t\ bc}{\rho_d}$$

or

$$W_d = B^2 v_s^2 \frac{2t}{a\ \rho_d} \text{ (abc)} \qquad 21$$

Neglecting viscous losses, the duct efficiency η_d may be defined as

$$\eta_d = \frac{W_o}{W_o + W_f + W_d} \qquad 22$$

Substituting equations 19, 20, and 21 into equation 22 and simplifying yields

$$\eta_d = \frac{1 - s}{1 + \frac{Y}{s}} \qquad 23$$

where

$$Y = \frac{2t\ \rho_f}{a\ \rho_d} \qquad 24$$

It may be shown that the maximum duct efficiency occurs at an optimum slip s_m

$$s_m = Y\left(\sqrt{1 + \frac{1}{Y}} - 1\right) \qquad 25$$

and is

$$\eta_d max = 1 - 2s_m \qquad 26$$

Equations 23 and 26 are plotted in Figure 27. This figure illustrates clearly the strong influence of duct wall loss in reducing pump efficiency. The diagonal line corresponding to Y = 0 shows duct efficiency as a function of slip when duct wall loss is zero. High duct efficiency requires a low value of the parameter Y .

b. Electrical Efficiency. In addition to the losses considered for duct efficiency above, this development considers the pump winding I^2R loss. The following assumptions, plus those for duct efficiency, are used:

1) Excitation is provided by balanced polyphase currents in windings distributed along the z axis.

2) Magnetomotive force caused by fluid and duct wall currents is compensated by current in the pump windings.

3) Time harmonics in the exciting current are neglected.

4) Space harmonics in exciting m.m.f. are neglected.

5) The leakage reactance of the fluid and duct wall circuits is negligible.

Relating winding loss to pump output necessitates relating winding current to the terms used in pump output equations 14 or 19. Winding current may be regarded as composed of two components 90 electrical degrees out of phase: one, the exciting current, produces the net flux density in the air gap; second, the load current compensates fluid and duct wall currents. Thus, where A_m and A_1 are magnetizing and load currents per unit length in the z axis, respectivel and k_1 is the winding pitch and distribution constant, it may be shown that

$$A_m = \frac{\pi g}{k_1 \mu \lambda} B \qquad 27$$

and

$$A_1 = \frac{a}{k_1} \left(1 + \frac{Y}{s} \right) j_f \qquad 28$$

Since A_m and A_1 are 90 electrical degrees out of phase, the winding loss may be related to the sum of their squares. Thus,

$$W_1 = r_1 \left(A_m^2 + A_1^2 \right) bc \qquad 29$$

where r_1 is the resistance of that part of the pump windings bounded by a region having unit length in both x and z axes. Using equations 17, 27, and 28, equation 29 may be expressed in the terms of equation 20. Thus,

$$W_1 = r_1 \left(\frac{B}{k_1} \right)^2 \left[\left(\frac{\pi g}{\lambda \mu} \right)^2 + \left(\frac{asv_s}{\rho_f} \right)^2 \left(1 + \frac{Y}{s} \right)^2 \right] bc \qquad 30$$

Neglecting viscous losses, electrical efficiency η_e may now be written

$$\eta_e = \frac{W_o}{W_o + W_f + W_d + W_1} \qquad 31$$

Using equations 19, 20, 21, and 30 and rearranging,

$$\eta_e = \frac{s(1 - s)}{(s + Y) + \frac{ar_1}{k_1^2 \rho_f} \left[(s + Y)^2 + \left(\frac{\pi g \rho_f}{\mu a \lambda v_s} \right)^2 \right]} \qquad 32$$

Equation 32 may be expressed in more convenient terms using the relationships

$$2f\lambda = v_s \qquad 33$$

$$v_f = (1 - s) v_s \qquad 34$$

Thus,

$$\eta_e = \frac{s(1 - s)}{(s + Y) + \frac{ar_1}{k_1^2 \rho_f} \left[(s + Y)^2 + \left(\frac{2\pi f g \rho_f}{\mu a v_f^2} \right)^2 (1 - s)^4 \right]} \qquad 35$$

It is interesting to substitute reasonable numbers for some of the terms in equation 35 and to plot η_e against the remaining variables. In Figure 28, η_e is shown as a function of slip and frequency for normally expected values of the ratios Y, $ar_1/k_1^2\rho_f$, and $2\pi g\rho_f/\mu a v_f^2$. Thus, assuming

$t = 0.025$ in.

$a = 0.25$ in.

$\rho_f = \rho_d = 20 \times 10^{-6}$ Ohm-in.

$k_1 = 0.8$ in.

$r_1 = 10 \times 10^{-6}$ Ohm

$g = 0.4$ in.

$\mu = 3.19$ line/amp-in.

$v_f = 25$ ft/sec

$$Y = 0.2 \qquad 36$$

$$\frac{ar_1}{k_1^2 f} = 0.156$$

$$2\pi \left(\frac{g}{a} \right) \frac{\rho_f}{\mu v_f^2} = 0.07 \qquad 37$$

Then,

$$\eta_e = \frac{s(1 - s)}{(s + 0.2) + 0.156 \left\{(s + 0.2)^2 + \left[0.07\, f(1 - s)^2\right]^2\right\}} \qquad 38$$

This equation is plotted in Figure 28.

2. Duct Specific Power

In the preceding development, no restrictions were placed on the space occupied by the pump. In this development, the specific power w of the pump duct is related to the various pump design parameters. It is defined as the ratio of duct output power W_o to duct volume abc.

Many factors will affect pump size, but the limitation in a particular design is generally winding temperature. Winding temperature is a function of winding power loss, fluid temperature, heat sink temperature, and the thermal properties of the paths through which the loss passes enroute from windings to heat sink. This development assumes that stator winding temperature limits the heat loss from the pump to q_1 units of power per unit surface area of the duct. Thus,

$$W_1 = q_1 bc \qquad 39$$

Equating equations 30 and 39, assuming negligible heat loss from the duct to the coolant,

$$q_1 = r_1 \left(\frac{B}{k_1}\right)^2 \left[\left(\frac{\pi g}{\lambda \mu}\right)^2 + \left(\frac{asv_s}{\rho_f}\right)^2 \left(1 + \frac{Y}{s}\right)^2\right] \qquad 40$$

Combining equations 19, for power output, and equation 40 and rearranging,

$$\frac{W_o}{abc} = w = \left(\frac{q_1}{a}\right) \frac{s(1 - s)}{\left(\frac{ar_1}{k_1^2 \rho_f}\right)\left[(s + Y)^2 + \left(\frac{\pi g \rho_f}{\mu a \lambda v_s}\right)^2\right]} \qquad 41$$

This equation is similar to equation 32 for electrical efficiency. Again, substituting for λ and v_s in terms of f, v_f and s,

$$w = \left(\frac{q_1}{a}\right) \frac{s(1 - s)}{\left(\frac{ar_1}{\rho_f k_1^2}\right)\left[(s + Y)^2 + \left(\frac{2\pi f g \rho_f}{\mu a \lambda v_f^2}\right)^2 (1 - s)^4\right]} \qquad 42$$

The expression for w has the dimensions of q_1/a since the remaining terms are dimensionless. In the flat EM pumps installed in the submarine Seawolf, q_1 was approximately 25 watts/in.^{2}. Using this value for q_1 and the values used to obtain Equation 38 for the remaining quantities, equation 42 becomes

$$w = \frac{641\ s(1 - s)}{(s + 0.2)^2 + \left[0.07\ f(1 - s)^2\right]^2} \qquad 43$$

This equation is plotted in Figure 29.

3. Power Factor and Stored Energy

The large air gaps inherent in EM pumps, coupled with the relatively high resistivities of the liquid alkali metals, lead inevitably to pumping configurations in which the energy stored in the magnetic fields associated with the air gap and the leakage flux paths is much greater, relative to input power, than is normally the case in motors and generators. Thus, ac EM pumps frequently have power factors less than 50%, particularly when efficiency has been maximized. In any power distribution system, supply of loads with low power factor is accomplished at the expense of either high current in all the power generation and distribution elements or the addition of capacitive load elements. Either approach adds weight and complexity to the power distribution system. The following development illustrates the extent to which pump power factor and electromagnetic stored energy are influenced by liquid metal properties, power supply frequency, and pump design.

In an inductive circuit, the relationships between the energy stored in the magnetic field and the reactive volt-amperes may be written:

$$U = \tfrac{1}{2} LI^2 \qquad 44$$

$$W_q = I^2X = I^2 (2\pi fL) \qquad 45$$

where I is rms current and U is the average value of the stored energy. It follows from equations 44 and 45 that

$$W_q = 4\pi fU \qquad 46$$

In the following derivation, the relationship between stored energy U and pump output W_o is developed in general terms and the results are plotted for selected constants and parameters. The configuration considered is shown in Figure 26.

Energy may be stored in the duct region (the air gap) and in the winding leakage flux paths. Thus, the energy stored in the magnetic gap U_g may be expressed:

$$U_g = \frac{1}{2}\frac{B^2}{\mu} gbc \qquad 47$$

The energy stored in the leakage flux paths U_l may be developed in the following manner. Equations 27 and 28 give expressions for magnetizing and load currents, respectively, per unit length in the z axis.

$$A_m = \frac{\pi g}{k_1 \mu \lambda} B \qquad 27$$

$$A_l = \frac{a}{k_1}\left(1 + \frac{Y}{s}\right) j_f \qquad 28$$

Since A_m and A_l have a mutually orthogonal relationship, the total sheet current density A is

$$A = \sqrt{A_m^2 + A_l^2} \qquad 48$$

Assuming that the windings have a leakage permeance Λ per unit length in the x and z axes, the energy stored in the leakage flux paths is

$$U_l = \tfrac{1}{2}A^2 \Lambda\, bc \qquad 49$$

The total stored energy is the sum of the components given by equations 47 and 49:

$$U = \frac{1}{2}\frac{B^2}{\mu} gbc + \frac{1}{2} A^2 \Lambda bc \qquad 50$$

Substituting for A,

$$U = \frac{1}{2} B^2 bc \left\{ \frac{g}{\mu} + \left[\left(\frac{\pi g}{k_1 \mu \lambda} \right)^2 + \left(\frac{a(s + Y)v_s}{k_1 \rho_f} \right)^2 \right] \Lambda \right\} \qquad 51$$

The leakage permeance is the sum of the permeance of the slots plus that of the end turns, if any. It may be shown that the slot permeance for completely filled slots with parallel sides, depth d_s, and a ratio of slot width to slot pitch τ is

$$\Lambda_s = \mu \frac{d_s}{3\tau} \qquad 52$$

It is reasonable to account for the permeance of the additional leakage flux paths using a multiplier $k_2 > 1$. Thus,

$$\Lambda = k_2 \mu \frac{d_s}{3\tau} \qquad 53$$

Neglecting hydraulic loss, the hydraulic power output of the duct is given by equation 19. From equations 50 and 19, the ratio of output to stored energy may be written

$$\frac{W_o}{U} = \frac{\mu v_s^2 s(1 - s)a}{2g\rho_f \left\{ 1 + \Lambda \left[\frac{g}{\mu} \left(\frac{\pi}{k_1 \lambda} \right)^2 + \frac{\mu}{g} \left(\frac{a(s + Y)v_s}{k_1 \rho_f} \right)^2 \right] \right\}} \qquad 54$$

Substituting for λ and v_s from the relationships in equations 33 and 34,

$$\frac{W_o}{U} = \frac{\mu v_f^2 \, as}{2g\rho_f(1-s)} \left\{ \frac{1}{1 + \Lambda \left[4\pi^2 \frac{g}{\mu} \left(\frac{f(1-s)}{k_1 v_f} \right)^2 + \frac{\mu}{g} \left(\frac{a(s+Y)v_f}{k_1 \rho_f (1-s)} \right)^2 \right]} \right\} \qquad 55$$

Equation 52 is a general expression for slot permeance derived on the tacit basis that only one stator is involved in supplying m.m.f. to the pump duct. When a stator is positioned on both sides of the pump duct, the current supplied to each stator need be only half that required with one stator. Accordingly, from equation 49, the total energy stored in the leakage flux paths when two stators are used will be only one half that stored when only one stator is used. Thus, employing equations 52 and 54, when one stator is used,

$$\left.\frac{W_o}{U}\right|_1 = \frac{\mu v_f \, as}{2g\rho_f(1-s)} \left\{ \frac{1}{1 + k_2 \left[\frac{4\pi^2 g d_s}{3\tau} \left(\frac{(1-s)f}{k_1 v_f} \right)^2 + \frac{d_s}{3\tau g} \left(\frac{a(s+Y)v_f}{k_1 \rho_f (1-s)} \right)^2 \right]} \right\} \qquad 56$$

Considering the foregoing, when two stators are used,

$$\left.\frac{W_o}{U}\right|_2 = \frac{\mu v_f^2 \, as}{2g\rho_f(1-s)} \left\{ \frac{1}{1 + \frac{k_2}{2} \left[\frac{4\pi^2 g d_s}{3\tau} \left(\frac{(1-s)f}{k_1 v_f} \right)^2 + \frac{d_s}{3\tau g} \left(\frac{a(s+Y)v_f}{k_1 \rho_f (1-s)} \right)^2 \right]} \right\} \qquad 57$$

Using the assumed values for the terms in equation 35, plus these additions,

$\tau = 0.5$

$k_2 = 2$

d_s = 1 in., when one stator is used

d_s = 0.5 in., when two stators are used

equations 56 and 57, in consistent units, become

$$\left.\frac{W_o}{U}\right|_1 = 44.9\,\frac{s}{1-s}\left\{\frac{1}{1 + 2.9\left[\frac{(1-s)f}{100}\right]^2 + 0.059\left(\frac{s+0.2}{1-s}\right)^2}\right\} \qquad 58$$

$$\left.\frac{W_o}{U}\right|_2 = 44.9\,\frac{s}{1-s}\left\{\frac{1}{1 + 0.725\left[\frac{(1-s)f}{100}\right]^2 + 0.0147\left(\frac{s+0.2}{1-s}\right)^2}\right\} \qquad 59$$

Equations 58 and 59 are plotted in Figures 30 and 31, respectively. These figures illustrate the sensitivity of stored energy to slip and frequency and also show the reduction in stored energy possible when stators can be located on both sides of a pump duct. While the minimum value of stored energy in a pump designed for high frequency may approach that in a pump designed for lower frequency, the reactive power (equation 46) will be at least proportional to frequency.

4. Hydraulic Pressure Drop

a. General. Hydraulic pressure drop in an EM pump is caused by entrance and exit losses and the viscous drag imparted to the fluid at the duct boundaries. Entrance and exit losses are usually expressed in terms of the velocity head

$$P_e = h\,\frac{\rho v^2}{2} \qquad 60$$

The number of velocity heads h depends upon the details of the entrance and exit conditions and may be approximated for a particular configuration by reference to various publications (Refs. 17 and 18).

Viscous loss is normally expressed in terms of the friction factor δ, the ratio of duct length to hydraulic diameter L/D, and velocity head. In a form of the Fanning equation,

$$P_\mu = 4\,\delta\left(\frac{L}{D}\right)\,\frac{\rho v^2}{2}$$

With the usual flow conditions, friction factor is a function of Reynolds number N_R, duct surface conditions, and duct curvature. When a conducting fluid flows through a magnetic field, circulating electrical currents flow within the fluid and introduce an additional body force on the fluid that influences the velocity distribution across the duct. This tends to modify the friction factor.

An analysis of hydraulic pressure drop for laminar flow of a viscous conducting fluid flowing in a straight duct through a magnetic field is given in this section. The resulting expression for fraction factor is

$$\delta = \frac{8\, N_H^2}{N_R} \left(\frac{1}{N_H \operatorname{Coth} N_H - 1} \right) \qquad 62$$

where the Hartmann number N_H (Ref. 19) is

$$N_H = \frac{BD}{4 \sqrt{\frac{\rho f \mu}{g}}} \qquad 63$$

and Reynolds number N_R (Ref. 17) is given by

$$N_R = \frac{\rho g v D}{\mu} \qquad 64$$

where μ is the viscosity of the fluid. A similar solution for the friction factor when flow is turbulent is unavailable. Physical reasoning and limited test data on mercury indicate that the magnetic field has very little effect on the friction factor when flow is turbulent. On this basis, the friction factor for turbulent flow (Ref. 17) is given by

$$\frac{1}{\sqrt{\delta}} = 4.0 \log_{10} \left(N_R \sqrt{\delta} \right) - 0.4 \qquad 65$$

Equations 62 and 65 are plotted in Figure 32. Friction factor is given for laminar flow by equation 62 and for turbulent flow by equation 65.

For curved ducts friction factor is greater than that given in Figure 32 for straight ducts. For laminar flow, Schlichting (Ref. 20) gives the effect of curvature as increasing friction factor by the multiplier

$$\left[1 + 0.075\, N_R \left(\frac{\text{Radius of Cross Section}}{\text{Radius of Curvature}} \right)^{\frac{1}{4}} \right] \qquad 66$$

No information is available concerning the effect of duct curvature when the Hartmann number is other than zero. The increase in friction factor caused by curvature results from secondary fluid flow patterns arising from the centrifugal force field produced by the variations in fluid velocity across the duct cross section. When a conducting fluid flows in a transverse magnetic field, velocity variations across the duct are reduced by the eddy current magnetic field reaction; hence, the effect of curvature is expected to decrease with increasing Hartmann number.

The velocity distribution across a wide rectangular duct is shown in Figure 33 for the range of practical values of Hartmann number. This velocity distribution is given in equation 80 in terms of average velocity. Higher values of pressure drop are associated with higher velocity gradients at the boundaries.

b. Effect of Magnetic Field. Consider the elementary duct section shown in Figure 26. Assume:

1) The field moves in the z direction at a constant velocity v_s.

2) The duct and air gap height in the y direction are much less than the other duct dimensions and the pole pitch, so that there are no variations in the field with respect to x and y.

3) Flow is laminar; velocity v varies only with y.

4) Current density has an x component only, and there are no conditions external to the elementary duct section shown which influence current density.

Taking the center of the duct section at $y = 0$, the current density anywhere is

$$j = \frac{B(v_s - v)}{\rho_f} \qquad 67$$

The body force on an element bounded by x-y planes at y and $y + dy$, therefore, is

$$F_b = B\, j\, dy = \frac{B^2(v_s - v)}{\rho_f}\, dy \qquad 68$$

The viscous force on the element is

$$F_{\mu} = \frac{\mu}{g} \frac{\partial^2 v}{\partial y^2} dy \qquad 69$$

The total force on the element is

$$F = F_b + F_{\mu} = \frac{B^2(v_s - v)}{\rho_f} dy + \frac{\mu}{g} \frac{\partial^2 v}{\partial y^2} dy \qquad 70$$

For laminar flow, the pressure across any cross section perpendicular to the flow must be constant. This requires that

$$\frac{\partial F}{\partial y} = 0 = - \frac{B^2}{\rho_f} \frac{\partial v}{\partial y} + \frac{\mu}{g} \frac{\partial^3 v}{\partial y^3} \qquad 71$$

Writing these partial differentials as total differentials in accordance with the assumptions

$$- \frac{B^2}{\rho_f} \frac{dv}{dy} + \frac{\mu}{g} \frac{d^3 v}{dy^3} = 0 \qquad 72$$

The solution of this differential equation may be written

$$v = K_1 + K_2 \cosh \alpha y + K_3 \sinh \alpha y \qquad 73$$

where

$$\alpha = \frac{B}{\sqrt{\rho_f \frac{\mu}{g}}} \qquad 74$$

Since v is an even function of y,

$$K_3 = 0$$

Thus,

$$v = K_1 + K_2 \cosh \alpha x \tag{75}$$

but $v = 0$, $y = \pm \frac{a}{2}$

Thus,

$$K_2 = - \frac{K_1}{\cosh \alpha \frac{a}{2}} \tag{76}$$

and

$$v = K_1 \left(1 - \frac{\cosh \alpha x}{\cosh \alpha \frac{a}{2}} \right) \tag{77}$$

The average velocity $\bar{v}$ is

$$\bar{v} = K_1 \left(1 - \frac{\tanh \alpha \frac{a}{2}}{\alpha \frac{a}{2}} \right) \tag{78}$$

hence,

$$v = \bar{v} \frac{1 - \frac{\cosh \alpha y}{\cosh \left(\alpha \frac{a}{2} \right)}}{1 - \frac{\tanh \left(\alpha \frac{a}{2} \right)}{\left(\frac{\alpha a}{2} \right)}} \tag{79}$$

The dimensionless constant $\alpha a/2$ is called the Hartmann number (Ref. 19).

$$N_H = \frac{\alpha a}{2} = \frac{B\left(\frac{a}{2}\right)}{\sqrt{\frac{\rho_f \mu}{g}}} \qquad 80$$

In terms of the Hartmann number,

$$v = \bar{v}\,\frac{1 - \dfrac{\cosh\left(N_H\,\dfrac{2y}{a}\right)}{\cosh N_H}}{1 - \dfrac{\tanh N_H}{N_H}} \qquad 81$$

The net hydraulic drag exerted on the fluid per unit area for each duct-fluid interface is

$$F_\mu = -\frac{\mu}{g}\frac{dv}{dy}\bigg|_{y=\frac{a}{2}} \qquad 82$$

$$F_\mu = \frac{2N_H \mu}{ga}\left(\frac{\tanh N_H}{1 - \dfrac{\tanh N_H}{N_H}}\right)\bar{v} \qquad 83$$

In terms of pressure drop per unit length of flow path for both duct-fluid interfaces:

$$P_{\mu} = \frac{2F_{\mu}}{a} = \frac{4 N_H^2 \mu}{ga^2} \bar{v} \left(\frac{1}{N_H \coth N_H - 1} \right) \qquad 84$$

Equating this expression for pressure drop to the expression of equation 61,

$$4 \delta \frac{\rho \bar{v}^2}{2} \left(\frac{1}{D} \right) = \frac{4 \mu N_H^2 \bar{v}}{ga^2} \left(\frac{1}{N_H \coth N_H - 1} \right) \qquad 85$$

Introducing Reynolds number given by equation 64 and equating the hydraulic diameter D to twice the duct height, it follows that

$$\delta = \frac{8 N_H^2}{N_R} \left(\frac{1}{N_H \coth N_H - 1} \right) \qquad 86$$

For large values of N_H, this expression becomes

$$\delta = \frac{8 N_H}{N_R} \qquad 87$$

When N_H becomes very small, approaching zero, (no magnetic field)

$$\delta \Big|_{N_H \to 0} \longrightarrow \frac{24}{N_R} \qquad 88$$

This is the classical expression given for friction factor for laminar flow in a wide rectangular duct (Ref. 21).

Expressing equation 80 in terms of hydraulic diameter D,

$$N_H = \frac{BD}{4\sqrt{\rho_f \frac{\mu}{g}}} \qquad 63$$

5. Cavitation Considerations

Cavitation, the phenomenon of formation and collapse of bubbles in a liquid, is generally associated with centrifugal pumps and propellers and has been the subject of extensive analyses and experimentation in these devices. The effect of cavitation may be either a deterioration in performance or physical damage to mechanical parts, or both.

Reasonable correlations of net positive suction head (NPSH) with cavitation inception and cavitation damage have been obtained for centrifugal pumps operating with water and liquid metal (Refs. 22 and 23). Similar criteria for EM pumps have not been well established. The duct passage of an EM pump consists, essentially, of an inlet section, an inlet transition region in which the fluid velocity is increased in magnitude and may be changed in direction, a pumping region in which the fluid is acted upon by the electromagnetic field, an outlet transition region leading to the pump outlet, and a pump outlet section. Thus, flow in EM pump passages can be considered as similar to flow through venturi type duct passages. Some insight concerning the cavitation performance of EM pumps may be developed by considering cavitation test data on venturi passages.

Cavitation inception data on venturi type passages are generally presented in relation to the cavitation number σ , given by the expression,

$$\sigma = \frac{P - P_v}{\frac{1}{2} \rho v^2} \qquad 89$$

where P is the ambient static pressure in the free stream, P_v is the vapor pressure, ρ is the mass density of the liquid, and v is the velocity in the free stream. Holl (Ref. 24) reports data on a cavitation tunnel test section with a cavitation number of 0.08. Hammitt (Ref. 25) reports data taken on a venturi test section showing a cavitation number of approximately 0.17 for sonic cavitation and approximately 0.06 for visible cavitation. The flow at the entrance to the pumping section of an EM pump may be less uniform than that in such test sections, since it may be affected adversely by fringing electromagnetic fields and a less favorable transition configuration. Thus, the range of cavitation numbers cited above probably represents a minimum for EM pumps and typical values, even for carefully designed pumps, may be considerably higher.

The total pressure necessary to avoid cavitation may be expressed

$$P_T - P_v = (1 + \sigma) \frac{1}{2} \rho v^2 + P_L + P_e \qquad 90$$

where P_T is the total pressure (static plus dynamic) present at the pump entrance; P_L is the pressure loss between the pump entrance and the first point in the pumping section at which a positive pressure gradient is developed; P_e is the peak value of any negative pressure caused by electromagnetic end conditions. In an ac pump, P_e may have both an average and a pulsating component. In a dc pump, it can have no pulsating component. The total pressure minus the vapor pressure, $P_T - P_v$, corresponds to NPSH. For turbulent flow, P_L may be written in terms of velocity head as

$$P_L = k_c \left(\frac{1}{2}\right) \rho v^2 \qquad 91$$

It is difficult to generalize on the pressure loss between the pump inlet and the entrance to the pumping section since it depends upon the configuration. The pressure loss, however, is probably less than that associated with a sudden contraction between the two regions. For turbulent flow, McAdams (Ref. 17) gives values of the contraction loss coefficient k_c ranging from zero to 0.5

depending upon the area ratio, i.e., the ratio between velocity at the pump entrance and the velocity in the pumping section. Additional viscous loss in the passages between pump inlet and pumping section entrance tend to increase k_c by an amount depending upon the configuration.

The value of P_e depends primarily upon the detailed design of the inlet end of the pumping section of the pump, including pole shape, winding distribution, and insulating baffles in the fluid stream. In a particular design, it is dependent upon the voltage (or current), frequency, and fluid velocity and resistivity. Although no general values for P_e may be given with assurance, the calculated value at the design point for the linear induction pump installed in the Experimental Breeder Reactor-II secondary loop (item 1, Table 24), was slightly less than one psi. It is convenient to rewrite equation 90 as follows.

$$P_T - \left(P_v + P_e\right) = \left(1 + \sigma + k_c\right) \rho \frac{v^2}{2} = K \left(\rho \frac{v^2}{2}\right) \qquad 92$$

where P_e represents an apparent increase in vapor pressure of the fluid, and K is a pump cavitation parameter. From the preceding discussion, it appears that the value of both σ and k_c will probably be approximately 0.4. Using this estimate, equation 92 becomes

$$P_T - \left(P_v + P_e\right) = 1.8 \left(\rho \frac{v^2}{2}\right) \qquad 93$$

where P_e is expected to be approximately one psi or 2 to 3 ft of head for most alkali metals.

Reference 26 reports cavitation test data on a flat linear induction pump rated at 1200 gpm, 37 psi, 700°F sodium. Figure 34 is reproduced for that reference. This figure shows test data for the relationship between flow (or fluid velocity) and a cavitation parameter which the authors defined as the ratio of the total head to the velocity head at the point of incipient cavitation. The data presented in Figure 34 were taken with sodium at 700°F. At this temperature, the vapor pressure is less than 0.01 psi.

From equation 92, the ratio of total head to velocity head may be written

$$\frac{P_T}{\rho \frac{v^2}{2}} = K + \frac{P_v + P_e}{\rho \frac{v^2}{2}} \qquad 94$$

In Figure 34, the left side of equation 94 is plotted against flow (proportional to velocity). From the figure, it may be deduced that $P_e/\rho g$ is quite small, approximately 3 ft.

The foregoing discussion deals exclusively with the inception of cavitation. Pressure in EM pumps is developed by body forces exerted on the fluid by electromagnetic interaction, and the pressure gradient is approximately constant throughout the pump section. The degree of cavitation tolerable will probably be limited by mechanical damage to the duct walls.

The conduction pumps have a special problem in that cavitation apparently is intensified in the areas where the bus bars contact the duct walls. Severe damage to the duct has been experienced in conduction pumps, probably because of high ohmic heating in that area. No evidence of cavitation damage has been reported for the several induction pumps tested. However, comprehensive tests are needed to provide sound criteria for the design of EM pumps for applications requiring low NPSH. Until the test data are available, careful design of the hydraulic inlet region should permit cavitation free operation as long as the NPSH is at least twice the velocity head at the entrance to the pumping section

6. Reliability

An inherently high reliability is the strongest virtue of the EM pump for alkali metals systems. Simplicity assists most in providing this high reliability. Other contributing factors include: no moving parts, no bearings, no seals, and fully hermetic containment of the pumped fluid. Electromagnetic pumps of certain types, however, have failed in service and these failures demonstrate certain reliability problems that must be considered in pump selection and design.

In the initial selection of EM pump types, reliability comparison has served as a guide. Here, the number of failure mechanisms and the severity of failure, together with experience in conventional EM pumps, have been the key considerations. These considerations are reviewed below.

1) Loss of pump cooling would adversely affect any of the pumps by increasing coil resistivities, reducing magnetic material performance, and deteriorating electrical insulation. The polyphase configurations would be most susceptible, however, because of the greater complexity of coils and electrical insulation systems and their proximity to the hot duct.

2) Interruption of flow in the duct is most damaging to the conduction type pump because of the high current density at the duct-to-bus connection. Fluctuations in flow can cause sudden local temperature excursions because of the high ohmic heating at the joint between the current conductor and duct wall. This type failure is common in conduction pumps operating at high temperatures and low NPSH and usually results in duct leakage at the electrode connection.

3) Pressure fluctuations across the duct walls can fatigue the duct. The duct configuration most susceptible is the flat induction pump where the mechanical arrangement allows duct wall support against internal pressure only. Reversal of the pressure can deform the duct. Very large conduction pumps have a similar duct weakness and are also subject to this problem. Pumps operating on single phase power experience greater pulsation in their developed head than other types of pumps.

4) Overpressure inside the duct is not a serious threat to any of the pumps since the ducts can be designed for the same pressure as other components in the loop. However, some configurations of the moving magnet pump make mechanical support of the duct difficult. If deformed, the duct may interfere with the rotor and thus cause pump failure.

5) Overtemperature in the pumped fluid, probably applicable only to the primary coolant, would reduce the performance and life of all types of pumps. The conduction pump, however, would be most immediately affected and failure would probably involve the duct-to-bus connection.

6) Mechanical shock poses a serious threat to the moving magnet pumps because of the weight and complexity of the rotating magnetic structures. For adequate performance, such pumps require a close clearance between the rotor and duct wall. Misalignment could result in a contact between the rotor and the duct wall.

7) Bearing lubricant or seal failure is applicable only to the moving magnet pumps, and the failure mechanism is obvious.

The preceding review indicates that as a class, the induction pumps have, potentially, the highest reliability. It must be recognized, however, that single phase induction pumps are relatively unknown since no operating experience is available to guide the reliability analyses. On the other hand,

much favorable experience has been accumulated on polyphase induction pumps.

In addition to providing a guide for selection, the foregoing discussion also points up those areas of weakness where design and development can mitigate or even eliminate the weakness. For example, the development of a higher temperature insulation system, allowing the polyphase pump windings to reject heat to the 1200 °F pumped fluid, would substantially eliminate damage caused by loss of cooling. Or, as another example, the development of better duct connections could substantially improve reliability of the conduction pumps. Further reliability study must await more detailed pump designs. Final proof of reliability must be obtained through endurance testing.

7. Choice of Pump Types for Analysis

The foregoing survey indicated that EM pumps can be designed in a large number of types and configurations. Detailed analysis of all types to insure the best selection for each application would be a prodigious task. But many of the pumps discussed in the survey had one or more characteristics unacceptable for space power applications and, thus, were disqualified from further consideration. To aid in this first selection, the pumps were classified into ten basic types. Figure 35 illustrates the method of classification. The first level of division, which separates pumps by the manner in which current is introduced into the fluid, establishes two main classes, i.e., conduction and induction. Next, the form of the power is considered. Under conduction pumps, two forms are possible; under induction pumps, three forms. Finally, the last division is made on the basis of the magnetic field or the shape and arrangement of the fluid passages within the field.

Comparing the pump characteristics within the two main divisions, the conduction pumps are less attractive because of reliability and power conditioning difficulties. However, the electromagnetic dc conduction pump should provide minimum weight and maximum efficiency. The dc conduction pump, therefore, was carried through the full detailed analysis and final selection process as a standard of comparison. Other conduction pumps were discarded.

Among the induction pumps, the moving magnet types were discounted since the presence of moving parts introduces additional modes of failure not burdening the static types. Finally, the spiral polyphase pump was eliminated because it serves the same applications as the helical polyphase type, with no advantage, but with additional problems in design and manufacture.

C. Performance Prediction Procedures

1. Direct Current Conduction Pump

Analyses of the performance of direct current conduction EM pumps appear in several references (Refs. 27 through 30). Since none of the references provide sufficient detail for complete design and performance calculation, an analysis was completed and is the basis for the conduction pump design and performance data given in this report. The analysis is summarized in this section. Any consistent system of units may be used in the analysis.

The conduction EM pump configuration considered is shown in Figure 36. Excitation is provided by a series winding of N turns carrying the total current I. The pump may be either compensated or uncompensated. For compensated pumps, the compensation is assumed to be perfect, although this is difficult to achieve in practice. The gross effects of the current and flux fringing into the fluid and duct walls outside the pumping section are considered, but the interrelationships between the fringing current and flux fields are neglected.

The equivalent circuit in Figure 37 is used as an aid in developing the analysis and calculating pump performance. Using Figure 37, the pump current I may be regarded as the sum of three components: I_f, which passes through the fluid in the pumping section; I_{fr}, which is the total fringing current in the fluid (outside the pumping section); and I_d, which is the current in the duct walls. The current in the pumping section I_f is opposed by a generated voltage V_g caused by the motion of the fluid in the magnetic field. The resistances of the fluid in the pumping section, the fluid fringing region, and the duct walls are R_f, R_{fr}, and R_d, respectively. The resistance of the circuit external to the pump duct R_e consists of electrodes, exciting winding, leads, and all associated parts. The calculation of the resistances R_f, R_{fr}, and R_d is discussed in several references (Refs. 27, 28, 29, 31, 32). The approach used in this analysis is similar to that used by Blake (Ref. 27) and Watt (Ref. 28). These resistances are defined as follows:

$$R_f = k_{rf} \rho_f \frac{b}{ac} \quad (95)$$

$$R_{fr} = k_{rfr} \rho_f \frac{b}{ac} \quad (96)$$

$$R_d = k_{rd} \rho_d \frac{b}{2tc} \quad (97)$$

Blake's Figure 13 (Ref. 27) and Watt's Figure 11 (Ref. 28) are suitable for evaluation of the constants, k_{rf}, k_{rfr}, and k_{rd}. The calculation of R_e is straightforward.

Flow Q and developed pressure P are given by

$$Q = abv \quad (98)$$

$$P = P_o + P_h \quad (99)$$

P_o is the net pressure output of the pump. Hydraulic pressure drop P_h may be calculated from Section III.B.4.

Inspecting Figures 37 and 38, the following relationships may be written for a fully compensated pump.

$$B_g = \frac{\mu N k_b I}{g} \quad (100)$$

$$V_g = B_g b v = \frac{\mu b v}{g} k_b N I \quad (101)$$

$$P = k_{ar} \frac{B_g I_f}{a} \quad (102)$$

From equations 100 and 102,

$$P = \frac{\mu N}{ga} \left(k_b k_{ar}\right) \left(\frac{I_f}{I}\right) I^2 \quad (103)$$

where k_b and k_{ar} are armature reaction constants. Both are 1.0 for fully compensated pumps. The analysis will demonstrate that these equations hold for uncompensated pumps. Expressions for k_b and k_{ar} will be developed. The relationships of equations 95 through 103 plus expressions for k_b and k_{ar}, used in conjunction with elementary analysis of the circuit in Figure 37, are sufficient for calculating the performance of dc conduction pumps.

The development of expressions for k_b and k_{ar} requires consideration of the differential relationships between the electromagnetic quantities in the pumping section, shown in Figure 38. Considering only the y component of magnetic field strength, the x component of current density, the z component of velocity, and neglecting all variations of these quantities with x and y,

$$\frac{\partial H}{\partial z} = -\frac{a}{g} j - \frac{i_d}{g} \qquad 104$$

$$\frac{\partial j}{\partial z} = -\frac{\mu v}{\rho_f} \frac{\partial H}{\partial z} \qquad 105$$

The solutions of equations 104 and 105 are

$$H = K_1 + K_2 e^{2\beta z} \qquad 106$$

$$j = \frac{i_d}{a} - 2\beta \frac{g}{a} K_2 e^{2\beta z} \qquad 107$$

where

$$2\beta = \frac{\mu v a}{\rho_f g} \qquad 108$$

The constants K_1 and K_2 may be expressed in terms of the average values, H_{av} and j_{av}, by

$$H_{av} = \frac{1}{c} \int_o^c H \, dz \qquad 109$$

$$j_{av} = \frac{1}{c} \int_o^c j \, dz \qquad 110$$

Recognizing that

$$ca\left(j_{av} + \frac{i_d}{a}\right) = I_f \left(1 + \frac{k_{rd}}{k_f}\frac{I_d}{I_f}\right) \qquad 111$$

it follows that

$$H = H_{av} + \frac{I_f}{g}\left(1 + \frac{k_{rd}}{k_{rf}}\frac{I_d}{I_f}\right)\left(\frac{1}{2\beta c} - \frac{e^{2\beta z}}{e^{2\beta c}-1}\right) \qquad 112$$

$$j = \frac{I_f}{ca}\left[\left(1 + \frac{k_{rd}}{k_{rf}}\frac{I_d}{I_f}\right)\frac{2\beta c\, e^{2\beta z}}{e^{2\beta c} - 1} - \frac{k_{rd}}{k_{rf}}\frac{I_d}{I_f}\right] \qquad 113$$

The validity of equation 101 for uncompensated pumps may be tested by examining the expression

$$V_d = b\,(\mu H v + \rho_f\, j) \qquad 114$$

Substituting equations 112 and 113 in this expression yields

$$V_d = \mu\, v\, H_{av}\, b + \rho_f \frac{b}{ca} I_f \qquad 115$$

But

$$V_g = B_g v b = \mu\, v\, H_{av}\, b \qquad 116$$

Hence,

$$V_d = V_g + R_f' I_f \qquad 117$$

This justifies the use of equation 101 for uncompensated pumps. In the equivalent circuit, the R_f is replaced by R_f' from equation 95 to account for current fringing at the ends of the pumping section.

It is necessary to relate H_{av} to the exciting m.m.f.

At z = 0,

$$H_o = H_{av} + \frac{I_f}{g} \left(1 + \frac{k_{rd}}{k_{rf}} \frac{I_d}{I_f}\right) \left(\frac{1}{2\beta c} - \frac{1}{e^{2\beta c} - 1}\right) \qquad 118$$

At z = c,

$$H_c = H_{av} + \frac{I_f}{g} \left(1 + \frac{k_{rd}}{k_{rf}} \frac{I_d}{I_f}\right) \left(\frac{1}{2\beta c} - \frac{e^{2\beta c}}{e^{2\beta c} - 1}\right) \qquad 119$$

From Figure 38, it may be shown that, approximately,

$$H_o = \frac{I}{g} \left(N + 0.5 - \frac{1}{2} \frac{I_{fr}}{I} - \frac{1}{2} \frac{k_{rd}}{k_{rfr}} \frac{I_d}{I}\right) \qquad 120$$

Thus, from equations 118 and 120,

$$H_{av} = \frac{I}{g} \left\{ N + 0.5 - \frac{1}{2} \frac{I_{fr}}{I} - \left[\frac{1}{2} \frac{k_{rd}}{k_{rfr}} + \frac{k_{rd}}{k_{rf}} \left(\frac{1}{2\beta c} - \frac{e^{2\beta c}}{e^{2\beta c}-1}\right)\right] \frac{I_d}{I} - \left(\frac{1}{2\beta c} - \frac{1}{e^{2\beta c}-1}\right) \frac{I_f}{I} \right\} \qquad 121$$

Then,

$$H_{av} = k_b \frac{NI}{g} \qquad 122$$

where

$$k_b = \frac{1}{N}\left\{(N + 0.5) - \frac{1}{2}\frac{I_{fr}}{I} - \left[\frac{1}{2}\frac{k_{rd}}{k_{rfr}} + \frac{k_{rd}}{k_{rf}}\left(\frac{1}{2\beta c} - \frac{e^{2\beta c}}{e^{2\beta c}-1}\right)\right]\frac{I_d}{I} - \left(\frac{1}{2\beta c} - \frac{e^{2\beta c}}{e^{2\beta c}-1}\right)\frac{I_f}{I}\right\} \quad 123$$

From equations 116 and 122, confirming equation 99,

$$V_g = \frac{\mu v b}{g} k_b N I \quad 124$$

The electrical pressure is

$$P = \int_o^c Hj\, dz \quad 125$$

Substituting from equations 112 and 113, integrating, and rearranging,

$$P = \mu H_{av}\frac{I_f}{a}\left[1 - \frac{1}{2g}\frac{I_f}{H_{av}}\left(1 + \frac{k_{rd}}{k_{rf}}\frac{I_d}{I_f}\right)\left(\coth \beta c - \frac{1}{\beta c}\right)\right] \quad 126$$

Then, as in equation 102, if

$$P = k_{ar}\,\mu H_{av}\frac{I_f}{a} = k_{ar} B_g \frac{I_f}{a} \quad 127$$

$$k_{ar} = 1 - \frac{1}{2g}\frac{I_f}{H_{av}}\left(1 + \frac{k_{rd}}{k_{rf}}\frac{I_d}{I_f}\right)^2\left(\coth \beta c - \frac{1}{\beta c}\right) \quad 128$$

Substituting from equation 122 in equation 128,

$$k_{ar} = 1 - \frac{1}{2Nk_b}\left(\frac{I_f}{I}\right)\left(1 + \frac{k_{rd}}{k_{rf}}\frac{I_d}{I_f}\right)^2\left(\coth \beta c - \frac{1}{\beta c}\right) \qquad 129$$

The current ratios $\frac{I_f}{I}$, $\frac{I_{fr}}{I}$, $\frac{I_d}{I}$ may be calculated from the equivalent circuit in Figure 37. For convenience, let

$$k_v = \frac{\mu b v k_b N}{g} \qquad 130$$

Then, equation 101 becomes

$$V_g = k_v I \qquad 131$$

From analysis of the circuit in Figure 37,

$$\frac{I_f}{I} = \frac{1 - k_v\left(\frac{1}{R_{fr}} + \frac{1}{R_d}\right)}{1 + R_f\left(\frac{1}{R_{fr}} + \frac{1}{R_d}\right)} \qquad 132$$

$$\frac{I_{fr}}{I} = \frac{1 + \frac{k_v}{R_f}}{1 + R_{fr}\left(\frac{1}{R_f} + \frac{1}{R_d}\right)} \qquad 133$$

$$\frac{I_d}{I} = \frac{1 + \frac{k_v}{R_f}}{1 + R_d\left(\frac{1}{R_f} + \frac{1}{R_{fr}}\right)} \qquad 134$$

This completes the calculation of armature reaction effects.

Pump output and hydraulic loss, in watts, where Q and P are gallons per minute and pounds per square inch, respectively, are

$$W_o = 0.435 \; P_o Q \tag{135}$$

$$W_h = 0.435 \; P_h Q \tag{136}$$

The various electrical losses in the pump may be calculated conveniently from the equivalent circuit in Figure 37.

$$W_d = I_d^2 \; R_d \tag{137}$$

$$W_{fr} = I_{fr}^2 \; R_{fr} \tag{138}$$

$$W_e = I^2 \; R_e \tag{139}$$

The fluid loss in the pumping section is

$$W_f = V_d \; I_f - \left(W_o + W_h \right) \tag{140}$$

The power input is

$$W_T = V \; I \tag{141}$$

The efficiency is

$$\eta = \frac{W_o}{W_T} \tag{142}$$

Relationships sufficient for performance calculation of both compensated and uncompensated conduction pumps have now been developed. The procedure is summarized as follows for an assumed configuration and fluid and the desired pressure and flow:

1) Calculate all parameters for the circuit in Figure 37.

2) Calculate P from equation 99.

3) Calculate the total current I . For compensated pumps, $k_b = k_{ar} = 1.0$. Hence, this calculation may be made directly using equations 130, 132 and 103. For uncompensated pumps, an iterative calculation is required between equations 123, 130, 132, 133, and 134 and for k_b. Current I may then be calculated directly using equations 123, 129, 130, 132, 133, 134 and 103.

4) Magnetic calculations for fringing flux density in the magnet, m.m.f. drop in the magnet, exciting winding length, etc. should be made by standard procedures.

5) Calculate all losses in accordance with equations 135 through 141.

2. Polyphase Induction Pumps

In Section III.A.4 the basic polyphase induction pumping configurations are described and illustrated. In Section V, preliminary designs and performance prediction calculations are reported for three of these configurations: flat linear, annular linear, and helical induction pumps. These calculations were made with computer programs developed during the past fifteen years and used much of that time in the design of induction pumps for various applications.

Reference 27 gives an excellent development and presentation of the basic electromagnetic relationships in polyphase induction pumps. Helical (spiral), flat, and annular pumps are considered. A more detailed and thorough analysis of flat induction pumps is given in Reference 33, which treats both transverse end (side) effects that arise when an end ring is not present at the duct sides and longitudinal end effects caused by the discontinuities in the magnetic field at the ends of the pumping section. Reference 34 is a mathematical analysis of longitudinal end effects in flat linear induction generators in which the assumed exciting current sheets extend uniformly over the entire length of the generator. Reference 35 reports a very detailed treatment of longitudinal end effects. Extensive numerical calculation is involved, and the results are not directly applicable to the general case.

The performance prediction procedure used in the calculation of helical induction pump performance was developed during the past five years. This procedure takes into account the end effects caused by imperfect end rings at the axial extremities of the pumping section; end effects caused by discontinuities in electromagnetic body force at the ends of the helical flow passages; the negative pressure gradient caused by the axial velocity of the fluid in the magnetic field; the effect of the curvature of the configuration on the magnetic field; the principal mutual effects of the various duct wall, stator can, and fluid currents. Other refinements frequently neglected in approximate performance calculation procedures are also incorporated here. This procedure has been used in conjunction with the design of helical induction pumps operative since 1962. Highly successful operation of these pumps confirms the validity of the performance prediction procedure.

The performance prediction procedure used in the calculations of annular and flat induction pump performance evolved from the development of the large flat induction pumps used in the nuclear submarine USS Seawolf. It has been employed in calculating performance of the pump used in the Experimental Breeder Reactor-II secondary loop and in numerous other applications of flat electromagnetic stators. Presently, the procedure is programmed for digital computer calculation and the calculations reported here were made by computer. The side effects caused by imperfect end rings, the end effects caused by the discontinuities of the electromagnetic field at the axial extremities of the pumping section, the effect of the air gap to pole pitch ratio on the electromagnetic field distribution, and the mutual effects of stator can and fluid currents are taken into account.

Temperature distribution calculations for the windings of helical, flat, and annular induction pumps were also developed and programmed for computer solution before this study was initiated. The calculations of winding temperature and heat transferred to the coolant reported in Section V were made by using these computer programs.

The basic induction pump relationships are developed in the following brief analysis. An idealized pump without side and end effects is considered, since treatment of these effects exceeds the scope of this report. The configuration considered is shown in Figure 39. Polyphase ac currents are supplied to distributed windings to produce a traveling wave of m.m.f. across the magnetic gap. It is convenient to replace the distributed exciting winding with a traveling current sheet which produces a space fundamental m.m.f. equal to that produced by the excited winding. The linear current density in the current sheet is sinusoidally distributed with a maximum value A, where

$$A = \frac{2mk_1 NI_s}{\lambda} \qquad 143$$

m is the number of phases, k_1 is the winding pitch and distribution factor, NI_s is the ampere turns per pole per phase in the stator winding, and λ is the pole pitch. The current sheet may be expressed

$$A = \mathrm{Re}\left\{ A_1 \, e^{i\left(\omega t - z\frac{\pi}{\lambda}\right)} \right\} \qquad 144$$

Neglecting variations in H and z with y and x and all components of H and j, except H_y and j_x, and assuming a uniform velocity v of the fluid in the z direction, the electromagnetic field relationships are expressed by the following:

$$\frac{\partial H}{\partial z} + \frac{a}{g} j_f + \frac{2t}{g} j_d + \frac{A}{g} = 0 \qquad 145$$

$$\rho_f \frac{\partial j_f}{\partial z} + v\mu \frac{\partial H}{\partial z} + \mu \frac{\partial H}{\partial t} = 0 \qquad 146$$

$$\rho_d \frac{\partial j_d}{\partial z} + \mu \frac{\partial H}{\partial t} = 0 \qquad 147$$

Letting

$$Y = 1 + \frac{2t}{a} \frac{\rho_f}{\rho_d} \qquad 148$$

equations 145, 146 and 147 may be combined to give

$$\frac{\partial^2 H}{\partial z^2} - \frac{\mu_{av}}{g\rho_f} \frac{\partial H}{\partial z} - \frac{\mu_a}{g\rho_f} (1 + Y) \frac{\partial H}{\partial t} + \frac{1}{g} \frac{\partial A}{\partial z} = 0 \qquad 149$$

Assuming

$$H = \mathrm{Re}\left\{ H_1 \, e^{\,i\left(\omega t - z\frac{\pi}{\lambda}\right)} \right\} \qquad 150$$

equation 149 may be solved for H_1, giving

$$H_1 = \frac{-i\,\frac{\lambda}{\pi g}\,A_1}{1 + i\,K_1} \qquad 151$$

where

$$K_1 = \frac{\omega\,\mu a}{g\rho_f}\left(\frac{\lambda}{\pi}\right)^2 (s + Y) \qquad 152$$

and slip s is

$$s = 1 - \frac{v}{\omega}\left(\frac{\pi}{\lambda}\right) \qquad 153$$

The current density in the fluid may be evaluated from equations 146 and 151, assuming

$$j_f = \mathrm{Re}\left\{ J_{f1} \, e^{\,i\left(\omega t - z\frac{\pi}{\lambda}\right)} \right\} \qquad 154$$

Then,

$$J_{f1} = \frac{\omega\,\mu s}{\rho_f}\left(\frac{\lambda}{\pi}\right) H_1 \qquad 155$$

The total pressure imparted to the fluid by the electromagnetic field, which is the output pressure plus the hydraulic pressure drop, is given by

$$P = \int_o^c \mu\, j_f\, H\, dz \qquad 156$$

Where c is an integral number of pole pitches, the time average of P may be written directly from equation 155:

$$P = \frac{c\omega s}{2\rho_f} \left(\frac{\lambda}{\pi}\right) \mu^2 \left|H_1\right|^2 \qquad 157$$

Then, substituting for $\left|H_1\right|^2$ from equation 151,

$$P = \frac{\frac{c\omega s}{2\rho_f} \left(\frac{\lambda}{\pi}\right)^3 \left(\frac{\mu A_1}{g}\right)^2}{1 + K_1^2} \qquad 158$$

The flow rate may be written

$$Q = abv = ab\omega \frac{\lambda}{\pi} (1 - s) \qquad 159$$

Neglecting hydraulic pressure drop, the power output is given by the product of equations 158 and 159,

$$W_o = \frac{\frac{abc\, s(1 - s)}{2\rho_f} \left[\omega \mu \left(\frac{\lambda}{\pi}\right)^2 \frac{A_1}{g}\right]^2}{1 + K_1^2} \qquad 160$$

The power and reactive volt ampere inputs to the magnetic gap may be calculated from the expressions

$$W_g = -\frac{bc}{2} \operatorname{Re}\left\{ E_1 A_1^* \right\} \tag{161}$$

and

$$W_{qg} = \frac{bc}{2} \operatorname{Im}\left\{ E_1 A_1^* \right\} \tag{162}$$

The choice of sign in equation 162 is arbitrary. At the location of the current sheets, the following applies

$$\nabla \times E = -\mu \frac{\partial H}{\partial t} \tag{163}$$

Using equations 150 and 163 and assuming no variations of E with x,

$$E_1 = \frac{\lambda}{\pi} \omega \mu H_1 \tag{164}$$

Substituting expressions for E_1 and H_1, from equations 164 and 151, into equations 161 and 162 and simplifying, gives the expression:

$$W_q = \frac{\frac{abc\,(s + Y)}{2\rho_f} \left[\omega\mu \left(\frac{\lambda}{\pi}\right)^2 \frac{A_1}{g} \right]^2}{1 + K_1^2} \tag{165}$$

$$W_{qg} = -\frac{\frac{bc\,\omega\,\mu}{2g} \left\{ \frac{\lambda}{\pi} A_1 \right\}^2}{1 + K_1^2} \tag{166}$$

The above treatment completes the development of the relationships between an exciting current sheet and the fluid and duct walls in an ideal induction pump. The current sheet is related to the pump winding by equation 143. For any chosen stator, the winding loss, iron loss, and winding reactive volt-amperes may be calculated by standard procedures. With this information and the preceding relationships, complete pump performance may be calculated.

In an actual pump, end and side effects degrade pump performance relative to an ideal pump. As indicated earlier, some of these effects have been treated adequately in the literature (Refs. 27, 33, 34, 35). For others, particularly the longitudinal end effect, no satisfactory general solution is available. The field equations for specific pump configurations and flow conditions have been integrated numerically to evaluate longitudinal end effects. General design guides may be established by further use of this technique.

3. Single Phase Induction Pump

An analysis of a single phase induction pump with an annular duct by D. A. Watt was published as a classified document in 1953. A declassified edition was published in 1956 (Ref. 36). The configuration treated in these references is shown in Figure 40. A more compact configuration, developed during the course of this EM pump design study, is shown in Figure 41. From an electromagnetic viewpoint, this configuration is equivalent to that studied by Watt. It is more compact and more symmetrical and, hence, better suited to space application where size, weight, and volt-ampere requirements must be minimized. As illustrated in Figure 41 both the duct and the exciting coil are annular in form. The basic magnetic flux pattern is axial and radial and, therefore, the laminations must be oriented with their major dimensions lying in planes passing through (or near) the axial centerline of the pump. To minimize hydraulic and electromagnetic inlet and exit losses, multiple inlet and outlet pipes are desirable. The symmetry of this configuration is such that the complex arrangement of chokes, described by Watt, to minimize circulating currents in the configuration in Figure 40 is unnecessary, provided entry and exit pipes are arranged with appropriate symmetry.

Figures 42 and 43 illustrate other compact single phase induction pump configurations similar to that in Figure 41. The Type B configuration in Figure 42 is somewhat more compact than Type A, but this compactness is achieved at the expense of poorer performance. The Type C configuration shown in Figure 43 has exciting coils located at each end of the annular duct.

When these coils are connected with their magnetomotive forces aiding, considering axial flux, Type C is equivalent to two Type A pumps hydraulically in parallel. Similarly, when the coils are connected with their magnetomotive forces opposing, Type C is equivalent to two Type B pumps hydraulically in parallel. In either case, pumping is from the ends of the duct toward the middle.

Compared with Types A and B, Type C pump does not appear to have any significant advantages.

The analysis of the performance of Type A and B single phase induction pumps proceeds along similar lines and is executed concurrently below. Throughout this analysis, the following assumptions are made:

1) The annular duct and air gap configuration may be treated as an equivalent rectangular configuration as shown in Figure 44. This introduces negligible error since the duct diameter is normally several integral multiples of the air gap radial height.

2) The flux density in the air gap has a y component only.

3) The fringing flux field at each end of the duct is negligible.

4) The permeability of the magnetic core is assumed infinite during the analysis of the air gap region. A correction for m.m.f. drop in the core may be made later.

5) Fluid and duct walls are isotropic and nonmagnetic with permeabilities the same as free space.

6) The fluid velocity has an x component only and is independent of y and z.

Root mean square values are used for all sinusoidally varying quantities. Any consistent system of units may be applied in the analysis.

The following basic relationships may be written for the configuration in Figure 44.

$$B = - \frac{1}{\pi d} \frac{\partial \phi}{\partial x} \tag{167}$$

$$j_f = - \frac{1}{\pi d \rho_f} \left(\frac{\partial \phi}{\partial t} + v \frac{\partial \phi}{\partial x} \right) \tag{168}$$

$$j_d = - \frac{1}{\pi d \rho_d} \frac{\partial \phi}{\partial t} \tag{169}$$

$$\frac{\partial B}{\partial x} = \frac{\mu}{g} \left(a\, j_f + 2t\, j_d \right) \tag{170}$$

For an assumed configuration and fluid velocity, equations 167 and 170 relate the four unknowns, B, ϕ, j_f, and j_d. They may be combined to yield one equation in one unknown, ϕ

$$\frac{\partial^2 \phi}{\partial x^2} = \frac{\mu a}{\rho_f g} \left[\left(1 + \frac{2t}{a} \frac{\rho_f}{\rho_d} \right) \frac{\partial \phi}{\partial t} + v \frac{\partial \phi}{\partial x} \right] \qquad 171$$

Assuming the exciting voltage sinusoidal in time and the fluid velocity constant, the system is linear and the resulting flux ϕ is also sinusoidal in time. Thus,

$$\phi = \mathrm{Re} \left\{ \Phi e^{i\omega t} \right\} \qquad 172$$

and

$$\frac{\partial \phi}{\partial t} = \mathrm{Re} \left\{ i\omega \Phi e^{i\omega t} \right\} \qquad 173$$

For convenience, let

$$Y = \left(1 + \frac{2t}{a} \frac{\rho_f}{\rho_d} \right) \qquad 174$$

Then, substituting these relationships in equation 171 and dropping the $\mathrm{Re}\{A\}$ designation, in the conventional manner, equation 171 may be written

$$\frac{\partial^2 \Phi}{\partial x^2} - \frac{\mu a v}{\rho_f g} \frac{\partial \Phi}{\partial x} - i \frac{\omega \mu Y a}{\rho_f g} \Phi = 0 \qquad 175$$

The solution of this equation is

$$\Phi = \Phi_1 \, e^{\alpha_1 x} + \Phi_2 \, e^{\alpha_2 x} \qquad 176$$

Where

$$\alpha_1 = \gamma_1 + i\beta_1 = \frac{\mu_{av}}{2\rho_f g} \left(1 - \sqrt{1 + i \frac{4\omega\rho_f g Y}{\mu_{av}^2}} \right) \qquad 177$$

$$\alpha_2 = \gamma_2 + i\beta_2 = \frac{\mu_{av}}{2\rho_f g} \left(1 + \sqrt{1 + i \frac{4\omega\rho_f g Y}{\mu_{av}^2}} \right) \qquad 178$$

It is apparent that

$$\beta_1 = -\beta_2$$

The terms Φ_1 and Φ_2 are constants which depend upon the boundary conditions. It is convenient to proceed with the analysis of the pump performance, expressing the performance in terms of these constants. They will be evaluated in terms of the boundary conditions for Type A and B pumps later.

Introducing a dimensionless constant C_1, where

$$C_1 = \frac{\Phi_2}{\Phi_1} \qquad 179$$

equation 176 may be written

$$\Phi = \Phi_1 \left(e^{\alpha_1 x} + C_1 \, e^{\alpha_2 x} \right) \qquad 180$$

Substituting from equation 180 into equations 167, 168, and 169,

$$B = -\frac{\Phi_1 \alpha_1}{\pi d}\left(e^{\alpha_1 x} + \frac{\alpha_2}{\alpha_1} C_1 e^{\alpha_2 x}\right) \qquad 181$$

$$J_f = -\frac{\Phi_1 \omega}{\pi d \rho_f}\left[\left(\frac{v}{\omega}\alpha_1 + i\right) e^{\alpha_1 x} + \left(\frac{v}{\omega}\alpha_2 + i\right) C_1 e^{\alpha_2 x}\right] \qquad 182$$

$$J_d = -\frac{\Phi_1 \omega}{\pi d \rho_d}\left(e^{\alpha_1 x} + C_1 e^{\alpha_2 x}\right) \qquad 183$$

The pressure developed by the pump is given by the product of the flux density and the current density in the fluid integrated over the length of the pump duct. The average value of the pressure is given by the expression

$$P = \mathrm{Re}\left\{\int_o^c - J_f B^* \, dx\right\} \qquad 184$$

where B* is the complex conjugate of B.

Thus,

$$P = \mathrm{Re}\left\{-\frac{\omega \Phi_1 \Phi_1^* \alpha_1^*}{(\pi d)^2 \rho_f}\int_o^c \left[\left(\frac{v}{\omega}\alpha_1 + i\right) e^{\alpha_1 x} + \left(\frac{v}{\omega}\alpha_2 + i\right) C_1 e^{\alpha_2 x}\right]\left[e^{\alpha_1^* x} + C_1 \frac{\alpha_2^*}{\alpha_1} e^{\alpha_2^* x}\right] dx\right\} \qquad 185$$

Equation 185 may be expanded, integrated, and expressed as follows:

$$P = -\frac{\omega \left|\Phi_1\right|^2}{\rho_f (\pi d)^2} \operatorname{Re}\left\{ \left(\frac{v}{\omega}\alpha_1 + i\right) \left[\frac{\alpha_1^* \left(e^{2\alpha_1 c} - 1\right)}{2\gamma_1} + \alpha_2^* C_2^*\right] + \left(\frac{v}{\omega}\alpha_2 + i\right)\left[\left|C_1\right|^2 \frac{\alpha_2^* \left(e^{2\alpha_2 c} - 1\right)}{2\gamma_2} + \alpha_1^* C_2\right]\right\} \quad 186$$

where

$$C_2 = C_1 \left[\frac{e^{\left(\alpha_1^* + \alpha_2\right) c} - 1}{\alpha_1^* + \alpha_2}\right] \quad 187$$

and $\left|\Phi\right|$ means the absolute value of Φ

From Figure 44 it is apparent that the total flux entering the duct is the value of the flux at x = 0 and that the total m.m.f. produced by the exciting coil, neglecting iron drop, may be written in terms of the air gap flux density at x = 0 and the m.m.f. produced by the inlet duct header. Thus,

$$\Phi_T = \Phi_1 \left(1 + C_1\right) \quad 188$$

$$M_w = \frac{g}{\mu} B\Big|_{x=o} + \frac{i\omega\Phi_T}{R_o} \quad 189$$

From equation 181,

$$M_w = -\frac{\omega\Phi_1}{R_o}\left[\left(\frac{gR_o}{\omega\mu\pi d}\alpha_1 - i\right) + \left(\frac{gR_o}{\omega\mu\pi d}\alpha_2 - i\right) C_1\right] \quad 190$$

The power input to the air gap region may be written

$$W_m = \mathrm{Re}\left\{ M_w \left.\frac{\partial \phi^*}{\partial t}\right|_{x=o} \right\} \qquad 191$$

From equation 180,

$$\left.\frac{\partial \phi}{\partial t}\right|_{x=o} = i\omega \Phi_1 \left(1 + C_1\right) \qquad 192$$

Then, substituting from equations 190 and 192 into equation 191,

$$W_m = \frac{\omega^2 \Phi_1 \Phi_1^*}{R_o} \mathrm{Re}\left\{ i \left(1 + C_1^*\right) \left[\frac{g R_o}{\omega \mu \pi d} \alpha_1 - i + \left(\frac{g R_o}{\omega \mu \pi d} \alpha_2 - i \right) C_1 \right] \right\} \qquad 193$$

In a similar manner, the reactive volt-amperes associated with the air gap region may be written

$$W_{qm} = \mathrm{Im}\left\{ M_w \left.\frac{\partial \phi^*}{\partial t}\right|_{x=o} \right\} \qquad 194$$

or

$$W_{qm} = \frac{\omega^2 \Phi_1 \Phi_1^*}{R_o} \mathrm{Im}\left\{ i \left(1 + C_1^*\right) \left[\frac{g R_o}{\omega \mu \pi d} \alpha_1 - i + \left(\frac{g R_o}{\omega \mu \pi d} \alpha_2 - i \right) C_1 \right] \right\} \qquad 195$$

Where R_w and X_w are exciting coil resistance and reactance on a one turn basis, expressions for coil loss and reactive volt-amperes may be written

$$W_w = |M_w|^2 R_w \qquad 196$$

$$W_{qw} = |M_w|^2 X_w \qquad 197$$

Equation 197 may be written in terms of the geometric permeance Λ of the coil leakage flux as

$$W_{qw} = |M_w|^2 \quad 2\pi \mu f \Lambda \qquad 198$$

The total loss is given by the sum of equations 193 and 196 and the total reactive volt-amperes is given by the sum of equations 195 and 198. Thus,

$$W_T = W_m + W_w \qquad 199$$

$$W_{qT} = W_{qm} + W_{qw} \qquad 200$$

Power output is the product of developed pressure and flow. Thus, in consistent units, efficiency η may be written

$$\eta = \frac{PQ}{W_T} \qquad 201$$

Power factor PF and turn voltage V_t are

$$PF = \frac{W_T}{\sqrt{\left(W_{qT}\right)^2 + \left(W_T\right)^2}} \qquad 202$$

$$V_t = \frac{\sqrt{\left(W_{qT}\right)^2 + \left(W_T\right)^2}}{M_w} \qquad 203$$

The analysis is now complete except for further consideration of the constants Φ_1 and C_1, which were defined by equation 180, i.e.,

$$\Phi = \Phi_1 \left\{ e^{\alpha_1 x} + C_1 e^{\alpha_2 x} \right\} \qquad 180$$

A boundary condition is common to both pumping configurations Type A and B; i.e., the total flux entering the duct Φ_T is the value of Φ at $x = o$. This condition has been expressed as

$$\Phi_T = \Phi_1 \left(1 + C_1\right) \qquad 188$$

A secondary boundary condition is imposed at the outlet end of the duct, at $x = c$. For pump Type A, m.m.f. relationships for a closed path crossing the duct at $x = c$ and returning to the starting point through the magnetic core to the

right of the duct (Figure 44), require that

$$I_c = -\frac{gB}{\mu}\bigg|_{x=c} = \frac{g\alpha_1}{\mu\pi d}\,\Phi_1\left(e^{\alpha_1 c} + \frac{\alpha_2}{\alpha_1}\,C_1\,e^{\alpha_2 c}\right) \qquad 204$$

where I_c is the current in the outlet duct header, having resistance R_c. Current I_c flows by virtue of the voltage induced by the flux at x = c; hence;

$$I_c = -\frac{i\omega\Phi}{R_c}\bigg|_{x=c} = -\frac{i\omega\Phi_1}{R_c}\left(e^{\alpha_1 c} + C_1\,e^{\alpha_2 c}\right) \qquad 205$$

Combining equations 189 and 190 and solving for C_1,

$$C_1 = -\frac{\left(\frac{gR_c}{\omega\mu\pi d}\,\alpha_1 + i\right)}{\left(\frac{gR_c}{\omega\mu\pi d}\,\alpha_2 + i\right)}\,e^{\left(\alpha_1 - \alpha_2\right)c} \qquad 206$$

For pump Type B, the boundary condition at x = c is more obvious. Neglecting fringing flux, the flux at x = c must be zero. Thus, from equation 180, at x = c,

$$C_1 = -e^{\left(\alpha_1 - \alpha_2\right)c} \qquad 207$$

The equations relating the performance of either Type A or B pumps to the parameters of the configuration and the fluid pumped are summarized below. The equations in the analysis are correct in any consistent system of units. Constants have been introduced into the equations listed below to correspond to the units indicated. Except for the suffix "a", the equations have numbers corresponding to those in the analysis.

$$Y = \left(1 + \frac{2t}{a} \frac{\rho_f}{\rho_d}\right) \text{ , dimensionless} \qquad 174a$$

$$\left.\begin{aligned} Z &= \sqrt{1 + i\ 5.475 \frac{f\rho_f gY}{av^2}} \\ \alpha_1 &= \gamma_1 + i\beta_1 \\ \alpha_2 &= \gamma_2 + i\beta_2 \\ \gamma_1 &= 0.1915 \frac{av}{\rho_f g} \left[1 + \text{Re}\left\{Z\right\}\right] \qquad 177a \\ \gamma_2 &= 0.1915 \frac{av}{\rho_f g} \left[1 - \text{Re}\left\{Z\right\}\right] \qquad 178a \\ \beta_1 &= -\beta_2 = 0.1915 \frac{av}{\rho_f g} \text{ Im}\left\{Z\right\} \end{aligned}\right\}$$

For Type A pump

$$C_1 = -\left[\frac{1.588 \times 10^6 \left(\frac{gR_c}{fd}\right)\alpha_1 + i}{1.588 \times 10^6 \left(\frac{gR_c}{fd}\right)\alpha_2 + i}\right] e^{(\alpha_1 - \alpha_2)c} \text{ , dimensionless} \qquad 206a$$

For Type B pump,

$$C_1 = - e^{(\alpha_1 - \alpha_2)c} \quad , \text{dimensionless} \qquad 207a$$

For both type pumps,

$$C_2 = C_1 \left[\frac{e^{(\alpha_1^* + \alpha_2)c} - 1}{\alpha_1^* + \alpha_2} \right] \quad , \text{in.} \qquad 187a$$

$$\Phi_T = \Phi_1 \left\{ \left| 1 + C_1 \right| \right\} , \text{megalines} \qquad 188a$$

$$P = - 562.5 \frac{f \left| \Phi_1 \right|^2}{d^2 \rho_f} \quad \text{Re} \left\{ \left(1.91 \frac{\alpha_1 v}{f} + i \right) \left[\frac{\alpha_1^* \left(e^{2\gamma_1 c} - 1 \right)}{2\gamma_1} + \alpha_2^* C_2^* \right] \right.$$

$$\left. + \left(1.91 \frac{\alpha_2 v}{f} + i \right) \left[\alpha_2^* \frac{\left(e^{2\gamma_2 c} - 1 \right)}{2\gamma_2} \left| C_1 \right|^2 + \alpha_1^* C_2 \right] \right\} \quad , \text{psi} \qquad 186a$$

$$G = \left[1.588 \times 10^6 \left(\frac{g R_o \alpha_1}{fd} \right) - i \right] + \left[1.588 \times 10^6 \left(\frac{g R_o \alpha_2}{fd} \right) - i \right] C_1$$

dimensionless

$$M_w = - 0.0628 \frac{f \Phi_1}{R_o} G \quad , \text{amp} \qquad 190a$$

$$KW_m = 3.95 \times 10^{-6} \frac{\left| f \left| \Phi_1 \right| \right|^2}{R_o} \quad Re \left\{ i \left(1 + C_1 \right) G \right\} \quad , kw \qquad 193a$$

$$KW_{qm} = 3.95 \times 10^{-6} \frac{\left| f \left| \Phi_1 \right| \right|^2}{R_o} \quad Im \left\{ i \left(1 + C_1 \right) G \right\} \quad , kvar \qquad 195a$$

$$KW_w = 10^{-3} \left| M_w \right|^2 R_w \quad , kw \qquad 196a$$

$$KW_{qm} = 20.05 \times 10^{-11} \Lambda f \left| M_w \right|^2 \quad , kvar \qquad 198a$$

$$KW_c = KW_c \quad , kw \qquad 199a$$

$$KW_{qT} = KW_{qm} + KW_{qw} \quad , kvar \qquad 200a$$

$$\text{Efficiency} = \eta = \frac{0.435\ PQ}{10^3\ KW_T} \quad , \text{dimensionless} \qquad 201a$$

$$PF = \frac{KW_T}{\sqrt{KW_{qT}^2 + KW_T^2}} \quad , \text{dimensionless} \qquad 202a$$

$$V_t = \frac{10^3 \sqrt{\left(KW_T \right)^2 + \left(KW_{qT} \right)^2}}{M_w} \quad , volts \qquad 203a$$

It follows from equations 180 and 181 that the flux Φ_c at x = c and gap flux densities B_o at x = o and B_c at x = c are

$$\Phi_c = \Phi_1 \; e^{\alpha_2 c} \left[e^{(\alpha_1 - \alpha_2)c} + C_1 \right] \quad \text{, megalines} \qquad 180a$$

$$\left.\begin{aligned} B_o &= - 10^3 \frac{\Phi_1 \alpha_1}{\pi d} \left\{ \left(1 + \frac{\alpha_2}{\alpha_1} C_1 \right) \right\} \quad \text{, kilolines/in.}^2 \\ B_c &= - 10^3 \frac{\Phi_1 \, e^{\alpha_2 c}}{\pi d} \frac{\alpha_1}{} \left[e^{(\alpha_1 - \alpha_2)c} + \frac{\alpha_2}{\alpha_1} C_1 \right] \quad \text{, kilolines/in.}^2 \end{aligned}\right\} \; 181a$$

D. Selection of Materials

Fundamental to design and evaluation of various electromagnetic pump applications is the selection of suitable materials. Complete and adequate information was not available on all materials chosen. Such gaps in the literature will become apparent in the discussion which follows. It is not feasible to include, in this final report, all the voluminous materials data reviewed throughout the study program nor to recount all details of composition, processing, and other prior history for the materials described. Such details are documented in the cited references and in the bibliography. The information is also limited to those materials properties directly applicable to design or performance calculation or those essential for a materials choice for the selected designs. A complete literature search or reconciliation of anomalies exceeded this program. The data reviewed in this report will adequately support preliminary design work. To accomodate final designs, considerable confirmation testing and some original data would be required.

The classes of materials which directly affect the design and construction of electromagnetic pumps for liquid metals include:

- Fluids
- Duct Materials
- Magnetic Materials
- Electrical Conductors and Insulation
- Thermal Insulation.

The section of materials was limited to these items. The choices made were intended to be within the present state-of-the-art and to be commercially available. Current work by Westinghouse Electric Co. on electric space generator materials under NASA Contract NAS 3-4162 had not been fully reported at the time of this publication. When published this information should be a valuable reference for EM pump development work. Discussion of the materials their properties and the choices made follows in the sequence cited above. In general, the tables and figures show the references from which the information was extracted.

1. Pumped Fluids

The pertinent fluids and their respective temperature ranges covered in this study include:

Liquid Metal	Temperature Range
NaK 78	(1000°F-1300°F)
Potassium	(1000°F-1400°F)
Lithium	(1000°F-2000°F)

Since the pumped fluids become current-carrying members within an electromagnetic device, the resistivities of the molten alkali metals are of primary interest. Viscosity and density data are required for hydraulic calculations, and vapor pressure data for cavitation considerations. Property information items necessary for design are shown in Figures 45 through 48, and enumerated below:

- Resistivity Vs. Temperature
- Density Vs. Temperature
- Viscosity Vs. Temperature
- Vapor Pressure Vs. Temperature

No information has been obtained regarding the wetting capability of the liquid metals for containment materials. Deem and Matolich (Ref. 37), however, noted slight irregularity in potassium resistivity measurements in a Cb-1Zr container at low temperatures which disappeared after the system was brought to a temperature of approximately 750°F. Thus it was suggested that an improvement in wetting had occurred. Neither has any information been noted regarding the influence of impurities on electrical resistivity of these liquid metals other than efforts by Blake et al. (Ref. 38), which indicated that change in oxygen concentration had only a minor effect on resistivity. The increase in resistivity with temperature far exceeds the

effects of oxygen concentration.

Documents reporting original work on the measurement of properties were consulted, and the values recorded here represent those believed to be most accurate. The extended temperature data of Deem and Matolich (Ref. 39) agrees at the lower temperatures with those by Kapelner and Bratton (Ref. 40). Because of agreement between the data in references 39 and 40 on potassium resistivity and the similarity in method used, Kapelner's (Ref. 41) data on lithium have been accepted as valid, despite an approximate 4% disagreement with Freedman and Robertson referenced therein and despite radical disagreement with the single point value of 17.81 μ-ohm-in. at 446 ^{o}F given by Weatherford (Ref. 42) and Lyon (Ref. 43). Difference in concavity (downward) compared to the other metals shown is unexplained. The resistivity of NaK (78) shown by Weatherford (Ref. 42) has been accepted as shown because no reports more recent than his references have been found. The data compiled by Weatherford appear consistent with Kapelner's (Ref. 41) data on NaK (46). The resistivities of a stainless steel, reference 44, and sodium, reference 45, are shown for comparison. These data are shown in Figure 45; additional information is presented in Table 4.

TABLE 4. CERTAIN PROPERTIES OF SELECTED ALKALI METALS
(Ref. 42)

	NaK (78)	Potassium	Lithium	Sodium
Atomic Weight		39.10	6.94	22.99
Melting Point, ^{o}F	12.0	145.8	357	208
Boiling Point, ^{o}F	1456	1395	2430	1630
Density of Solid, lb/ft^{3}, at Melting Point	54.18	53.69	33.34	60.62
Surface Tension, lb/ft, at Melting Point	7.4×10^{-8}	0.0059	0.027	0.0131

Density and viscosity data, necessary for hydrodynamic and other calculations, are shown in Figures 46 and 47. The only interpretative comment is that the values of viscosity stated by Hall and Blocher (Ref. 46) for potassium are the highest temperature values available and lie within the extremes of previously documented data

The vapor pressure of the liquid metal is significant in considering cavitation problems. Figure 48 presents this data. Walling and Lemmon (Ref. 47) and Ewing et al. (Ref. 48) agree substantially on potassium. No recent work was found on lithium and Stull's survey data (Ref. 49) was combined with Weatherford's (Ref. 42) data. The most recent information on NaK (78) was Weatherford's (Ref. 42) survey. Sodium (Ref. 42) is shown for comparison.

As design sophistication improves and as experience accumulates in the design, construction, and operation of electromagnetic pumps, investigation of these items may be warranted;

1) Wetting of containment material by alkali metals and contact resistance.

2) Influence of dissolved or dispersed materials upon electrical resistivity of liquid metals.

2. Duct Materials

to p. 83

The choice of duct material for the electromagnetic pump is predominantly governed by over-all system requirements rather than pump considerations alone. Compatibility with all other materials in the alkali metal system is a superseding necessity. The main factors which influence the material choice are

- Fluid to be Pumped
- Electrical Losses in the Pump
- System Materials Compatibility
- Fluid Velocity
- Alkali Metal Corrosion,
- Temperatures and Temperature Gradients
- Mechanical Loads and Material Strength
- Dissimilar Thermal Expansions
- Time of Exposure at Various Temperatures
- Cyclic Operation

Although considerable information exists on corrosion of the containment materials, because of the high temperatures and long design life required here, the choice of alkali-metal resistant duct materials for EM pumps is not obvious. Most of the corrosion test information is based on static environment, capsule tests, and simple refluxing capsule tests. Thus, the materials choices here are also preliminary and require further confirmation to support detailed design work.

A consideration of containment metal corrosion mechanisms and rates under exposure to liquid alkali metals at elevated temperatures is given by Amateau (Ref. 50) and by DiSteffano and Hoffman (Refs. 51 and 52). The latter emphasize the necessity of controlled composition in both containment

and liquid metal materials, particularly with regard to interstitial elements, such as carbon, nitrogen, hydrogen and oxygen. A review of these three reports and numerous other documents led to the tabulation of probable candidate duct materials presented in Table 5. System compatibility, corrosion, and allowable temperatures were considered based on the temperature differentials in the systems described in Section IV.

The properties of duct materials which are of primary importance to the pump designer include:

- o Resistivity
- o Thermal Expansion
- o Tensile Strength
- o Creep Properties
- o Stress Rupture Properties
- o Magnetic Permeability
- o Fabricability

The electrical resistivity of the duct material significantly influences the design of EM pumps. The duct material is electrically in parallel with the pumped fluid; it is desirable, therefore, to have high resistance duct walls. Thus, to minimize losses, metallic duct walls should be as thin as is consistent with mechanical considerations. For manufacturing purposes and corrosion considerations, it is recommended that the wall thickness be at least 0.025 inch. Electrical resistivity data versus temperature data are shown in Figure 49. The resistivity of potassium is also indicated for comparison.

Measurements of electrical resistivity of structural materials are not frequently made; therefore, fewer data are available. It should also be noted that composition, impurities, and chemical or metallurgical conditions, such as grain size or precipitation upon aging, can have a significant influence both on electrical resistivity and other properties. Such differences in composition, etc., could very well account for resistivity data differences of 5% or higher such as those between Smith (Ref. 53) and Weiss (Ref. 54); Kapelner (Ref. 41) and Weiss (Ref. 54); and Bennethum (Ref. 55) and Haynes (Ref. 56). Tottle (Ref. 57) shows the influence of oxygen, zirconium and titanium on the properties of columbium.

Regarding the choice of materials for data presentation, except for the newer refractory alloys, (see footnote, Table 5), and the improved superalloys, the materials shown are well documented for long-time use in alkali metals. The remaining candidate materials shown in Table 5, and other concurrently under development, (some of which show considerable promise of improved characteristics) have not yet been evaluated in alkali metal service representative of space power applications.

TABLE 5. PROBABLE DUCT MATERIALS

Type[a]	Alloy	Composition, %								Suggested Temp. (°F) Limitations		
		Cb	Ta	Mo	W	Ti	Zr	Hf	C	Li	K	NaK (78)
A	Ta T111[b]	---	Bal.	---	8	---	---	2	---			
	Ta T222[b]	---	Bal.	---	9.6	---	---	2.4	0.01			
	Mo TZM	---	---	Bal.	---	0.5	0.08	---	---			
	Mo Mo-0.5Ti	---	---	Bal.	---	0.5	---	---	---	2000	1600	1600
	Cb FS-85[b]	Bal.	28	---	10.5	---	0.9	---	---			
	Cb AS-55[b,c]	Bal.	---	---	5	---	1	---	0.06			
	Cb D-43[b]	Bal.	---	---	10	---	1	---	---			
	Cb Cb-1Zr	Bal.	---	---	---	---	1	---	---			
		Co	Ni	Cr	Mo	W	Fe	C	Cb			
B	Co B L-605[d]	Bal.	10	20	---	15	3	0.1	---		1600	1600
C	Type SS 316L SS[d]	---	12	17	2.5	---	Bal.	0.03	---			
C	Type SS 347 SS[d]	---	10.5	18	0.5	---	Bal.	0.08	1.1		1400	1400

[a]Alloy types: A, refractory alloys; B, superalloys; C, austenitic stainless steel.

[b]New refractory alloy; limited information available on alkali metals compatibility.

[c]Melted with an yttrium addition to improve weldability.

[d]1.0Si, 2.0Mn, 0.04P, 0.03S max.

Figures 50 through 53 show thermal expansion, tensile yield, elastic modulus and creep-ruture for representative alloys. Although many properties, such as rupture and creep, are properly presented as bands, lines have been used to approximate median values to avoid confusion. Density and melting point data on some of the duct materials are presented in Table 6.

TABLE 6. DENSITY AND MELTING POINT OF SOME DUCT ALLOYS

	Alloy				
Property	T111	Cb-1Zr	L-605	Type 316-L SS	Mo-0.5Ti
Density, lbs/in.^{3}	0.604	0.31	0.33	0.29	.367
Melting Point, ^oF	5400[a]	4350	2425-2570	2500-2550	4370

[a]Estimated.

As cited in Section V, the dc electromagnetic pumps generally have the lowest specific weight. However, a serious state-of-the-art limitation for conduction pumps exists in the electrical connection to the pump duct. Realization of the high performance of dc pumps requires the use of copper or a material of similarly low resistivity. The difficulty in making a reliable metallurgical bond between the duct material and the conductor material constitutes a problem.

Copper has been brazed successfully to Type 316 SS. Such joints, however, have not been subjected to tests adequate to qualify them for these EM pump applications. Electron beam welding of copper to Type 316 SS with a Monel metal insert is also promising. It is probable that welds or brazes of copper to L-605 alloy would be as successful as those of copper to Type 316 SS. A copper to Cb-1Zr diffusion bonded joint showed no brittle intermetallic zone nor interdiffusion of metals when subjected to a 100-hour, 1600^{o}F isothermal test (Ref. 58). How this joint would behave under thermal cycling is unknown. Subsequent brief development efforts to join copper to other refractory alloys for service temperatures above approximately 1300^{o}F have not been particularly encouraging; prospects for other high conductivity metals are no brighter. Certainly, similar or worse joining problems would be encountered in using aluminum, and even the lower design duct temperatures are dangerously close to the melting point of aluminum.

In addition to the metallurgical aspects of duct to conductor joints cited above, the high temperature mechanical strength of copper alone (with the possible exception of dispersion hardened materials) may be insufficient to meet the requirements of a hot duct to conductor connection. However, the containment of a good conductor within a supporting sheath, e.g., stainless steel, may be an attractive approach to the problem. (Some related discussion appears subsequently under "Electrical Conductors and Insulation"; Figures 59 through 63 will assist in the consideration of the present topic.)

Possibly, a compromise material may be selected for the electrical connection to the duct; for example, Mo-0.5Ti alloy has adequate high temperature strength and moderate thermal conductivity, with significant, but perhaps not unacceptable, increase in electrical resistivity. Such a joint may provide an optimum compromise between a mechanically strong joint and acceptable electrical and thermal losses. Although such a joint has not been required previously, it is conceivable that a process for joining Mo-0.5Ti to the other candidate duct refractory metals could be developed.

As design sophistication increases, or as the needs for greater accuracy and weight control arise, certain deficient areas in the data may have to be resolved, i.e.,

1) Resistivity of duct materials: The resistivity data presented are adequate for present purposes; however, the influence of prior history, condition, and composition upon the resistivity of the materials must be determined.

2) Creep and stress rupture: There is considerable variation, undoubtedly influenced by differences in details of composition, manufacture, forming, heat treatment, testing, etc., in the reported values for many of the materials. The effect of total duct material on electrical losses is significant in most designs. Therefore, when optimum flight hardware must be designed, more precise information on the duct material will be needed.

3) New materials: As the corrosion resistance of new materials is demonstrated, information on properties and processing must be obtained. For example, the later developmental columbium alloys promise improved high temperature strength over Cb-1Zr while simultaneously retaining good corrosion resistance. More fabricability and creep information is required, however, and no resistivity data appear to be available.

4) New processes: Ducts offering lower electrical losses and higher thermal resistance, while retaining high reliability, might be achieved using sandwich structures. More intricate shapes of flow passages can reduce hydraulic losses. To exploit the potential weight advantage of the conduction pump, a process for accomplishing suitable high temperature metallurgical bonds between a good electrical conductor and the duct material should be developed.

3. Magnetic Materials

The dc conduction pump can be designed to isolate the coils and most of the magnetic material thermally from the liquid being pumped. In polyphase induction pumps, thermal insulation is required between the high temperature liquid metal duct and the stator to protect the windings from overtemperature. Generally, the designs are based on the following magnetic material conditions:

Stator Temperature	800 °F max.
Core Temperature	1600 °F max.
Atmosphere	Inert Gas at ~15 psi
Power Input	DC AC, Single Phase, 25-100 Cps AC, 3-Phase, 50-200 Cps

to p. 9

It is anticipated that pumps with these winding and stator operating temperatures are first generation designs. As the higher temperature performance of insulation systems is assured, these temperatures may be increased. The development of new materials and new insulation systems may also permit increased temperatures.

The basic principle of electromagnetic pumping requires that the duct and fluid be a nonmagnetic portion of the pump's magnetic circuit. Thus, electromagnetic pumps are inherently large air gap devices. Since the m.m.f. required for the nonmagnetic gap is much greater than that necessary for the rest of the magnetic circuit, there is little advantage in using high permeability magnetic materials. Other properties, therefore, were examined to guide the initial choice. Those properties of soft magnetic materials of interest to the pump engineer, arranged more or less in order of importance, include:

- Curie Temperature
- Aging Characteristics
- Thermal Conductivity
- Core Loss Vs. Induction Vs. Temperature
- Volt-Amperes Vs. Induction Vs. Temperature
- Stress Sensitivity
- Magnetic Anisotropy

The state-of-the-art appropriate to the materials selection for this program yields a less than optimum amount of information applicable to soft magnetic materials. Few of the candidate materials have been tested at elevated temperature in the absence of air or, in some instances, to a sufficiently high temperature. Uncertainty about processing details makes reconciliation of anomalous results difficult. Nevertheless, there is a body of information which indicates areas of probable success and the direction for future development. The pertinent materials are silicon-iron alloys and cobalt-iron alloys. Nickel and the nickel alloys do not have characteristics approaching the requisite high-temperature/high-flux-density properties.

to p.90

The Curie temperature of a magnetic material is the first criterion for selection. Usually, the material must be held well below the Curie temperature to maintain useful magnetic properties. Figure 54 shows the data for Curie temperature and saturation induction versus silicon content of silicon-iron alloys; Figure 55 is a novel presentation of saturation induction isotherms versus cobalt content of cobalt-iron alloys. The following suggestions are made for the design limits of silicon-iron alloys:

1) A maximum induction of 100,000 lines/in.^{2} at 800 ^{o}F for 0.25% or lower silicon content.

2) Reduction of the above flux density with increasing silicon content.

3) Reduction of the above flux density with increasing temperature.

4) A maximum operating temperature of 1250 ^{o}F.

The following suggestions are made for the design limits of cobalt-iron alloys in the 25% to 35% cobalt range:*

*Fifty percent cobalt alloys should not be employed until anomalous behavior ascribed to atomic ordering is clarified (Refs. 68 and 69).

1) A maximum induction of 120 kilolines/in.^{2} (18 kilogauss) at 1200 °F for 35% cobalt content.

2) Reduction of the above flux density with departure of cobalt content from 35%.

3) Reduction of flux density with increasing temperature.

4) A maximum operating temperature of 1600 °F.

There is fragmentary evidence to indicate that high temperature magnetic characteristics in an inert atmosphere, such as that proposed for these electromagnetic pumps, will not change appreciably with time at these suggested, or even higher, values of temperature and flux density. The reports examined indicate that virtually all previous tests provide an inadequate basis for rejecting the proposed design limits because of one or more of the following reasons: 1) oxidation (testing or aging in air); 2) interlaminar insulation; 3) pre-test anneal; or 4) mechanical stress. In the case of low silicon content steel, a balance may have to be effected between increased coercive force and core loss upon aging versus other properties.

To determine the heat balance in an electromagnetic pump design, the thermal conductivity of the magnetic material used in the stator must be known. The winding losses, the heat transferred through the thermal insulation between duct and stator, and the losses generated by ac flux in the magnetic material itself must all be transmitted to the heat sink through the stator. Improved design may be achieved with a high thermal conductivity material, even at the cost of higher core losses in the material itself. The thermal conductivities of several candidate magnetic alloys, including an estimated characteristic for cobalt alloys based on a reported room temperature value, are shown in Figure 56. Thermal conductivity of magnetic material for central cores is not a problem, but higher temperature flux-carrying capability must be considered.

Normal magnetization information, primarily useful for dc applications, can indicate maximum useful flux densitites (and required m.m.f.) in electrical apparatus. Guides to ac performance may also be obtained from normal magnetization curves. Although many of the reports on elevated temperature that were reviewed do not show normal magnetization curves, Figure 57 shows some data which are available.

As noted previously, there are inconsistencies in data reported by various investigators. Figure 58 verifies, for a silicon steel, the general observation that core loss decreases with increasing temperature. A substantial inconsistency in the data, probably caused by lack of pre-test annealing and by less than optimum interlaminar insulation, is also indicated by the individual points for the same nominal grade of steel (AISI-M 36). The

elevated temperature data for silicon steels are reproduced in Figure 58 because they best represent the characteristic reduction of loss with temperature, although the tests were made in air on unannealed samples with questionable interlaminar insulation. Figure 58 also reports losses on 27% and 35% cobalt-iron alloys. Few investigators have reported elevated temperature exciting current or excitation volt-amperes in a form useful to this program. Table 7 presents values of excitation volt-amperes per pound estimated on the basis of various pieces of data. No elevated temperature data were found for low silicon iron alloys.

TABLE 7. ESTIMATED 60 CYCLE MAGNETIZING EXCITATION

Material	Flux Density, Kl/in.^{2}	Excitation, Volt-Amperes/lb		
		212°F	800°F	1100°F
1.25% Si (M-36)	64	2.6	3.0	4.0
	97	20	31	40
27% Co	64	5	4.5	4
	97	18	20	22
	116	40	45	60

Many of the reports reviewed, e.g., references 75 through 78, indicated that sensitivity to mechanical stress, particularly in aging tests, was caused primarily by oxidation. This was especially true in wound cores and for oriented materials. Because of the inert atmosphere for the magnetic material, no difficulty is anticipated from oxidation in electromagnetic pumps studied for this program.

Magnetic anisotropy, the easier magnetization of a material in one direction than another, is established (Ref. 79) as the cause of increased loss for magnetization in one direction compared to the loss for magnetization in another direction; the relative increase is greater in oriented materials than in nonoriented materials. Not so well known is the fact that a rotational flux causes a more significant loss than that caused by the simple alternating flux (Refs. 80 through 82). A rotational flux is one constant in magnitude but time variant in direction as contrasted with the simple alternating flux, which is unidirectional but time variant in magnitude. This effect is greater in oriented materials. The increased loss with rotational flux is ascribed to the doubled frequency of magnetic domain wall movement (Ref. 83). In polyphase pumps, rotational flux exists in the magnetic material behind the slots and teeth.

Deterioration of interlaminar insulation will cause increasing losses on aging tests. Some of the various reports reviewed, e.g., references 74, 76, and 84, stated that the laminar coating may have provided insufficient interlaminar resistance for long-time, high temperature service. No well documented investigation of a suitable lamination insulating material was found. Tentatively, a material which can withstand the stress relief anneal temperature, such as Carlite coating or Sterling Varnish Co. S-678 material with aluminum oxide added is recommended. An alternative would be to flame spray the laminations with aluminum oxide. Aluminum orthophosphate laminar coating has yielded anomalous results for different investigators.

The reports surveyed, e.g., references 85 through 87, indicated a very low probability of permanent degradation of magnetic materials considered for these pumps under the expected service conditions. The cobalt alloys will, of course, become radioactive under neutron bombardment and will remain radioactive for considerable time.

The higher indicated thermal conductivity and the higher permissible ac flux densities, at modest increase in losses (over silicon steel losses), apparently favor the use of the cobalt-iron alloys. Except where the temperature requirement indicates otherwise, the 27% cobalt steel is preferable to the 35% alloy because of better mechanical properties and somewhat lower cost. For highest temperature use in cast or forged magnetic structures, the 35% cobalt steel is suggested. Conversely, if the temperature is favorable and the lower flux density is acceptable, a silicon-iron or very low carbon iron will allow substantial reductions in the costs of core material and processing.

As indicated earlier in this discussion, test information to verify that the candidate materials will suffer no appreciable degradation in an inert atmosphere at the pertinent temperatures and times is needed. Also, the development of adequate interlaminar insulation is required.

4. Electrical Conductors and Insulation

Since conductors are rarely used alone, it is difficult to treat conductors and their insulation separately. The service conditions, the manufacturing processes employed, and the over-all electrical insulation must be considered. Numerous study and experimental projects have been directed at the development of insulated wire and insulation systems for service at 900°F to 1100°F. Varying degrees of success, with only experimental quantities carried through manufacture, were achieved. Most development work was on component materials and mock-ups of insulation systems; most development units manufactured were transformers and inductive reactors with aging tests of approximately 1,000 hours. This is an insufficient basis for recommending 18,000-hour high reliability space mission application. Establishing 750°F to 800°F as the expected working temperature for the windings of these electromagnetic pumps, therefore, constitutes a conservative approach. As additional experience is acquired with presently available materials and with newly developed materials and insulation systems, higher permissible temperatures are anticipated.

Selecting electrical conductor materials for liquid metal EM pumps requires a knowledge of the electrical resistivity and strength characteristics of basic conductor materials. Where needed, consideration must then be given to modifying these characteristics using metallic claddings, coatings, or metallurgical variations. For the polyphase pumps, the conductor strength should be sufficient for unsupported end turns. The thermal conductivity of the conductor is important to the transfer of heat within the windings and, as mentioned earlier regarding conduction pumps, where high current density conductors must operate in contact with the duct wall.

Figures 59 and 60 show the electrical resistivities and thermal conductivities of various conductor materials. The short-time strengths of various types of conductor materials at elevated temperatures are depicted in Figure 61, which shows their yield strengths as a function of temperature. There is a lack of creep and rupture data on conductor materials. Most of that which is available is shown in Figure 62. No information was available on creep under thermal cycling, although copper is known to perform poorly in this regard at elevated temperatures.

The advantages of the low electrical resistivity and the favorable temperature coefficients of resistivity of copper and silver, compared with other conductor materials, is clearly apparent. Except for elevated temperature strength and stability considerations, low electrical resistivity is the criterion for selection of a conductor material. The high thermal conductivities of silver and copper are also beneficial in the transfer of heat from the conductor and the consequent maintenance of low electrical resistivity.

SAP aluminum (sintered aluminum powder), the best alternative after copper, has considerable advantage in strength over pure copper and silver up to approximately 1000 ^{o}F. Also, aluminum can be readily anodized as an insulation for low voltage applications. Except on a strength-to-weight basis, the new dispersion hardened coppers exhibit strengths superior to those of SAP. Simultaneously, these materials retain the high conductivity advantage of copper. Also, the dispersion hardened materials apparently have a lesser tendency to grain growth on extended exposure to high temperature. For very high temperature service, molybdenum should be considered. For applications below approximately 1000 ^{o}F, the strength advantages of molybdenum are not sufficient to offset its high resistivity and density.

In pump designs, in which protective atmospheres minimize or eliminate the oxidation problem and assist in cooling the electrical conductors to a temperature near 800 ^{o}F, beryllia or zirconium dispersion hardened copper and, to a lesser extent, clad copper appear to be the best choices. The electrical conductivities of conductors of these types are not seriously reduced from that of pure copper. (See Figures 59 and 63 and Table 8.) As indicated in Figure 63 and Table 8, the thermal diffusion stability of higher strength clad copper conductors has been studied to some extent. While

top p93
to p. 93

TABLE 8. CHANGE IN RESISTANCE OF WIRES AGED AT 1100°F
2000 HOURS IN ARGON
(Ref. 97)

Wire Type	AWG Gauge	Resistance Increase, %
OFHC Cu	20	-0.9
Annealed Cu	28	-0.2
Be-Cu, Ag Plate	20	15.6
Cu, 1¼% Ag Plate	36	11.7
Cu, Single Glass Served, Silicone Treated	28	-1.3
Cu-3% Ag	42	-3.5
Cu-3% Ag, Secon Type C Insulation	28	-1.9
Sterling Ag	30	7.0
Cu, 27% Ni Clad, Bare	28	124
Cu, 27% Ni Clad, Bare	36	360 (570 hrs)
Cu, 27% Ni Clad, Ceramatemp Insulation	28	60.6
Cu, 27% Ni Clad, Ceramicite Insulation	28	75.9
Cu, 27% Ni Clad, Ceroc Insulation	28	70.6
Cu, Type 430 SS Clad	28	30.0
Cu, Type 430 SS Clad	36	59.3
Cu, Inconel Clad	28	31.3
Cu, Inconel Clad	36	144.2
Cu, Anodized Ta Clad	30	Too Brittle
Cu, 4% Ni Plate	28	55.7
Cu, 4% Ni Plate	36	210 (570 hrs)
Cu, 10% Ni Plate	28	79.3
Cu, 10% Ni Plate	36	228.0
Cu, Ag Barrier, Ni Plate	28	23.4
Cu, Cr Barrier, Ni Plate	28	108.2
Cu, Fe Barrier, Ni Plate	28	196
Cu, Cr Plate	28	3.7
Cu, Re Plate	28	0.4
Cu, Fe Plate	28	11.2
Ag, Cr Plate	28	1.9
Ag, Re Plate	28	46.7
Ag, Fe Plate	28	21.2
Ag, Fe Barrier, Ni Plate	28	32.8

there are some limited indications that a nickel clad copper conductor would exhibit very little, if any, diffusion between nickel and copper at 800 °F and possess fairly stable electrical resistivity for long periods of time, appreciable evidence to the contrary also exists. Nickel clad silver, satisfactory in this and many other respects, appears to lack satisfactory high temperature strength. Primarily because of the uncertainty of reliable long-time resistivity in the clad conductor approach, the unclad dispersion hardened conductors are presently favored for EM pump application.

More extensive creep test evaluation, long-time stability evaluation in appropriate atmospheres, and electrical resistivity measurements over the appropriate temperature range will be required, however, to confirm these characteristics in the conductor selected. In attempting to achieve improved conductor strength, the effect of conductor composition and processing treatment on the electrical resistivity of the final conductor and its ability to be satisfactorily joined to other conductor or duct materials must also be considered. Conductor composition, processing, and joining do not present extremely difficult problems in the application of the selected conductor materials to EM pump designs.

Electrical conductor insulations for the EM pump must operate at 800°F in an inert atmosphere and provide adequate insulation at a maximum of 20 volts turn-to-turn after shaping. Several types of conductor insulations have been studied over the past several years for temperatures in the 800°F range and for applications in air. The protective atmosphere contemplated in the EM pumps protects the conductor from oxidation.

to p 94 →

Previous high temperature insulations have employed the following concepts: 1) anodized aluminum, 2) matured glass enamel coatings, 3) flame sprayed oxides and nitrides. 4) glass frit impregnated glass-serving, and 5) granular glass coatings. Anodized aluminum has been used successfully as a high temperature insulated conductor. This system is limited, however, by the higher resistivity and the lower mechanical strength of the aluminum conductor compared to dispersion hardened or clad copper or silver. The matured glass enamels are difficult to apply uniformly on small radii conductors and on corner radii of rectangular conductors, and, in general, lack satisfactory electrical insulating characteristics at elevated temperatures. Flame sprayed conductors lack workability and coating adherence. At elevated temperatures, both the low melting, glass impregnated glass-served insulations and the glass-fritted coatings that mature in place exhibit unsatisfactory current leakage and high dissipation factors at low frequencies. Untreated glass-served wire performs well at elevated temperatures but is impractical because of its poor handling characteristics. Conventional resin impregnated insulations result in carbonaceous deposits during vacuum burnout that produce poor insulating characteristics. Burnout of the resin in air eliminates carbon but requires undesirably high temperatures (1200°F) and protection of the conductor from oxidation.

The devitrification temperature of the glass of conventionally impregnated glass serving is approached during burnout at these temperatures. The excellent high temperature electrical characteristics of E glass, a borosilicate glass, is indicated by its elevated temperature resistivity in Table 9 and by successful tests of unimpregnated, double glass-served #36 AWG silver conductor in argon for 2,000 hours at 1112°F.

TABLE 9. VOLUME RESISTIVITY OF E GLASS AT SEVERAL TEMPERATURES

Resistivity, ohms/cm^3	Temperature, °F
2 - 5 x 10^{12}	72
1 x 10^7	1320
1 x 10^6	1450
1 x 10^5	1600

To utilize the desirable high temperature electrical characteristics of resinless insulation and the room temperature handling characteristics of resin impregnated glass-served insulation and simultaneously avoid carbon deposits during resin burnout in air, the following procedure is recommended:

1) Preparation of the glass filament serving with the inclusion of inorganic lubricants, such as boron nitride, which are suspended in a film forming, low temperature, fugitive (temporary) binder, such as polybutene, polyvinyl acetate, polyurethane, or similar material.

2) Preparation of double glass-served conductors using the glass filamentary materials cited above with additional lubricant, filler, and fugitive binder to produce an insulated conductor with good handling characteristics.

3) Fabrication of the conductor into its required shapes, application of glass-mica tape coil/phase insulation, and installation into the slots. (The need for wedges or for further insulation in the form of slot liners or tubes is not anticipated.)

4) Bakeout of the fugitive binder in vacuum or under protective atmosphere at low temperature, leaving only glass serving, fillers and lubricants on the conductor in its final manufactured component configuration.

5) Impregnation of the conductor/insulation system with ethyl silicate, aluminum phosphate, or colloidal silicic acid to produce an inorganic bond of the assembled conductor/insulation system.

to p 96

Some unreported preliminary work, currently being performed on this approach, offers the possibility of developing a satisfactory high temperature conductor insulation system. The final details of the processing may differ from those outlined above. Developing the process will require high temperature electrical stability tests, mechanical and vibration tests, and coil forming experiments.

The heat transfer design approach for polyphase induction pumps, as discussed in Section V-A, prescribes a gas filled stator enclosure. The selection of gases for this application requires attention to thermal conductivity, dielectric strength, and chemical stability in the expected environment. On the basis of thermal conductivity, helium or hydrogen are the obvious choices. Other properties of these gases, however, are not favorable. Table 10, which presents some comparative data on electrical and thermal properties of selected gases, indicates that helium, neon, and argon have poor dielectric strength. Nitrogen has been selected as the best

TABLE 10. SELECTED ELECTRICAL AND THERMAL PROPERTIES OF CERTAIN GASES[a] (Refs. 98 and 99)

Gas	Arc-Over Voltage,[b] Volts	Thermal Conductivity at 32 °F, Btu/hr-ft^2-°F/in.	Watts/°F-in.
Air	1700	16.5×10^{-3}	3.4×10^{-4}
Nitrogen	1800	16.2×10^{-3}	3.3×10^{-4}
Neon	360	32.0×10^{-3}	6.5×10^{-4}
Helium	350	97.4×10^{-3}	20×10^{-4}
Hydrogen	950	112.1×10^{-3}	23×10^{-4}
Argon	590	11.2×10^{-3}	2.3×10^{-4}

[a]Values at room or other indicated temperature and one atmosphere.
[b]For 0.010-in. uniform gap, dc, gas only.

compromise gas for the stator cavity. Although other gases have individual properties that are superior, nitrogen has the best combination of engineering properties. In addition, it has exhibited satisfactory characteristics in past service in air insulated pumps. A gas filled and sealed stator cavity permits the selection of immediately available electrical insulation systems, whereas a cavity open to space vacuum would not.

Within certain limits, the electrical sparkover of a gap in a gas is constant for a constant product of gap stress and gas pressure. The sparkover value falls to a minimum which generally occurs at various pressure X gap products for different gases. This relationship was formalized by F. Paschen and, hence, curves showing the relationship, such as those in Figure 64, bear his name. It is desirable to limit the filling pressure to approximately one atmosphere at normal operating temperature. Although hydrogen has desirable thermal conductivity, it has only fair electrical strength. In addition, there is concern regarding 1) the possible loss of hydrogen by diffusion through the wall at elevated temperature and 2) uncertain metallurgical effects with hydrogen. The use or addition of electronegative gases to improve the breakdown situation was rejected because of the possibility of the dissociation of the more complex gas under radiation. No specific information on this point was obtained.

5. Thermal Insulation

Experience with previous designs in electromagnetic pumps has indicated that a multilayer metal foil and wire cloth is suitable for the pump designs of this study. The data in Table 11 indicates that four layers each of foil and wire would provide a barrier with a conductivity of approximately 0.015 to 0.003 watt/^{o}F-in. It was estimated that the conductivity would drop to below 0.015 watt/^{o}F-in. in vacuum with a 1200 ^{o}F duct wall. For design purposes, a value of 0.002 watt/^{o}F-in. was chosen. This value is used in the design calculations of Section V.

TABLE 11. THERMAL CONDUCTIVITIES OF COMPOSITE METAL THERMAL SHIELDS[a]

Sample No.	Composite Construction	Wire Dia., in.	Av. Thk., in.	Mesh. Size, no./in.	Open Area %	Total Thk., in.	Compress. psi	Mean Temp., °F	Thermal Conductivity Btu-in / hr-ft²-°F	Thermal Conductivity Watts / °F-in. x 10³
1	Type 347 SS Screen Type 347 SS Sheet Type 347 SS Screen	0.010 0.010	0.020 0.010 0.020	18 x 18 18 x 18		0.050	100 100 100 35	561 574 621 640	1.06 1.23 1.59 1.10	2.14 2.50 3.23 2.23
2	Type 347 SS Screen Type 347 SS Sheet Type 347 SS Screen Type 347 SS Sheet Type 347 SS Screen	0.010 0.010 0.010	0.020 0.010 0.020 0.010 0.020	18 x 18 18 x 18 18 x 18		0.080	100	550	1.23	2.50
3	Type 347 SS Screen Type 347 SS Sheet Type 347 SS Screen Type 347 SS Sheet	0.0055 0.0055	0.013 0.003 0.013 0.003	54 x 54 54 x 54	49.4 49.4	0.032	25	496	1.06	2.14
4	Type 347 SS Sheet Type 347 SS Screen Type 347 SS Sheet	0.010	0.003 0.026 0.003	40 x 40	36.0	0.032	25	496	1.23	2.50
5	Type 347 SS Screen Type 347 SS Solara-amic Sheet Type 347 SS Screen Type 347 SS Solara-amic Sheet	0.0055 0.0055	0.013 0.003 0.013 0.003	54 x 54 54 x 54	49.4 49.4	0.032	25	496	0.867	1.75
6	Type 347 SS Screen	0.0025	0.006	160 x 160	37	0.006	100	682	0.632	1.28
7	2 Layers Type 347 SS Screen	0.0025	0.006	160 x 160	37	0.0105	100	689	0.929	1.88
8	2 Layers Type 347 SS Screen	0.0019	0.005	165 x 165	47.1	0.0085	100	676	0.750	1.52

[a]Air environment (Ref.100).

IV. SPACE POWER SYSTEMS CONSIDERATIONS

A. System Criteria for Pump Selection

After reliability, the most important characteristic of space power systems components is weight. Nor is it sufficient to consider the weight of the component alone. Rather, to select the best components and systems, the total contribution that each component makes to the over-all power plant weight must be determined. The customary approach is to calculate weights of each identifiable component and to assign weight penalties for the contribution that each component makes to over-all power plant weight. Power consumed by a component, for example, contributes to the over-all power plant weight and the associated penalty can be defined as plant weight increment per unit of power consumed. Similarly, the lagging power factor characteristic of induction pumps requires added capacitance in the power supply. Thus, a weight penalty is assigned on the basis of the reactive power demand of the pump.

As a power plant design progresses, the weight analysis becomes increasingly detailed and the resultant weight estimate becomes more refined. Obviously, at this developmental stage, highly detailed weight analyses of EM pumps are unwarranted. It is important only that the major items of weight be recognized and that each be considered sufficiently to insure proper preliminary selections relative to pump type and major characteristics affecting preliminary pump design. Within the preceding limitations, those items considered beyond pump weight are:

1) Weight penalty for power consumed by the pump and its power supply.

2) Power supply equipment weight.

3) Cooling.

   a. Equipment weight, i.e., radiator, coolant pump, and its power supply and piping.

   b. Weight penalty for power consumed by the coolant pump.

4) Reactive power penalty occasioned by using ac pumps.

Items that can be recognized at this time but which have not been included in this study are:

1) Power cabling and control and instrument wiring that require preliminary space craft layouts to evaluate. In ac pumps, this item is small compared to the over-all pump equivalent weights. Because of the very high

currents requiring large bus bar cross sections, dc conduction pump weight may be substantially increased by this item.

2) Control and protective switchgear.

B. Power Weight Penalty

The incremental addition to the over-all power plant weight caused by using electrically driven components was set at 10 lb/kw electrical power drawn from the main electric power source for the turboelectric system and at 9 lb/kw for the thermionic system. These values were established as basic assumptions at the initiation of the study program. The weight penalty is assumed to cover the entire nuclear power plant except the pumps and directly related equipment covered below. This weight penalty is usually as large in magnitude as the weight of the pump itself. The sum of power weight penalty and pump weight constitute over three-quarters of the total weight criterion for most pumps and is, therefore, used for initial optimization with the performance prediction computations discussed in Section V.

C. Power Conditioning

To cover the range of EM pump applications which are under investigation, different types of power conditioning equipment must be considered:

1) High frequency ac to low frequency ac converter (required for application of ac pumps to turboelectric systems).

2) DC to three-phase ac converter (required for application of ac pumps to thermionic systems).

3) AC to low voltage dc converter (required for application of dc pumps to turboelectric systems).

4) DC to low voltage dc converter (required for dc pumps in thermionic systems).

1. AC Frequency Converter

For applying three-phase ac pumps in turboelectric power systems, the cycloconverter device in Figure 65 was selected. This type frequency converter is optimum where the frequency conversion ratio is reasonably

high (above 10/1) and where the high frequency is at the input side. The principal power handling components of this device are the eighteen controlled rectifier type, high speed electronic switches. These are arranged in six commutating groups, one for each of the low frequency output phases. The air core reactors, connected between the three pairs of forward and reverse output phases, serve as protection against high frequency line-to-line shorts resulting from spurious misfiring of the controlled rectifiers. These reactors have a large reactance at the high frequency but a low impedance (in series with the load) at the low frequency. Firing the controlled rectifiers is timed and actuated by low power level control circuits, which represent a small fraction of the total weight and power loss of the device. This control circuitry provides for both rectifier and inverter action of the controlled rectifiers so that the circuit may handle low frequency loads of any power factor. Another feature of the cycloconverter is the fact that it can be readily designed to provide variable pump input voltage to control pump flow. The fact that the induction type EM pump provides for continuous variation of flow using input voltage variation is certainly one of its important advantages over alternate types of pumps that require throttle valve type flow control.

Cesium vapor thyratron tubes, currently under development, are proposed as the ultimately available controlled rectifier switches. These tubes will be suitable for service in a space power cycloconverter powering loads, such as 60 cycle ac pumps from a high frequency (1000 cps to 3200 cps) inductor alternator power source. The tubes are highly radiation resistant and operate at a high temperature, 1475 ^{o}F. The efficiency of the cycloconverter using projected cesium vapor thyratrons can be estimated conservatively at 90%. The heaviest components of the device are the "air core" reactors. Their specific weight is plotted as a function of capacity level in Figure 66. Including the controls and cooling equipment, the cycloconverter can be estimated conservatively at one lb/kw.

2. Low Voltage Rectifier Circuit

For applying dc pumps in ac power systems, a low voltage, three-phase rectifier circuit, such as that shown in Figure 67 is required. The double Y, six-phase rectifier using the interphase transformer is a good selection for this application, since it provides low dc voltage ripple and high transformer utilization and has only a fixed diode forward voltage drop in the dc output circuit. High temperature, low forward voltage drop (one volt or less) cesium vapor diode tubes are currently under development. These are probably the best type rectifier components for this application.

The weight of this transformer rectifier is principally in the transformer component. Figure 68 shows the specific weight of three-phase transformers in the 400 cps frequency range. This agrees with results reported in references 101 and 102. To allow for excess transformer

capacity required for the rectifier circuit application and to provide for cooling equipment, rectifiers, and cabling, a specific weight of one lb/kw has been estimated for this type power supply equipment.

For a dc output voltage level of 3 to 5 volts (which would provide power to several dc pumps in series), an efficiency of 80% can be estimated using projected performance data for the cesium vapor diodes. In this connection, the assumption that dc conduction pumps may be connected in series should be underlined. As indicated subsequently, the design voltages for these devices are near 1/2 volt. If reliability considerations prevent using the series arrangement, then the dc conduction pump will be burdened with a greater weight penalty than that presented in this section because of reduced power conversion efficiency.

3. Three-Phase Inverter Circuit

This device is very similar, insofar as its power handling components are concerned, to the rectifier circuit in Figure 67. In addition, a cycloconverter has been added between the inverter and the final output. The advantages of using the cycloconverter in this manner are the following:

1) By using a high frequency inverter, the weight of the transformers (and capacitors) is significantly reduced.

2) The power factor of the inverter circuit is nearly unity regardless of the low frequency ac pump power factor. This basic characteristic of the cycloconverter device is explained in reference 103. A high power factor reduces weight and electrical losses in the inverter. Cesium vapor controlled rectifiers are selected for both inverter and cycloconverter electronic switches.

The over-all efficiency of the pump power supply in Figure 69 is estimated at 87% and the specific weight is 1.6 lbs/kw. This is based on the weights of transformers and cycloconverters as discussed above and the weights of capacitors as reported in reference 104.

4. DC to DC Voltage Converter

This device, shown in Figure 70, comprises a single phase auto-impulse commutated (square wave) inverter combined with a low voltage rectifier. Cesium vapor thyratrons are selected for the inverter circuit switching devices. A center-tapped transformer is used to provide only a single diode forward drop voltage loss in the output circuit. This affords maximum efficiency but results in a higher transformer specific weight than those discussed above. Estimated efficiency is 80% using a cesium vapor diode for the output rectifiers. A reasonable design specific weight is 1.5 lbs/kw. This is somewhat more conservative than values for similar circuits reported in reference 104.

D. Reactive Power

Reactive power delivered to the electromagnetic pumps necessarily carries a weight penalty for these reasons:

1) Increased current in alternator windings, distribution busses, and power conditioning components results in increased losses and/or weight of these components.

2) The total flux in an inductor alternator magnetic circuit is a sensitive function of the machine load power factor. This results from the effects of armature reaction upon the unwound homopolar rotor portion of the magnetic circuit. The weight of the machine, in turn, depends heavily upon the total flux which must be carried by the magnetic circuit. Figures 71 and 72 show the variation of machine weight and efficiency with load for a typical 500 kw inductor alternator design. Figure 73 shows the relationship between percent power factor, kvar reactive power, and kw real power input to the pump.

In a typical turboelectric space power system using ac induction type EM pumps, it is probable that the pumps will be located in close proximity to the generator and that the pump power supply equipment will receive power directly from the alternator. For such a system, the weight penalty assignable to the reactive power load of the EM pumps can be based upon the effects of this load on alternator weight and efficiency. The effects of this reactive power load upon the weight and losses of the frequency converter are, for typical EM pump loads, safely covered by the assumptions of 90% efficiency and one lb/kw for the frequency converter equipment. Additionally, an important characteristic of the cycloconverter type frequency converter is the fact that, although a low power factor load may be placed on the low frequency output of the converter, the load seen by the high frequency power source is a near unity power factor load of varying amplitude. Reference 103 explains this characteristic of the cycloconverter. By connecting several cycloconverter units in parallel operating out of phase with each other, the ideal result of a constant unity power factor apparent load on the high frequency power source can be approached. For the present study, the possibility of high power factor will be ignored, and a reactive power weight penalty will be assigned.

For turboelectric power systems, this weight penalty will be based upon the effects of reactive kva upon alternator weight and efficiency. For thermionic power systems, this weight penalty will be based on the weight of capacitors required to neutralize the pump reactive kva at the high frequency output of the inverter circuit.

1. AC Pumps Applied to Turboelectric Systems

$$\text{KVAR Wt. Penalty} = \frac{\text{Lbs}}{\text{KVAR at Pump Input}} = \frac{\Delta\,(\text{Alternator Wt.})}{\Delta\ \text{KVAR}}$$

$$+ \frac{\Delta\,(\text{Alternator Output})}{\Delta\ \text{KVAR}} \times \frac{\text{Lbs}}{\text{KW Output}}$$

The quantities Δ alternator weight/Δ kvar and Δ alternator output/Δ kvar are evaulated from Figure 71 at a machine power factor of 0.85 (which is assumed to be a reasonable over-all load power factor at the alternator output), with the results that

$$\text{KVAR Wt. Penalty} = \frac{10}{40} + \frac{10}{200} \times 10 = 0.75 \text{ lb/kvar}$$

2. AC Pumps Applied to Thermionic Power Systems

For this application, the reactive kva weight penalty will be based upon the weight of capacitors required to neutralize the lagging power factor of the EM pump load in the inverter circuit. The power conditioning circuit shown in Figure 69, in which a frequency converter is used between a high frequency inverter and the EM pump, will be the basis for calculation. An inverter output phase voltage of 500 and a frequency of 2,000 cps are also assumed.

$$\text{Required Capacitive KVAR} = \frac{E^2}{X_c} = E^2\ 2\ \pi f C \times 1000 = 0.32\ \mu\text{f/KVAR}$$

$$\text{KVAR Wt. Penalty} = \frac{\text{Required Capacitance}}{\text{KVAR}} \times \frac{\text{Lbs}}{\text{Capacitance}}$$

It is estimated that a weight of one lb/μf is a reasonable development goal for high temperature radiation resistance capacitors of the specified voltage and frequency rating. Using this value:

$$\text{Reactive KVA Wt. Penalty} = \frac{0.32 \text{ lb}}{\text{KVAR}}$$

To account for capacitor losses and cooling, this value will be increased approximately 50% to 1/2 lb/kvar. Because of the relatively low value of this weight penalty, further refinement in its evaluation seems unwarranted.

E. Cooling

To define and evaluate basic parameters involved in the computation of cooling weight penalties for electromagnetic pumps and their associated power supply equipment, typical turboelectric and thermionic power system configurations have been defined and analyzed from the standpoint of pump and pump cooling requirements. Figures 74 and 75 show schematic flow diagrams of these two system configurations. Flow rates and pump power levels corresponding to an output capacity of one MW have been determined for these alternate systems. Table 12 summarizes pump and pump power conditioning design data pertaining to these two systems. These data include values for both ac and dc pumps in each of the defined pumping functions estimated from Tables 17-30 using the pump capability parameter concept as discussed in Sections V.C. and D.

The turboelectric system flow network has three main flow loops: 1) primary coolant all liquid flow loop, 2) turbine working fluid two-phase loop, and 3) the all liquid heat rejection loop. (The latter loop has been subdivided for reliability.) In addition, there is a low temperature heat rejection loop powered by an EM cooling pump that transfers heat from a coolant heat exchanger to a low temperature radiator. The coolant in the side of this heat exchanger opposite the low temperature radiator flow loop is turbine working fluid circulated by a turbogenerator shaft mounted pump. This type flow network permits using NaK in all radiator loops and, thus, minimizes the system pre-start freezing problems. The use of EM pumps in the auxiliary system of both the turboelectric and thermionic systems avoids the power plant startup problem of bearing lubrication supply common to rotating pumps.

The thermionic system has two main circuits: 1) primary thermionic reactor anode coolant loop, and 2) the heat rejection loop, which is subdivided for reliability. In addition, there is a low temperature coolant flow loop powered by an EM pump that circulates NaK coolant through the system EM pumps, controls, and power conditioning equipment and through a low temperature radiator. All radiator flow loops employ NaK coolant.

Table 12 provides the information necessary to evaluate the component parts of an over-all pump and pump power conditioning cooling weight penalty. These component parts are the cooling pumping power weight penalty, the cooling radiator and associated connecting plumbing weight penalty, and the weight of cooling pump and related ducting and power conditioning equipment. The Cooling Pumping Power Weight penalty may be defined as:

$$\text{CPPW} = \frac{\text{Pump and Pump PC Cooling Power Wt. Penalty}}{\text{KW Input to All System EM Pump Power Supplies}}$$

TABLE 12. WEIGHT FACTORS FOR SPACE POWER EM PUMPS
(One MW Power Plant)[a]

Pump Function[b]	Pump Power Output, kw[c]	AC Pumps			DC Pumps		
		Eff., %	Power Input, kw[d]	Heat To Coolant, kw[e]	Eff., %	Power Input, kw[d]	Heat To Coolant, kw[e]
Turboelectric System							
Primary Coolant Circulation	6.5	18	36	15	20	32	13
Boiler Feed	3.5	12	29	13	20	18	7.0
Radiator Coolant Circulation	11	16	69	29	20	55	22
Pump Coolant Circulation	0.25	10	2.5	2.5	18	1.4	1.4
Totals	21	--	135	60	--	106	43
Coolant Pump Wt., lb.	60				15		
Thermionic System							
Primary Coolant Circulation	2.6	18	15	6.0	20	13	5.2
Radiator Coolant Circulation	11	16	69	29	20	55	22
Pump Coolant Circulation	0.12	10	1.2	1.2	18	0.6	28
Totals	13	--	85	36	--	69	28
Coolant Pump Wt., lb.	35				12		

[a] All estimates in this table are based on a 1 MW electrical output space power plant.
[b] The main pumping functions in the respective power plants.
[c] Hydraulic power developed by the pump.
[d] Includes power supply losses.
[e] Includes heat load to the cooling system from the pump and its power supply.

The CPPW parameter can also be expressed as:

$$\frac{\text{Power Input to System Cooling Pumps}}{\text{Total Power Input to all System Pump Power Supplies}} \times \text{Power Wt. Penalty}$$

From the data in Table 12, the following numbers may be obtained:

For ac pump application to turboelectric system,

$$\text{CPPW} = \frac{2.5}{136} \times 10 = 0.18 \text{ lb/kw}$$

For dc pump application to turboelectric system,

$$\text{CPPW} = \frac{1.4}{106} \times 10 = 0.13 \text{ lb/kw}$$

For ac pumps in thermionic system,

$$\text{CPPW} = \frac{1.20}{85} \times 9 = 0.13 \text{ lb/kw}$$

For dc pumps in thermionic system,

$$\text{CPPW} = \frac{0.6}{69} \times 9 = 0.08 \text{ lb/kw}$$

From space power system design studies, such as those reported in reference 100, the weight of a heat rejection radiator structure designed for operation in the temperature range of 600 ^{o}F to 800 ^{o}F can be estimated at 2 lbs/kw loss heat. To arrive at a pump and pump power supply cooling weight penalty which is referred to the power input to the pump power supply, the fact that not all the pump and pump power supply losses are transferred to the low temperature radiator coolant must be considered. The pump losses delivered to this coolant as heat are indicated for each pump application defined in Table 12.

$$\frac{\text{Cooling Radiator Wt. Penalty}}{\text{KW power Input to Pumps}} = \frac{\text{2 lbs/kw x Loss Delivered to Coolant}}{\text{Total Power Input to Pump Power Supply}}$$

For the four cases under consideration, this weight penalty is (from Table 12) as follows:

For ac pumps in turboelectric systems,

$$2.0 \times \frac{59.4}{136} = 0.9 \text{ lb/kw}$$

For dc pumps in turboelectric systems,

$$2.0 \times \frac{43.4}{106} = 0.8 \text{ lb/kw}$$

For ac pumps in thermionic systems,

$$2.0 \times \frac{36.2}{85} = 0.85 \text{ lb/kw}$$

For dc pumps in thermionic systems,

$$2.0 \times \frac{27.8}{69} = 0.8 \text{ lb/kw}$$

The quantity: Cooling Pump Weight Penalty/Total Power Input to System Pumps for the four cases of interest from the data in Table 12 are

For ac pumps in turboelectric system,

$$\frac{60}{136} = 0.44 \text{ lb/kw}$$

For dc pumps in turboelectric system,

$$\frac{15}{106} = 0.14 \text{ lb/kw}$$

For ac pumps in thermionic system,

$$\frac{35}{85} = 0.41 \text{ lb/kw}$$

$$\frac{12}{69} = 0.17 \text{ lb/kw}$$

By combining the three components of the pump cooling weight penalty, a total pump cooling weight penalty can be obtained for each of the four cases of interest:

$$\frac{\text{Total Pump and Pump Power Supply Cooling Weight Penalty}}{\text{Total Power Input to System Pump Power Supplies}}$$

For alternating current pumps in turboelectric system,

$$\begin{array}{l} 0.18 \\ 0.90 \\ \underline{0.44} \\ 1.52 \end{array} \simeq 1.5 \text{ lbs/kw}$$

Similarly:

For direct current pumps in turboelectric system $\simeq$ 1.1 lbs/kw

For alternating current pumps in thermionic system $\simeq$ 1.4 lbs/kw

For direct current pumps in thermionic system $\simeq$ 1.1 lbs/kw

Since, obviously, the cooling weight penalty is a small fraction of the pump total equivalent weight, it is reasonable to assume a blanket weight penalty of 1.5 lbs/kw pump and a pump power conditioning cooling weight penalty for all types of EM pumps in either turboelectric or thermionic power systems.

F. Summary of Weights and Penalties

To summarize the results of the preceding analyses, the weights and penalties to be used in the final selection of pumps are presented in Table 13. In the concluding form presented here, all weight items, except the power factor penalty, are evaluated in pounds per kilowatt power input to the pump power supply. The summation renders a simple two-part total that permits easy computation of the weight criteria for pump selection which appear in Section V. Note that the weight penalty varies not only with the type power plant but also with the form of power input.

TABLE 13. WEIGHTS AND PENALTIES FOR EM PUMPS IN SPACE POWER PLANTS

Weight Item	Weights and Penalties			
	Turboelectric System		Thermionic System	
	AC Pump	DC Pump	AC Pump	DC Pump
Power Input, lb/kw	10	10	9	9
Power Supply, lb/kw	1	1	1.6	1.5
Efficiency, %	90	80	87	80
Cooling, Pump and Power Supply, lb/kw	1.5	1.5	1.5	1.5
Power Factor, lb/kvar	0.75	---	0.5	---
Total Wt. Penalties				
Power and Cooling, lb/kw[a]	12.5	12.5	12.1	12
Power Factor, lb/kvar[b]	0.75	----	0.50	---

[a] To be applied to the power input to the pump power supply.
[b] To be applied to the reactive power of the pump only.

V. PUMP SELECTION AND DESIGN

A. Design Guides and Restraints

EM pump design for this program comprised a broad study of a variety of pump types for diverse combinations of pumped fluids, flows, developed pressures, and temperatures. Detailed mechanical designs, requiring complete layouts, stress analysis, temperature distribution analysis, metal joining procedures, etc., have not been made for any of the ratings. To maintain reasonable consistency between designs, preferred ranges and limits for certain sensitive quantities have been established and observed. These quantities and a rationale for their choice are discussed here.

1. Fluid Velocities

Increasing the velocity of the fluid in the pumping section tends to reduce the size and weight of an EM pump. Erosion, hydraulic loss, or cavitation considerations may limit the maximum velocity. With the fluids and the containment materials considered in this study, erosion should not impose any practical limitations. Within the velocity limits for which hydraulic loss is acceptable, from a pump efficiency standpoint, the pump suction pressures specified will provide sufficient static pressure at the entrance to the pumping section to prevent cavitation for all cases, except the condensate boost pump at a rated NPSH of 10 ft and lower. For this application, the fluid velocity must be limited at the pump suction to maintain a static pressure which exceeds the vapor pressure. This can be accomplished, at the cost of additional weight, by using low fluid velocities throughout the pump. The effect of using low fluid velocity is shown in Section V.B. Alternatively, flow passages of varying cross section may be employed to limit the fluid velocity at the pump entrance to prevent cavitation then increase it to the desired pumping velocity as the fluid moves into the pumping section and the static pressure is increased. The design of duct passages of varying cross section appears feasible, but the details have not been developed.

The pump characteristics presented in this report are based on duct velocities selected primarily on the basis of a weight-efficiency compromise. Duct fluid velocities are 20 to 30 ft/sec in the helical pump designs, 30 to 40 ft/sec in the annular and flat pump designs, and 20 to 40 ft/sec in the dc pump designs. These are approximately the same velocities used in presently operative pumps and somewhat less than the fluid velocities in the EM pumps used in the USS Seawolf and the Experimental Breeder Reactor II secondary loop.

2. Duct Wall Thickness

The choice of duct wall thickness was a compromise between efficiency and reliability. Ducts may be either conducting (metallic) or nonconducting (nonmetallic, e.g., ceramic). Nonconducting duct walls of minimum thickness minimize pump losses. Using ceramic materials for duct walls, however, adds extremely difficult problems and certainty of a significantly lower reliability than is realizable with a metallic duct constructed of the material used in the remainder of the system. The losses associated with conducting duct walls of practical thickness in EM pumps are approximately 10% of the power input. All the pump designs reported, therefore, use conducting duct walls constructed of the material selected for the system involved. This avoids bimetallic joints and stresses caused by different coefficients of expansion of the materials and thus contributes to simplicity and reliability.

Pump sizes and pressures are such that metallurgical and fabrication considerations, rather than stress considerations, will determine minimum duct wall thickness in most of the pump ratings. Since duct losses are approximately proportional to duct wall thickness in all EM pumps considered, maximum pump efficiency is associated with minimum duct wall thickness. Electromagnetic pump designs which are ultimately proved for use in space power plants will doubtless have duct wall thicknesses that vary with parameters, such as pump type, duct material, pump size, and fluid pressure. For this study, however, a duct wall thickness of 0.025 in. has been used arbitrarily in all the pump designs reported.

3. Heat Transfer

In electromagnetic devices, winding temperature is usually a major design limitation. Its accurate prediction is also one of the more difficult design tasks, particularly when design proportions, boundary conditions, and thermal circuit materials differ considerably from designs which have been thoroughly tested. In the application of EM pumps in space, the thermal design problem is compounded by the hard vacuum environment which, if permitted to apply in the region occupied by the pump windings, severely affects the transfer of the I^2R loss in the windings to the heat sink. The vacuum also limits the choice of insulating materials to those which will maintain physical and dielectric integrity after prolonged outgassing at operating temperature in vacuum.

In a broad study such as this, a comprehensive investigation of the heat transfer in each pump design considered is not possible. Accordingly, establishing a general approach to heat transfer, which will lead to reasonable, but relatively simple, criteria for thermal design of all the EM pump windings, is necessary. With this background, the following approach to heat transfer was adopted:

1) It is assumed that the windings operate at an average temperature of 750 °F and that the pump coolant is supplied at 600 °F, the bearing and generator coolant temperature in the systems shown in Figures 74 and 75.

2) The winding cavity is completely sealed by a suitable metallic material, e.g., stainless steel. This region is charged with gas, probably nitrogen, at approximately one atmosphere pressure at operating temperature. To minimize the heat flow from the duct to the pump magnetic structure, the pump duct is excluded from the enclosed region.

3) Either the magnetic structure of the pump or the exterior surface of the sealed envelope will be conduction cooled by the liquid metal coolant.

This approach appears reasonable, considering the current state of the art, and can be modified or changed to incorporate advances in related arts as they occur. The approach, however, does have certain disadvantages:

1) The necessity of maintaining a sealed envelope for containing the windings introduces an additional failure mode. The resultant improvement in insulation system reliability and the improved pump performance permitted by the favorable heat transfer realized, however, is believed to more than compensate for this tendency to reduce reliability.

2) In induction pumps, the portion of the metallic envelope in the magnetic field experiences eddy current loss, which is proportional to the wall thickness and the electrical conductivity of the envelope. Since the envelope has no physical connection to the liquid metal system, it may be fabricated from a material having relatively low electrical conductivity. The helical, annular, and flat pump performance data reported are based on an envelope fabricated from austenitic stainless steel with a wall thickness of 0.015 in.

Winding temperature distribution calculations were made for all the final designs reported in Section V.B and the maximum and average temperature rises above the coolant temperature are indicated. These calculations were based on standard heat flow calculational procedures, using computer programs. Pertinent thermal resistivities are cited in Section III.D.

4. Current Densities

No restrictions have been placed on current densities in the fluids, the duct walls, and the stator envelope. These current densities are determined by the pump weight and efficiency design optimization procedure. Pump characteristics, particularly efficiency, weight, and winding temperature, are quite dependent upon the current density in the pump windings. Trial designs and experience suggested that, for induction pumps, winding current densities would be limited by allowable winding temperatures. For helical and flat induction pumps, current densities of approximately 3300 amp/in.^{2} were used; for annular pumps, current densities of approximately 3600 amp/in.^{2} were used. The higher values used in annular pumps reflect slightly better heat transfer from the pump windings because of the shorter lengths of coils external to the slots in the magnetic steel. In dc pumps, the choice of winding current density is based on a weight-efficiency compromise. Trial calculations indicated an optimum in the 4000 to 5000 amp/in.^{2} range, and, therefore, a current density of 4500 amp/in.^{2} was used in all dc pump designs reported.

5. Flux Densities

In electromagnetic devices, the choice of flux density is usually based on a compromise between weight and performance. Using higher flux densities permits lower weight at the cost of a tendency to reduce efficiency and increase winding temperatures. The nonlinearity of the magnetization characteristics of most ferromagnetic materials is such that saturation places a fairly well defined upper limit on the value of the flux density which is practical to use. In certain pumps using distributed windings, such as helical and flat induction pumps, winding end turn considerations, rather than saturation considerations, often limit magnetic tooth and slot proportions. Precise determination of the optimum requires detailed layout and study of each pump type at each rating. In the induction pump designs reported, peak flux densities of 90 to 100 kilolines/in.^{2} and a tooth width to slot width ratio of approximately 0.5 were used. In the dc pumps, peak flux densities of 120 kilolines/in.^{2} were used.

6. Insulation Allowances

Insulation allowances are selected as a compromise between dielectric strength and pump weight. The improvement in pump weight, which may be made by reduction in insulation allowances, is proportional to the ratio of the volume of insulation associated with a conductor to the volume of the conductor itself. Direct current pump windings operate at voltages in the order of one volt, and each conductor normally has a cross section in the order of one in.^{2}. Insulation allowances are very low, and pump weight is not sensitive to proportionally large changes in insulation allowances. Consequently, insulation allowances, as such, are included in the general requirement that the area in the dc magnet through which the series windings pass be twice the maximum total cross-sectional area of the conductor passing through the area (also known as the window area).

System considerations lead to the design of ac induction pumps for voltages of approximately 100 volts. Pump current is relatively low, therefore, and insulation volume is a substantial fraction of conductor volume. Based on an appraisal of available insulating materials, anticipated environmental conditions, and experience, insulation allowances of 0.005 in. between strands and 0.0275 in. from conductor to slot walls were chosen for all induction pumps reported. These allowances are consistent with the dielectric strength of nitrogen, proposed for the stator winding cavity in Section III.D.

7. Frequency

The general study of EM pumps reported in Section III.B indicates the desirability of low frequency as a source of power for EM pumps. Accordingly, since frequency reduction is required, the designs are based on a free choice for frequency. In practice, trial designs were made for most ratings at 50, 100, 200 and 400 cps and final selections were made from this group.

B. Characteristics of Selected EM Pumps

Table 2 lists the pump applications to be studied in this program and the ranges for the various parameters. A series of separate pump designs were made for each application with parameters chosen systematically from the study ranges specified. The specific parameters for which separate designs were made for all applications are shown in Table 14. Designs were made for seven pressure-flow-temperature combinations for each application. To illustrate the effect of very low suction pressure on pump weight and performance additional designs were made for the condensate boost application. Design and performance calculations are reported for at least one polyphase induction pump type for the seven ratings indicated. Similar calculations are reported for dc conduction pumps for the first five ratings.

Primary emphasis was on the design point rating, i.e., the rating at which all parameters have design point values. Design calculations for the design point were made for at least three frequencies between 50 cps and 400 cps for the induction pump type selected. At each frequency, an optimum configuration was derived by varying the design parameters systematically to determine the combination for which pump weight plus ten times the power input in kilowatts was minimum. Thus, a first optimization was obtained based on the fact that pump weight and power penalty constitute the major part of the weight criterion of an EM pump. Only those configurations with proportions deemed reasonable for construction were considered. Optimum designs for dc conduction pumps were derived similarly. Optimization of the other ratings in the study range was conducted in a similar manner

TABLE 14. PUMP DESIGN PARAMETER COMBINATIONS

Rating Number	FLOW			PRESSURE			TEMPERATURE		
	Min.	Design Pt.	Max.	Min.	Design Pt.	Max.	Min.	Design Pt.	Max.
1		X			X			X	
2	X				X			X	
3			X		X			X	
4		X		X				X	
5		X				X		X	
6		X			X		X		
7		X			X				X

but fewer frequencies were considered and the process was not carried as far as for the design point ratings. Computations were made on approximately 1000 designs. Of these, 89 are reported in the following discussion. Various physical properties of the liquid metals and the duct materials were taken from the curves in Section III.D. Other design parameters were based on the design guides in Section V.A.

1. Condensate Boost Pump: Potassium

Performance characteristics for nineteen EM pump designs for the condensate boost pump application are summarized in Table 15. Designs 1 through 5 are for the design point. Designs 6 through 17 are for other ratings selected from the study range, and designs 18 and 19 are for the design point with the fluid velocity reduced severely to prevent cavitation when the suction pressure is very low.

TABLE 15. CHARACTERISTICS OF SELECTED EM PUMP DESIGNS
I Turboelectric Condensate Boost: Potassium

Selected Characteristics[a]							Resultant Characteristics[b]								
Design No.	Pump Type[c]	Fluid Temp., °F	Flow, gpm	Press. Rise, psi	Fluid Vel., ft/sec	Power Freq., cps	Power Output, kw[d]	Power Input, kw	Eff., %	PF, %	Cooling Load, kw	Winding Temp., °F Max.	Winding Temp., °F Av.	Pump Wt., lbs	Sp. Wt., lbs/kw[e]
1	HI	1200	16	30	22	100	0.20	2.0	10	49	1.5	790	750	33	160
2	↓	↓	↓	↓	24	150	↓	1.9	10	40	1.3	780	740	30	160
3*					25	200		2.0	10	43	1.1	760	720	26	130
4					27	400		2.8	7	46	1.1	760	730	22	110
5	DC		↓		27	---		1.5	14	--	0.6	---	---	9	44
6	HI		11		22	200	0.14	1.4	10	34	---	---	---	20	150
7	DC		11		27	---	0.14	1.1	12	--	---	---	---	7	51
8	AI		130		29	50	1.6	7.7	21	44	---	---	---	140	84
9	↓		↓		39	100	↓	8.8	19	43	---	---	---	76	47
10	↓				40	200		8.9	18	28	---	---	---	87	54
11	DC		↓	↓	27	---		7.2	23	--	---	---	---	69	43
12	HI		16	3.0	11	200	0.02	0.7	3.0	44	---	---	---	11	540
13	DC		↓	3.0	27	---	0.02	0.3	6.0	--	---	---	---	3	120
14	HI			60	28	200	0.41	3.0	14	34	---	---	---	38	90
15	DC	↓	↓	60	27	---	0.41	2.6	16	--	---	---	---	13	32
16	HI	1000	15	30	24	200	0.20	2.0	10	46	---	---	---	25	120
17	↓	1400	16	↓	26	200	0.21	2.1	10	39	---	---	---	27	130
18		1200	↓		13	100	0.20	2.5	8.0	53	---	---	---	38	190
19	↓	1200	↓	↓	15	200	0.20	2.7	7.5	45	---	---	---	32	160

*Optimum Design. See Table 25.

[a]Most significant input to the performance prediction procedures. Based on design requirements Table 3 and design guides Section V.A.

[b]Most significant output from the performance prediction procedures.

[c]HI = helical induction; DC = direct current conduction; AI = annular induction; FI = flat induction; SPI = single phase induction.

[d]Hydraulic power developed by the pump.

[e]"Pump Weight" divided by "Power Output" as shown in this table.

a. Description of Pump Designs, Design Point

1. Helical Induction Pump. Designs 1 through 4 in Table 15 are helical induction pumps designed for 100, 150, 200, and 400 cps, respectively. In general, the designs for the higher frequencies tend to be somewhat lighter and less efficient, although the changes are slight over this frequency range. As indicated in Section V.D, pump design 3 at 200 cps gives the best system performance of the induction pump designs for the design point. The distribution of the losses for this design is indicated in Table 16. Figure 76 is a reduced size layout. Performance curves are shown in Figure 77. Other helical induction designs for the design point are quite similar to that in Figure 76. Many of the detailed design features in Figure 76, such as weld preparations, would doubtless be modified if a complete mechanical design were made.

The duct is AISI Type 316-L SS. The duct assembly comprises an outer cylinder, an intermediate cylinder in which helical passages are machined, an assembly of magnetic core laminations, an inner cylinder, end members connecting and closing the cylinders at the ends, and inlet and outlet connections. The radial wall thicknesses of both outer and intermediate duct cylinders are 0.025 in. The helical passages are approximately square with a side width of approximately 0.34 in.; there are two such passages hydraulically in parallel. The axial width of the boundaries of the flow passages is 0.02 in. The inner cylinder is not linked by the magnetic field and, hence, it may have any convenient wall thickness. The pipe illustrated is 3/4 in. schedule 40. The core is composed of one-piece laminations with the principal planes of the laminations perpendicular to the axial centerline of the duct. Any of the available cobalt iron alloys appear adequate, since the flux density may be maintained at 50,000 lines/in.^{2} without significant weight penalty. Because of the low flux density and low frequency, lamination thickness is not critical. An inorganic interlaminar insulation which is not subject to continued outgassing or reaction with the magnetic core at 1200 °F is required. Possible materials are discussed in Section III.D.

The stator assembly comprises the cooling coil assembly, which is welded or brazed to the radial periphery of the cylindrical frame; the cylindrical frame; the stator laminations; the stator winding; and the stator can. The cooling coil assembly, which is made of stainless steel tubing 3/8-in. OD by 0.028-in. wall thickness, constitutes the heat sink for the pump. It is supplied with NaK at 600 °F. Pump winding temperature is relatively insensitive to coolant flow rate at flows of one gpm or higher.

Since the cylindrical frame must support the stator lamination assembly and contain the gas in the stator winding cavity, its design is determined by structural considerations. A nominal wall thickness of 1/8 in. has been used and, to simplify the stator frame to stator can connection, austenitic stainless steel, also used for the stator can, is preferred.

TABLE 16. POWER DISTRIBUTION FOR CONDENSATE BOOST PUMP (Design Point; Helical Induction Application; 200 cps)[a]

Item	Design Point Data	
	KW	Percent Input
Pump Output	0.20	10
Stator Winding Loss	0.52	26
Secondary (Fluid) Loss	0.88	43
Iron Loss	0.2	10
Duct Wall Loss (0.025 in.)	0.11	5
Stator Can Loss	0.05	3
Hydraulic Loss	0.07	3
Total Power Input	2.03	100

[a]See Design 3, Table 15.

The stator laminations will be at a temperature of approximately 700°F. As indicated in Part A of this section; flux densities are approximately 90,000 lines/in.^{2}. Because an important function of the stator laminations is to conduct the losses to the heat sink, high thermal conductivity is desirable. The low silicon magnetic steels, common iron, or the cobalt-iron alloys afford a satisfactory combination of thermal and magnetic properties. Calculations are based on common iron. Lamination thickness is not critical and may be 0.025 in. or less. A stable interlaminar insulation is required to avoid pressure buildup in the stator winding cavity and to avoid interlaminar eddy current.

The stator winding is two pole, three phase, lap wound, two coil sides per slot. Eighteen slots, 0.32-in. wide by 0.75-in. deep, are used and the individual coils are form wound using rectangular wire. (Random wound coil construction using round wire is possible and may prove preferable.) A total conductor cross section of 2.65 in.^{2} is used, with a mean length of turn of 26 inches. Performance calculations are based on copper windings with a resistivity of 1.75 μ-ohm-in. at 750°F. Ground wall insulation and insulation between turns are assumed to be 0.025 in. and 0.005 in., respectively. This design has eight turns per coil. When the coils are wye connected, one circuit per phase, the line voltage is 76 volts and the line current 31.5 amp. The voltage and current combination may be changed by changing the number of turns per coil. The stator winding cavity is filled with nitrogen at approximately one atmosphere of pressure at 700°F. Section III.D and Section V.A discuss electrical conductors, electrical insulation, and dielectric gases further. Eddy currents produce loss in the stator can. Austenitic stainless steel, 0.015-in. thick, is chosen for the can. Power is supplied to the stator windings through a ceramic to metal seal assembly in the stator envelope.

The thermal insulation between the pump duct and the stator can consists of alternate layers of austenitic stainless steel cloth and strip that is laminated to reduce eddy current loss. Strip dimensions are approximately 0.003-in. thick by 0.3-in. wide; cloth thickness per layer, approximately 0.010-in. thick. Thus, about four layers of the strip and cloth combination may be placed in the 0.05 in. available for thermal insulation. Section III.D gives data on similar insulation in air.

The velocity head associated with the fluid velocity of 25 ft/sec in the pump duct is 9.8 ft. The design point NPSH of 10 ft is not sufficient to insure the absence of cavitation. As indicated in Section III.B, if only 10 ft NPSH is available, the duct entrance velocity should be limited to approximately 18 ft/sec. To avoid cavitation with an NPSH of 10 ft, either of two approaches appear feasible. In the most direct approach, the pump duct velocity is simply limited to 18 ft/sec. This results in somewhat greater pump weight and lower efficiency. Line 19, Table 15 indicates approximate characteristics for a 200 cps pump for the design point characteristics and a duct velocity of 15 ft/sec. Compared with design 3, this pump has a weight increase of approximately 23% and a power input increase

of approximately 31%. Because the design procedure is not sufficiently precise to indicate accurately such a small change in inlet velocity, specific design calculations were not made for a pump design with a duct velocity of 18 ft/sec.

In another approach, variable cross-section helical passages may be used to limit the fluid velocity to 18 ft/sec, or less, in the entrance region of the pump until an increase in pressure is developed by the electromagnetic reaction. Then, the cross section of the passages may be reduced until the fluid velocity is consistent with low pump weight and power input. Although this approach has not been used in designs developed to date, it appears feasible.

Figure 77 shows developed pressure, power input, and power factor as a function of flow for pump design 3 in Table 15. Developed pressure is shown for four different voltages. Power input varies as the square of the voltage and is illustrated for rated voltage. Power factor is independent of voltage. Both power input and power factor are relatively insensitive to flow. The shape of the pressure-flow rate curves illustrates the suitability of this pump for control of flow by voltage variation.

Table 16 shows the disposition of the power input to pump design 3. The predominant losses occur in the stator winding and as resistive loss in the potassium. To a good approximation, duct losses are directly proportional to radial duct wall thickness and inversely proportional to the electrical resistivity of the duct material. That little will be gained by using a thinner duct wall or a material of higher resistivity is apparent. Because of its low resistivity, however, columbium as a duct material introduces significant additional duct wall loss, unless the wall thickness is reduced.

2. DC Conduction Pump. Calculated performance characteristics and pump weight for a dc conduction EM pump for the design point rating are given in Table 15, design 5. Figure 78 shows several views of this pump configuration. This pump is of the uncompensated series excited conduction type with 1-1/2 effective turns in the exciting winding. At the rated point, a current of 2310 amp is required at 0.63 volt.

The duct material is AISI Type 316-L SS. The cross-sectional dimensions of the fluid passage are 0.125 in. by 1.5 in. The length of the pumping section, in the direction of flow, is 2 in. The wall thickness is 0.025 in. The magnet operates at the approximate temperature of the fluid pumped, 1200^{o}F, and, hence, no thermal insulation is required between the duct and the magnet. To prevent leakage currents in the magnets, however, electrical insulation is required. A space of 0.003 in. on either side of the duct is allowed for this insulation. The insulation is not specified, but any mechanically suitable ceramic would be adequate. Two layers of metallic foil, seal welded at the edges and ceramic coated on the inner surfaces, could also be used at some increase in insulation thickness but with a negligible change in performance.

The fluid streams in the inlet and outlet flow transition sections at either end of the pumping section are separated into three sections to limit the fringing current in the fluid and the duct walls. Thus, separate sections are parelleled by headers several diameters removed from the pumping section. In Figure 78 the three flow sections of the transition regions are depicted as separate in the pumping section, with the adjacent walls welded solidly together. If the metallic walls between adjacent flow passages in the pumping section are omitted, leaving one rectangular passage, performance will be improved slightly. Detailed design and development work is necessary to select the best arrangement in this region.

The magnet is cobalt-iron, probably 35% cobalt. Flux densities are 43,000 lines/in.^{2} and 120,000 lines/in.^{2} in the air gap and the magnet, respectively. No conduction cooling of the magnet is shown in Figure 78, Section III.D discusses properties and limitations of various magnetic materials at high temperatures. Although operation at 1200 °F appears feasible, the magnet temperature may be reduced readily, if this becomes desirable, by using cooling coils attached to the periphery of the magnet in conjunction with thermal insulation between duct and magnet surfaces. Pump performance and weight would be adversely affected, but only slightly.

The performance shown for design 5, Table 15, is based on series windings of the size illustrated in Figure 78 having an electrical resistivity of 2.37 μ-ohm-in., the resistivity of copper at 1200 °F. In the illustration, the windings are cooled by radiation to space. Elementary calculations indicate that such a cooling arrangement may be feasible at the selected current density of 4500 amp/in.^{2}, assuming that the pump is located so that the windings can effectively radiate to space or to objects at temperatures considerably less than 1200 °F. If such a location is infeasible, the windings may be conduction cooled by a liquid metal at an appropriate temperature less than 1200 °F in tubes attached to the surface of the windings or enclosed within the surface of the windings. The winding-electrode joint region poses a difficult design problem In the design illustrated, the electrode is an extension of the duct and, hence, is AISI Type 316-L SS. The electrode may be an integral part of the duct structure or it may be welded to the sides of the duct. The winding is welded or brazed to the electrode in the joint configuration illustrated to provide maximum contact area. This leads to low current densities in the joint and electrode area; hence, low loss, low temperature rise, and low voltage drop in this region. This concept involving a bimetallic joint with abrupt changes in cross-sectional area of adjoining parts, and the development and demonstration of a reliable design in a formidable task.

b. Pump Requirement Parameter Range. Performance for EM pumps designed for various ratings over the study range (Table 14) is shown in Table 15 under design 6 through 17. In all these designs, duct velocity was chosen without regard for the specified design point NPSH of 10 ft. Rather, the basis for selecting velocity was the efficiency-weight trade-off. It is assumed that the duct passages can be made larger in the inlet section of the pumping region so that cavitation can be avoided with an NPSH of 10 ft. Lines 18 and 19 show performance calculations for designs utilizing much lower fluid velocities than those derived from an efficiency-weight compromise.

Except those whose performance is given by lines 8 through 10, all designs covered in Table 15 are either the helical induction type or the dc series excited conduction type. Although individual dimensions differ greatly, the general appearance and arrangement of these pump designs is similar to that illustrated in Figures 77 and 78. Because the pump rating applicable to designs 8,, 9 and 10 involves a flow-pressure combination which is better suited to the annular induction pump than the helical induction pump, designs of the annular induction type were chosen for this rating. This type pump is shown in Figure 79 and described below.

2. Radiator Coolant Pump: NaK

a. Description of Pump Designs, Design Point. The design point pressure flow combination for this pump is such that induction pumps of both annular and helical types are applicable. Accordingly, performance calculations were made for designs for both types. Design and performance calculations were made for power supply frequencies of 50, 100, 200, and 400 cps. Table 17 lists the most important results of these calculations. At equivalent or slightly lower weights, the best annular designs have somewhat better performance than the best helical designs. The choice, however, is narrow.

1. Annular Induction Pump. Designs 1 through 4 in Table 17 are annular induction pump designs for 50, 100, 200, and 400 cps, respectively. The efficiency is a maximum for the 100 cps design (line 2). Pump weight is highest for the 50 cps design. It decreases rapidly with increasing frequency to 200 cps but rises slightly for the 400 cps design. The best combination of efficiency and weight is at 100 to 200 cps. The 200 cps design, described briefly below, is the basis for the illustration in Figure 79, the loss distribution in Table 18 and the performance characteristics curves in Figure 80.

The duct is AISI Type 316-L SS. The duct assembly comprises an outer cylinder with a diameter of approximately 1.3 in., an inner cylinder with a diameter of approximately 1.0 in., a magnetic core sealed within the inner cylinder, and a means of maintaining the inner cylinder concentric with the outer cylinder. The wall thickness of each cylinder is 0.025 in. Thus, the flow passage is an annulus of mean diameter 1.15 in. and radial

TABLE 17. CHARACTERISTICS OF SELECTED EM PUMP DESIGNS
II Turboelectric Radiator Coolant: NaK
V Thermionic Radiator Coolant: NaK

Selected Characteristics[a]							Resultant Characteristics[b]								
Design No.	Pump Type[c]	Fluid Temp., °F	Flow, gpm	Press. Rise, psi	Fluid Vel., ft/sec	Power Freq., cps	Power Output, kw[d]	Power Input, kw	Eff., %	PF, %	Cooling Load, kw	Winding Temp., °F Max.	Winding Temp., °F Av.	Pump Wt., lbs	Sp. Wt., lbs/kw[e]
1	AI	1200	60	25	25	50	0.66	5.05	13	0.43	2.4	730	720	120	180
2	↓	↓	↓	↓	32	100	↓	4.51	15	0.39	2.0	740	720	52	79
3*	↓	↓	↓	↓	40	200	↓	5.36	12	0.39	1.7	750	730	38	58
4	↓	↓	↓	↓	37	400	↓	6.53	10	0.31	1.6	780	740	41	62
5	HI	↓	↓	↓	21	50	↓	5.15	13	0.41	3.4	910	850	92	140
6	↓	↓	↓	↓	24	100	↓	5.36	12	0.38	2.7	830	780	66	100
7	↓	↓	↓	↓	25	200	↓	7.19	9	0.46	2.5	830	770	51	77
8	↓	↓	↓	↓	26	400	↓	11.3	6	0.49	2.6	780	730	58	88
9	DC	↓	↓	↓	39	---	↓	4.35	15	----	1.9	---	---	19	29
10	DC	↓	↓	↓	29	---	↓	3.41	19	----	1.3	---	---	27	41
11	HI	↓	30	↓	23	100	0.33	2.96	11	0.31	---	---	---	51	150
12	DC	↓	30	↓	34	---	0.33	2.47	13	----	---	---	---	11	33
13	AI	↓	360	↓	30	50	3.9	18.3	22	0.47	---	---	---	240	63
14	↓	↓	↓	↓	33	100	↓	19.8	20	0.25	---	---	---	190	48
15	↓	↓	↓	↓	42	200	↓	24.6	16	0.28	---	---	---	140	37
16	DC	↓	↓	↓	29	---	↓	17.5	23	----	---	---	---	150	38
17	AI	↓	60	10	27	100	0.26	2.55	10	0.42	---	---	---	32	120
18	AI	↓	↓	↓	35	200	↓	3.02	9	0.35	---	---	---	23	89
19	HI	↓	↓	↓	18	100	↓	3.48	7.5	0.36	---	---	---	54	210
20	DC	↓	↓	↓	21	---	↓	1.70	15	----	---	---	---	18	69
21	AI	↓	↓	100	36	100	2.6	15.3	17	0.35	---	---	---	160	61
22	AI	↓	↓	↓	43	200	↓	16.2	16	0.34	---	---	---	98	38
23	HI	↓	↓	↓	32	100	↓	12.1	22	0.26	---	---	---	170	65
24	DC	↓	↓	↓	26	---	↓	12.0	22	----	---	---	---	100	39
25	AI	1000	↓	25	39	200	0.66	5.13	12	0.39	---	---	---	36	59
26	AI	1300	↓	25	41	200	0.66	5.65	12	0.31	---	---	---	42	64

*Optimum Design. See Tables 26 and 29.

See Table 15 for applicable footnotes.

TABLE 18. POWER DISTRIBUTION FOR RADIATOR COOLANT PUMP (NAK)
(Design Point; Annular Induction Application; 200 cps)[a]

Item	Design Point Data	
	KW	Percent Input
Pump Output	0.66	12
Stator Winding Loss	0.81	15
Secondary (Fluid) Loss	1.71	32
Iron Loss	0.3	6
Duct Wall Loss (0.025 in.)	1.23	23
Stator Can Loss	0.45	8
Hydraulic Loss	0.2	4
Total Power Input	5.36	100

[a]See design 3, Table 17.

depth 0.15 in. In the illustration, the core is depicted as comprising an assembly of axially oriented square wires of cobalt-iron alloy. Alternatively, laminations, which are oriented with the planes containing the major dimensions passing through, or near, the axis of the pump, can be used. Core material and interlaminar insulation requirements are the same as those discussed in Section V.B.1. The inner duct cylinder and core assembly are subject to axial forces transmitted from the fluid, axial forces caused by eddy currents in the cylinder walls, and radial magnetic forces proportional to the radial offset of the assembly from the central position in the stator bore. All these forces are modest. The positioning means illustrated in Figure 79 provides axial flexibility to avoid high stresses caused by differential expansion. The pump duct assembly is not connected mechanically to the stator assembly since performance is not affected by small changes in the axial position of the duct assembly.

The stator assembly comprises the cooling jacket on the radial periphery of the frame, the frame, the stator laminations, the stator winding, and the stator can. The cooling jacket illustrated permits passing the 600 °F NaK coolant across the entire radial periphery of the frame. Obviously, other arrangements, such as the cooling coils illustrated in the preceding section, are possible. The calculated heat flow to the coolant is 1.7 kw and, hence, a flow of 2 gpm will give a coolant temperature rise of approximately 35 °F. The stator frame serves principally to support the cooling jacket and the stator can. For compatibility with the stator can and the coolant, austenitic stainless steel is selected for the frame. Considerations governing the choice of stator laminations, interlaminar insulation, and dielectric gas in the stator winding region are similar to those discussed in Section V.B.1, and the choices are identical.

The stator winding is six pole, three phase, one coil side per slot, two slots per phase per pole. The coils are toroidal in form with eighteen turns per coil. Each turn consists of one strand of rectangular wire 0.075 in. by 0.135 in in cross section. Ground insulation and turn-to-turn insulation are 0.025 in. and 0.005 in. thick, respectively. Windings are assumed to be copper with a resistivity of 1.75 μ-ohm-in. at 750 °F. Winding interconnections are made at the outside diameter of the coils. When the windings are wye connected, one circuit per phase, a line voltage of 152 volts and a line current of 56 amp are required for the design point rating. The voltage and current combination may be changed by changing the number of turns per coil and the connection arrangement. Sections III.D and V.A discuss electrical conductors, electrical insulation, magnetic materials, and dielectric gases further. The stator can passes through the magnetic field in the stator bore and, hence, experiences loss caused by eddy currents. Austenitic stainless steel 0.015 in. thick is chosen for the stator can. Power is supplied to the windings through ceramic to metal seals in the stator envelope.

Thermal insulation with the same construction and thickness described in Section V.B.1 is located in the space between the duct outside diameter and the stator can. The fluid velocity in the duct is 40 ft/sec. The design point suction pressure of 30 psia is sufficient to prevent cavitation.

Table 18 gives the loss distribution. The resistive loss in the NaK pumped is the predominant loss; duct wall loss and stator winding loss are next in magnitude. The performance curves shown in Figure 80 are similar to those for the condensate boost pump discussed in Section V.B.1.

2. Helical Induction Pump. Designs 5 through 8 in Table 17 are helical induction pump designs for 50, 100, 200, and 400 cps, respectively. Pump efficiency is best for the 50 cps design; it decreases with increasing frequency for the 100, 200, and 400 cps designs. Pump weight is a minimum for the 200 cps design. The 100 cps design, line 6, offers the best combination of efficiency and weight. Layouts have not been made for these designs. Aside from dimensional changes, however, the general arrangements, materials choices, power disposition, and performance characteristic curves are similar to those cited in Section V.B.1, Figures 76 and 77, and Table 16.

3. DC Conduction Pump. Designs 9 and 10 in Table 17 are uncompensated series excited dc conduction pump designs. Design 9 is light weight with relatively low efficiency, while design 10 is heavier with higher efficiency. Evaluated on a 10 lbs/kw input basis, they appear to be about equally attractive. These designs illustrate the trade-off relationship for weight and efficiency.

A layout has not been made for a dc conduction pump for this rating. Both designs 9 and 10, Table 17, however, have 1-1/2 turns in the exciting winding and have the same general arrangement and materials as those illustrated in Figure 78 and described in Section V.B.1. The calculated terminal voltage and current combination for the designs are 0.69 volt-6290 amp, and 0.7 volt-4863 amp, respectively.

b. Pump Requirement Parameter Range. Performance for EM pumps designed for various ratings over the study range (Table 14) is shown in Table 17, designs 11 through 26. For each specific pressure flow combination, designs were made for a dc conduction pump and either helical or annular, or both, induction pumps. For most ratings, designs were made for more than one frequency. Detailed comparisons of performance and the effect of changes in ratings are best derived directly from Table 17. As expected, designs for larger ratings have higher efficiency and lower specific weight than those for smaller ratings. Power factor varies little for the various induction pump designs for which performance is tabulated.

The lowest value of suction pressure specified in the study range is 20 psia. At 1300 ^{o}F, the vapor pressure of NaK is 6.5 psi and, hence, the suction pressure exceeds the vapor pressure by 13.5 psi, or 44.3 ft. Assuming that the velocity head at the duct inlet should not exceed one half this head, 22.2 ft, inlet duct velocity is limited to 26.7 ft/sec. Although this is somewhat less than some duct velocities listed in Table 17, it is sufficiently close that the duct velocity could be reduced to this value with little change

in weight and performance. As illustrated by designs 3 25 and 26 the effect of changes in NaK temperature on pump performance and weight over the specified study range is slight. Layouts have not been made for these designs. In general arrangement and materials choice, pumps for these ratings would be quite similar to pumps of the same type which have been illustrated and described.

3. Radiator Coolant Pump: Lithium

a. Description of Pump Designs, Design Point.

1. Helical Induction Pump. Of the induction pump applications, the helical induction pump is best suited to the design point pressure flow combination for this application. Accordingly, designs 1 through 4, Table 19, are helical induction pump designs for 100, 150, 200, and 400 cps frequencies. A comparison of performance characteristics and weight for these designs shows that both pump weight and efficiency decrease with increasing frequency. On a weight basis, allowing 10 lbs/kw, the 100, 150, and 200 cps designs are equivalent; the 400 cps design, however, because of low efficiency, is definitely inferior. Table 20 and Figure 81 show the distribution of losses and the performance characteristics curves, respectively, for design 1, Table 19. A layout has not been made for this design. In general arrangement, approximate size, and materials choice (except the duct material), it is very similar to the condensate boost pump illustrated in Figure 76

The duct material is Cb-1Zr. Outer and inner duct cylinders have diameters of 2.65 in. and 1.7 in., respectively. Duct wall thicknesses are 0.025 in., and the axial thickness of the members separating the helical flow passages is 0.02 in. The two flow passages, hydraulically in parallel, are square in cross section with a side width of 0.44 in. The inner core and the stator assembly are similar to those detailed in Section V.B.1. Various combinations of line current and voltage, consistent with the power input and power factor indicated for design 1, Table 19, may be achieved by proper selection of the turns per coil and the winding interconnection. Although the detailed properties of the electrical insulation will impose some restriction, it is anticipated that line voltages up to 100 volts or so may be used without incurring a significant penalty in pump weight or performance.

The loss distribution is given in Table 20. The principal losses occur in the stator windings and as resistive loss in the lithium. Although the duct resistivity is quite low, duct loss has been kept at a relatively low value. This is largely attributable to the low resistivity of lithium. Potassium or NaK pumps with columbium ducts would tend to have considerably higher per unit duct loss. The specified suction pressure of 30 psia is sufficient to avoid cavitation at the duct velocities used. The characteristics curves shown in Figure 81 are similar to those discussed in Section V.B.1.

TABLE 19. CHARACTERISTICS OF SELECTED EM PUMP DESIGNS
III Turboelectric Radiator Coolant: Lithium
VI Thermionic Radiator Coolant: Lithium

Selected Characteristics[a]							Resultant Characteristics[b]								
Design No.	Pump Type[c]	Fluid Temp., °F	Flow, gpm	Press. Rise, psi	Fluid Vel., ft/sec	Power Freq., cps	Power Output, kw[d]	Power Input, kw	Eff., %	PF, %	Cooling Load, kw	Winding Temp., °F Max.	Winding Temp., °F Av.	Pump Wt., lbs	Sp. Wt., lbs/kw[e]
1*	HI	1200	31	20	25	100	0.27	2.1	13	0.55	1.6	780	740	33	120
2	↓	↓	↓	↓	29	150	↓	2.4	11	0.53	1.5	790	750	29	110
3					28	200		2.5	11	0.53	1.5	770	730	28	110
4	↓				33	400		3.8	7	0.47	1.5	760	720	26	98
5	DC		↓		20	---		1.8	15	----	0.8	---	---	13	49
6	HI		15		27	200	0.13	1.2	11	0.38	---	---	---	18	120
7	DC		15		22	---	0.13	1.2	11	----	---	---	---	7	45
8	AI		180		30	50	1.6	7.5	22	0.53	---	---	---	98	61
9	↓				38	100		8.5	19	0.47	---	---	---	58	36
10	↓				44	200		9.8	16	0.38	---	---	---	56	35
11	AI				33	100		9.8	16	0.59	---	---	---	78	49
12	DC		↓	↓	24	---		7.5	22	----	---	---	---	70	44
13	HI		31	10	25	200	0.13	1.6	8.5	0.33	---	---	---	21	160
14	DC			10	22	---	0.13	1.1	12	----	---	---	---	8	60
15	HI			60	25	100	0.80	4.0	20	0.27	---	---	---	59	74
16	HI			↓	34	200		4.9	16	0.50	---	---	---	47	59
17	DC	↓	↓		24	---	↓	4.7	17	----	---	---	---	34	43
18	HI	1000	30	20	28	200	0.26	2.6	10	0.54	---	---	---	27	100
19	HI	1500	32	20	29	200	0.28	2.5	11	0.52	---	---	---	29	110

*Optimum Design. See Tables 27 and 30.

See Table 15 for applicable footnotes.

TABLE 20. POWER DISTRIBUTION FOR RADIATOR COOLANT PUMP (LITHIUM)
(Design Point; Helical Induction Application; 100 cps)[a]

Item	Design Point Data	
	KW	Percent Input
Pump Output	0.27	13
Stator Winding Loss	0.70	33
Secondary (Fluid) Loss	0.65	31
Iron Loss	0.15	7
Duct Wall Loss (0.025 in.)	0.22	11
Stator Can Loss	0.03	1
Hydraulic Loss	0.08	4
Total Power Input	2.10	100

[a]See design 1, Table 19.

2. DC Conduction Pumps. Design 5, Table 19, is a series excited dc conduction pump for the design point rating. A layout has not been made for this design, but, in general arrangement and materials choices (except the duct material, which is Cb-1Zr), it is similar to the design described in Section V.B.1 and illustrated in Figure 78. The calculated terminal voltage and current for this design are 0.44 volt and 4,086 amp.

b. Pump Requirement Parameter Range. Performance for EM pumps designed for various ratings over the study range (Table 14) is shown in Table 19, designs 6 through 19. For each specific pressure flow combination, designs were made for a dc conduction pump and either helical or annular induction pumps. In some cases, induction pump designs were made for more than one frequency. For the configuration combining design point pressure and maximum flow requirement, annular induction pumps were designed both for a straight-through duct configuration, illustrated in Figure 79, and, since it offers several attractive features, a reverse flow configuration, illustrated in Figure 82. This latter configuration is design 11, Table 19. Perhaps the most attractive aspect of this design is the fact that the pump duct may be completely isolated from pipe reactions transmitted from the radiator coolant loop, thus improving reliability and simplifying loop arrangement.

Detailed comparisons of performance and the affect of changes in ratings are best made directly from Table 19. As expected, designs for larger ratings have higher efficiency and lower specific weight than designs for smaller ratings. Power factor varies little for the various induction pump designs. The lowest value of suction pressure specified is 20 psia. This is sufficient to avoid cavitation for all the designs tabulated. As indicated by designs 3, 18, and 19, Table 19, the effect of lithium temperature on pump performance and weight over the specified study range is slight.

Since the helical induction, annular induction, and dc conduction pump designs reported in this section are similar in general arrangement and features to those described and illustrated in preceding sections of this report, layouts for these designs have not been made. Figure 82 does show the annular induction pump with reverse flow, which has not been illustrated previously. Except for the reverse flow feature and the Cb-1Zr duct, this design is similar in arrangement and materials choices to the annular induction pump design described in Section V.B.2.

4. Primary Coolant Pump: Lithium

a. Description of Pump Designs, Design Point. Designs were made for flat induction pumps, annular induction pumps, single phase induction pumps, and dc conduction pumps for the design point rating. Performance and weight for several such designs are indicated in Table 21, designs 1 through 8. The dc conduction pump shows both the highest efficiency and the lowest weight. The pump output power for this application is greater than that for the other applications, hence higher efficiency and lower specific weight

TABLE 21. CHARACTERISTICS OF SELECTED EM PUMP DESIGNS
IV Thermionic Primary Coolant: Lithium

Selected Characteristics[a]							Resultant Characteristics[b]								
Design No.	Pump Type[c]	Fluid Temp., °F	Flow, gpm	Press. Rise, psi	Fluid Vel., ft/sec	Power Freq., cps	Power Output, kw[d]	Power Input, kw	Eff., %	PF, %	Cooling Load, kw	Winding Temp., °F Max.	Winding Temp., °F Av.	Pump Wt., lbs	Sp. Wt., lbs/kw[e]
1	FI	1700	640	6	25	50	1.7	14	12	0.49	9.9	910	830	270	160
2	↓	↓	↓	↓	30	100	↓	14	12	0.51	7.7	830	780	210	120
3	↓	↓	↓	↓	31	200	↓	17	10	0.40	8.6	800	740	220	130
4*	AI	↓	↓	↓	25	50	↓	10	16	0.39	5.0	750	740	160	94
5	↓	↓	↓	↓	29	100	↓	14	12	0.33	5.1	800	790	130	77
6	↓	↓	↓	↓	36	200	↓	22	8	0.23	6.0	780	770	150	86
7	SPI	↓	↓	↓	20	20	↓	16	11	0.62	2.0[f]	---	---	230	94
8	DC	↓	↓	↓	26	---	↓	10	16	----	4.8	---	---	110	64
9	AI	↓	560	↓	25	50	1.5	9.9	15	0.36	---	---	---	140	94
10	DC	↓	560	↓	26	---	1.5	9.5	15	----	---	---	---	100	68
11	AI	↓	3200	↓	37	50	8.4	59	14	0.25	---	---	---	510	61
12	AI	↓	↓	↓	46	100	↓	83	10	0.18	---	---	---	800	96
13	FI	↓	↓	↓	30	100	↓	60	14	0.43	---	---	---	830	99
14	DC	↓	↓	↓	42	---	↓	53	16	----	---	---	---	460	55
15	AI	↓	640	3	25	50	0.84	7.1	12	0.39	---	---	---	120	140
16	AI	↓	↓	↓	27	100	↓	11	7.5	0.22	---	---	---	120	140
17	DC	↓	↓	↓	26	---	↓	6.6	13	----	---	---	---	75	89
18	AI	↓	↓	50	55	100	14	62	23	0.50	---	---	---	250	18
19	FI	↓	↓	↓	41	100	↓	55	26	0.37	---	---	---	460	33
20	DC	↓	↓	↓	37	---	↓	56	25	----	---	---	---	300	22
21	FI	1200	610	6	29	100	1.6	14	12	0.55	---	---	---	200	120
22	FI	2000	660	6	32	100	1.7	15	12	0.49	---	---	---	210	120

*Optimum design. See Table 28.

See Table 15 for applicable footnotes.

might be anticipated. The very low pressure, 6 psi, required for the study application and the high fluid temperature, 1700 °F, however, prevent attaining these objectives.

1. Flat Linear Induction Pump. Flat induction pumps, with all magnetic parts readily accessible for cooling, are particularly well suited to this application where the fluid temperature is very close to the Curie point of the available magnetic materials. Designs 1, 2, and 3, Table 21, are flat induction pumps designed for 50, 100, and 200 cps, respectively. Pump weight is lowest for the 100 cps design. Pump efficiency, which decreases with increasing frequency, is best for the 50 cps design. The best combination of efficiency and weight is at 100 cps. This design is illustrated in Figure 83. The power distribution is shown in Table 22, and the performance curves are shown in Figure 84.

The duct is Cb-1Zr. The duct assembly consists of a pumping section of rectangular cross section, measuring approximately 0.75 in. by 9 in. by 22 in. long, and flow transition sections are offset cones. In the inlet transition section, flow enters at the circular base of the cone, makes a 90° turn, and enters the pumping section through an opening along one side of the cone. The outlet transition section is identical, but, with reversed direction of flow. Two continuous webs connecting the flat surfaces of the pumping section to provide axial stiffness are illustrated. The pump duct is not connected mechanically to the stator assembly, although duct guides are shown at the ends to limit gross displacements.

Two identical stator assemblies and structural members to position them relative to each other are required. Each stator assembly comprises a coolant jacket along the surface farthest from the duct, the stator laminations, the stator winding, and a sealed metallic envelope to maintain the desired dielectric gas in the winding region. Temperatures of stator laminations, winding, and dielectric gas are the same as those for the induction pump designs described previously and, therefore, material considerations and choices are the same. (See Section V.B.1 for discussion of these materials and the various allowances for insulation, etc.) The stator coils have three turns, each turn consisting of two strands of rectangular wire, 0.082 in. by 0.157 in. in cross section. Each stator is lap wound, two coil sides per slot. The winding is four pole, three phase, three slots per pole per phase. With a wye connection, one circuit per phase, line voltage and current at the design point are 183 volts and 88 amp. This voltage current combination may be modified by changing the number of turns per coil and the winding interconnection. The cooling arrangement incorporates rectangular passages in the stator envelope at the back of the laminations. The coolant is assumed to be NaK at 600 °F. In passing through the cooling passages of each stator, coolant flow of 4 gpm will experience a temperature rise of approximately 40 °F. The metallic envelope enclosing each stator includes a 0.015 in. thick sheet passing through the magnetic gap between the thermal insulation and the stator surface. In the performance calculations it is assumed that this

TABLE 22. POWER DISTRIBUTION FOR PRIMARY COOLANT PUMP
(Design Point; Flat Induction Application; 100 cps)[a]

Item	Design Point Data	
	KW	Percent Input
Pump Output	1.68	12
Stator Winding Loss	3.97	28
Secondary (Fluid) Loss	5.64	39
Iron Loss	1.0	7
Duct Wall Loss (0.025 in.)	0.98	7
Stator Can Loss	0.31	2
Hydraulic Loss	0.75	5
Total Power Input	14.33	100

[a]See design 2, Table 21.

material is austenitic stainless steel. The structural members holding the stators in the proper relationship are I-beams of varying depth. Because the duct is not self-supporting, the load produced by the fluid pressure acting on the flat duct surfaces is transmitted through the thermal insulation and the stator lamination assemblies to the I-beams, which, therefore, must be quite stiff.

Thermal insulation of the type described in Section V.B.1 is located between the duct and each stator. Spaces 0.15 in. in depth are allowed for this insulation. This accommodates eleven or twelve layers of metallic cloth and strip. Those layers in contact with the duct are Cb-1Zr; the remaining layers may be Cb-1Zr or austenitic stainless steel. The fluid velocity in the duct is 30 ft/sec, the design point suction pressure is 10 psia, and the vapor pressure of lithium at the design point temperature of 1700 ^{o}F is approximately 0.3 psia. Thus, assuming low velocity at the pump suction, the NPSH corresponding to 9.7 psi is 50 ft. The velocity head corresponding to 30 ft/sec is 14 ft; hence, the NPSH is sufficient to prevent cavitation.

Table 22 gives the loss distribution for this design. The principal losses are the electrical losses in the lithium and in the stator winding. The duct wall loss is less than 10% of the power input and, hence, some increase in the duct wall thickness, which is assumed to be 0.025 in., can be tolerated.

2. Annular Induction Pump. For the primary coolant application, the annular induction pump shows better performance and weight than the flat induction pump. The lithium temperature, however, is sufficiently high to preclude using any known magnetic core material without cooling. In designs 4 through 6, Table 21, it was assumed that the core would be cooled to approximately 1200^{o}F. Accordingly, space was provided for coolant passages in the core, and a radial space of approximately 0.04 in. was provided for thermal insulation between the duct and the core. No layouts of this region were made, however, and insufficient study has been made to substantiate that the core can be adequately cooled in designs with the performance indicated in Table 21. Of annular induction pump designs 4 through 6, Table 21, the 50 cps design, line 4, has the best performance and weight combination. Table 23 and Figure 85 give the power distribution and calculated performance curves, respectively, for this design. For the three frequencies considered, efficiency decreases with increasing frequency, and weight is a minimum at the intermediate frequency of 100 cps.

Layouts have not been made for these designs. Calculations were based on using Cb-1Zr of 0.025-in. wall thickness for the duct, thermal insulation of 0.130-in. thickness between the duct and the stator can, and thermal insulation of 0.040-in. thickness between the duct and the core. The general arrangement is similar to that illustrated in Figure 79. In design 4, the mean diameter of the annular duct is 3 in., and the radial height is 0.88 in. The length of the pumping section is 30.2 in. The stator slots are 0.92 in.

TABLE 23. POWER DISTRIBUTION FOR PRIMARY COOLANT PUMP
(Design Point; Annular Induction Application; 50 cps)[a]

Item	Design Point Data	
	KW	Percent Input
Pump Output	1.68	16
Stator Winding Loss	2.75	27
Secondary (Fluid) Loss	3.72	36
Iron Loss	0.50	5
Duct Wall Loss (0.025 in.)	0.97	9
Stator Can Loss	0.17	2
Hydraulic Loss	0.50	5
Total Power Input	10.29	100

[a]See design 4, Table 21

deep, and the winding is four pole, three slots per phase per pole, one coil side per slot, ten turns per coil, wye connected, one circuit per phase. Line voltage and current at the design point are 140 volts and 217 amp, respectively.

3. Single Phase Induction Pump. The principle of operation and the general arrangement of components of the single phase induction pump are described in Section III.A. The performance prediction procedure is developed in Section III.C.3. Very little work has been reported on pumps of this type, and the arrangement described in this report is believed to be completely new. Since there is no experience in the design, fabrication, and operation of these pumps, performance prediction and arrangement details are less certain than for those pumps where more experience is available. Design 7, Table 21, is a single phase induction pump application for the design point rating. Although somewhat inferior to the best designs for pumps of other types, it does have attractive features and subsequent study may produce a better design. This pump is designed for 20 cps.

The pump configuration, illustrated in Figure 86, comprises a duct assembly, a magnetic core assembly, and an annular winding. The duct material is Cb-1Zr with a wall thickness in the pumping section of 0.040 in. The fluid annulus in the pumping section has a mean diameter of 5.43 in., a radial depth of 0.6 in., and a length of 3 in. The fluid velocity is 20 ft/sec. The flow transition from pump inlet to pumping section and from pumping section to pump outlet is via twelve one-inch pipes equally distributed circumferentially around the pumping section annulus. The header at each end of the pumping section constitutes a conducting path linked by the flux in the pump core. It carries eddy currents, which oppose the m.m.f. of the exciting coil and create undesirable losses. To reduce these losses, insulating baffles, one located between each adjacent pair of transition pipes, are shown in each header. The magnetic portion of the pump consists of a laminated core and twelve E-shaped packages of laminations. The planes containing the principal dimensions of the laminations pass through, or near, the axial center line of the pump. Figure 86 illustrates the arrangement. Cooling the magnetic parts is necessary and may be accomplished with cooling coils around the periphery of the parts. Cooling coils are not shown in the illustration. The exciting winding is a concentrated annular coil located at one end of the pumping section. The conductor is copper and is formed around a thin walled austenitic stainless steel tube through which coolant is circulated.

Space for thermal insulation was not allowed in the performance prediction calculations for design 7, Table 21, and is not illustrated in Figure 86. Since the nonmagnetic gap in the pumping section is 0.68 in., space may be allowed for thermal insulation without significantly changing indicated pump performance.

4. DC Conduction Pump. Design 8, Table 21, is a series excited compensated dc conduction pump for the design point rating. This pump design has a combination of calculated efficiency and weight superior to that of any other design listed. In general arrangement, it is similar to the design illustrated in Figure 78 except that the series winding has one turn and the pump is compensated.

The duct material is Cb-1Zr with a wall thickness of 0.025 in. in the pumping section. The rectangular pumping section is 2-in. high by 4-in. wide by 2-in. long. The flow velocity is 25 ft/sec. To limit end fringing current, inlet and discharge transition regions are composed of six parallel flow passages. A 0.1-in. space between each side of the duct and the magnet is filled with thermal insulation of the metallic cloth and sheet type. Since the fluid exceeds the upper temperature limit for operation of available magnetic materials, auxiliary cooling of the magnet is necessary. The conductor material also must be cooled. The conductor to duct joint has not been designed, and, since the calculations are based on using a conductor material with the resistivity of copper at 1200 ^{o}F with an electrode of Cb-1Zr, some depreciation in performance may be incurred at this point.

b. Pump Requirement Parameter Range. Designs 9 through 22, Table 21, are conduction and induction pump designs for the various ratings chosen in the specified study range (Table 14). For each pressure flow combination considered, designs were made for a dc conduction pump and for either flat or annular, or both, induction pumps.

Primarily because of the low values of developed pressure specified, the efficiency of most of the designs calculated is low. Exceptions are the 50 psi, 640 gpm designs, which show efficiencies exceeding 22%. The power factor of the induction pumps is low, and it is less for annular than for flat pumps.

The lowest value of suction pressure specified in the study range is 5 psia. At 2000 ^{o}F, the vapor pressure of lithium is 2 psi. Thus, the NPSH is approximately 3 psi, or 16 ft, and fluid velocity at the entrance to the pumping section should be limited to approximately 23 ft/sec. Tapering the duct passages at the entrance to the pumping section will accomplish this.

Designs 2, 21, and 22, Table 21, indicate that lithium temperature alone has little effect on pump performance. This comparison is not completely accurate, however, since the allowances for thermal insulation were constant for the three temperatures. Compared with designs for lithium temperatures of 1700 ^{o}F and 2000 ^{o}F, at a lithium temperature of 1200 ^{o}F, material stress capability is much higher, thermal expansion is significantly reduced, and much design simplification is possible.

C. Pump Weight Improvement

It has been observed that, in EM pumps designed on a consistent basis, a fairly constant correlation exists between the weight of the various pumps and a parameter given by the product of flow rate, developed pressure, and fluid electrical resistivity. This parameter has been designated the pump capability parameter. In Figure 87 the ratio of pump weight to this capability parameter is plotted against the capability parameter for thirteen induction pumps designed during the past fifteen years and for eight designs developed during the course of this study. The specific pump ratings shown on the chart are indicated in Table 24. Data points 1 through 13 represent actual pumps, many of which have operated tens of thousands of hours with virtually no maintenance and with outstanding reliability. Data points a through h represent designs selected from those whose characteristics are summarized in Tables 15 through 23.

The data in Figure 87 show that the weight of EM pumps designed specifically for space power application may be less than one tenth that of EM pumps developed for conventional applications. This weight reduction has been achieved by: 1) Virtually eliminating the pump frame, 2)using somewhat higher current and flux densities in the active parts of the pump, and 3) using a magnetic flux return path inside the pump duct. To achieve low weight of the frame, cylindrical configurations have been chosen because they provide optimum utilization of structural material for pressure containment. The EM pumps used in the Submarine USS Seawolf, in which only 22% of the pump weight was active magnetic or conducting material, illustrate the potential of this approach to weight minimization. Current densities in the designs proposed for space applications are approximately 3300 to 5000 amp/in.^{2} compared with 2500 to 3500 amp/in.^{2} in earlier designs. Because of the large air gaps necessary in EM pumps, flux densities are usually low, particularly in high temperature helical induction pumps. In the designs for space applications, flux densities of approximately 90,000 lines/in.^{2}, compared with flux densities of approximately 40,000 lines/in.^{2} in earlier pumps, are used in the magnetic materials. The use of a magnetic core in the stator bore, when compared with the nonmagnetic core construction in the helical pumps presently operative, permits substantial reductions in stator conducting and magnetic material.

The observed correlation of pump weight with pump capability parameter may be rationalized in the following manner. In a particular induction pumping configuration with a magnetic field of fixed peak amplitude moving at a fixed synchronous velocity, a conducting fluid passing through the pump duct at a fixed velocity less than that of the moving magnetic field experiences a pressure rise inversely proportional to its electrical resistivity. Accordingly, since the flow is the same for all fluids for the assumed conditions, the product of flow rate, pressure, and electrical resistivity is constant. Thus the pumping configuration has a capability related to the product of pressure, flow and electrical resistivity. The weight of a pump, therefore, is a function of the parameter. This neglects significant variables such as fluid temperature, density, and viscosity. It should be employed carefully, particularly in

TABLE 24. PUMP IDENTIFICATION, EM PUMP WEIGHT CORRELATION

Ident. No.[a]	Flow, gpm	Head, psi	Fluid	Temp., °F	Wt., lb	Fluid Resistivity, μ-ohm-in.	Capability Parameter, gpm-psi-μ-ohm-in-10^{-3}	Eff., %	Pump Type[b]	Location or Application
Existing Pumps										
1	6500	53	Na	700	18,500	8.5	2930	44	FI	EBR-II Secondary Loop
2	5000	40		700	14,000	8.5	1700	40		Argonne Natl. Lab.
3	3300	85		600	11,400	7.1	1990	43		USS Seawolf
4	1200	40		700	6,430	8.5	408	33		KAPL Test Pump
5	60	30		700	800	8.5	15.3	15		KAPL Service/EBR-II Service
6	500	40		900	2,250	10.6	212	17	HI	LASL
7	42	150	K	1600	1,500	35.0	220	10		SPPS Turbine Loop
8	200	20		1850	1,500	37.5	150	6		SPPS 300 KW Loop
9	20	67		1850	1,100	37.5	50.1	5		SPPS 300 KW Loop[c]
10	50	50		1400	1,000	29.0	72.5	11		AiResearch Corp.
11	4	120		1400	300	29.0	13.9	3.5		AiResearch Corp.
12	3	75		2200	570	45.0	10.1	1		SPPS 100 KW Loop[c]
13	4	80		500	250	10.2	3.3	4		SPPS Bearing, Seal Service
Study Pumps										
a	16	30	K	1200	26	23.5	11	10	HI	Turboelectric Condensate Boost
b	16	30	K	1200	9	23.5	11	14	DC	Turboelectric Condensate Boost
c	60	25	NaK	1200	38	32.5	49	12	AI	Thermionic Radiator Coolant
d	60	25	NaK	1200	19	32.5	49	15	DC	Radiator Coolant
e	31	20	Li	1200	33	15.4	9.45	13	HI	Radiator Coolant
f	31	20	Li	1200	13	15.4	9.45	15	DC	Radiator Coolant
g	643	6	Li	1700	160	17.7	68.4	16	AI	Primary Coolant
h	643	6	Li	1700	110	17.7	68.4	16	DC	Primary Coolant

[a] Refers to identification in Figure 89.
[b] FI = flat induction; HI = helical induction; DC = direct current conduction; AI = Annular Induction
[c] These are double rated pumps. The higher output rating is used.

comparing pumps for fluids with widely different characteristics or pumps designed for completely different applications or environments.

D. Weight Evaluations For The Selected Pumps

Consideration of the several pump concepts enumerated and discussed in Section III for applicability to space power systems led to the choice of five general pump types for more detailed design study. This preliminary selection was based on quantitative comparison of the various pump concepts, emphasising reliability. Following this selection, preliminary designs and performance predictions were made for approximately 1000 pump rating combinations for the various pump applications considered in this study. From these, 89 preliminary designs having the best combination of performance and weight were selected. Descriptive information and performance for these designs are summarized in Section V.C.

In the second step of the selection, the 89 pump designs were integrated into the space power plant, applying system considerations, weights and penalties presented in Section IV. This second selection step culminated in a weight analysis for each of the 89 pump designs. This weight analysis was based on the weights and weight penalties listed in Table 13 and the pump data reported in Tables 15 through 23. The results of this analysis are given in Tables 25 through 30. Final pump choices to satisfy the six study applications were based on minimum evaluated weight as indicated in the columns designated Weight Criteria. The pumps chosen are indicated by an asterisk in the column designated Pump Design Number. Pertinent data for the six selections are summarized in Table 31. All numbers have been rounded off to two significant figures.

Inasmuch as the pump ratings for the radiator coolant pumps for turboelectric and thermionic power systems were identical, separate pump designs were not required for the two systems. Identical pump designs when integrated into the turboelectric and thermionic power systems resulted in different values, hence separate lists appear for the same pumps in the two systems.

Some useful generalizations can be drawn from the information given in Tables 25 through 30.

1. DC conduction pumps permit minimum system weight. There is some indication that this effect is reduced as pump size increases.

2. Pump specific weight decreases with increased pump output. Thus, a compromise between pumping system weight and reliability improvement through redundance by using several small pumps in parallel must be made.

TABLE 25. WEIGHT ANALYSIS FOR SELECTED EM PUMP DESIGNS
I Turboelectric Condensate Boost Pump: Potassium

Pump Characteristics						Weights and Penalties			Weight Criteria	
Design No.[a]	Pump Type[b]	Power Output, kw[c]	Power Input, kw[d]	Eff., %	Reactive Power, kvar	Pump Wt., lbs	Power and Cooling Penalty, lbs [e]	PF Penalty, lbs [e]	Total Wt., lbs	Over-all Sp. Wt., lbs/kw
1	HI	0.20	2.3	8.9	3.6	33	29	2.7	65	320
2	↓	↓	2.1	9.3	4.4	30	26	3.3	59	300
3*			2.3	8.9	4.2	26	29	3.1	58	290
4			3.2	6.3	5.4	22	40	4.1	66	330
5	DC		1.8	11	---	9	23	---	32	160
6	HI	0.14	1.5	9.3	3.9	20	19	2.9	42	300
7	DC	0.14	1.4	10	---	7	18	---	25	180
8	AI	1.6	8.6	19	16	136	110	12	260	160
9	↓	↓	9.7	17	18	76	120	14	210	130
10			9.9	16	30	87	120	23	230	140
11	DC		9.0	18	---	69	110	---	180	110
12	HI	0.02	0.78	2.6	1.4	11	9.8	1.0	22	1100
13	DC	0.02	0.43	4.7	---	3	5.4	---	8.4	420
14	HI	0.41	3.3	12	8.4	38	41	6.3	85	210
15	DC	0.41	3.2	13	---	13	40	---	53	130
16	HI	0.20	2.3	8.7	3.9	25	29	2.9	57	280
17	↓	0.21	2.3	9.1	5.2	27	29	3.9	60	290
18		0.20	2.7	7.4	4.0	38	34	3.0	75	380
19		0.20	3.0	6.7	5.3	32	38	4.0	74	370

*Optimum Design

[a] See Tables 15 to 23 under the same design number for other pump characteristics.

[b] HI = helical induction; DC = direct current conduction; AI = annular induction; FI = flat induction SPI = single phase induction.

[c] Hydraulic power developed by the pump.

[d] Input to the pump power supply. Includes power supply losses.

[e] See Table 13.

TABLE 26. WEIGHT ANALYSIS FOR SELECTED EM PUMP DESIGNS

II Turboelectric Radiator Coolant Pump: NaK

Pump Characteristics						Weights and Penalties			Weight Criteria	
Design No.[a]	Pump Type[b]	Power Output, kw[c]	Power Input, kw[d]	Eff., %	Reactive Power, kvar	Pump Wt., lbs	Power and Cooling Penalty, lbs[e]	PF Penalty, lbs[e]	Total Wt., lbs	Over-all Sp. Wt., lbs/kw
1	AI	0.66	5.6	12	11	120	70	8.3	200	300
2	↓	↓	5.0	13	11	52	62	8.3	120	190
3*	↓	↓	5.9	11	13	38	74	9.7	120	180
4	↓	↓	7.2	9.2	20	41	90	15	150	220
5	HI	↓	5.7	12	11	92	71	8.3	170	260
6	↓	↓	5.9	11	13	66	74	9.7	150	230
7	↓	↓	8.0	8.3	14	51	100	10	160	240
8	↓	↓	13	5.1	20	58	160	15	230	350
9	DC	↓	5.4	12	---	19	68	---	87	130
10	DC	↓	4.3	15	---	27	54	---	81	120
11	HI	0.33	3.3	10	9.1	51	41	6.8	99	300
12	DC	0.33	3.1	11	---	11	39	---	50	150
13	AI	3.9	20	20	34	240	250	25	520	130
14	↓	↓	22	18	77	190	270	58	520	130
15	↓	↓	27	14	84	140	340	63	540	140
16	DC	↓	22	18	---	150	270	---	420	110
17	AI	0.26	2.8	9.3	5.6	32	35	4.2	71	270
18	AI	↓	3.4	7.7	8.1	23	42	6.1	71	270
19	HI	↓	3.9	6.7	9.0	54	49	6.7	110	420
20	DC	↓	2.1	12	---	18	26	---	44	170
21	AI	2.6	17	15	41	160	210	31	400	150
22	AI	↓	18	14	45	98	220	34	350	130
23	HI	↓	13	20	45	170	160	34	360	140
24	DC	↓	15	17	---	100	190	---	290	110
25	AI	0.66	5.7	12	12	36	71	9.0	120	180
26	AI	0.66	6.3	10	17	42	79	13	130	200

*Optimum Design.

See Table 25 for applicable footnotes.

TABLE 27. WEIGHT ANALYSIS FOR SELECTED EM PUMP DESIGNS
III Turboelectric Radiator Coolant Pump: Lithium

Pump Characteristics						Weights and Penalties			Weight Criteria	
Design No. [a]	Pump Type [b]	Power Output, kw [c]	Power Input, kw [d]	Eff., %	Reactive Power, kvar	Pump Wt., lbs	Power and Cooling Penalty, lbs [e]	PF Penalty, lbs [e]	Total Wt., lbs	Over-all Sp. Wt., lbs/kw
1*	HI	0.27	2.3	12	3.0	33	29	2.2	64	240
2			2.7	9.9	3.8	29	34	2.8	66	240
3			2.8	9.5	4.0	28	35	3.0	66	240
4			4.2	6.4	7.0	26	53	5.2	84	310
5	DC		2.3	12	---	13	29	---	42	160
6	HI	0.13	1.3	10	2.8	18	16	2.1	36	280
7	DC	0.13	1.5	8.8	---	7	19	---	26	200
8	AI	1.6	8.3	19	12	98	100	9.0	210	130
9			9.5	17	16	58	120	12	190	120
10			11	15	24	56	140	18	210	130
11			11	15	13	78	140	9.8	230	140
12	DC		9.3	17	---	70	120	---	190	120
13	HI	0.13	1.8	7.3	4.3	21	22	3.2	46	350
14	DC	0.13	1.3	10	---	8	16	---	24	180
15	HI	0.80	4.4	18	14	59	55	11	130	160
16	HI		5.5	15	8.5	47	69	6.4	120	150
17	DC		5.9	14	---	34	74	---	110	140
18	HI	0.26	2.8	9.3	4.0	27	35	3.0	65	250
19	HI	0.28	2.8	10	4.1	29	35	3.1	67	240

*Optimum Design.
See Table 25 for applicable footnotes.

TABLE 28. WEIGHT ANALYSIS FOR SELECTED EM PUMP DESIGNS

IV Thermionic Primary Coolant Pump: Lithium

Pump Characteristics						Weights and Penalties			Weight Criteria	
Design No. [a]	Pump Type [b]	Power Output, kw [c]	Power Input, kw [d]	Eff., %	Reactive Power, kvar	Pump Wt., lbs	Power and Cooling Penalty, lbs [e]	PF Penalty, lbs [e]	Total Wt., lbs	Over-all Sp. Wt., lbs/kw
1	FI	1.7	16	11	24	270	190	12	470	280
2	↓	↓	16	10	24	210	190	12	410	240
3	↓	↓	19	8.8	38	220	230	19	470	280
4*	AI	↓	12	14	24	160	150	12	320	190
5	↓	↓	16	10	41	130	190	21	340	200
6	↓	↓	25	6.8	91	150	300	46	500	290
7	SPI	↓	19	8.7	20	230	230	10	470	280
8	DC	↓	13	13	---	110	160	---	270	160
9	AI	1.5	11	13	25	140	130	13	283	190
10	DC	1.5	12	12	---	100	140	---	240	160
11	AI	8.4	67	13	230	570	810	120	1400	170
12	AI	↓	95	8.8	450	800	1100	230	2100	250
13	FI	↓	69	12	130	830	840	65	1700	210
14	DC	↓	66	13	---	460	790	---	1300	150
15	AI	0.84	8.2	10	17	120	99	8.5	230	270
16	AI	↓	13	6.6	49	120	160	25	300	360
17	DC	↓	8.2	10	---	75	98	---	170	210
18	AI	14	72	19	110	250	870	55	1200	84
19	FI	↓	63	22	140	460	760	70	1300	92
20	DC	↓	70	20	---	300	840	---	1100	82
21	FI	1.6	16	9.8	22	200	190	11	400	250
22	FI	1.7	17	9.8	24	210	210	12	430	250

*Optimum Design.

See Table 25 for applicable footnotes.

TABLE 29. WEIGHT ANALYSIS FOR SELECTED EM PUMP DESIGNS
V Thermionic Radiator Coolant Pump: NaK

Pump Characteristics						Weights and Penalties			Weight Criteria	
Design No. [a]	Pump Type [b]	Power Output, kw [c]	Power Input, kw [d]	Eff., %	Reactive Power, kvar	Pump Wt., lbs	Power and Cooling Penalty, lbs [e]	PF Penalty, lbs [e]	Total Wt., lbs	Over-all Sp. Wt., lbs/kw
1	AI	0.66	5.8	11	11	120	70	5.5	200	300
2		0.66	5.2	13	11	52	63	5.5	120	180
3*			6.2	11	13	38	75	6.5	120	180
4			7.5	8.8	20	41	91	10	140	210
5	HI		5.9	11	11	92	71	5.5	170	260
6			6.2	11	13	66	75	6.5	150	220
7			8.3	8.0	14	51	100	7.0	160	240
8			13	5.1	20	58	160	10	230	350
9	DC		5.4	12	---	19	65	---	84	130
10	DC		4.3	15	---	27	52	---	79	120
11	HI	0.33	3.4	9.7	9.1	51	41	4.6	97	290
12	DC	0.33	3.1	11	---	11	37	---	48	150
13	AI	3.9	21	19	34	240	250	17	510	130
14			23	17	77	190	270	39	500	130
15			28	14	84	140	340	42	520	130
16	DC		22	18	---	150	260	---	410	110
17	AI	0.26	2.9	9.0	5.6	32	35	2.8	70	270
18	AI		3.5	7.4	8.1	23	42	4.1	69	270
19	HI		4.0	6.5	9.0	54	48	4.5	110	410
20	DC		2.1	12	---	18	25	---	43	160
21	AI	2.6	18	14	41	160	220	21	400	150
22	AI		19	14	45	98	230	23	350	130
23	HI		14	19	45	170	170	23	360	140
24	DC		15	17	---	100	180	---	280	110
25	AI	0.66	5.9	11	12	36	71	6.0	110	170
26	AI	0.66	6.5	10	17	42	79	8.5	130	200

*Optimum Design.
See Table 25 for applicable footnotes.

TABLE 30. WEIGHT ANALYSIS FOR SELECTED EM PUMP DESIGNS
VI Thermionic Radiator Coolant Pump: Lithium

Pump Characteristics						Weights and Penalties			Weight Criteria	
Design No. [a]	Pump Type [b]	Power Output, kw [c]	Power Input, kw [d]	Eff., %	Reactive Power, kvar	Pump Wt., lbs	Power and Cooling Penalty, lbs [e]	PF Penalty, lbs [e]	Total Wt., lbs	Over-all Sp. Wt., lbs/kw
1*	HI	0.27	2.4	11	3.0	33	28	1.5	63	230
2	↓	↓	2.8	9.5	3.8	29	34	1.4	64	240
3	↓	↓	2.9	9.2	4.0	28	35	2.0	65	240
4	↓	↓	4.3	6.2	7.0	26	52	3.5	82	300
5	DC	↓	2.3	12	---	13	28	---	41	150
6	HI	0.13	1.4	9.5	2.8	18	17	1.4	36	280
7	DC	0.13	1.5	8.8	---	7	18	---	25	190
8	AI	1.6	8.6	19	12	98	100	6.0	200	130
9	↓	↓	9.8	16	16	58	120	8.0	190	120
10	↓	↓	11	15	24	56	130	12	200	120
11	↓	↓	11	15	13	78	130	6.5	210	130
12	DC	↓	9.3	17	---	70	110	---	180	110
13	HI	0.13	1.8	7.3	4.3	21	22	2.2	45	350
14	DC	0.13	1.3	10	---	8	16	---	24	180
15	HI	0.80	4.6	17	14	59	56	7.0	120	150
16	HI	↓	5.7	14	8.5	47	69	4.3	120	150
17	DC	↓	5.9	14	---	34	71	---	110	130
18	HI	0.26	2.9	9.0	4.0	27	35	2.0	64	250
19	HI	0.28	2.9	9.7	4.1	29	35	2.1	66	240

*Optimum Design.
See Table 25 for applicable footnotes.

TABLE 31. EM PUMPS FOR SIX SPACE POWER APPLICATIONS

Characteristic	Application					
	Turboelectric			Thermionic		
	Condensate Boost	Radiator Coolant		Primary Coolant	Radiator Coolant	
		NaK	Lithium		NaK	Lithium
Pump Design No.[a]	I-3	II-3	III-1	IV-4	V-3	VI-1
Type[b]	HI	AI	HI	AI	AI	Hi
Fluid	K	NaK-78	Li	Li	NaK-78	Li
Fluid Temp., ^{o}F	1200	1200	1200	1700	1200	1200
Flow, gpm	16	60	31	640	60	31
Dev. Press., psi	30	25	20	6	25	20
Power Output, kw[c]	0.20	0.66	0.27	1.7	0.66	0.27
Power Input, kw	2.0	5.4	2.1	10	5.4	2.1
Voltage[d]	100	100	100	100	100	100
Freq., cps	200	200	100	50	200	100
PF, %	43	39	55	39	39	55
Eff., %	10	12	13	16	12	13
Wt., lbs.	26	38	33	160	38	33
Sp. Wt., lbs/kw[e]	130	58	120	94	58	120
Power Supply	← Freq. Changer →			Invert. + Transf. + Freq. Changer		
Input Power, kw	2.3	5.9	2.3	12	6.2	2.4
Voltage	500	500	500	100	100	100
Freq., cps	2000	2000	2000	DC	DC	DC
Eff., %	90	90	90	87	87	87
Power Plant Wt. Penalty, lbs.	29	74	29	150	75	29
PF Wt. Penalty, lbs.	3.1	9.7	2.2	12	6.5	1.5
Total Wt., lbs/pump	58	120	64	320	120	63
Pumps per Power Plant	4	16	16	1	16	16
Total Pump Sys. Wt., lbs.	230	1900	1000	320	1900	1000
Over-All Sp. Wt., lbs/kw	290	180	240	190	180	230
Over-All Eff., %	8.9	11	12	14	11	11

[a] See Tables 15, 17, 19, and 21 for additional design information.
[b] HI = helical induction; AI = annular induction.
[c] Hydraulic power output = flow gpm x developed pressure psi x 4.35×10^{-4}.
[d] Voltage below 300 volts is not critical to pump design.
[e] Pump weight ÷ power output.

3. Pumping systems using lithium are significantly lighter than those using NaK.

4. Minimum pump system weight is not necessarily associated with the minimum pump weight.

Interpolation of these tables is possible without significant loss of accuracy provided extremes in flow, pressure, and temperature are avoided.

Since system weight penalties are typically comparable to pump weight, and since system weight penalties are dominated by efficiency, improvements in pump efficiency should receive as much emphasis as improvement in pump weight. The pump designs for which performance data is reported here are based on conservative values for the critical quantities, such as flux density, current density, thermal and electrical insulation allowances, etc. It is anticipated that detailed designs will show performance at least as good as that indicated in this report.

Some improvement in system weight may be achieved if the pumps can be designed to reject winding losses to the pump fluid. Obviously, this requires a winding temperature of 200 to 300 ^{o}F above the fluid temperature, which is 1200 ^{o}F for all applications other than the primary coolant. In addition to elimination of the weight penalty associated with the cooling system, this would permit elimination of the thermal insulation, hence some performance improvement due to the consequent reduction in the length of the nonmagnetic gap. Some additional loss due to the increased resistivity of the conductor material will be associated with such an arrangement. Thus, the major gain will be in the reduction in weight penalties for cooling and improvement in reliability rather than reduced pump weight or higher efficiency.

In conclusion, the results of this study show that electromagnetic pumps are a good choice for applications in the alkali metal systems of large space power plants. As indicated in Section V.C, substantial weight improvement can be achieved over present practice within existing technology. The greatest asset of the EM pump is reliability through simplicity. Within present technology, the polyphase induction pump will best insure high reliability. Other features especially valuable to space power systems are good controllability and the elimination of startup problems mentioned in Section IV. Also interesting is the possibility that induction pumps can circumvent the cavitation problems discussed in Section III.B. Figure 88 depicts possible flight configurations for the helical and the annular induction pumps.

VI. BIBLIOGRAPHY

(EM Pump Technology)

Armstrong, D. S., "Electromagnetic Pumps for Liquid Metals," AEI Engineering, November - December 1962.

Asti, J. F., "Development of Electromagnetic Pumps Suitable for Pumping Liquid Metals," Final Report, Contract NObs 47750, Report No. 43-109, Allis-Chalmers Mfg. Company.

Baker, R. S., "Design of Direct-Current Electromagnetic Pump," Report NAA-SR-6583, North American Aviation, July 20, 1961.

Baker, R. S., "Design of an Eddy-Current Brake for a Sodium-Cooled Nuclear Power Reactor," Report NAA-SR-2986, North American Aviation, September 15, 1958.

Baker, R. S., "Tests of Linear Induction Electromagnetic Pump for HNPF," Report TDR-5777, Atomics International, October 26, 1960.

Baker, R. S., "Weights and Efficiencies of Helical-Rotor EM Pumps for Sodium Service," NAA-SR-Memo-7955, North American Aviation, November 12, 1962.

Blake, L. R., "A.C. and D.C. Conduction Pumps for Liquid Metals," Engineer, Vol. 202, 1956, No. 526, pp. 541-544, No. 527, pp. 572-576.

Blake, L. R., "Dynamo-Electric Machines," U.S. Patent 2,905,089, September 22, 1959.

Blake, L. R., "Electromagnetic Pumps for Liquid Metals," Nuclear, Pt. B. Reactor Technology, Vol. 1, August 1959, pp. 65-76.

Branover, H., and Lielausis, O., "The Effect of a Transverse Magnetic Field on Internal Structure and Hydraulic Resistance in Turbulent Flows of Liquid Metals," Physics Institute of the Academy of Science of the Latvian SSR, August 5, 1960 (tr.).

Brill, E. F., "Development of Special Pumps for Liquid Metals," Mech. Eng., No. 6, June 1953.

Bruckel, W., "Elektrodynamische Pumpe," German Patent 511,137, October 1930.

Cage, J. F., Jr., "Electromagnetic Pumps," Machine Design, March 1953.

Cage, J. F., Jr., "Electromagnetic Pumps for High-Temperature Liquid Metal", Mech. Eng., June 1953.

Cambillard, E., Polyphase Annular Electromagnetic Induction Pumps for Liquid Metals, Liquid Metal Colloquium of the European Society of Atomic Energy, Aix-en-Provence, September 30 - October 2, 1963.

Chepele, Tu. M., "A Pump for Pumping Liquid (Molten) Metal," Russian Patent 143,982, Qr. FTD-TT-63-496/1 and 2.

Cole, R. H., "Modulated Electromagnetic Pump," U. S. Patent 3,066,607, December 4, 1962.

Crever, F. E., "Electromagnetic Centrifugal Pump," U. S. Patent 2,652,778, September 25, 1953.

Donelian, K. O., "Electromagnetic Pump," U. S. Patent 2,658,452, November 10, 1953.

Eisenberg, P., "Cavitation Damage," Technical Report 233-1, Hydronautics, Inc., Astia AD-602833, December 1963.

Fenemore, A. S., "Linear Induction Pumps for Liquid Metals," The Engineer, May 17, 1957.

Findlay, G. R., "Research on Fundamental Electrodynamic and Hydrodynamic Phenomena Involved in Electromagnetic Pumping of Liquid Metals," Final Report, Contract NASr-33, Liquid Metals, Inc., March 31, 1962.

Findlay, J. M., "Apparatus for Pumping Liquid Metal," British Patent 746,456, March 1956. U. S. Patent 2,915,973, December 8, 1959.

Fishman, F., "End Effects in Magnetohydrodynamic Channel Flow," Research Note 135, AVCO-Everett Research Laboratory, June 1959.

Fraser, W. J., "DC Electromagnetic Pump Study for Thermionic Conversion Reactors," NAA-SR-Memo-5501, North American Aviation, July 15, 1960.

Germeles, A. E., "Channel-Flow of Conducting Fluids Under an Applied Transverse Magnetic Flow," J. Appl. Mech., Trans. ASME, June 1964.

Hammitt, F. G., and Summers, J. L., "Similarity Relations for Electromagnetic Pumps," Nuclear Power, No. 71, March 1962.

Hilditch, J. A. S., "The Electromagnetic Pumping of Liquid Metals-1," Atomics and Nuclear Energy, February 1958.

Hilditch, J. A. S., "The Electromagnetic Pumping of Liquid Metals-2," Atomics and Nuclear Energy, April 1958.

Jackson, W. D., Pierson, E. S., and Porter, R. P. "Design Consideration for MHD Induction Generators," Paper No. 61, National Symposium of Magnetohydrodynamic Electrical Power Generation, Paris, July 6-11, 1964.

Jackson, W. D., "Liquid Metal Faraday-Type MHD Generators," Paper No. 62-1401, AIEE Conference, October 7, 1962.

Jackson, W. D., "Liquid Metal Faraday-Type MHD Generators," IEEE Trans. on Power Apparatus and Sys., December 1963.

Jaross, R. A., and Barnes, A. H., "Design and Operation of a 10,000 GPM DC Electromagnetic Sodium Pump and 250,000 Ampere Homopolar Generator," Second United Nations International Conference on the Peaceful Uses of Atomic Energy, A/CONF. 15/P/2157, June 1958.

Laithwaite, E. R., "Linear Induction Motors," Paper No. 2433 U, IEE, December 1957.

Laithwaite, E. R., "Rotor Windings for Induction Motors with Arc-Shaped Stators," Proc. IEE, Vol. III, No. 2, February 1964.

Lebedev, A. A., "The Magnetic Field, Excited by the Primary Winding, in the Air Gap of an Induction Machine with a Curved Stator," Electromekhanika, No. 5, 1959, pp. 14-23, (tr.).

Miley, D. C., "A Toroidal Thermoelectric - Magnetic Liquid Metal Pump for Space Application," Report R59FPD624, Flight Propulsion Division, General Electric Company, July 1959.

Murgatroyd, W., " Experiments on Magneto-Hydrodynamic Channel Flow," Phil. Mag., Series 7, December 1953.

Murgatroyd, W., "Theory of the Ideal A.C. Conduction Pump," Report ED/R 1566, A.E.R.E., Harwell, December 2, 1954.

Okhremenko, N. M., "Optimum Geometrical Ratios in Induction Pumps for Liquid Metals," Elektrichestro, No. 9, 1961.

Osterle, J. F., and Angrist, S. W., "The Thermoelectric-Hydromagnetic Pump," J. Heat Transfer, Trans. ASME, May 1964, pp. 166-168.

Pedersen, E. S., "Nuclear-Thermoelectric Space Power System," Martin Co.

Petrick, M., and Lee, Kung-You, "Performance Characteristics of a Liquid Metal MHD Generator," Paper No. 62, National Symposium of Magnetohydrodynamic Electrical Power Generation, Paris, July 6-11, 1964.

Pierson, E. S., "A Hydromagnetic DC Converter," Contract Nr AF33(616)-7624, Report DSR7672, Res. Lab. of Electronics, MIT, January 1961.

Preiser, H. S., Thiruvengadam, A., and Couchman, C. E., III, "Cavitation Damage in Liquid Sodium," NASA-CR-54071, April 1, 1964.

_____, "Problems of Magnetohydrodynamics and Plasma Dynamics," Proceedings of the Conference on Magnetohydrodynamics, Riga, July 2-10, 1958, Tr. AEC-tr-4509.

_____, "Problems of Magnetohydrodynamics and Plasma Dynamics II," Proceedings of the Conference on Theoretical and Applied Magnetohydrodynamics, Riga, June 27-July 2, 1960, FTD-TT-62-1301.

Pully, O. O., "Electromagnetic Pump," U. S. Patent 2,686,474, August 17, 1954.

Rossow, V. J., "On Flow of Electrically Conducting Fluids Over a Flat Plate in the Presence of a Transverse Magnetic Field," Report 1358, NASA.

Seim, O. S., and Jaross, R. A., "Characteristics and Performance of 5,000 GPM AC Linear Induction and Mechanical Centrifugal Sodium Pumps," Proceedings of United Nations Conference on the Peaceful Uses of Atomic Energy, A/Conf. 15/1, 7, 1958.

Sherman, A., "Exact Solutions for Magnetohydrodynamic Channel Flows," Report R62SD991, Missile and Space Division, General Electric Company, December 1962.

Shturman, G. I., and Aronov, R. L., "Edge Effect in Induction Machines with an Open Magnetic Circuit," Elektrichestvo, 1947, pp. 54-59.

Sudar, S., "Snap 2 Reactor Pump Development Program," Report NAA-SR-5244, North American Aviation, September 1, 1961.

Vandenberg, L. B., "Heat Exchanger Pump," U. S. Patent 2,478,710, June 1956.

Vandenberg, L. B., "Homopolar Generator Pump for Liquid Metals," Report No. 590, Knolls Atomic Power Laboratory, General Electric Company, August 1951.

Vol'dek, A. I., "Electromagnetic Pumps for Liquid Metals," Elektrichestvo, No. 5, 1960.

Von Hufnagel, S., "Die Thermoelektromagnetische Pumps," Aus dem Institut fur Thermodynamik der Technischen Hockschule Munchen (Tr.).

Wakefield, K. W., "Electromagnetic Pump," U. S. Patent 2,612,109, September 30 1952.

Watt, D. A., "The Design of EM Pumps for Liquid Metal," J. Inst. Elec. Engrs. (London), December 1958.

Watt, D. A., "Design of Travelling Field Induction Pumps for Liquid Metals," Report R/M 144, A.E.R.E., Harwell, September 1957.

Watt, D. A., "Electromagnetic Pumps for Liquid Metals," Engineering, April 27 1956.

Watt, D. A., O'Connor, R. I., and Holland, E., "Tests on an Experimental DC Pump for Liquid Metals," Report R/R 2274, A.E.R.E., Harwell, 1957.

Weber, H. E., and Marston, C. H., "Liquid Metal Vortex MHD Generator," Paper No. 63-WA-209, ASME, September 9, 1963.

(Materials Support)

_____, Allegheny Ludlum 316 & 316-L, Alloy Digest, Oct. 1956, Engineering Alloys Digest, Montclair, N. J.

Bartlett, E. S. and Houck, J. A., "Physical and Mechanical Properties of Columbium and Columbium-Base Alloys," DMIC Report 125, Feb. 29, 1960.

Becker, J. J., "Recent Development in Magnetic Metals and Alloys," Metallurgical Rev., Vol. 7, No. 28, 1962, p. 371.

Bober, E. S., Stapleton, R. E., and Snavely, W. H., "Alkali Metal Resistant Wire," APL-TDR-64-42, April 15, 1964.

Chen, C. W., "Soft Magnetic Cobalt-Iron Alloys," No. 22, March 1964.

_____, "CS1200 Ceramic Coil System," Publication No. EB-39, Anaconda Wire and Cable Company, 1963.

Dotson, L. E., "Emittance Coating Studies of Columbium-1 Zirconium," Report R61FPD571, Flight Propulsion Division, General Electric Company, 1962.

Goldberg, M. E., and Hamre, H. G., "Electronic Component Parts Research for 500°C Operation," TR-57-362, WADC, February 1958.

Gordon, D. I., "Magnetic Cores and Permanent Magnets in Hyper-Environments," Proceedings of Institute of Environmental Sciences National Meeting, Los Angeles, April 1960, pp. 205-228.

Graham, Jr., C. D., "Temperature Dependence of Anisotropy and Saturation Magnetism in Iron and Iron Silicon Alloys," J. Appl. Phys., Vol. 30, Supp., No. 5, May 1960.

Heasing, H., and Rosenblum, L., ed., NASA-AEC Liquid Metals Corrosion Meeting, Washington, D. C., December 7-8, 1960, NASA TN-D-769.

Helms, Jr., H. H., "Review of Aluminum-Iron Magnetic Alloys and Associated Systems," Technical Report 62-144, Naval Ordinance Laboratory, October 23, 1962.

_____, "Hiperco Soft Magnetic Material for High Flux Levels," Hiperco 50, Technical Data Bulletin 52-163, Westinghouse Electric Company, March 1963, pp. 9-12.

Javitz, A. E., and Barkan, H. E., "Transformer Materials for Extreme Environments," Elec. Mfg., 1960.

Knowlton, A. E., ed., Standard Handbook for Electrical Engineers, McGraw-Hill Book Company, New York, 1957.

Matheson Gas Data Book, The Matheson Co., Inc., East Rutherford, N.J., 1961.

Meek, J. M., and Craggs, J. D., "Electrical Breakdown of Gases," Claredon Press, Oxford, 1953.

Minges, M. L., "Thermal Insulations for Aerospace Applications -423° to 3000°F," TDR-63-699, Aeronautical Systems Division, September 1963.

Pasnak, M., and Lundsten, R. H. "Effects of Extremely High Temperature on Magnetic Properties of Core Material," Report 6132, NAVORD, July 10, 1958.

Schindler, A. I., and Salkovitz, E. I., "Effect of Applying a Magnetic Field During Neutron Irradiation on Magnetic Properties of Fe-Ni Alloys," J. Appl. Phys., Vol. 31, Supp., No. 5, May 1960.

Schmidt, F. F., "Tantalum and Tantalum Alloys," DMIC Report 133, Defense Metals Information Center, Battelle Memorial Institute, July 25, 1960.

_____, "Tantalum Base Alloy, T-111," Special Technical Data Bulletin 52-365, Westinghouse Electric Corp., March 1963.

Stanley, J. K., Electrical and Magnetic Properties of Metals, ASM, Cleveland, Ohio, 1963.

REFERENCES

1. Faraday, M., "Bakerian Lecture Series," (January 12, 1832), Phil. Trans. Roy. Soc., vol. 15, 1832, p. 125.

2. Holden, Frank, "Mercury Meter," U.S. Patent 853,789, May 14, 1907..

3. Northrup, E.A., "Some Newly Observed Manifestations of Forces in the Interior of an Electric Conductor," Phys. Rev., vol. 24, 1907, p. 474.

4. Hartmann, J.F.G.P., "Improvements in or Relating to Apparatus for Producing a Continuous Electrically Conducting Liquid Jet," British Patent 126,947, December 1919.

5. Hartmann, J., "Mercury Dynamics. I. Theory of the Laminar Flow of an Electrically Conductive Liquid in a Homogeneous Magnetic Field," Kgl.. Danske Videnskab. Selskab Math. - fys. Medd., vol. 15, no. 6, 1937.

6. Hartmann, J., and Lazarus, F., "Mercury Dynamics. II. Experimental Investigations of the Flow of Mercury in a Homogeneous Magnetic Field," Kgl. Danske Videnskab. Selskab Math. - fys. Medd., vol. 15, no. 7, 1937.

7. Phillips, J.H., "Improvements in Pumps for Producing a Flow of Conducting Liquid," British Patent 528,091, October 22, 1940.

8. Einstein, A., and Szillard, L., "Pump, Especially for Refrigerating Machine," British Patent 344,881, 1931.

9. Spencer, U.S. Patent 1,792,449, February 10, 1931.

10. Lago, U.S. Patent 2,258,415, October 7, 1941.

11. Berthier, L.J., "Pompe Electro-Magnetique," French Patent 888,532, December 15, 1943.

12. Bainbridge, K.T., "Liquid Conductor Pump," U.S. Patent 1,660,407, February 1928.

13. Tama, M., "Electromagnetic Pumping of Molten Metals," Iron Age, December 4, 1947.

14. "Research on Spacecraft and Power Plant Integration Problems", Topical Report, NAS-CR-54159, Contract NAS3-2533; 64SD892 Missile and Space Division, General Electric Co., July 24, 1964.

15. Panholzer, R., "Electromagnetic Pumps," Electrical Engineering, vol. 82, no. 2, February 1963.

16. Baker, R.S., "Theory, Design, and Performance of Helical-Rotor, Electromagnetic Pump," Report NAA-SR-7455, Contract AT(11-1)-GEN-8, North American Aviation, May 31, 1963.

17. McAdams, W.H., Heat Transmission, McGraw Hill Book Company, New York.

18. Marks, L.S., Mechanical Engineering Handbook, McGraw Hill Book Company, New York.

19. Cowling, T.G., Magnetohydrodynamics, Interscience Publishers, New York.

20. Schlichting, H., Boundary Layer Theory, McGraw Hill Book Company, New York.

21. Lamb, H., Hydrodynamics, Cambridge University Press, London.

22. Grindell, A.G., "Correlation of Cavitation Inception Data for a Centrifugal Pump Operating in Water and in Sodium-Potassium Alloy (NaK)," Trans. ASME, Series D.,vol. 82, December 1960, pp. 821-828.

23. Wood, G.M., "Cavitation Testing Techniques for High Temperature Liquid Metal Systems," ASME Symposium on Cavitation Research Facilities and Techniques, May 1964.

24. Holl, J.W., "Cavitation Research Facilities at the Ordnance Research Laboratory of the Pennsylvania State University," ASME Symposium on Cavitation Research Facilities and Techniques, May 1964.

25. Hammitt, F.G., "Observations on Cavitation Damage in a Flowing System," Trans. ASME, Series D, September 1963, pp. 347-359.

26. Barnard, J., and Collins, G.D., "Test of 1200 GPM Linear AC Electromagnetic Pump," Report AECD-3460, Knolls Atomic Power Laboratory, General Electric Company.

27. Blake, L.R., "Conduction and Induction Pumps for Liquid Metals," Proc. IEE, Part A, vol. 104, no. 13, February 1957.

28. Watt, D.A., "The Design of Electromagnetic Pumps for Liquid Metals," Paper No. 2763 U, IEE, December 1958.

29. Barnes, A.H., "Direct-Current Electromagnetic Pumps," Nucleonics, January 1953.

30. Woodrow, J., "The D.C. Electromagnetic Pump for Liquid Metals," Paper No. E/R 452, A.E.R.E., Harwell, December 2, 1949.

31. Rossow, V.J., Jones, W.P., and Huerta, R.H., "On the Induced Flow of an Electrically Conducting Liquid in a Rectangular Duct by Electric and Magnetic Fields of Finite Extent," Technical Note D-347, NASA, January 1961.

32. Sutton, G.W., Hurwitz, H., Jr., and Poritsky, H., "Electrical and Pressure Losses in a Magnetohydrodynamic Channel Due to Current Loops, AIEE Paper No. 61-1078, October 15, 1961.

33. Okhremenko, N.M., "Electromagnetic Phenomena in Flat-Type Induction Pumps for Molten Metal," J. ARS, Supp., September, 1962. (Translated and Reprinted from Elektrichestvo, no. 3, March 1960.)

34. Schwab, B., "Theory of Annular Electromagnetic Pumps and Comparison with Experiments," Liquid Metal Colloquium of the European Society of Atomic Energy, Aix-en-Provence, September 30 - October 2, 1963.

35. Sudan, R.N., "Interaction of a Conducting Fluid Stream with a Traveling Wave of Magnetic Field of Finite Extension," J. Appl. Phys., vol. 34, no. 3, March 1963.

36. Watt, D.A., "A Single Phase Annular Induction Pump for Liquid Metals," Report ED/R 1844, A.E.R.E., Harwell, January 1956.

37. Matolich, J., Jr., Private Communication, August 1964.

38. Blake, L.R., "Resistivity Monitor to Indicate Oxide Content of Sodium," Paper No. 3278M, IEE, August 1960.

39. Deem, H.W., and Matolich, J., Jr., "The Thermal Conductivity and Electrical Resistivity of Liquid Potassium and the Alloy Niobium- 1 Zirconium," Report BATT-4673-T6, Battelle Memorial Institute, 1963.

40. Kapelner, S.M., and Bratton, W.D., "The Electrical Resistivity of Sodium, Potassium, Rubidium and Cesium in the Liquid State," Report PWAC 376, United Aircraft Corp., 1962.

41. Kapelner, S.M., "The Electrical Resistivity of Lithium and 46NaK," Report PWAC 349, United Aircraft Corp., 1961.

42. Weatherford, D.W., et al., "The Properties of Inorganic Energy-Conversion and Heat-Transfer Fluids for Space Applications," WADD-TR-61-96, Southwest Research Institute, 1961.

43. Lyon, R.N., ed., Liquid Metals Handbook, revised 2nd ed., U.S. Govt. Printing Office, Washington, D.C.

44. A-L Stainless Steel Handbook, Allegheny-Ludlum Steel Company, 1959.

45. Jackson, C.B., ed., Liquid Metals Handbook: NaK Supplement, U.S. Govt. Printing Office, Washington, D.C., 1955.

46. Hall, E.H., and Blocher, J.M., Jr., "The Viscosity of Saturated Liquid Potassium from 70 to 1150°C by the Oscillating-Cylinder Method," Report BATT-4763-T1, Battelle Memorial Institute, 1962.

47. Walling, J.F., Nuzum, H.K., and Lemmon, A.W., Jr., "The Vapor Pressure and Heat of Vaporization of Potassium from 480 to 1150°C," Report BATT 4673-T3, Battelle Memorial Institute, 1963.

48. Ewing, C.T., et al., "High Temperature Properties of Sodium and Potassium," Progress Report 12, Contract NASA C-76320, Report No. 6094, Naval Research Laboratory, June 2, 1964.

49. Stull, D.R., "Vapor Pressures of Pure Substances - Inorganic Compounds," Ind. Eng. Chem., vol. 39, 1947, p. 517.

50. Amateau, M.F., "The Effect of Molten Alkali Metals on Containment Metals and Alloys at High Temperatures," DMIC Report No. 169, Defense Metals Information Center, Battelle Memorial Institute, 1962.

51. Di Stefano, J.R., and Hoffman, E.E., "Corrosion Mechanisms in Refractory Metal-Alkali Metal Systems," Report ORNL 3424, Oak Ridge National Laboratory, 1963.

52. Hoffman, E.E., "Corrosion of Materials by Lithium at High Temperatures," Report ORNL 2924, Oak Ridge National Laboratory, 1960.

53. Smith, E.R., "Design of a Linear Induction Electromagnetic Pump," NAA-SA-Memo 5184, Rev. B, North American Aviation, 1960.

54. Weiss, V., ed., Aerospace Structural Metals Handbook. Vol. 1. Ferrous Alloys, Aeronautical Systems Division, USAF.

55. Bennethum, W.H., General Electric Company, Evendale, Private Communication, September 1963.

56. Haynes No. 25 Alloy (L-605), Haynes Stellite Company Bulletin.

57. Tottle, C.A., "The Physical and Mechanical Properties of Niobium," J. Inst. Metals, vol. 85, 1956-57, p. 1757.

58. Young, W. R. and E. S. Jones "Joining of Refractory Metals by Brazing and Diffusion Bonding" ASD-TDR-63-88, AF 33(616)- 7484 General Electric Company Jan. 1963 p.51.

59. Schmidt, F.F., and Ogden, H.R., "The Engineering Properties of Molybdenum and Molybdenum Alloys," DMIC Report 190, Defense Metals Information Center, Battelle Memorial Institute, September 20, 1963.

60. Schmidt, F.F., and Ogden, H.R., "The Engineering Properties of Tantalum and Tantalum Alloys," DMIC Report 189, Defense Metals Information Center, Battelle Memorial Institute, September 13, 1963.

61. Weiss, V., ed., Aerospace Structural Metals Handbook. Vol. 2. Non-ferrous Alloys, Aeronautical Systems Division, USAF.

62. Sisco, F.T., and Epremian, E., Columbium and Tantalum, John Wiley Son, New York, 1963.

63. Houck, J.A., "Physical & Mechanical Properties of Commercial Molybdenum-Base Alloys," DMIC Report 140, Defense Metals Information Center, Battelle Memorial Institute, November 30, 1960.

64. Schmidt, F.F., and Ogden, H.R., "The Engineering Properties of Columbium and Columbium Alloys," DMIC Report 188, Defense Metals Information Center, Battelle Memorial Institute, September 6, 1963.

65. Steels for Elevated Temperature Service, United States Steel Co., 1961.

66. Helms, H.H., Jr., "Adaptability of Iron-Silicon Magnetic Alloys for Special Environments," NAVWEPS Report 7331, October 26, 1960.

67. Pshechenkova, G.V., and Skokov, A.D., "Temperature Dependence of the Magnetic Saturation Induction of Alloys of the Iron-Cobalt System," Institute of Precision Alloys, USSR, Physics of Metals and Metallography, vol. 14, no. 5, 1962, pp. 798-799.

68. Martin, D.L., and Geisler, A.H., "Constitution and Properties of Cobalt-Iron-Vanadium Alloys," Trans. ASM, vol. 44, 1952, pp. 461-483.

69. "Research and Development Program on Magnetic, Electrical Inductor, Electrical Insulation, and Bare Seal Materials," Quarterly Report 3, NASA-CR-54089, June 1964.

70. "Hiperco Soft Magnetic Alloy for High Flux Levels, Hiperco 27," Technical Data Bulletin 52-163, Westinghouse Electric Company, 1963, pp. 1-4.

71. "Hiperco Soft Magnetic Alloy for High Flux Levels, Hiperco 35," Technical Data Bulleting 52-163, Westinghouse Electric Company, March 1962, pp. 5-8.

72. Goldsmith, A., et al., Handbook of Thermophysical Properties of Solid Materials, WADC-TR-58-476, vol. 2, revd. ed., November 1960.

73. Electric Steel Sheet Engineering Manual, 4th ed., United States Steel Corp., 1955.

74. Clark, J.J., and Fritz, J.F., "The Effect of Temperature on the Magnetic Properties of Silicon Iron, Cobalt Iron and Aluminum Iron Alloys," WADC-TN-59-240, July 1959.

75. Chen, C.W., "Temperature Dependence of Magnetic Properties of Silicon Iron," J. App. Phys, vol. 29, no. 9, 1958, p.1337.

76. Greene, C.K., Lee, R.E., and Lietzau, K.E., "Evaluation of Magnetic Cores at Ultra High Temperature," WADC-TR-58-483, April 1959.

77. Lauriente, M., and Lyon, G.E., "Characteristics of Supermendur at 500°C, J. App. Phys., vol. 32, Supp., no. 3, March 1961, p. 3725.

78. Pavlik, N., "High Temperature Stability of Magnetic Materials," J. Appl. Phys., vol. 32, Supp., no. 3, March 1961.

79. Bozorth, R.M., Ferromagnetism, D. Van Nostrand, New York, 1951.

80. Kaplan, Asa, "Magnetic Core Losses Resulting from a Rotating Flux," J. App. Phys., vol. 32, Supp., no. 3, March 1961.

81. Young, F.J., and Schenk, H.L., "Method for Measuring Iron Losses in Elliptically Polarized Magnetic Fields," J. App. Phys., vol. 31, Supp., no. 5, May 1960.

82. Stratton, R.D., and Young, F.J., "Iron Losses in Elliptically Rotating Fields," J. App. Phys., vol. 33, Supp., no. 3, March 1962.

83. Kaplan, A., "Origin of Excess Loss in a Generator Stator Core. Pt. 2. Losses Resulting From a Rotating Flux," Report DF 59SL303, General Electric Company, December 1959.

84. Harms, H.B., and Fraser, J.C., "Ultra High Temperature Miniaturized Power Transformers and Inductor Materials," WADC-TR-57-492, vols. 1 and 2, May 1958.

85. Sery, R.S., Fischell, R.E., and Gordon, D.I., "Effect of Nuclear Irradiation on Magnetic Properties of Core Materials," Report NAVORD 4381, December 19, 1956.

86. Sery, R.S., and Gordon, D.I., "Nuclear Irradiation Effects on Ferromagnetic Core Materials," Report NAVORD 6127, June 3, 1958.

87. Harms, H.B., and Fraser, J.C., "Ultra High Temperature (500°C) Transformers and Inductors," WADC-TR-59-348, July 1959.

88. Goldsmith, A., et al,, Thermophysical Properties of Solid Materials, WADC-TR-58-476, vol. 1, revd. ed., November 1960.

89. AMZIRK, Technical Handbook, American Metal Climax, Inc., New York, 1961.

90. New Product Information Bulletin, Cube Alloy, Handy and Harmon Company, January 1964.

91. O'Rourke, R.G., Private Communication, Brush Beryllium Corp., August 1964.

92. Frank, R.G., and Zimmerman, W.F., Materials for Rockets and Missiles, Macmillan Company, New York, 1959.

93. Soiber, R., Private Communication, C.G. Hussey Company, August 1964.

94. Metals Handbook, vol. 1, ASM, 1961.

95. Unpublished Data, American Metal Climax, Inc., April/September 1964.

96. "Alternate Turbine Generator Development Program for the 350 KW SPUR System," Final Report, General Electric Company, Cincinnati, Ohio, March 1963. (Confidential, information quoted not restricted).

97. "Development of High Temperature Transformers with New Configurations for Missiles and Aircraft," Final Report, Contract Nobsr-72671, Raytheon Company, November 1960.

98. Clark, F.M., Insulating Materials for Design and Engineering Practice, John Wiley Sons, New York, 1962.

99. Farrall, G.A., "Paschen Curves for Various Gases," Memo Report P-215, Research Laboratory, General Electric Company, December 1959.

100. Unpublished data, Advanced Technology Laboratories, General Electric Company.

101. "Research on Spacecraft and Power Plant Integration Problems," Quarterly Reports 3 and 4, Contract NAS 3-2533, 64SD700, Missile and Space Division, General Electric Company, April 26, 1964.

102. Vincent, J.L., "Transformer Design Study," Flight Propulsion Division, General Electric Company, May 1961.

103. "Space Power Systems Study D.C. to D.C. Converters for Nuclear-Thermionic Energy Sources," Final Report, Contract NAS 5-1234, WAED 63.11E, Westinghouse Electric Corp., December 3, 1963.

104. Vaughn, G.F., "Design of a Digital Static Frequency Converter. Pt. I. Circuit Design," Report DMS 64-2, Space Power and Propulsion Section, Missile and Space Division, General Electric Company, May 14, 1964.

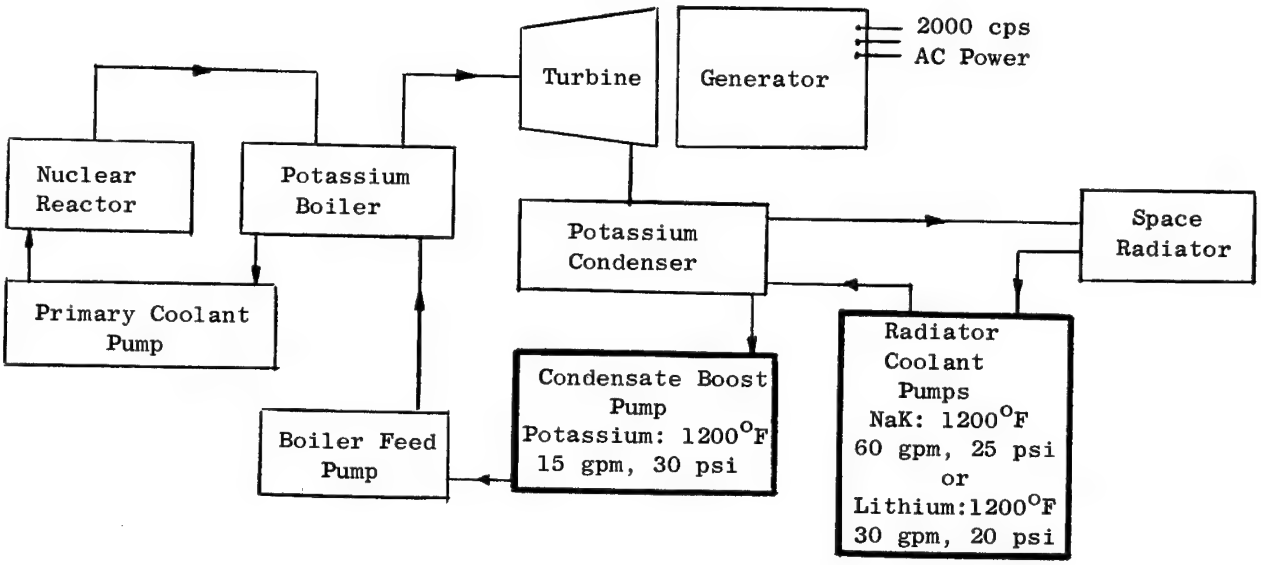

a. Turboelectric Power Plant

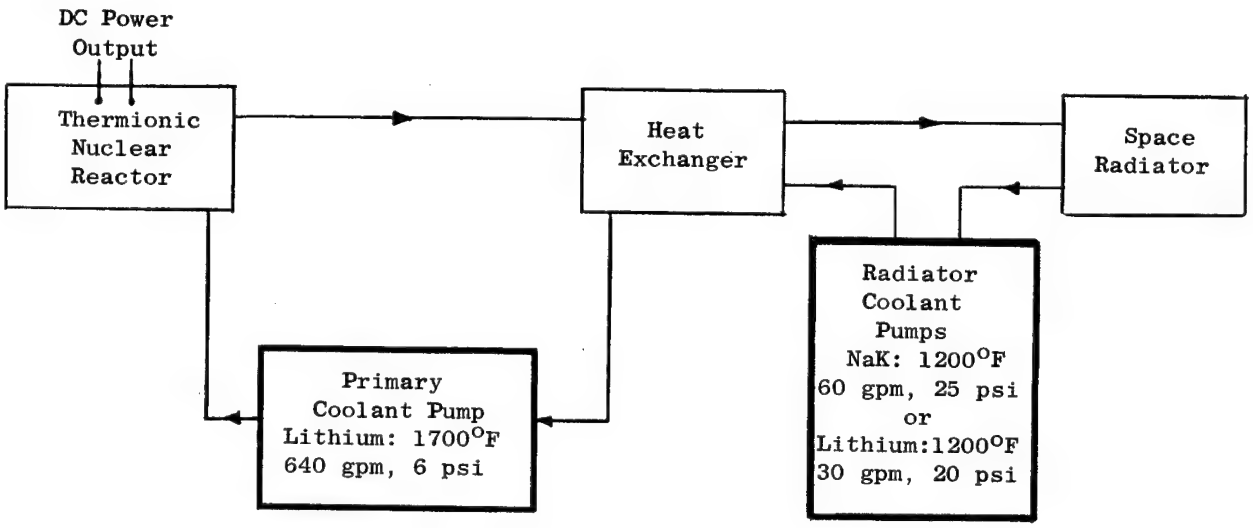

b. Thermionic Power Plant

Figure 1. Nuclear Space Electric Power Plants Schematic Diagrams.

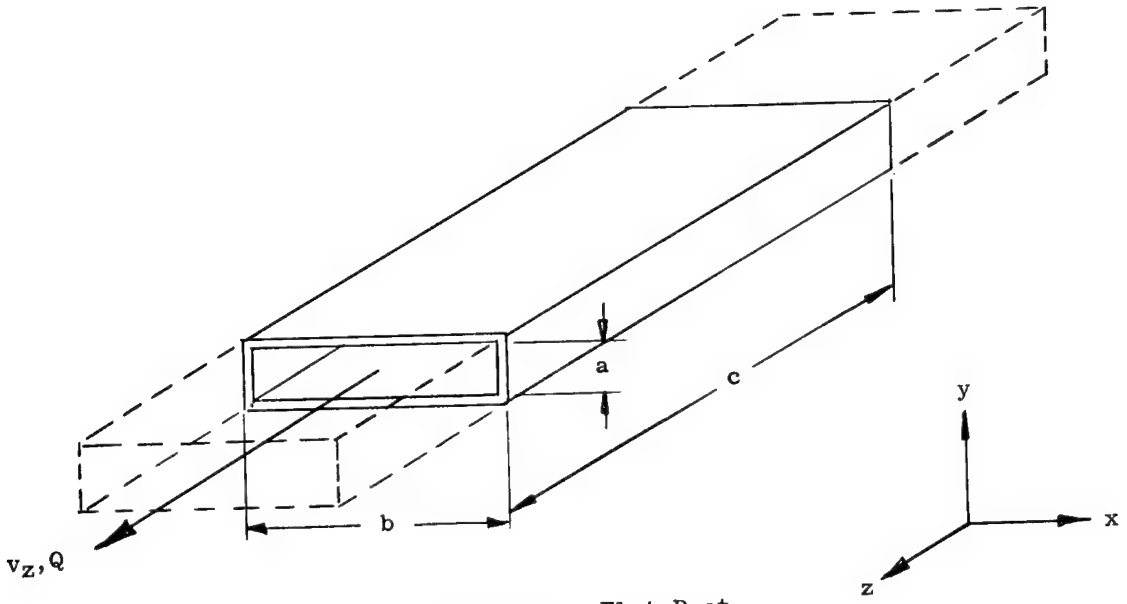

Figure 2. Flat Duct.

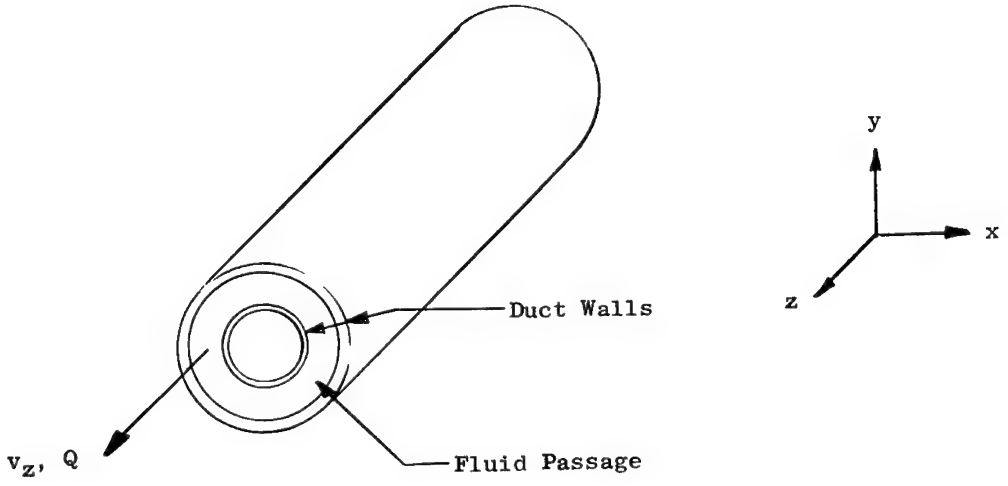

Figure 3. Axial Flow Annular Duct.

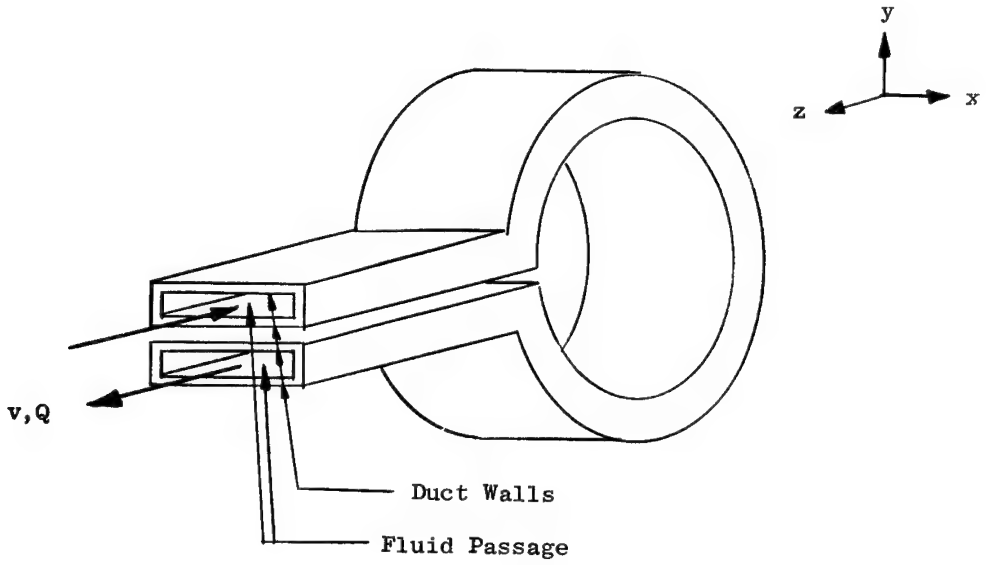

Figure 4. Tangential Flow Annular Duct.

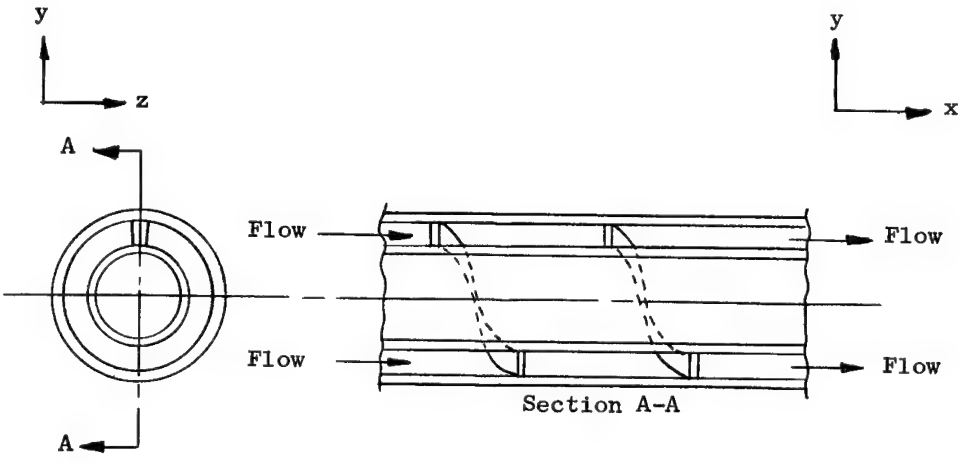

Figure 5. Helical Flow Annular Duct.

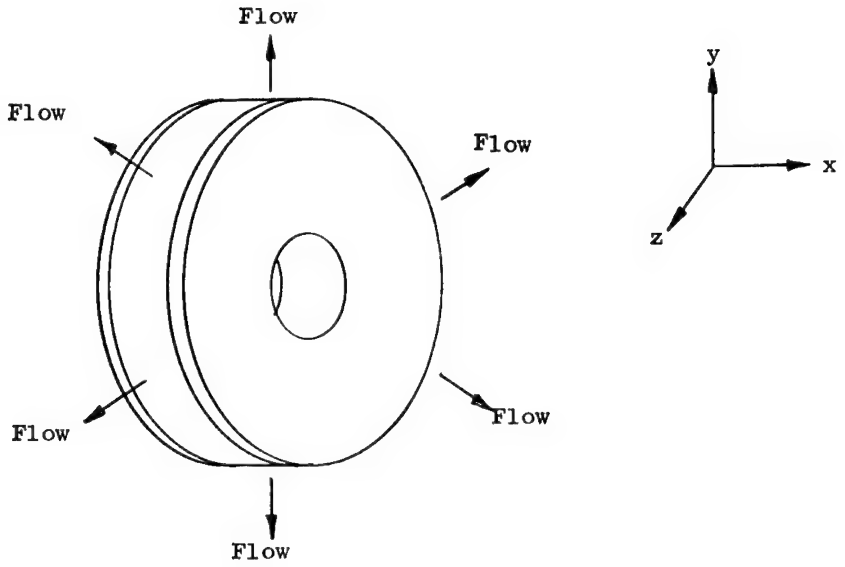

Figure 6. Radial Flow Disc.

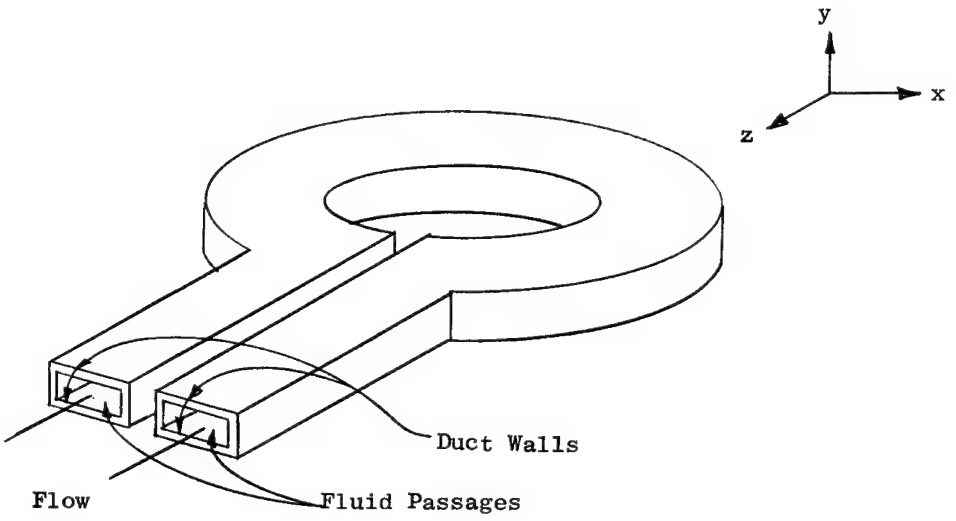

Figure 7. Tangential Flow Disc.

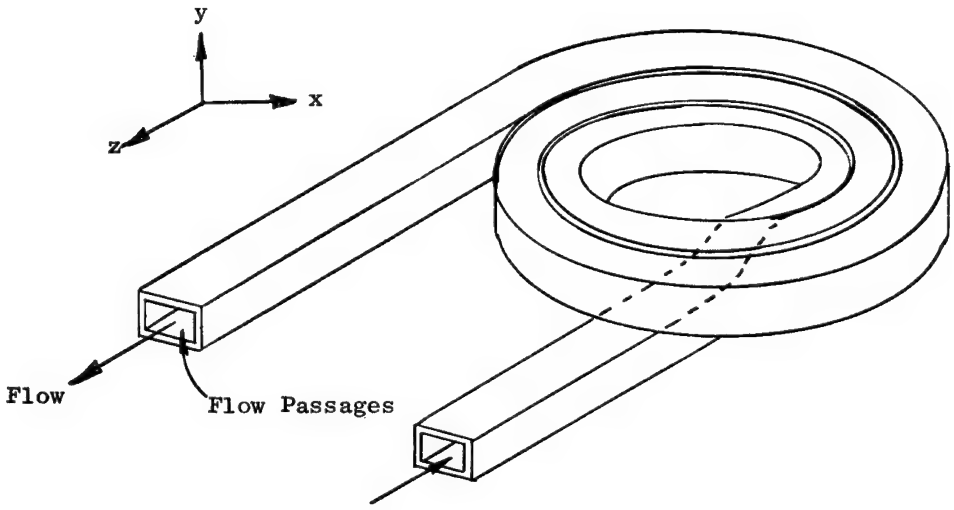

Figure 8. Spiral Flow Disc.

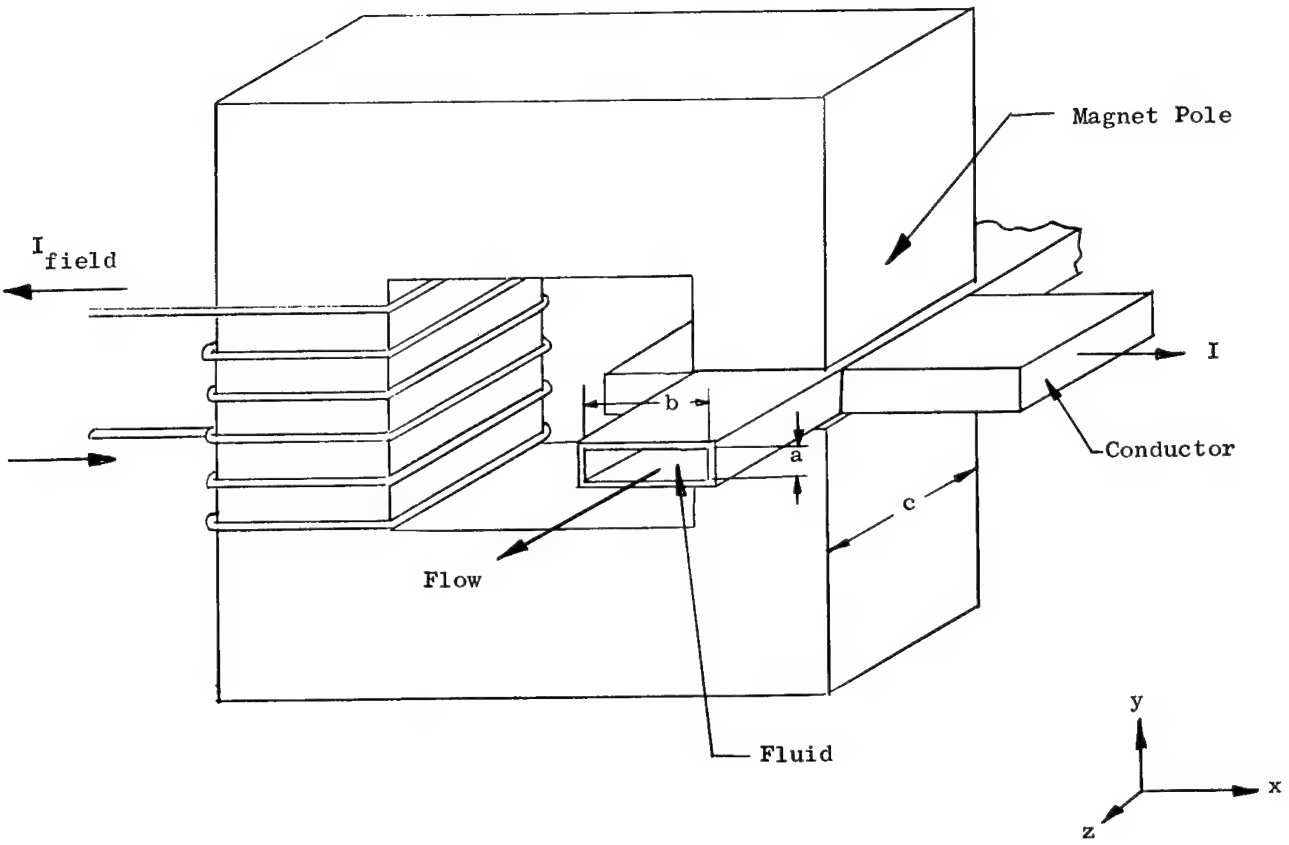

Figure 9. Conduction EM Pump.

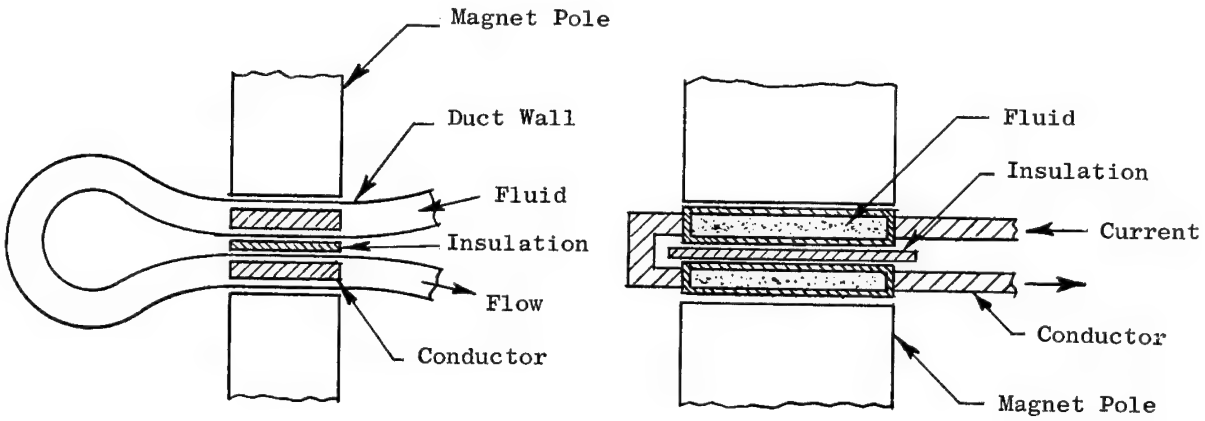

a. Common Flux, Common Current.

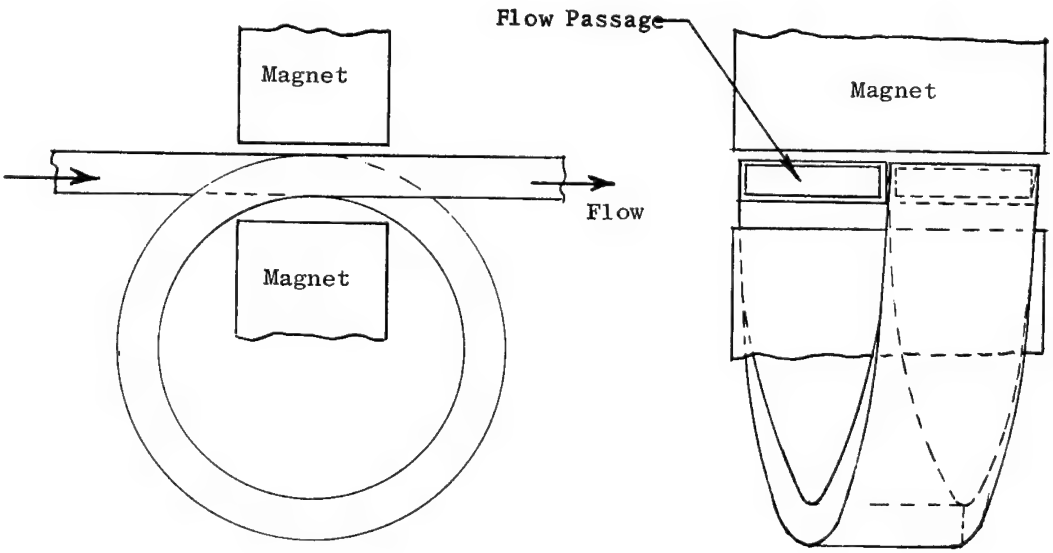

b. Common M.M.F., Common Current.

Figure 10. Two-Stage Flat Duct Conduction Pump

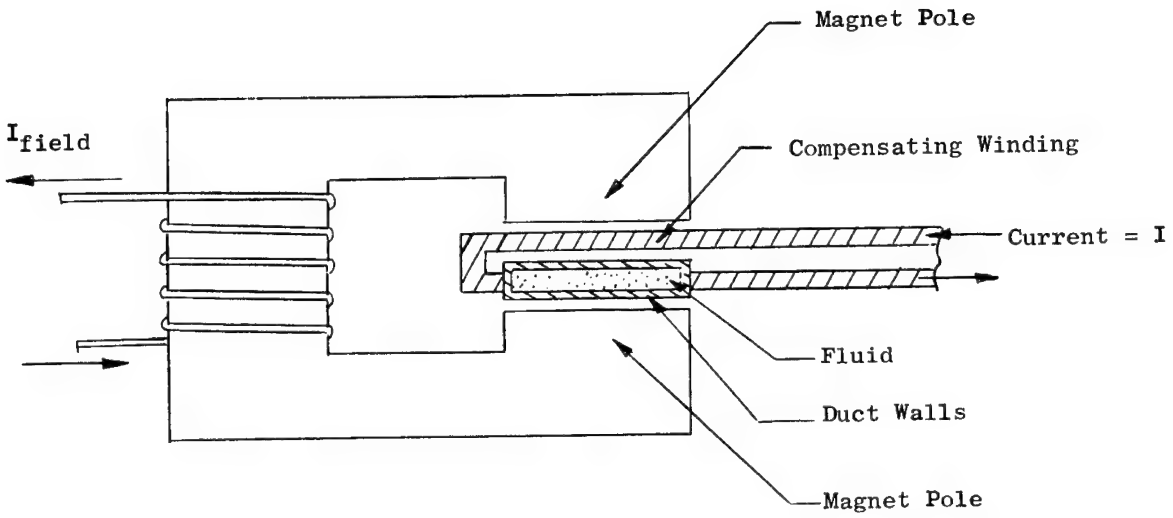

Figure 11. Compensated Conduction EM Pump.

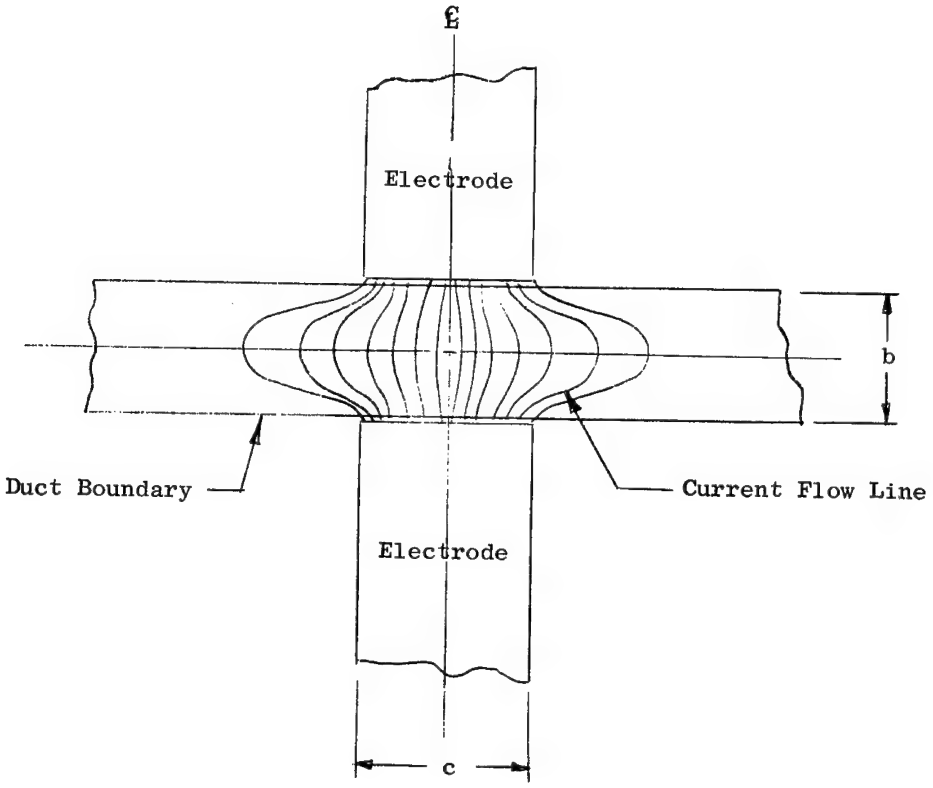

a. Current Fringing, No Insulating Barrier.

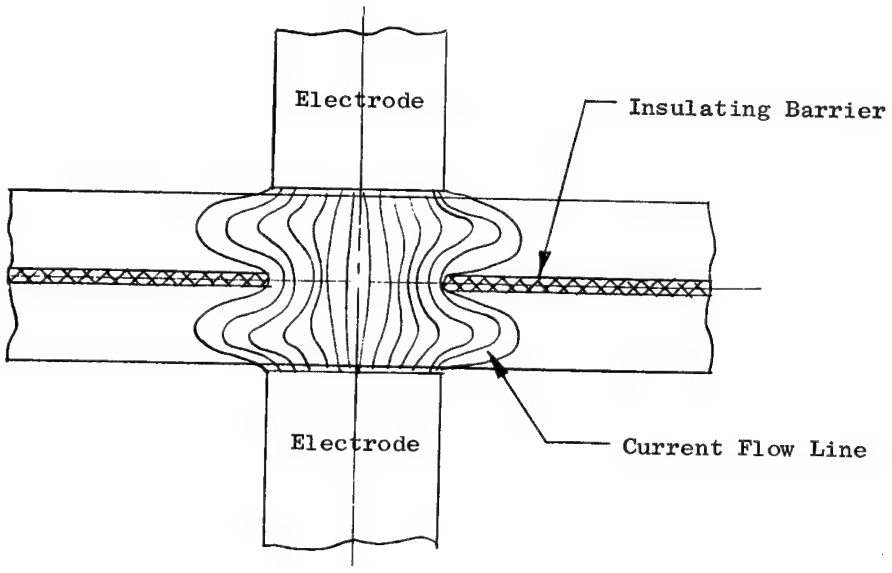

b. Current Fringing, One Insulation Barrier.

Figure 12. Current Fringing at Ends of Conduction Pump.

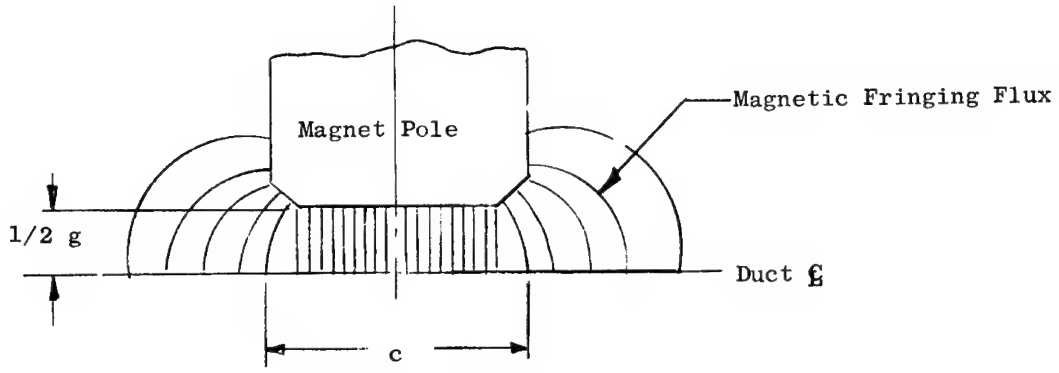

Figure 13. Flux Fringing Conduction Pump Duct.

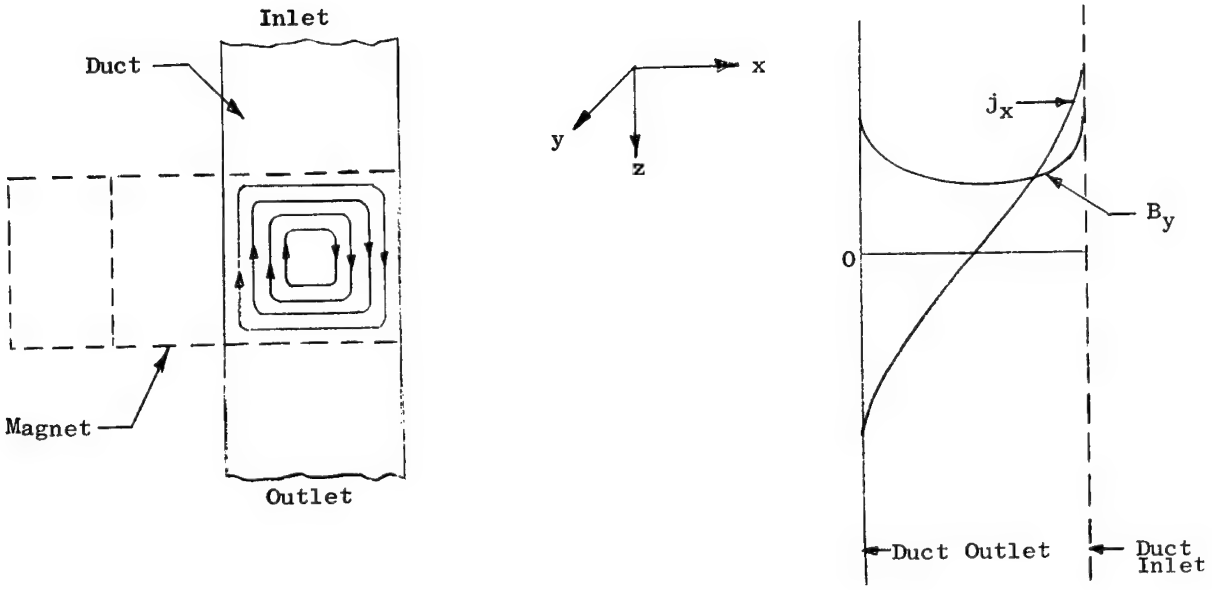

Figure 14. Eddy Current and Flux Density: Single Phase AC Conduction Pump

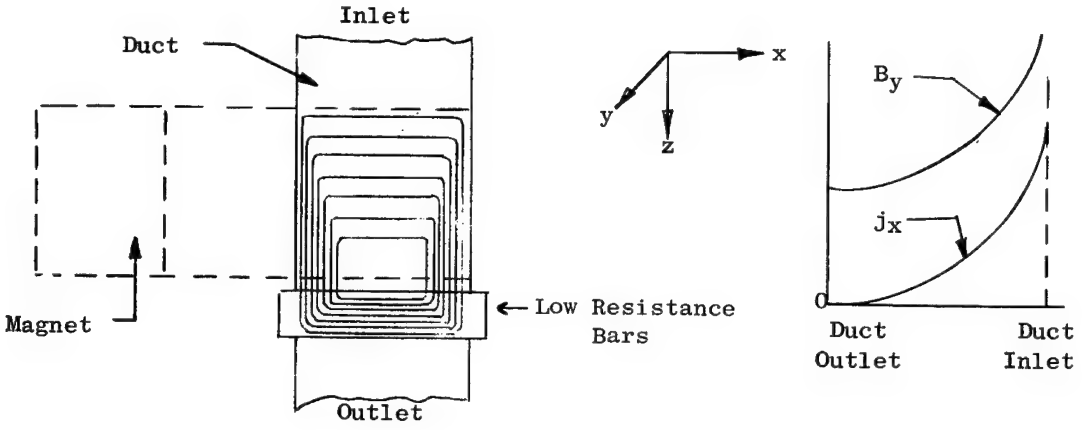

Figure 15. Eddy Current and Flux Density; Single Phase Induction Pump.

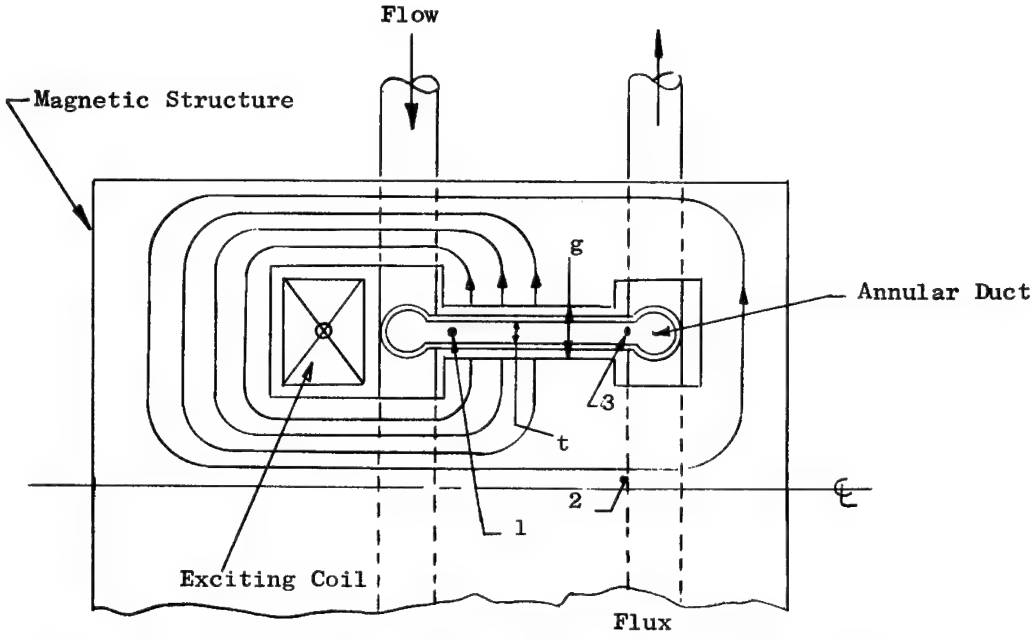

Figure 16. Annular Duct, Single Phase, Induction Pump, Type A

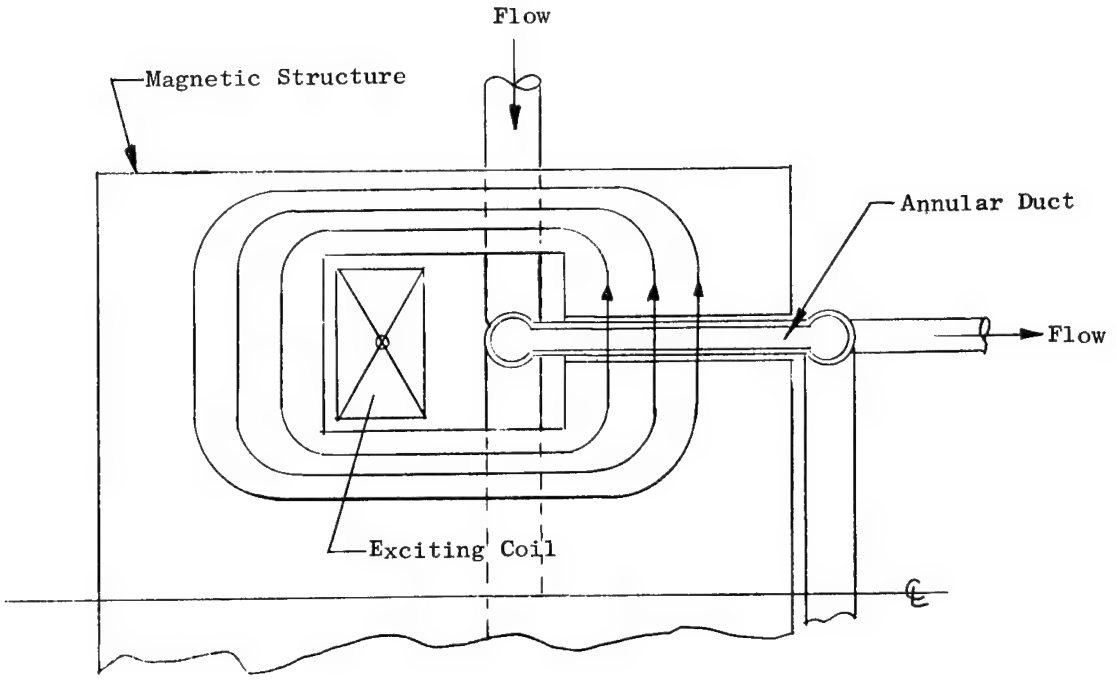

Figure 17. Annular Duct, Single Phase, Induction Pump, Type B

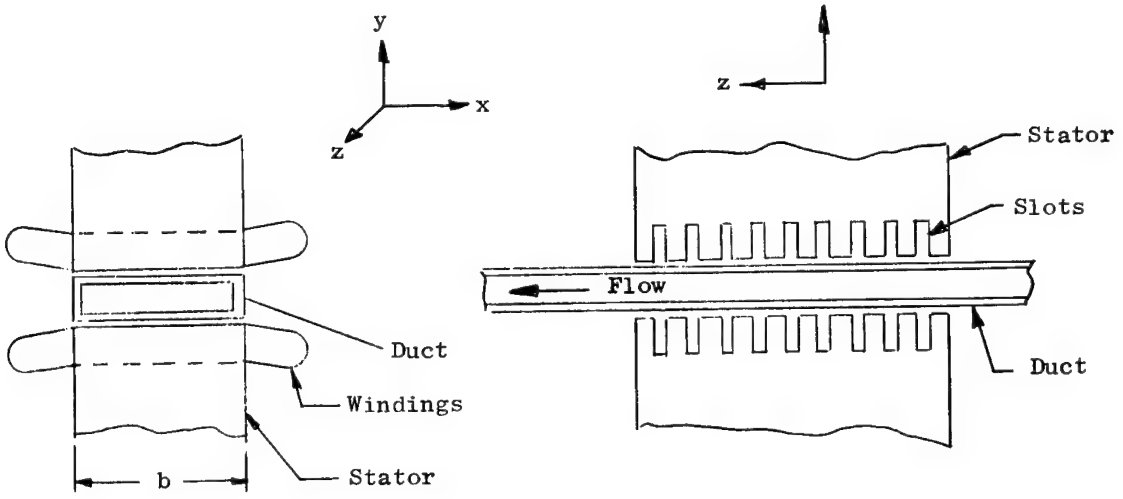

Figure 18. Flat Linear Induction Pump.

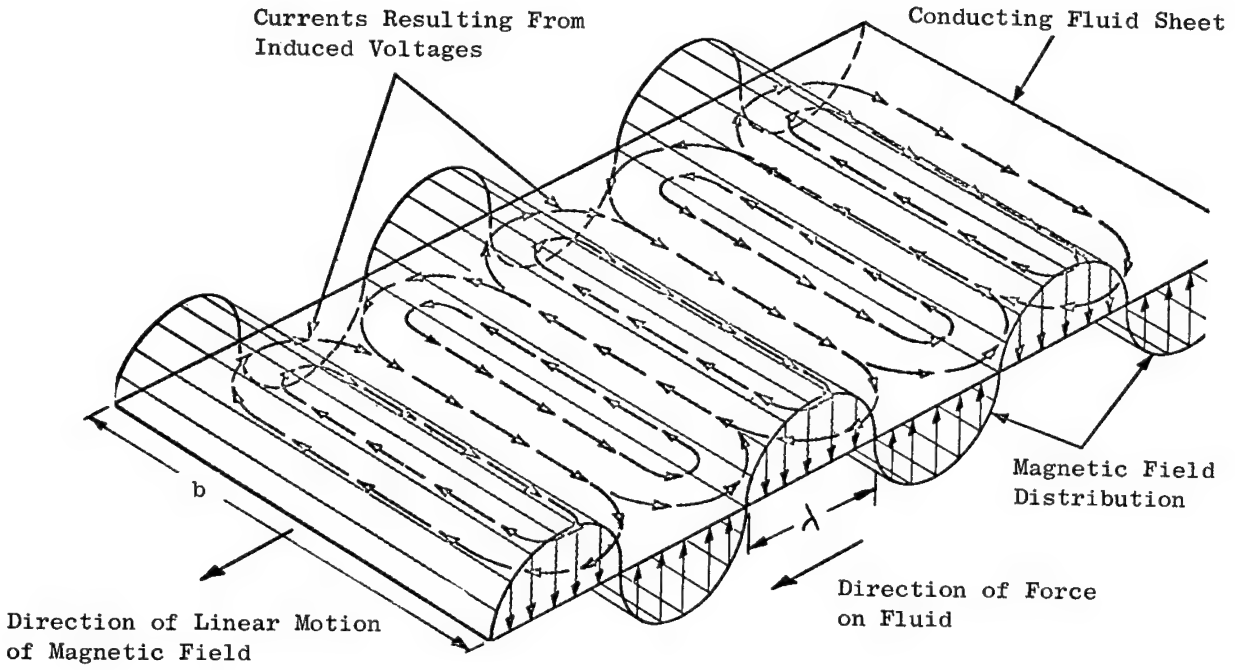

Figure 19. Field and Current Relationships in Flat Linear Induction Pump.

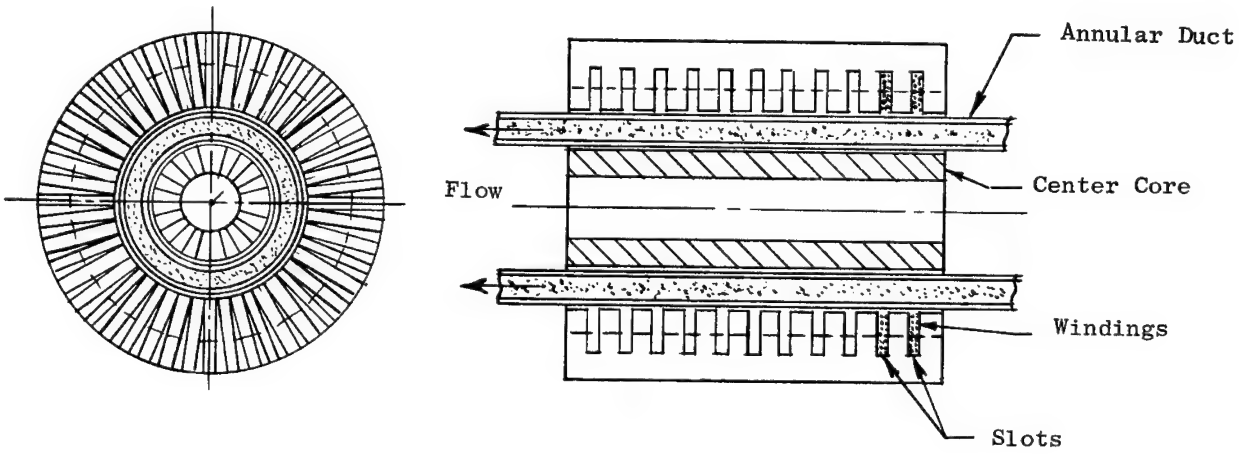

Figure 20. Annular Linear Induction Pump.

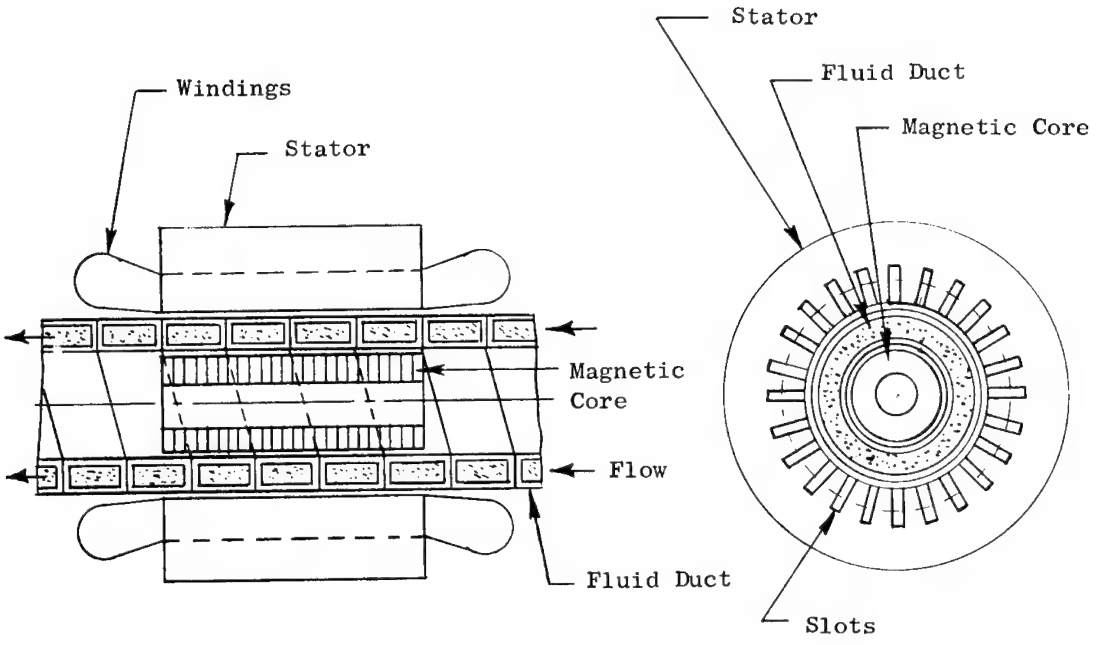

Figure 21. Helical Induction Pump.

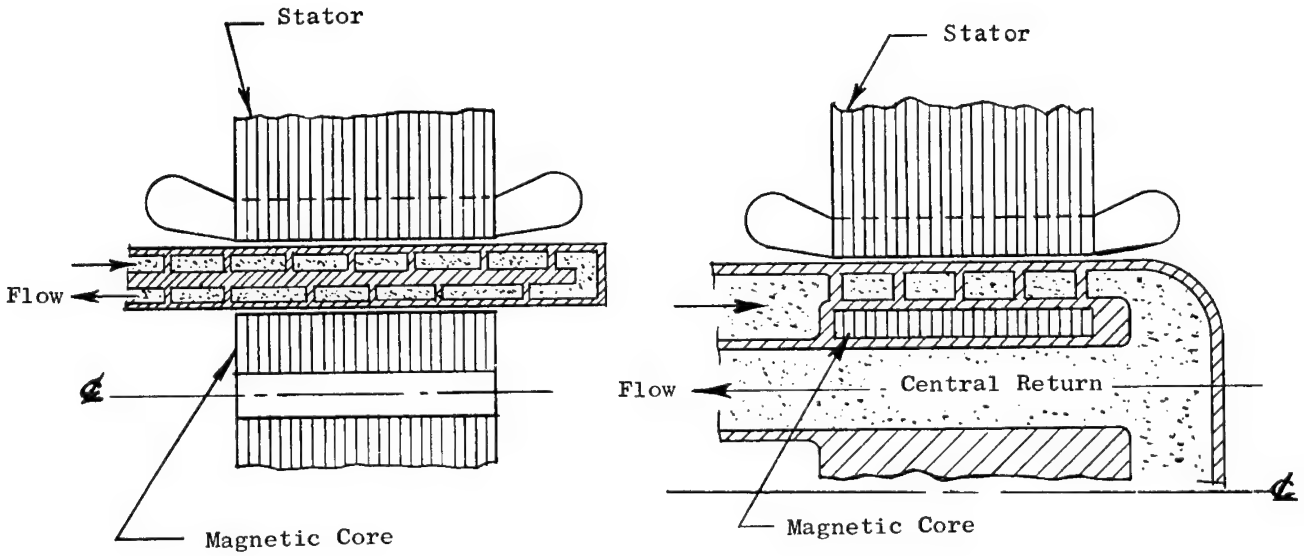

a. Two-Pass

b. One-Pass, Center Return

Figure 22. Helical Induction EM Pumps

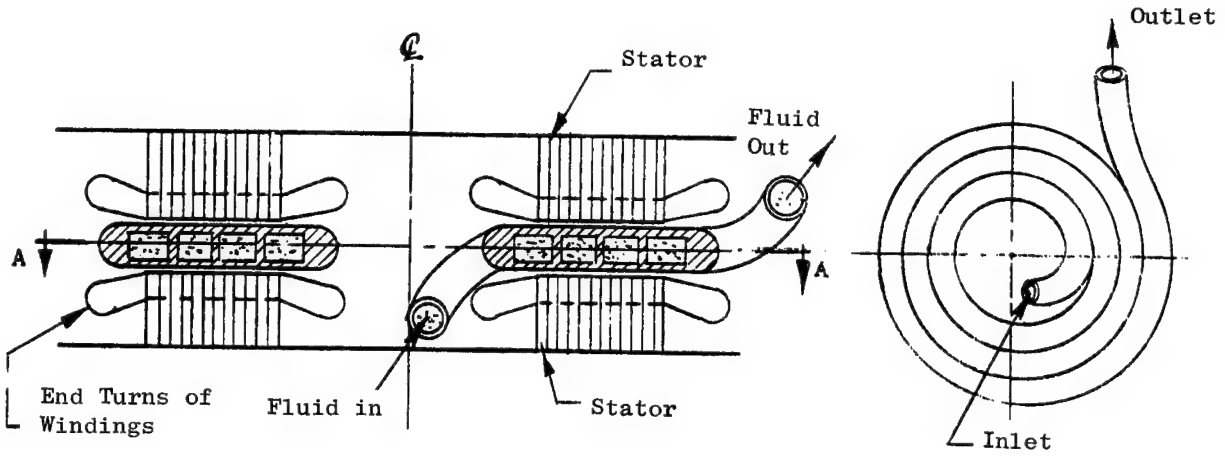

Figure 23. Spiral Induction Pump.

Section A-A
(Reduced Scale)

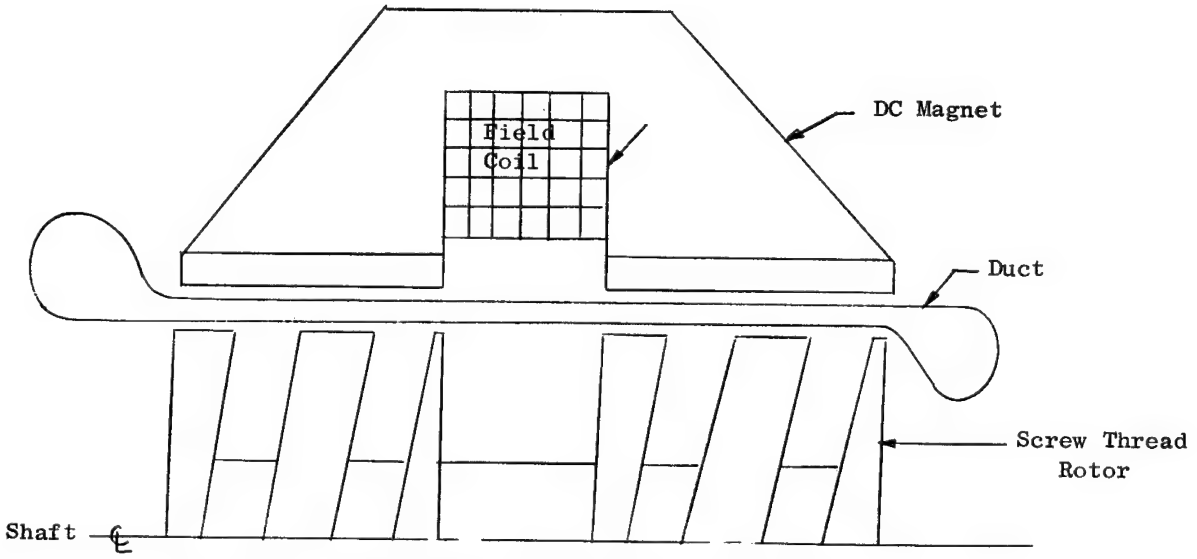

Figure 24. Moving Magnet Pump, Inductor Type I

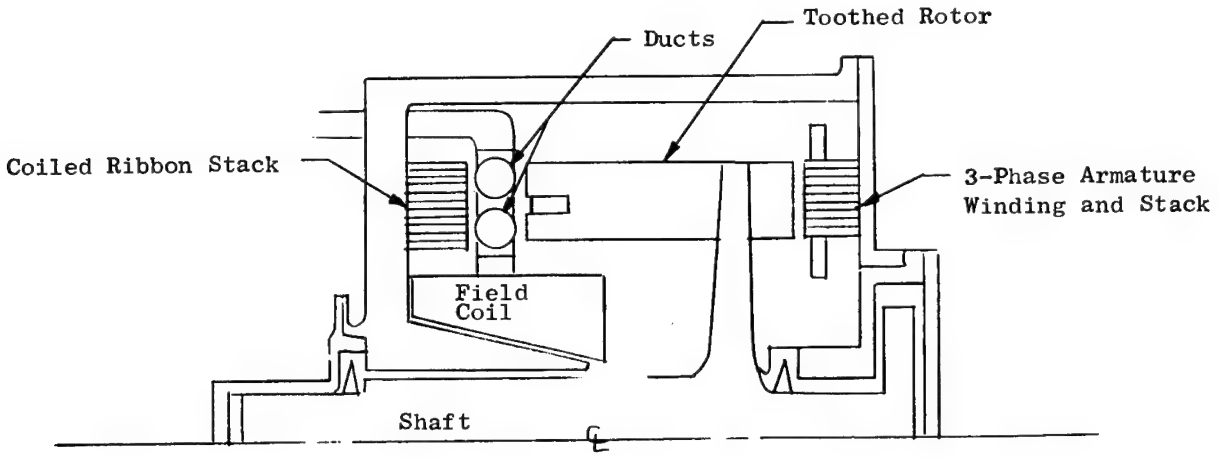

Figure 25. Moving Magnet Pump, Inductor Type.II.

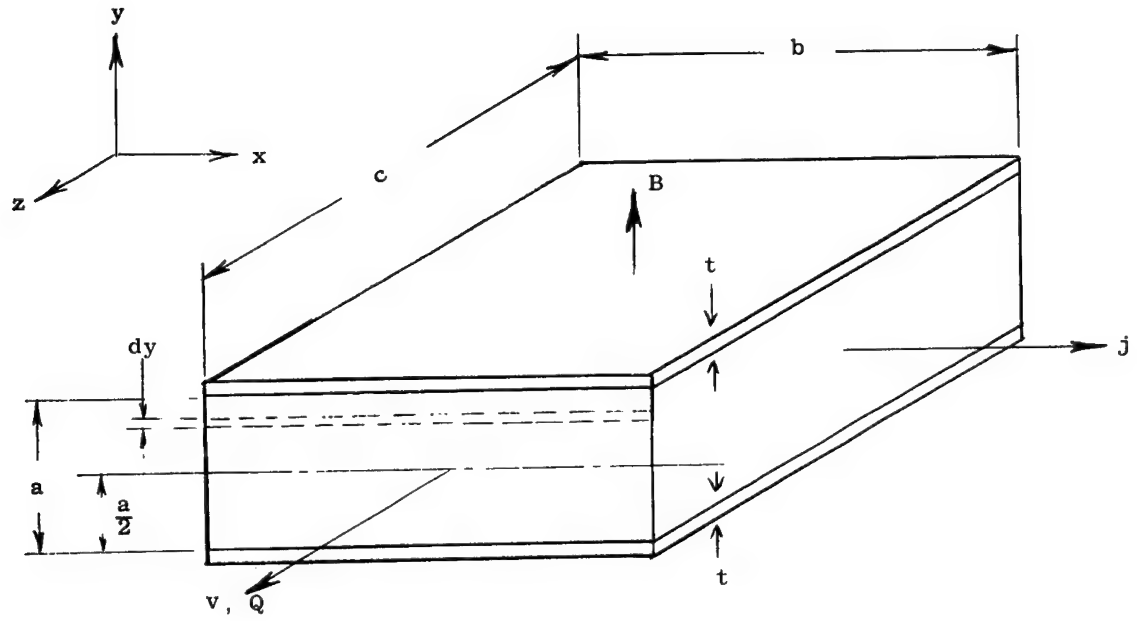

Figure 26. Pump Duct Element

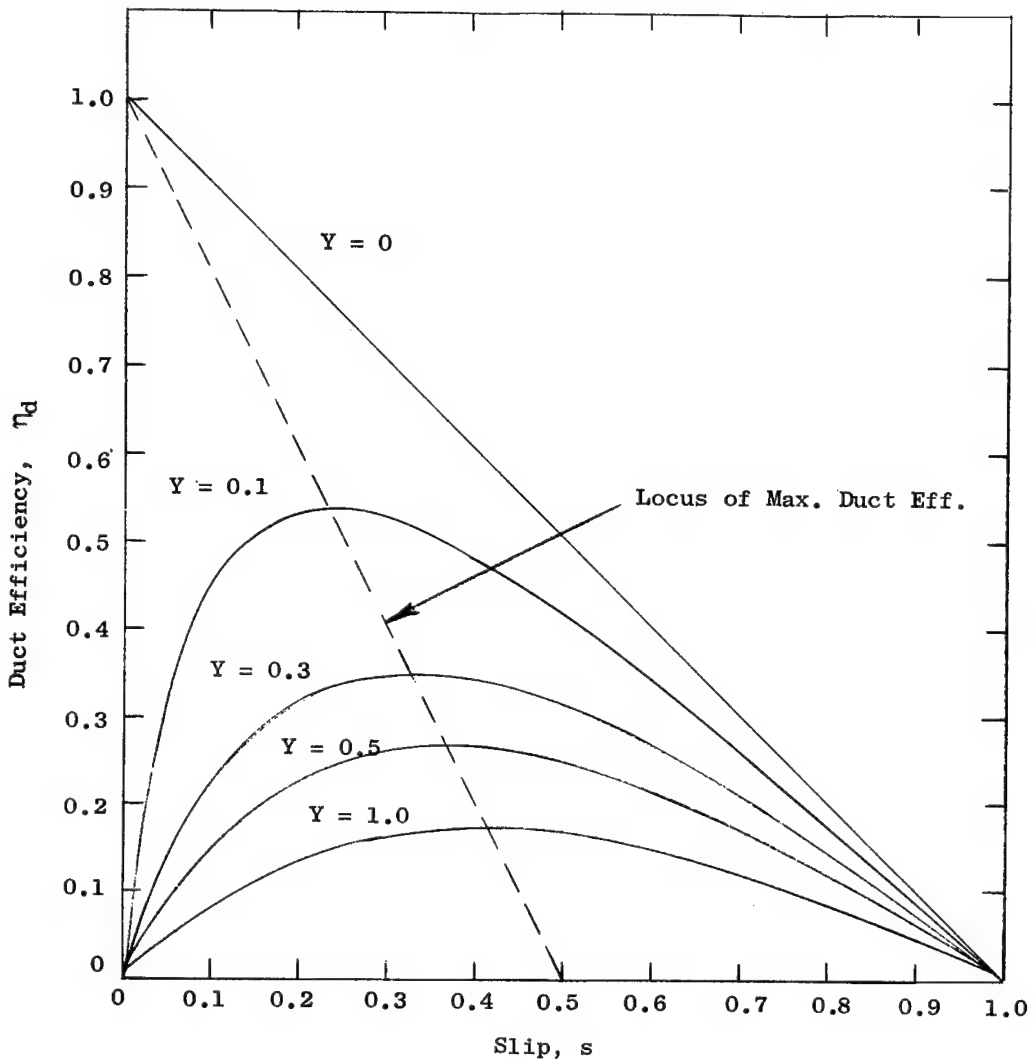

Figure 27. Duct Efficiency Vs. Slip (Includes I^2R Loss in Fluid and Duct Only).

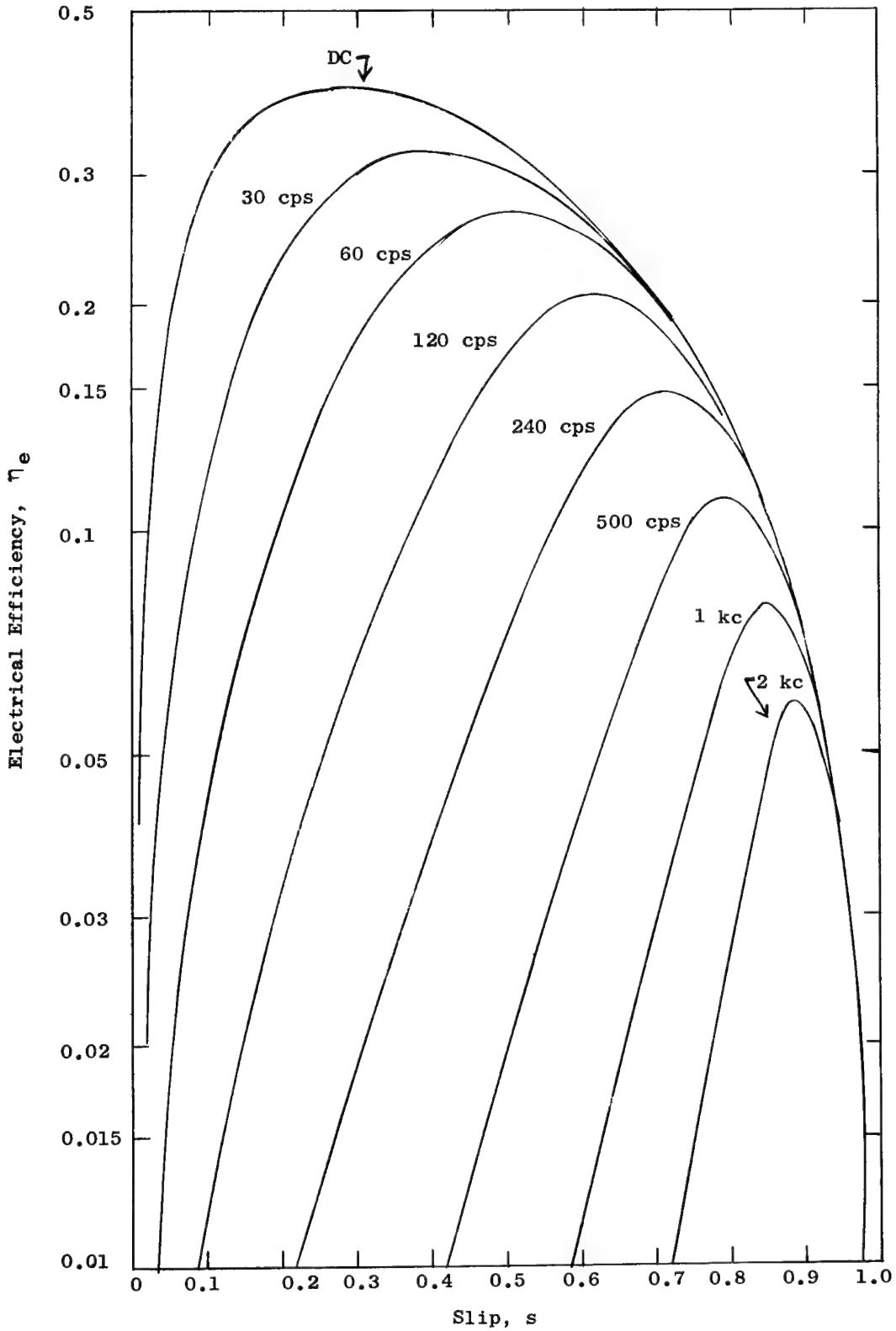

Figure 28. Electrical Efficiency Vs. Slip for Various Power Input Frequencies.

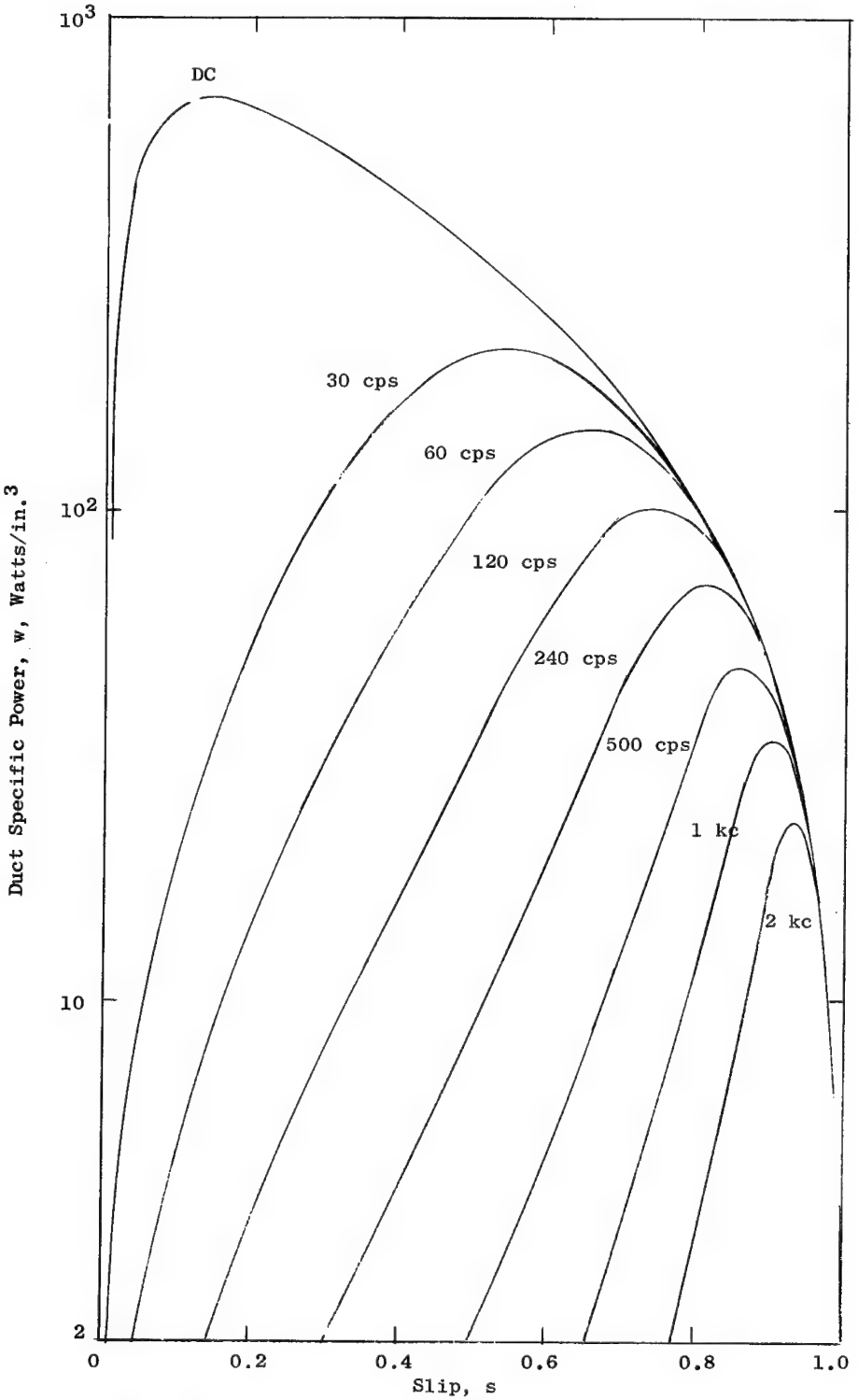

Figure 29. Duct Specific Power Vs. Slip for Various Power Input Frequencies.

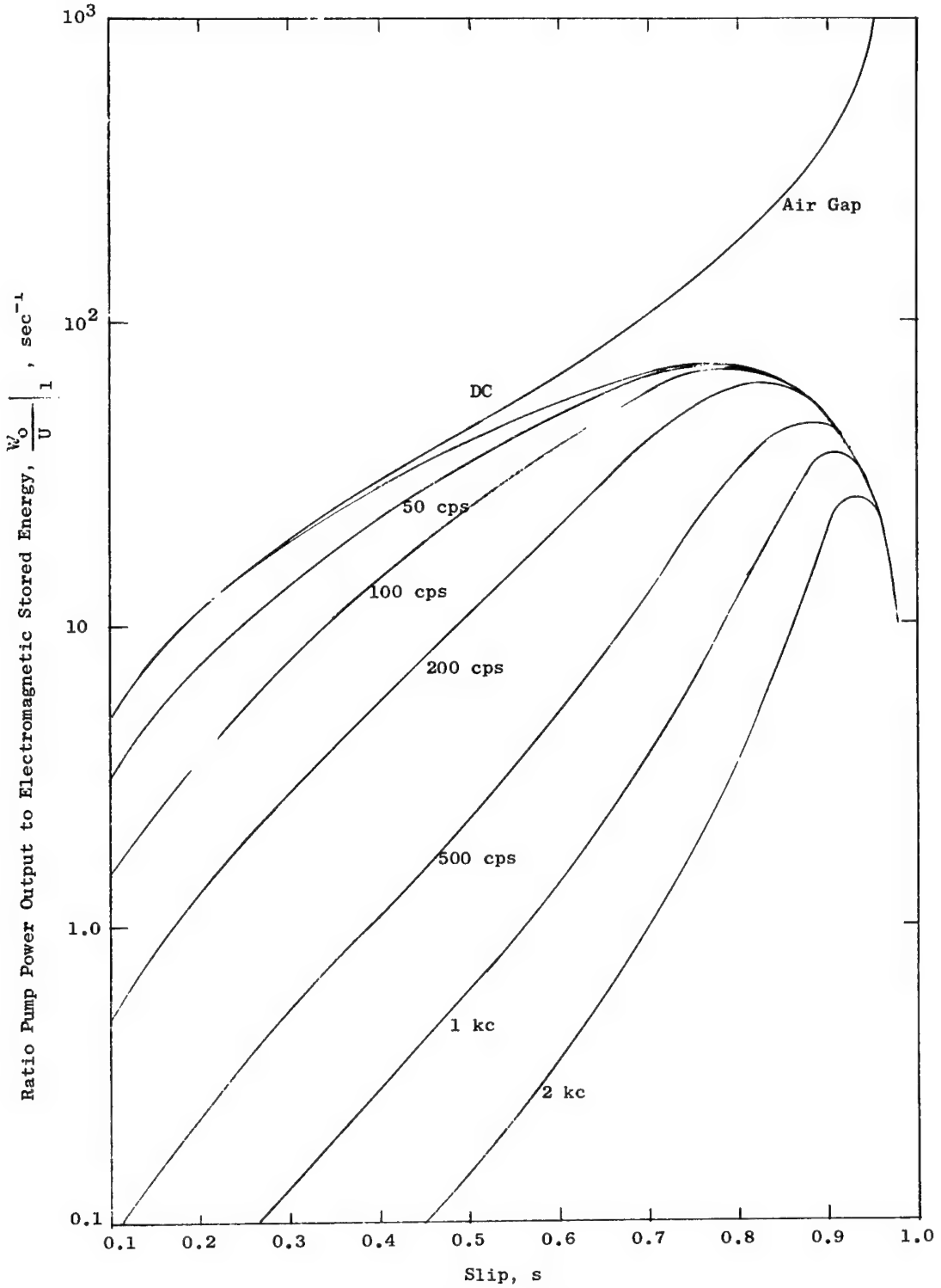

Figure 30. Stored Energy Relationships for Various Power Input Frequencies (Wound Stator on One Side of Duct).

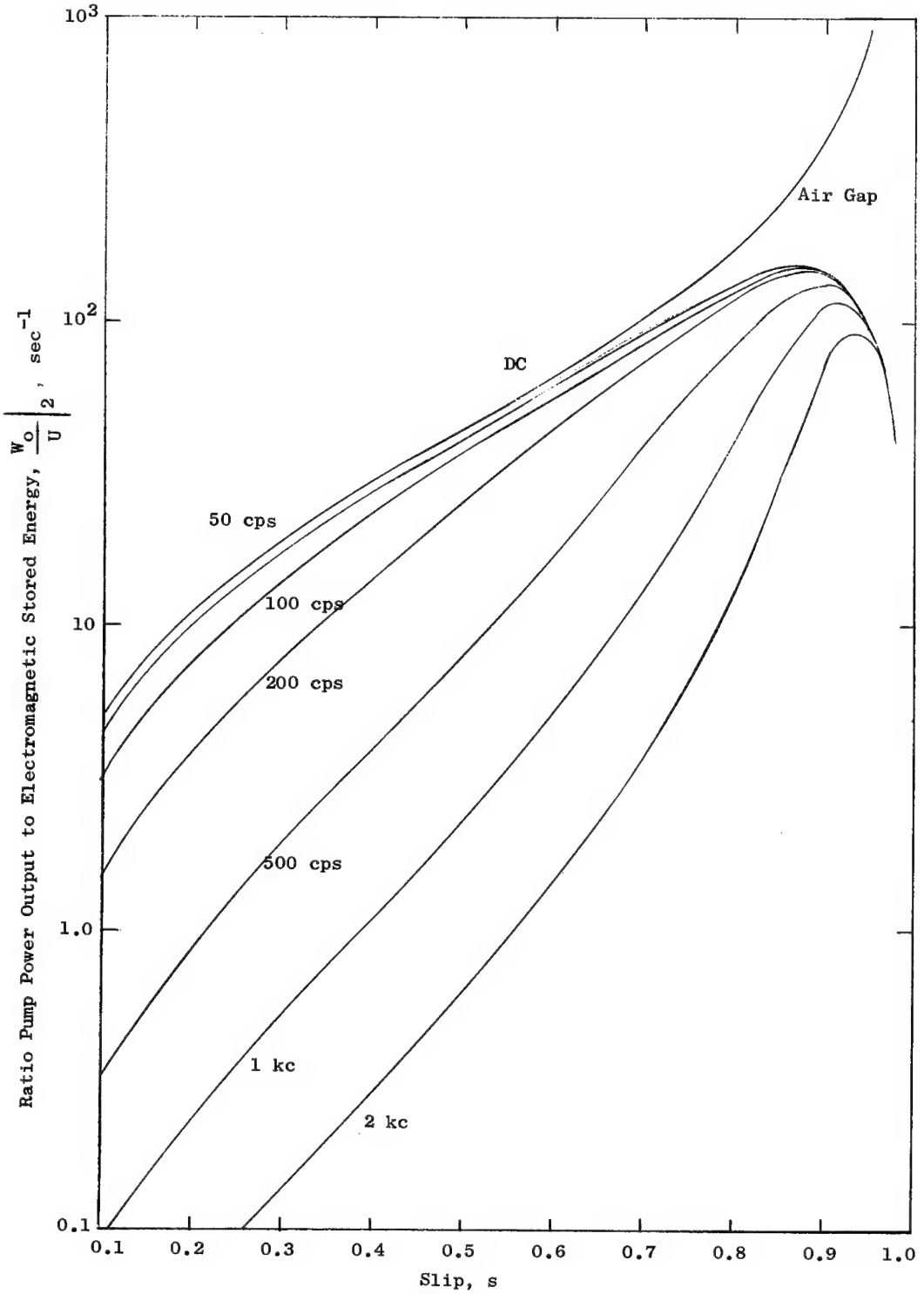

Figure 31. Stored Energy Relationships for Various Power Input Frequencies (Wound Stators on Both Sides of Duct).

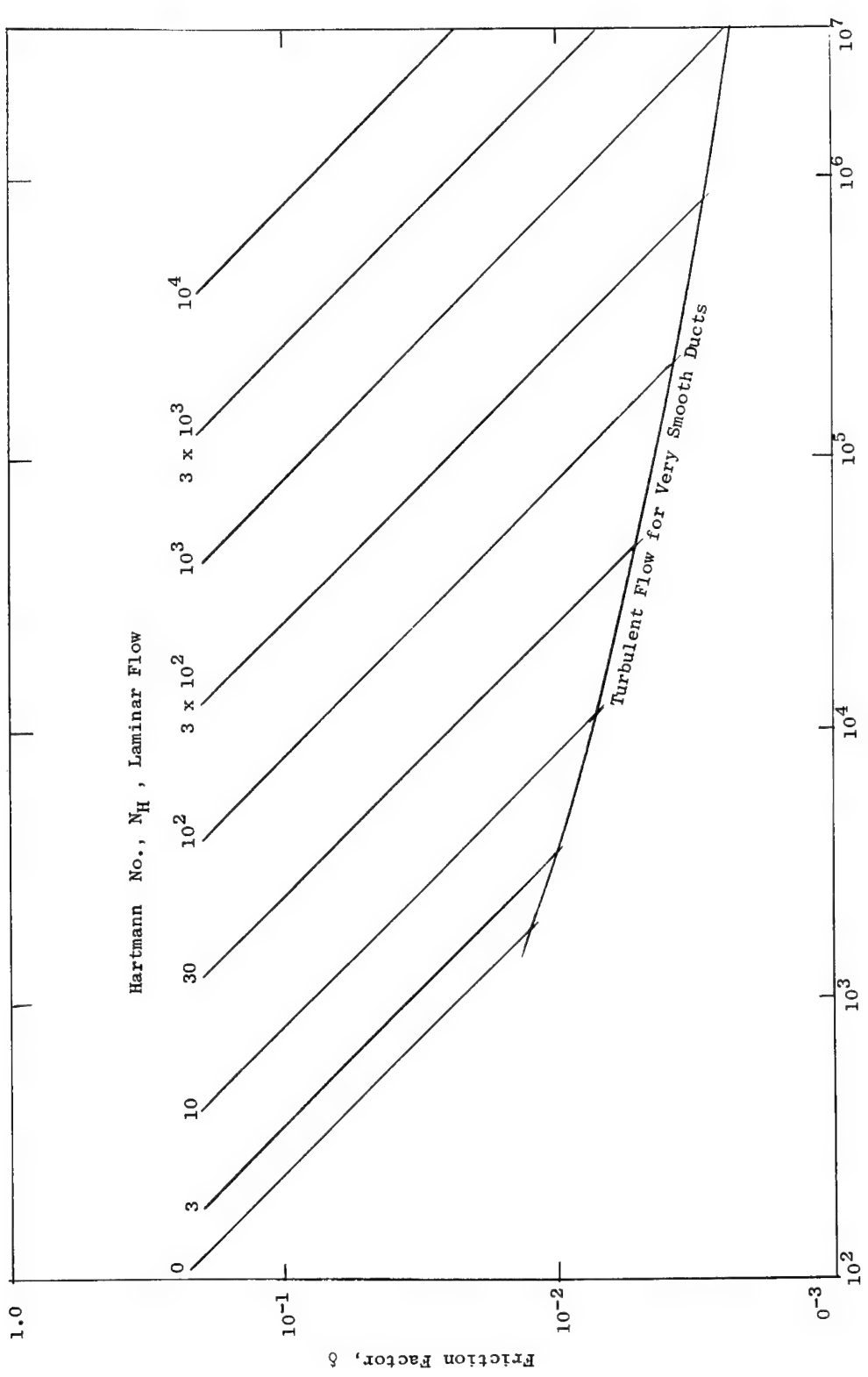

Figure 32. Friction Factor, Flow of Conducting Fluid in a Magnetic Field.

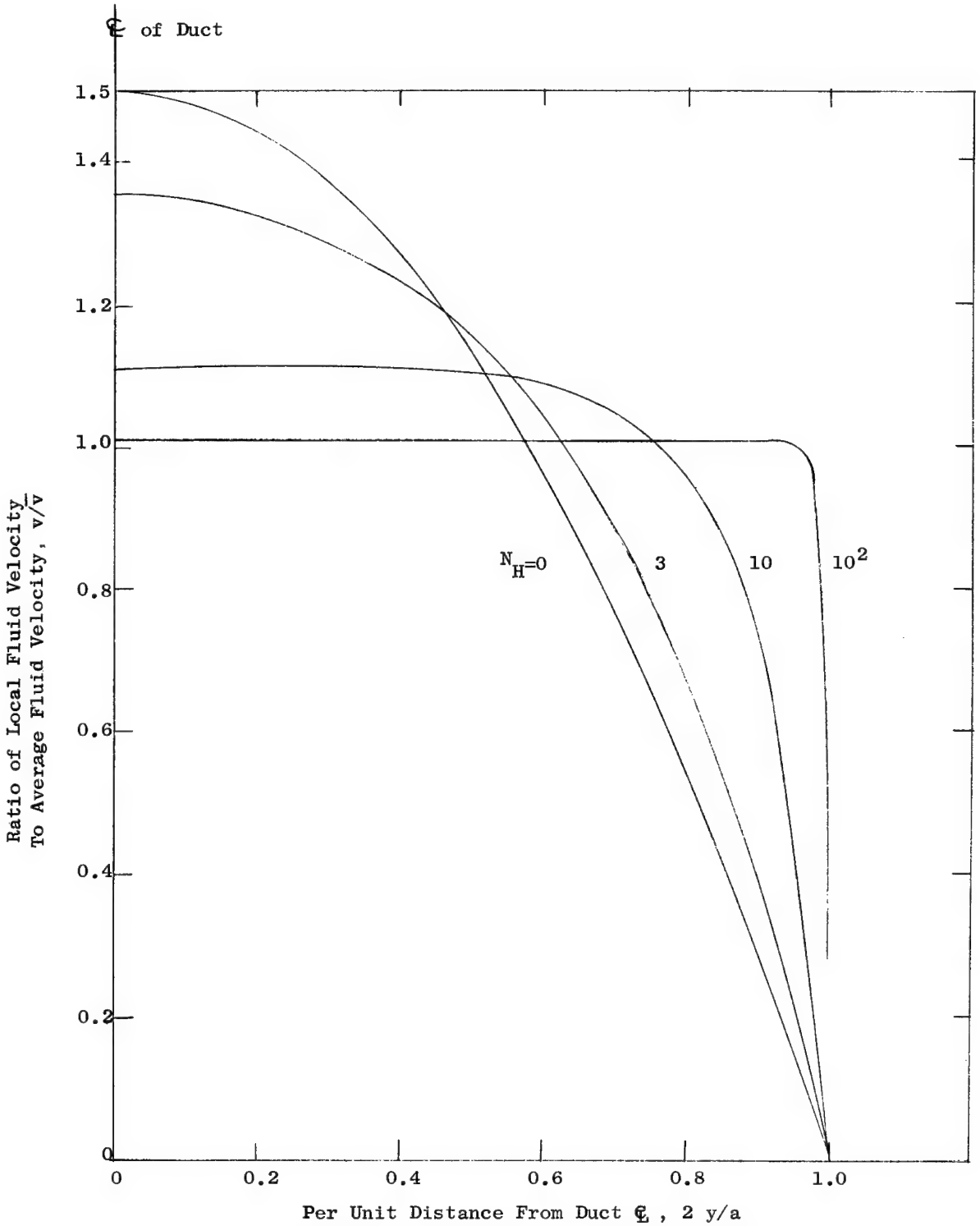

Figure 33. Fluid Velocity Profile in a Rectangular Duct as a Function of Hartmann Number (Laminar Flow).

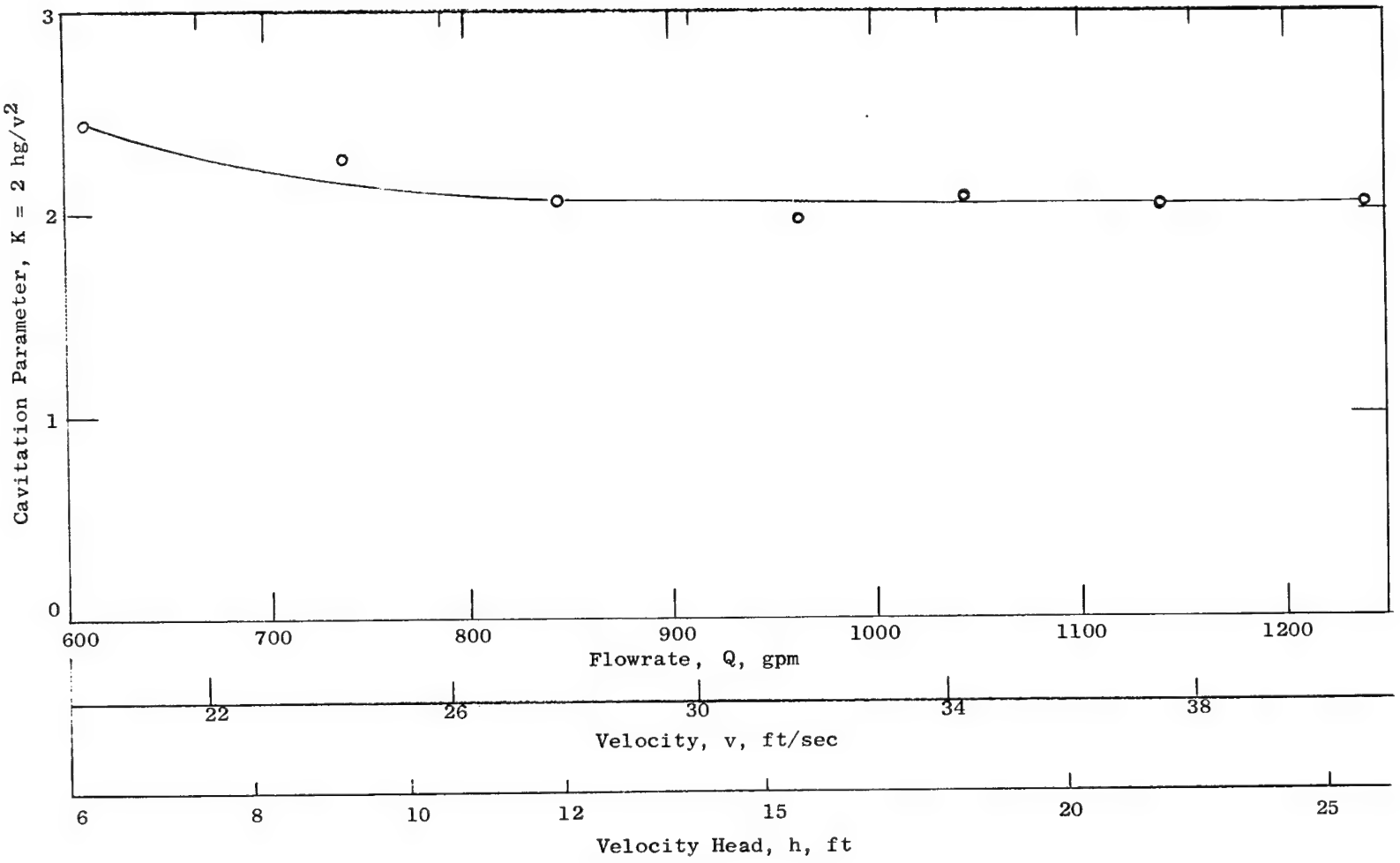

Figure 34. Cavitation Parameter Vs. Flow Flat Induction Pump. (From Ref. 26)

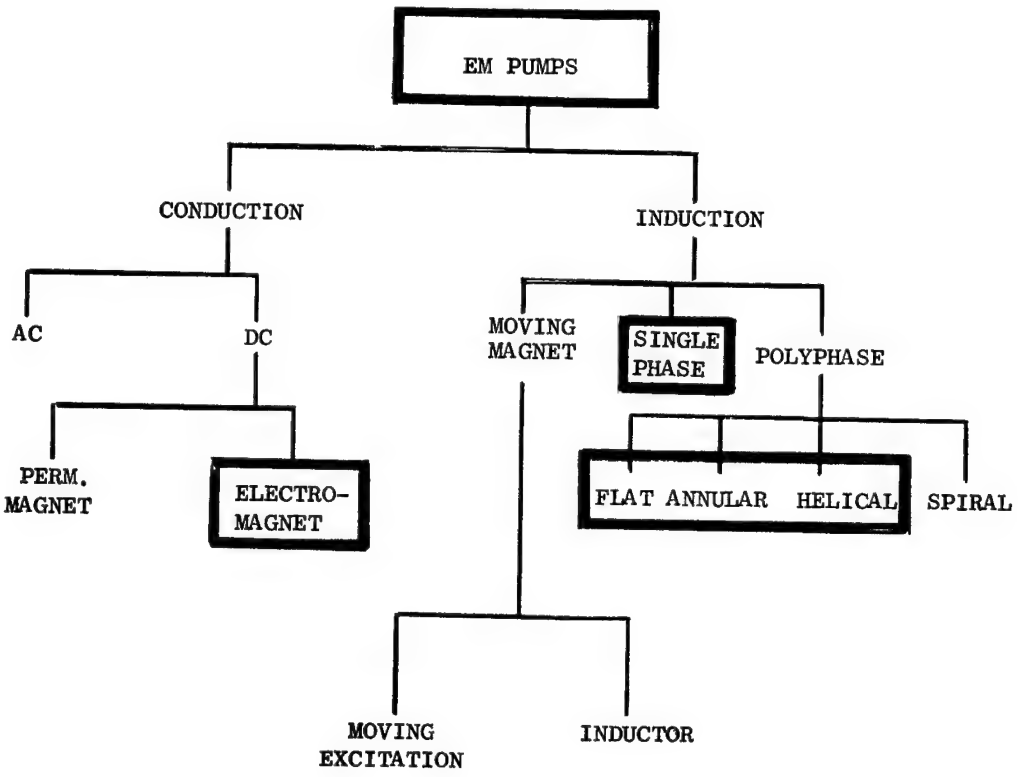

Figure 35. EM Pump Classification.

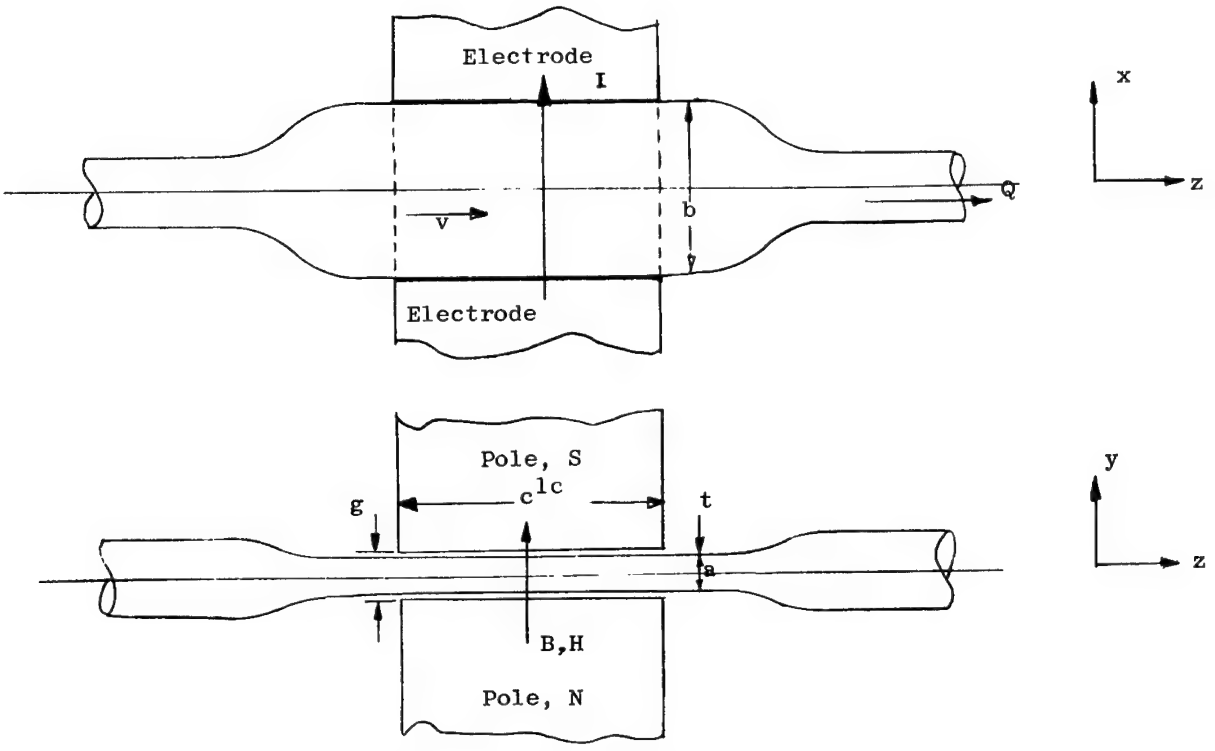

Figure 36. Conduction Pump Configuration.

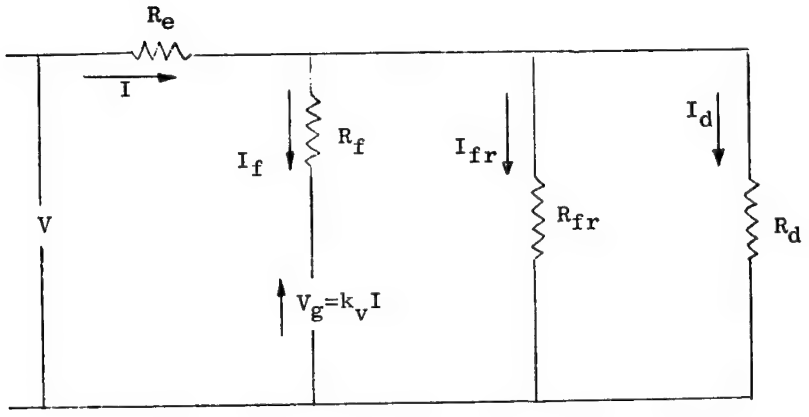

Figure 37. DC Conduction Pump Equivalent Circuit.

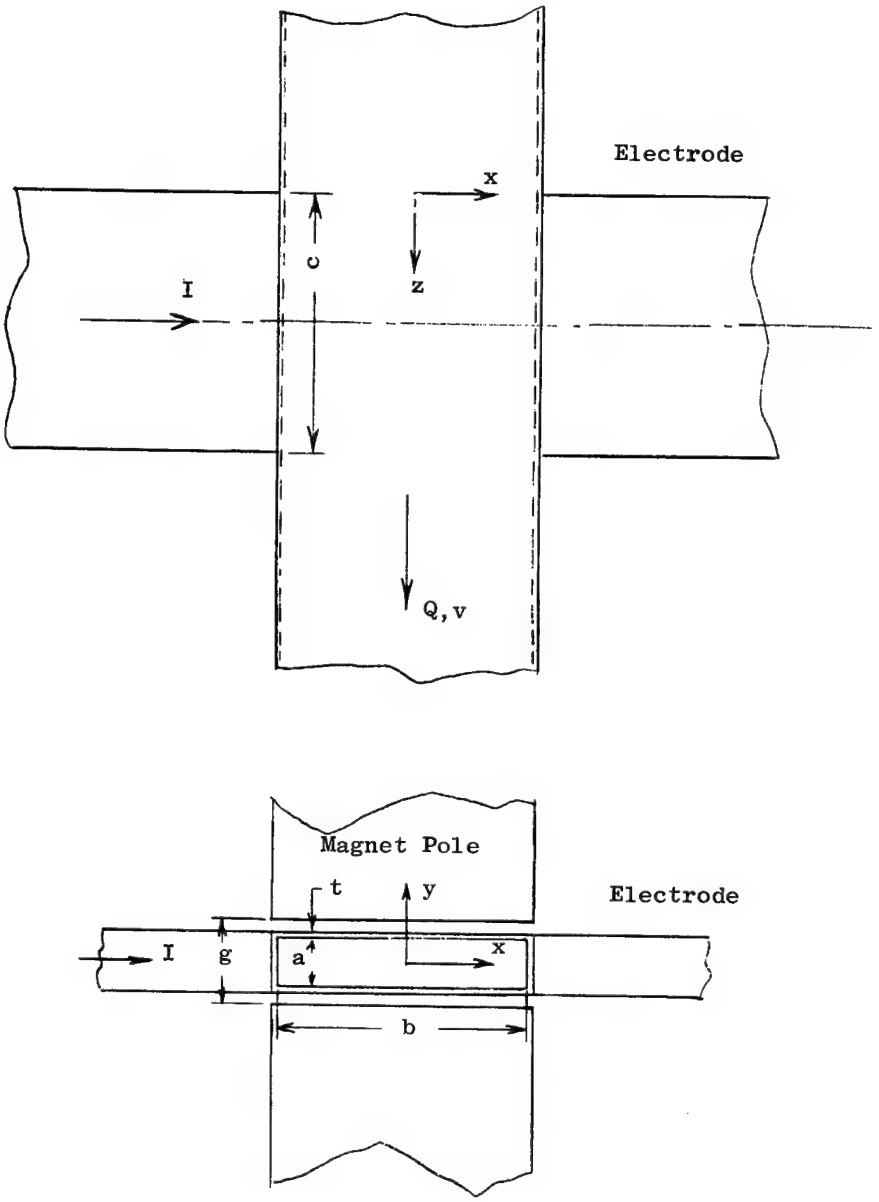

Figure 38. Uncompensated DC Conduction Pump Pumping Section.

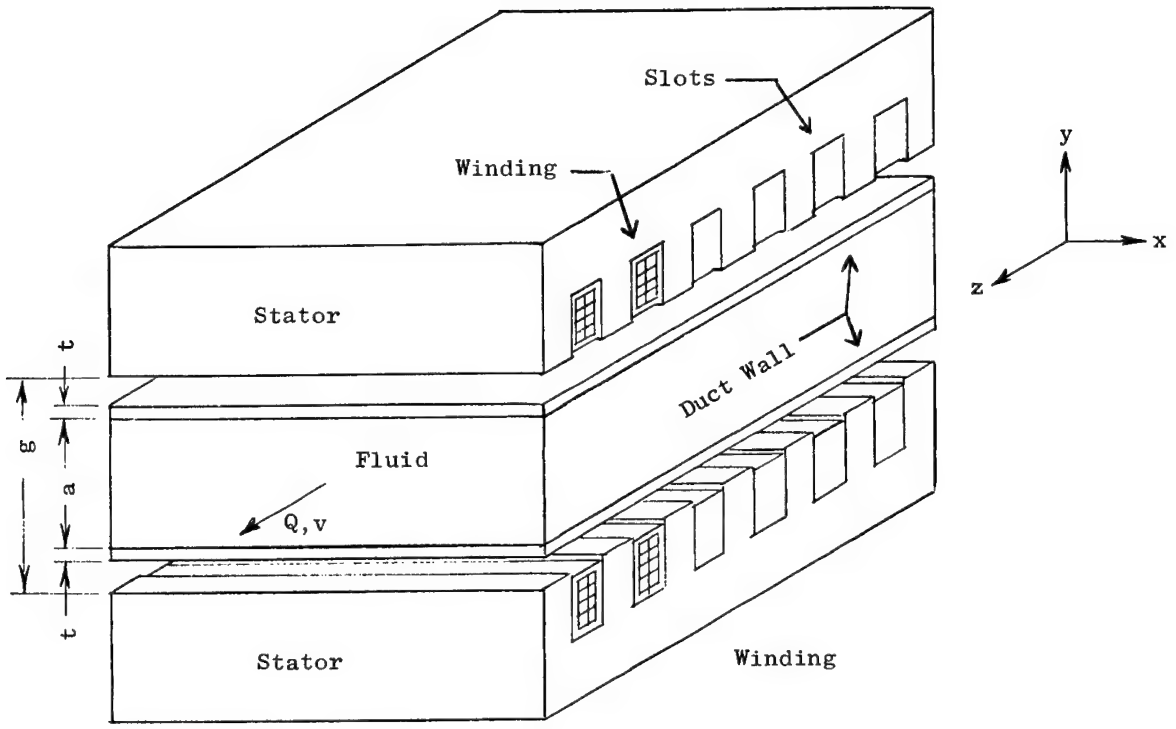

Figure 39. Elementary Pump Section, Induction EM Pump.

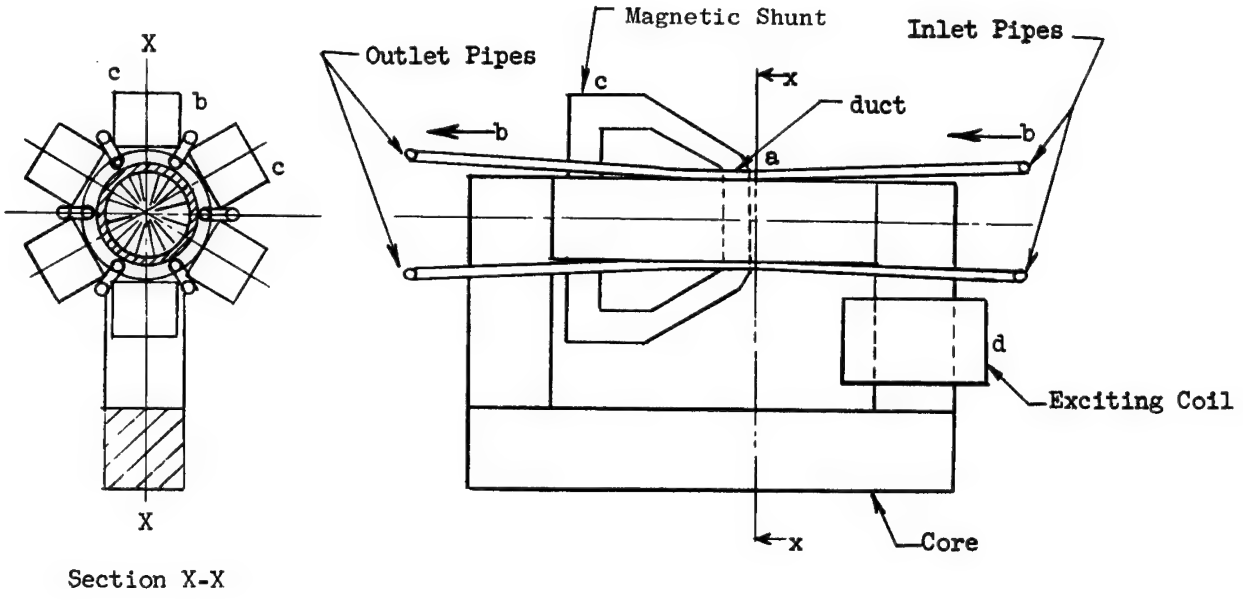

Figure 40. Single Phase Induction Pump Studied by Watt.

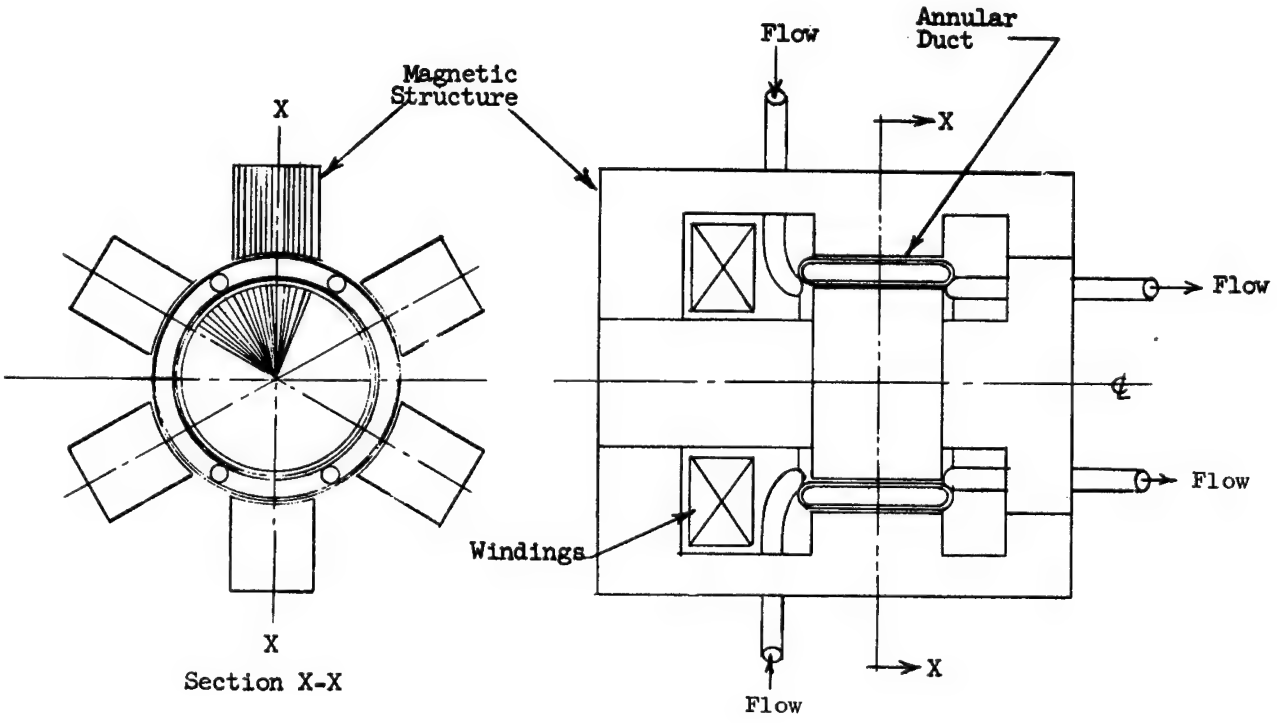

Figure 41. Single Phase Induction Pump Type A.

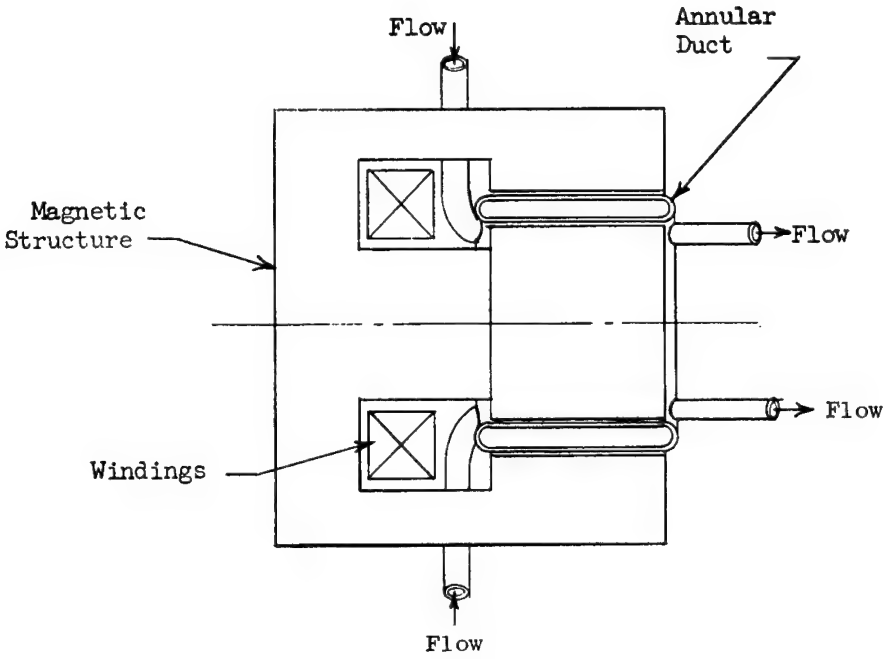

Figure 42. Single Phase Induction Pump Type B.

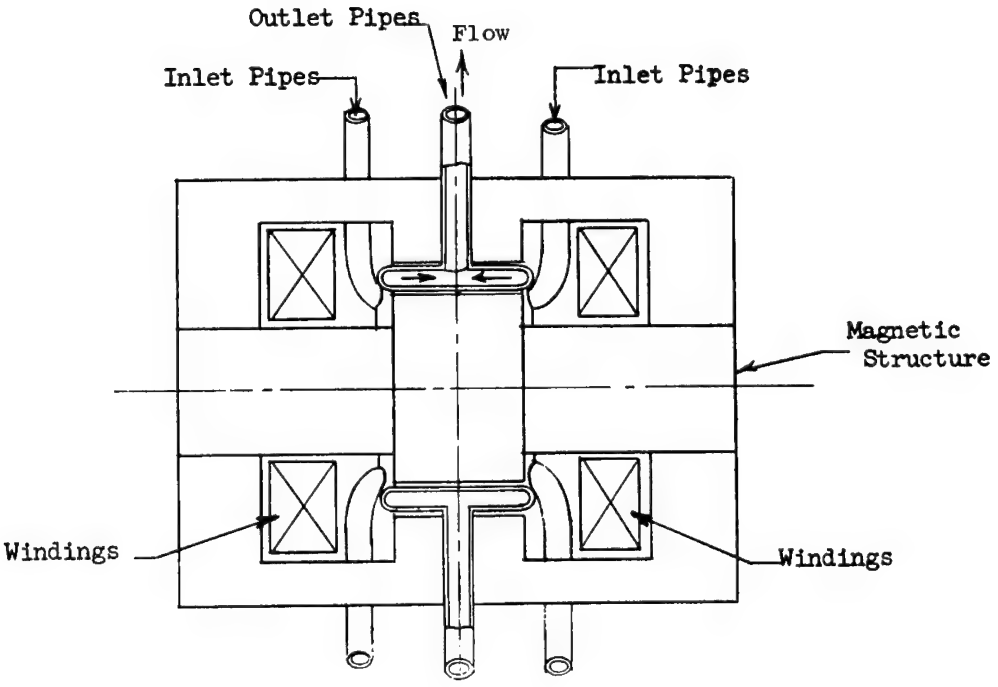

Figure 43. Single Phase Induction Pump Type C.

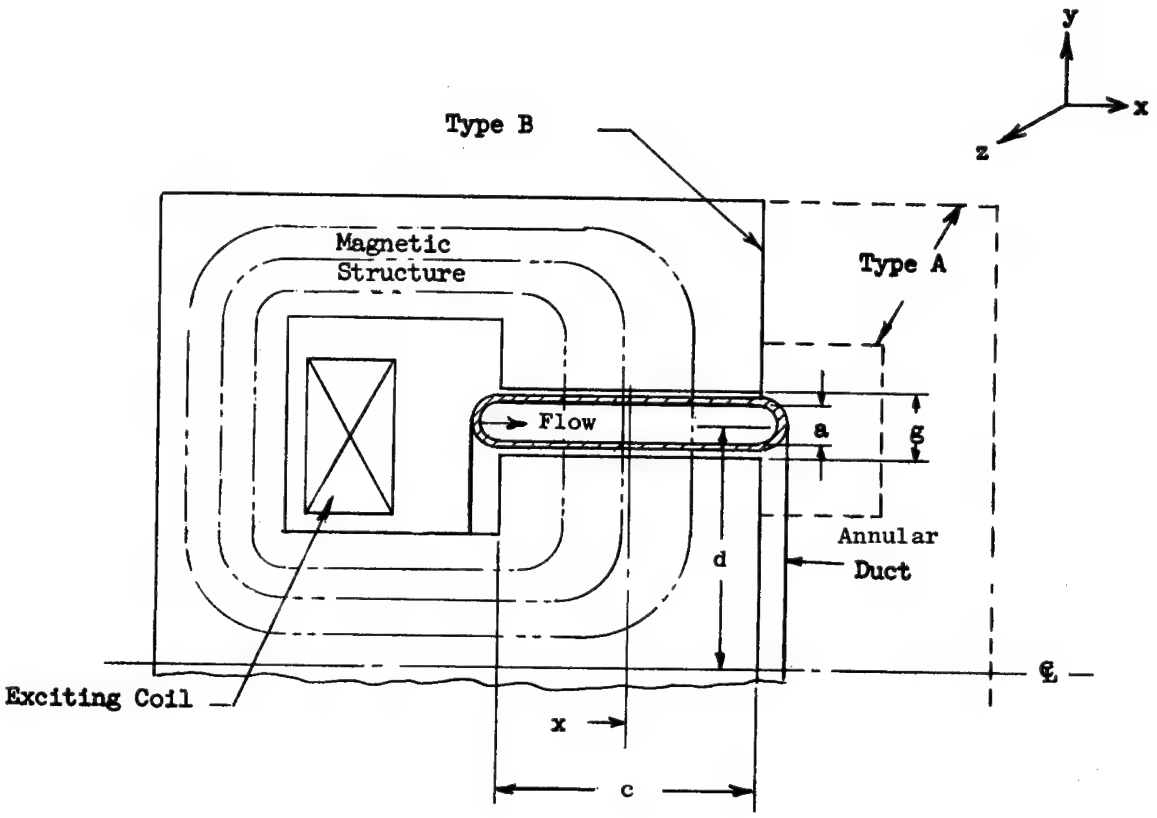

Figure 44. Schematic Single Phase Induction Pump

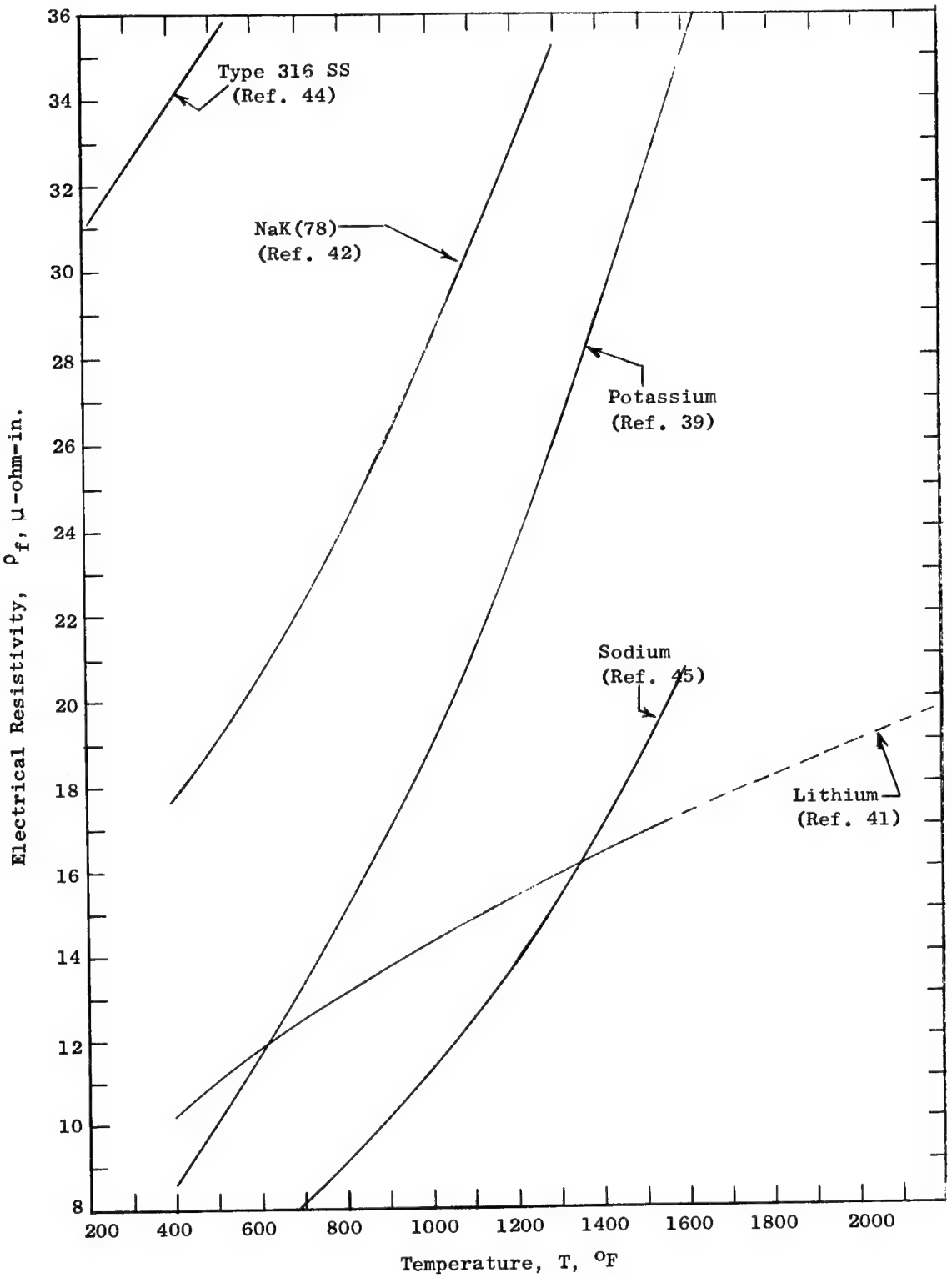

Figure 45. Electrical Resistivity Vs. Temperature for Selected Alkali Metals.

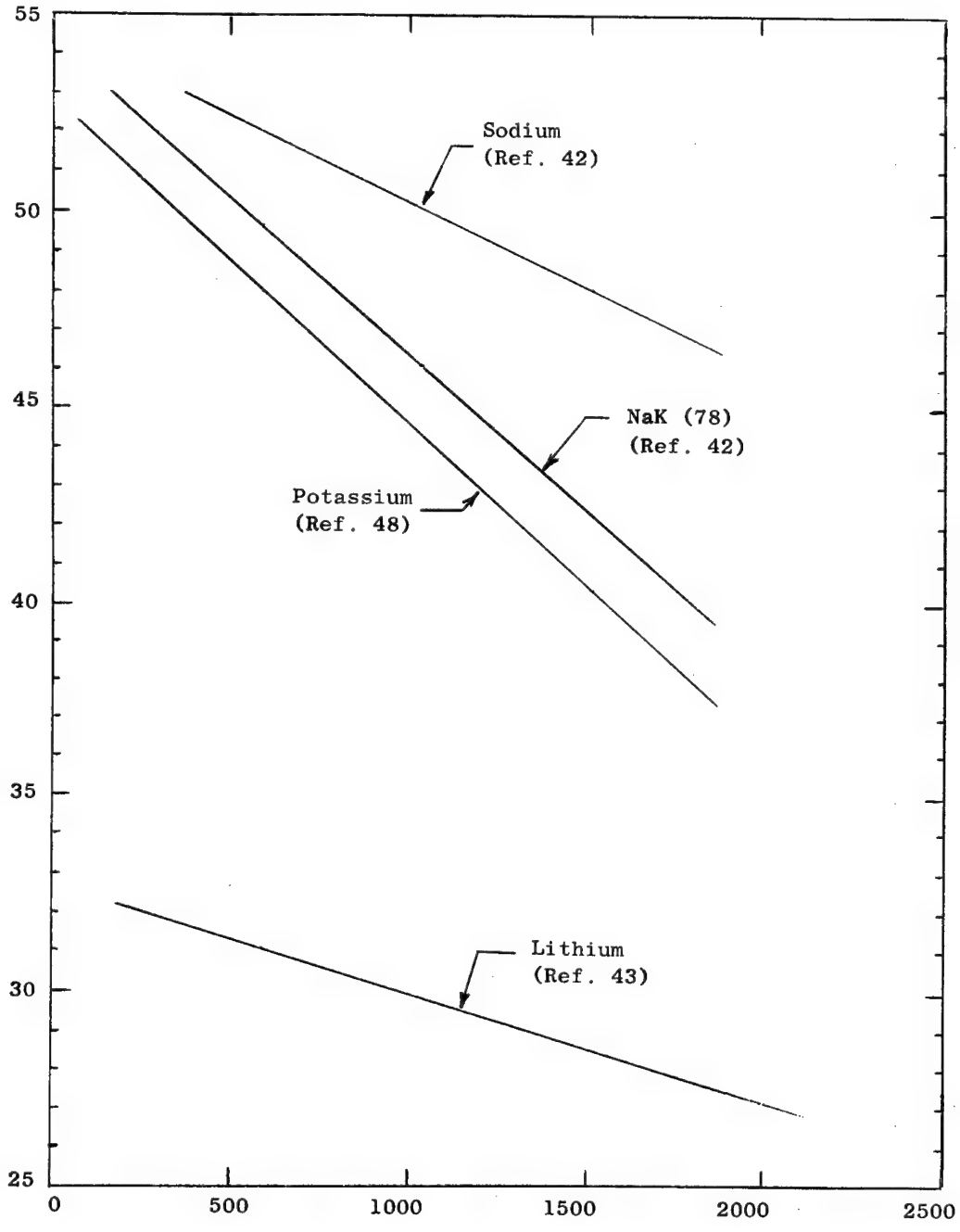

Figure 46. Density of Liquid Metals.

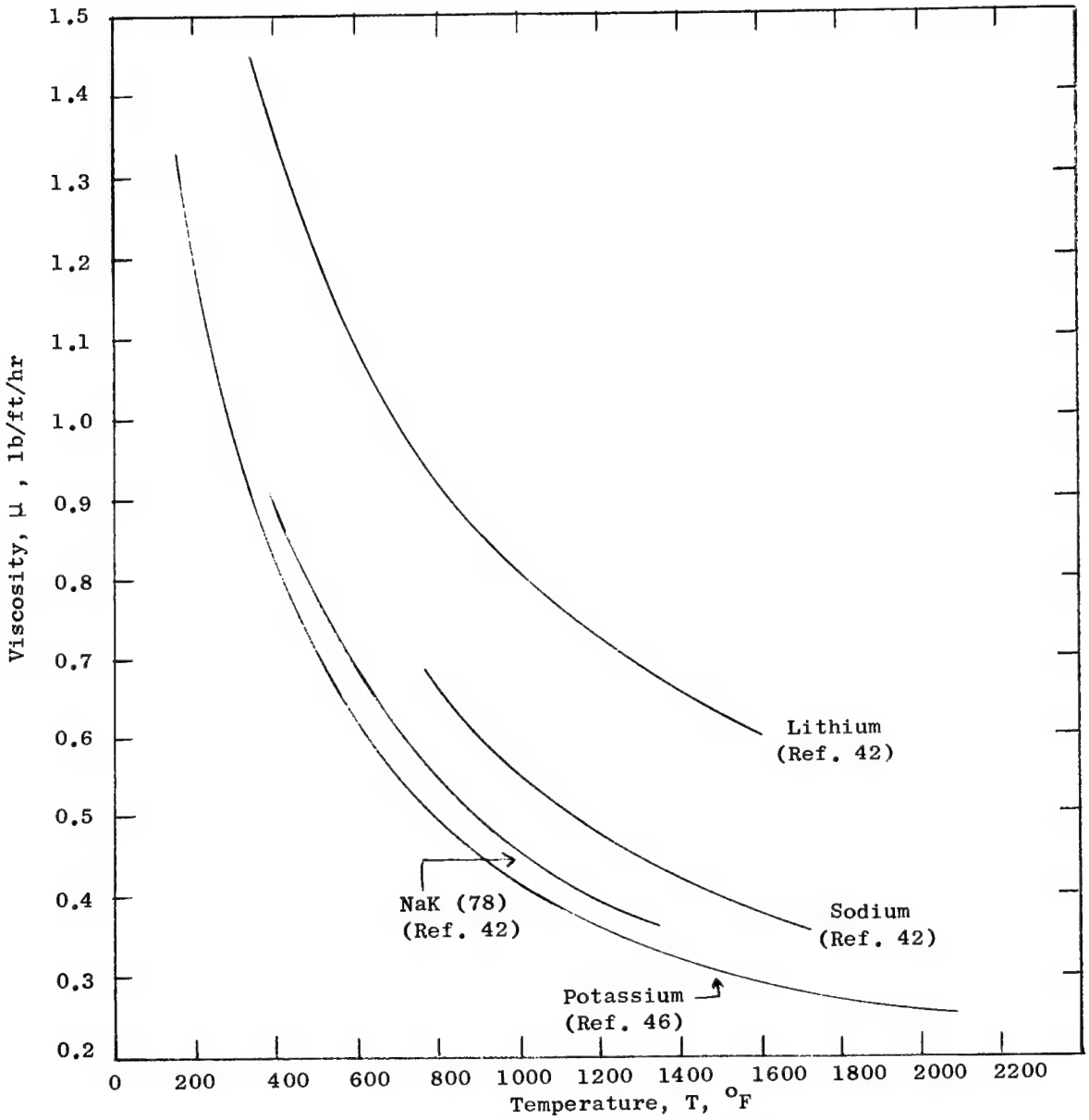

Figure 47. Molten Alkali Metal Viscosity Vs. Temperature

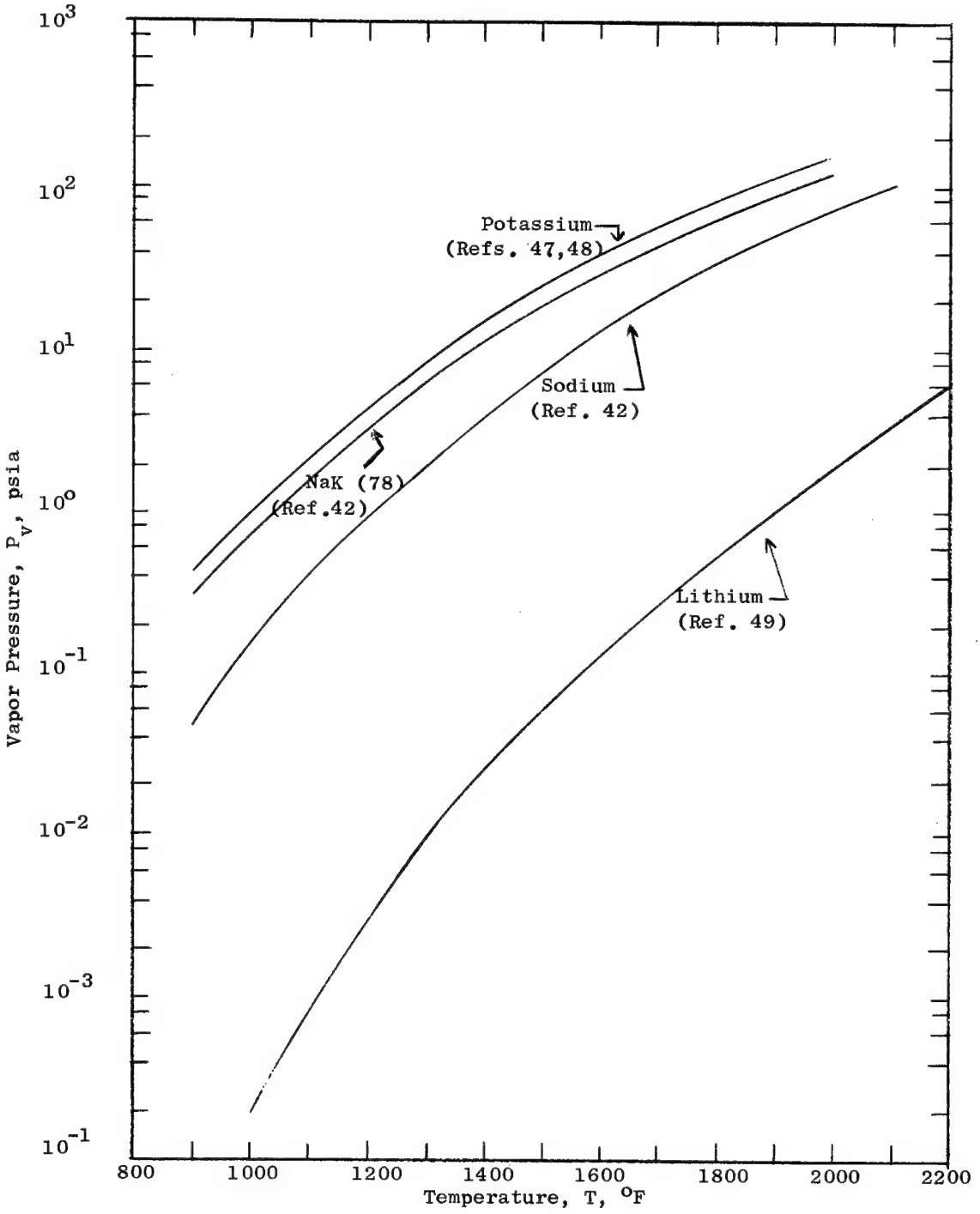

Figure 48. Vapor Pressure of Alkali Metal Working Fluids.

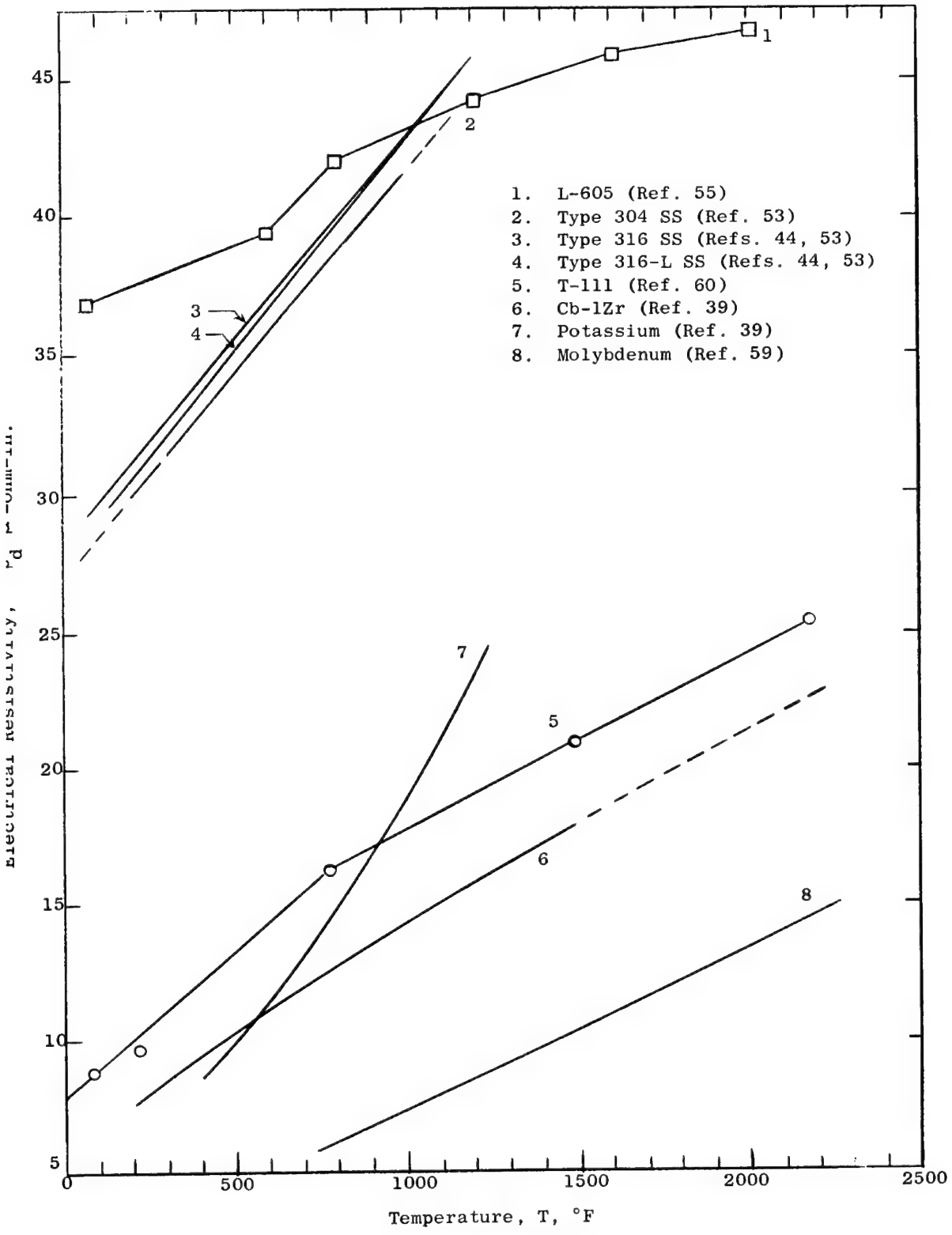

Figure 49. Electrical Resistivity of Duct Materials: Variation with Temperature.

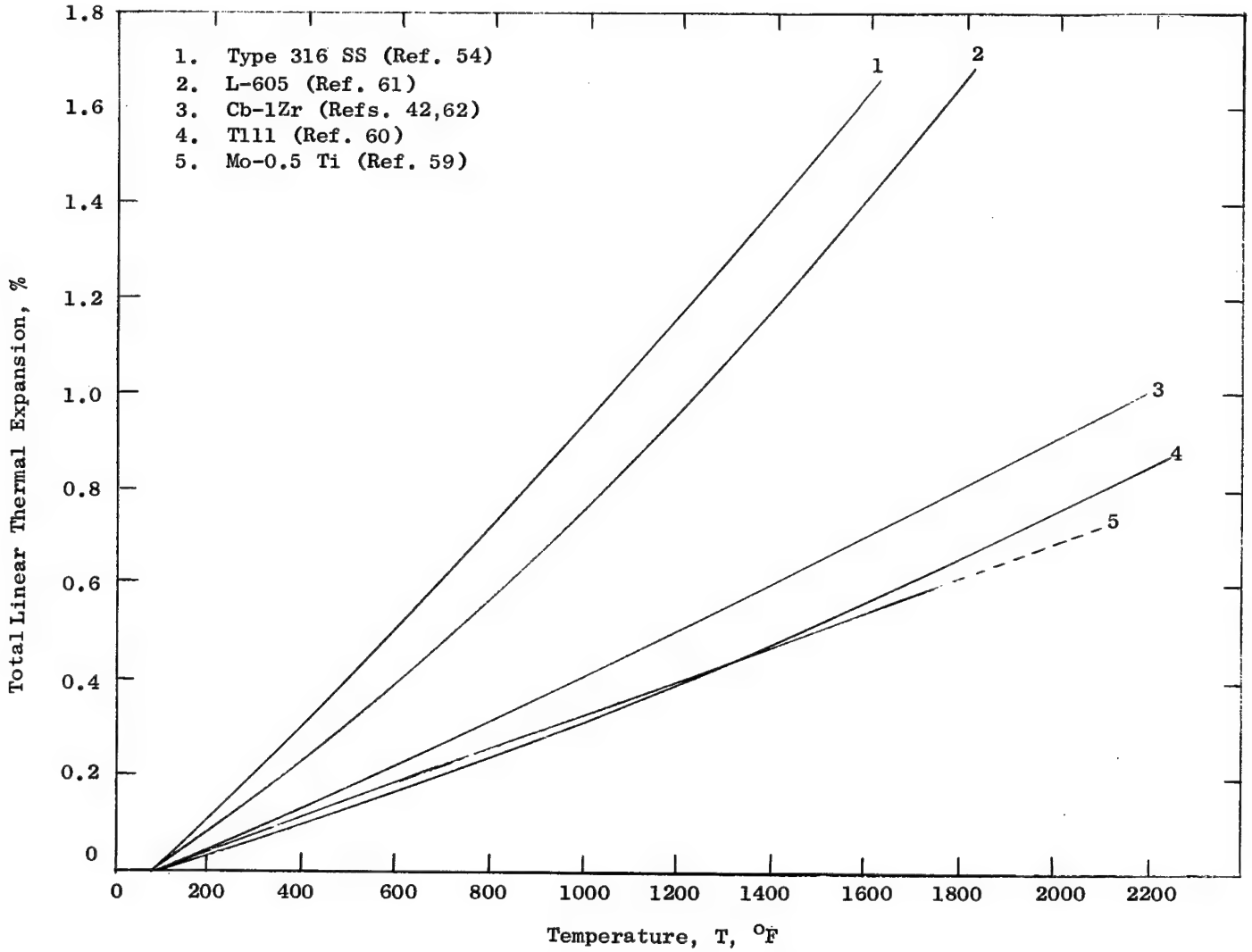

Figure 50. Linear Thermal Expansion of Duct Materials Vs. Temperature.

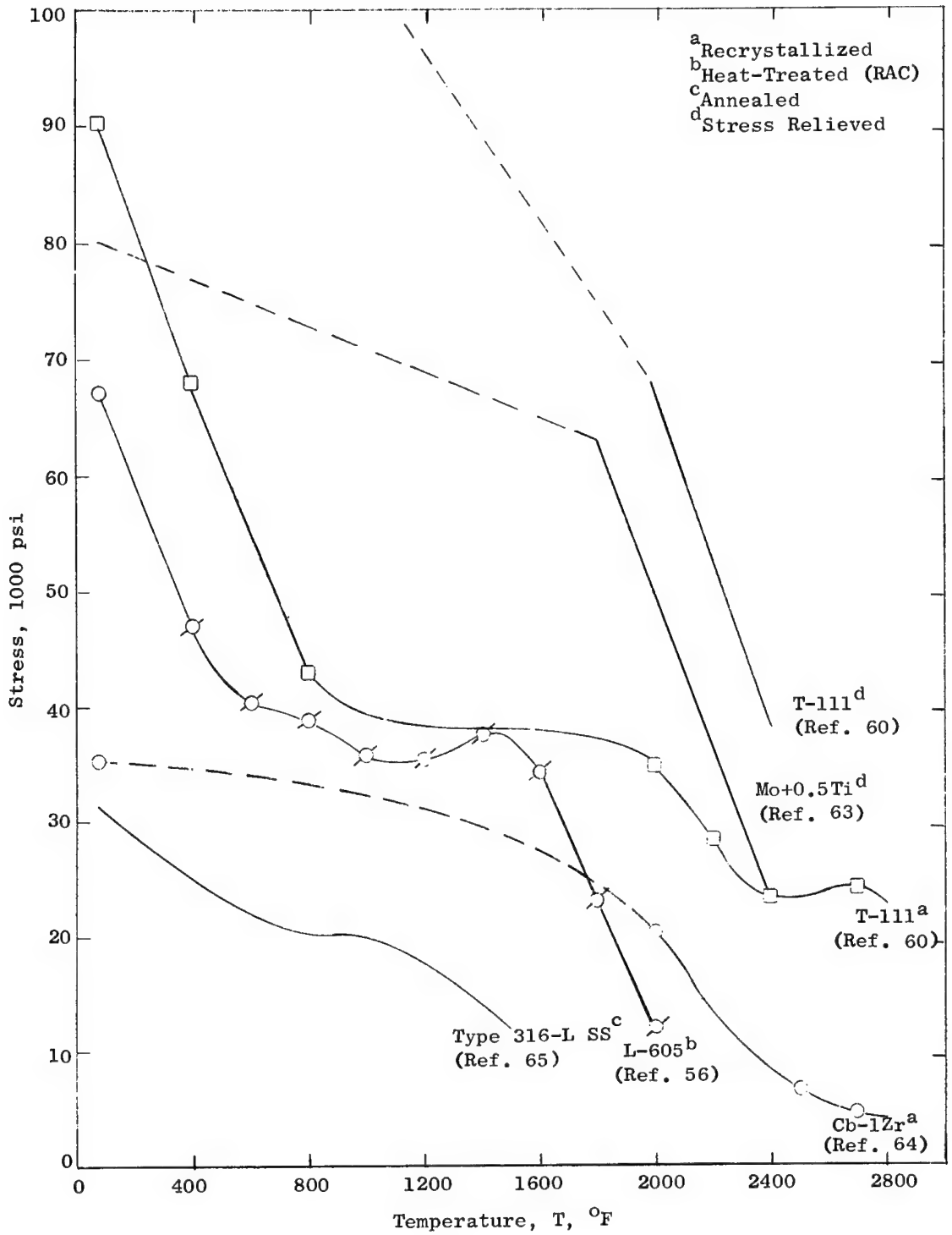

Figure 51. Tensile Yield of Selected Duct Materials, 0.2% Offset, Short-Time at Elevated Temperature.

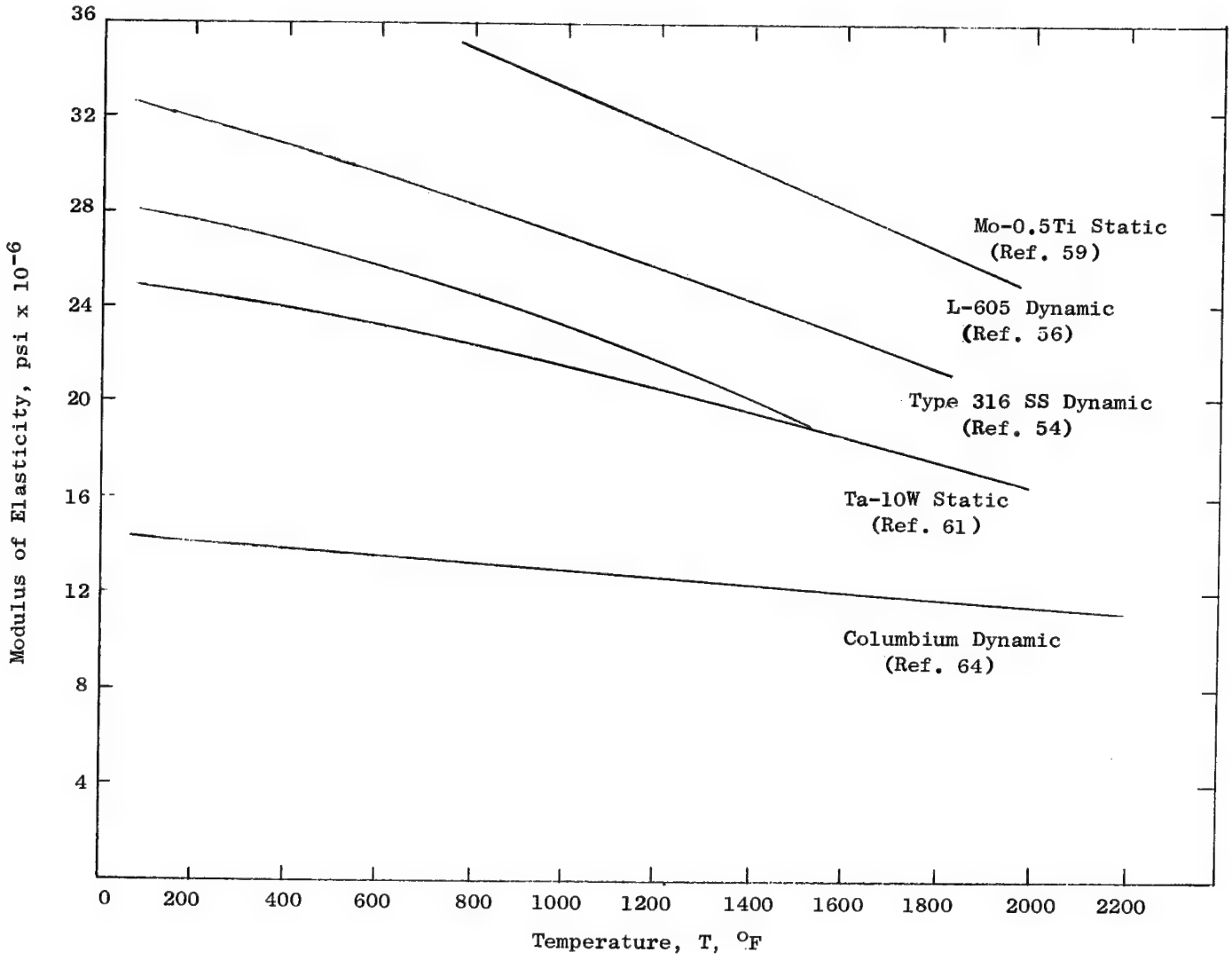

Figure 52. Modulus of Elasticity of Duct Materials.

(1) T-111: Stress-Rel; Rupture; Test at 2400°F Only (Ref. 60)
(2) Mo-0.5 Ti: Stress-Rel.; Rupture; 2000°F Max. Test (Ref. 59)
(3) Mo-0.5 Ti: Stress-Rel; 1% Creep; 2000°F Max. Test (Ref. 59)
(4) Cb-1Zr: Annealed; Rupture; Test at 1800°F and 2000°F Only (Ref. 64)
(5) L-605: Stress-Rel; Rupture; 1800°F Max. Test (Ref. 56)
(6) L-605: Stress-Rel; 1% Creep; 1800°F Max. Test (Ref. 56)
(7) Type 316 SS: Stress-Rel; Rupture; 1500°F Max. Test (Ref. 65)
(8) Type 316 SS: Stress-Rel; 1% Creep; 1500°F Max. Test (Ref. 65)

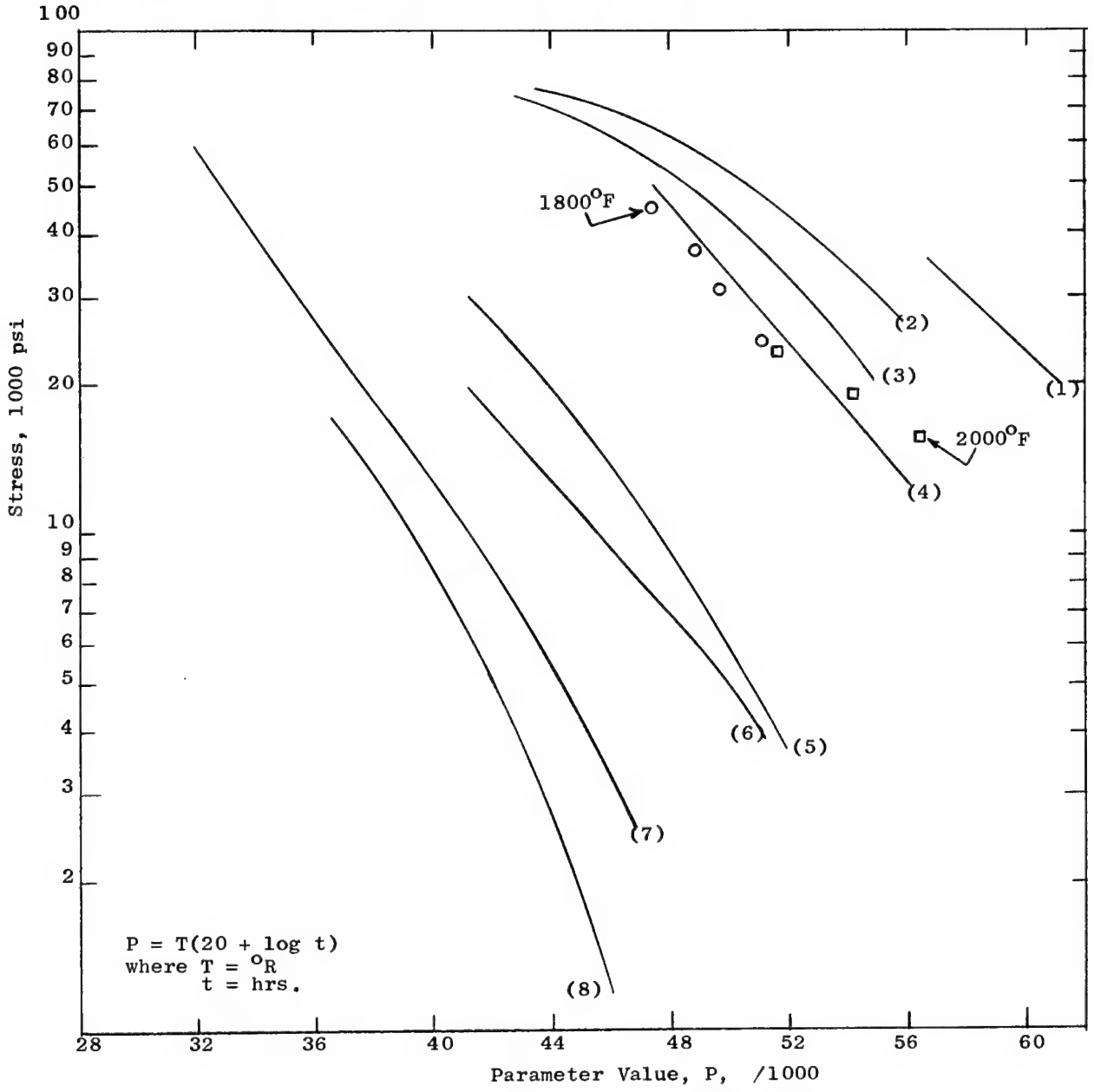

Figure 53. Creep and Rupture Strengths of Duct Materials.

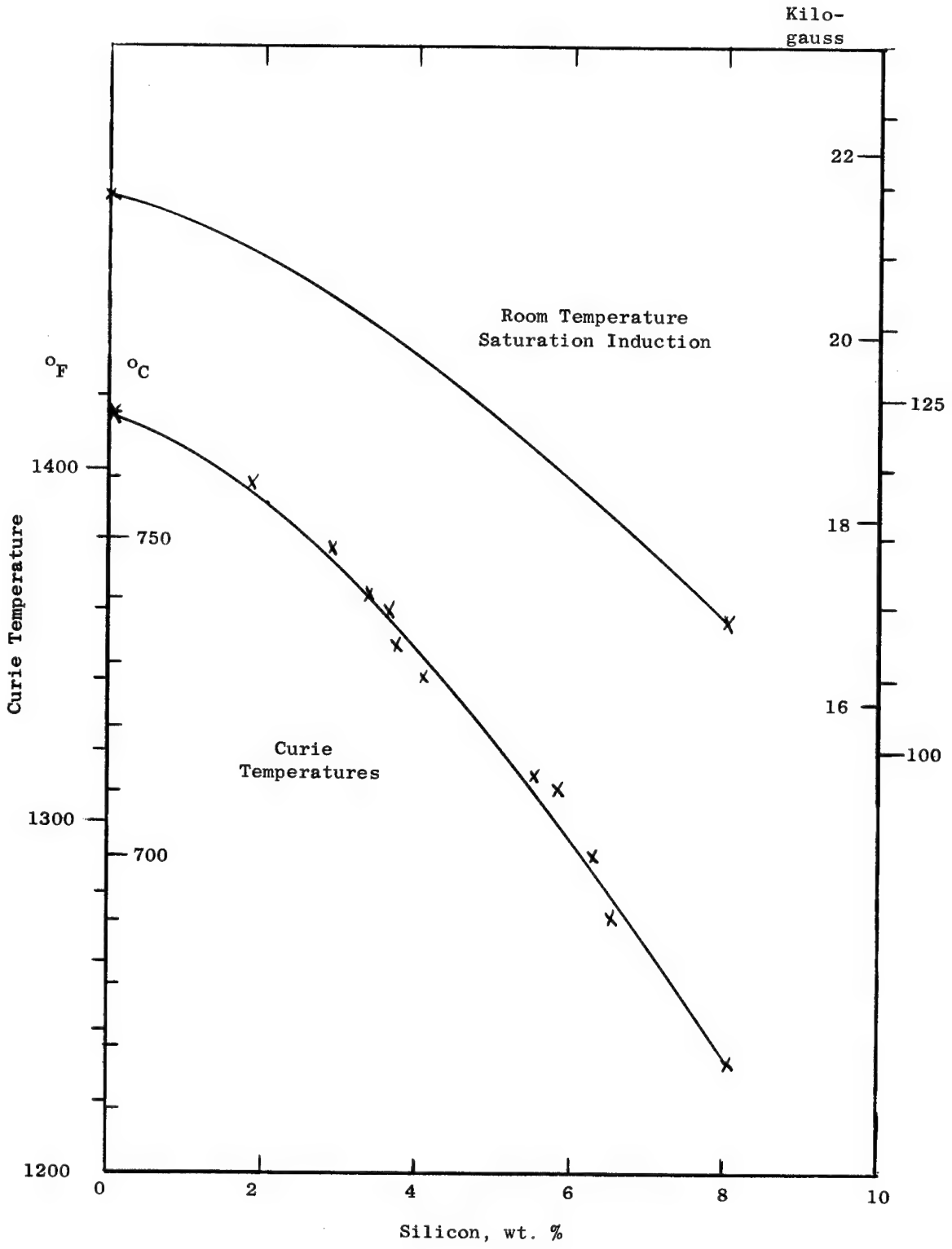

Figure 54. Variation of Important Properties of Iron-Silicon Alloys with Composition (Ref. 66).

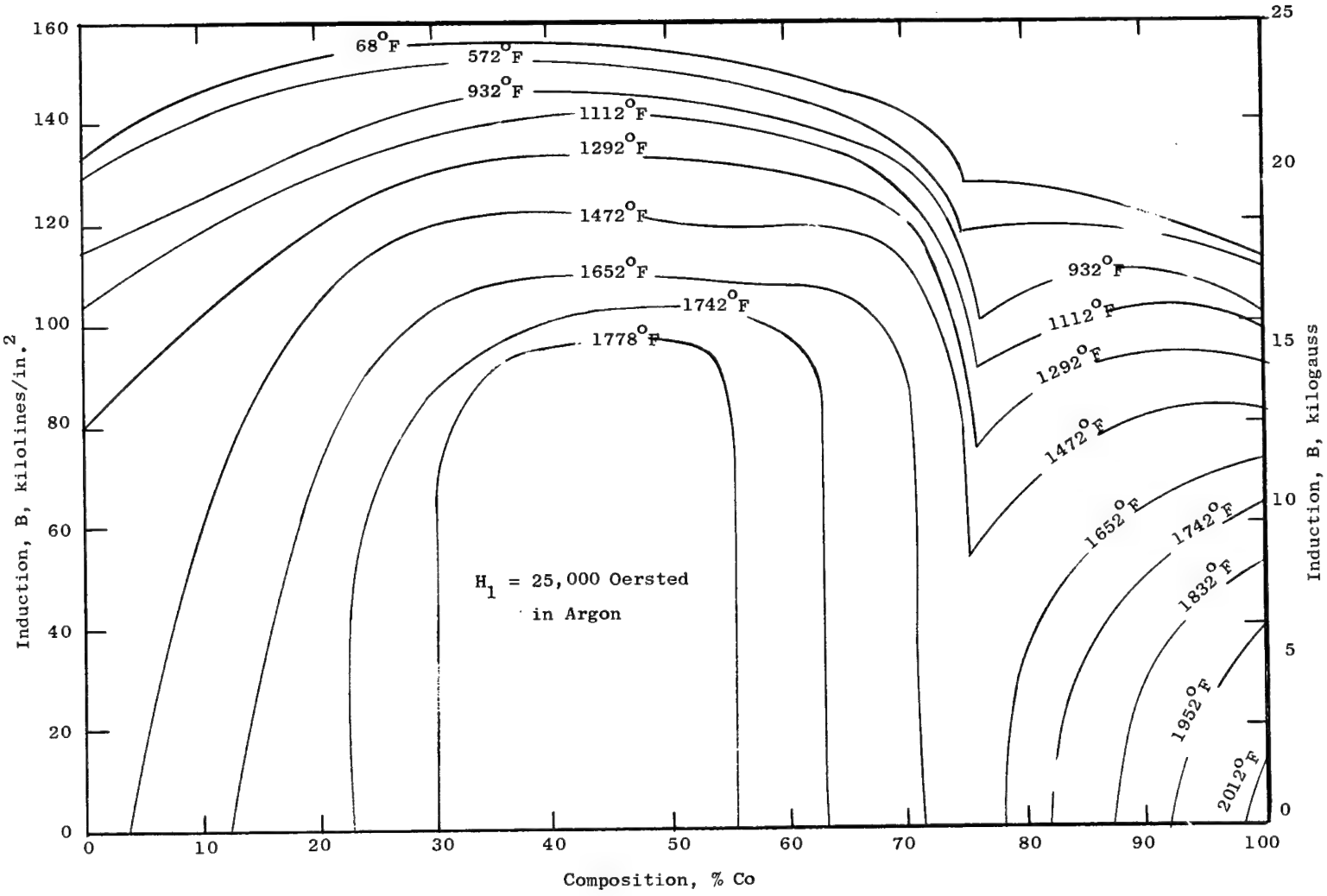

Figure 55. Saturation Induction Isotherms Iron-Cobalt Alloys (Ref. 67).

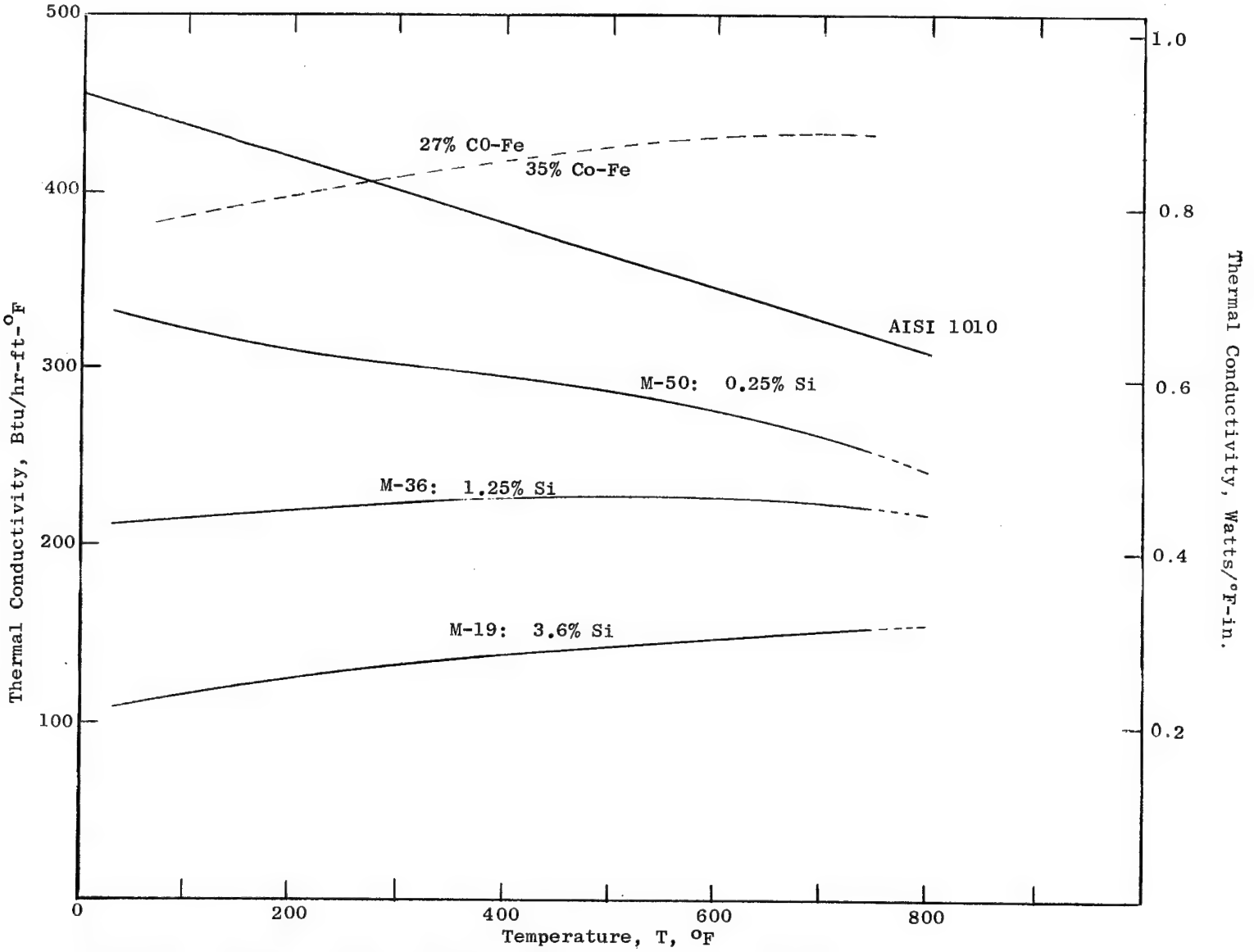

Figure 56. Thermal Conductivities of Selected Magnetic Materials (Refs. 70 through 73).

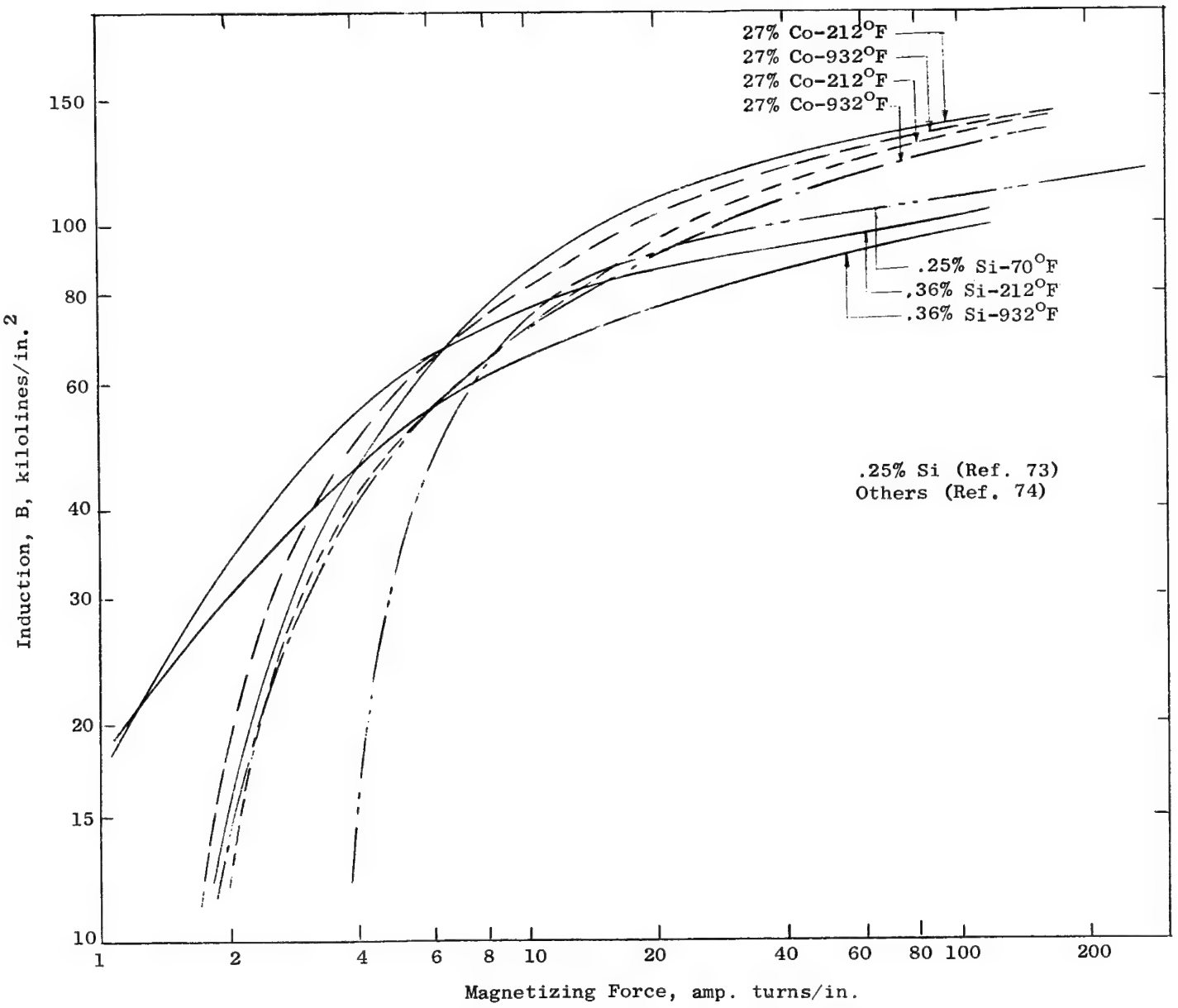

Figure 57. Normal Magnetization Curves for Selected Iron Alloys.

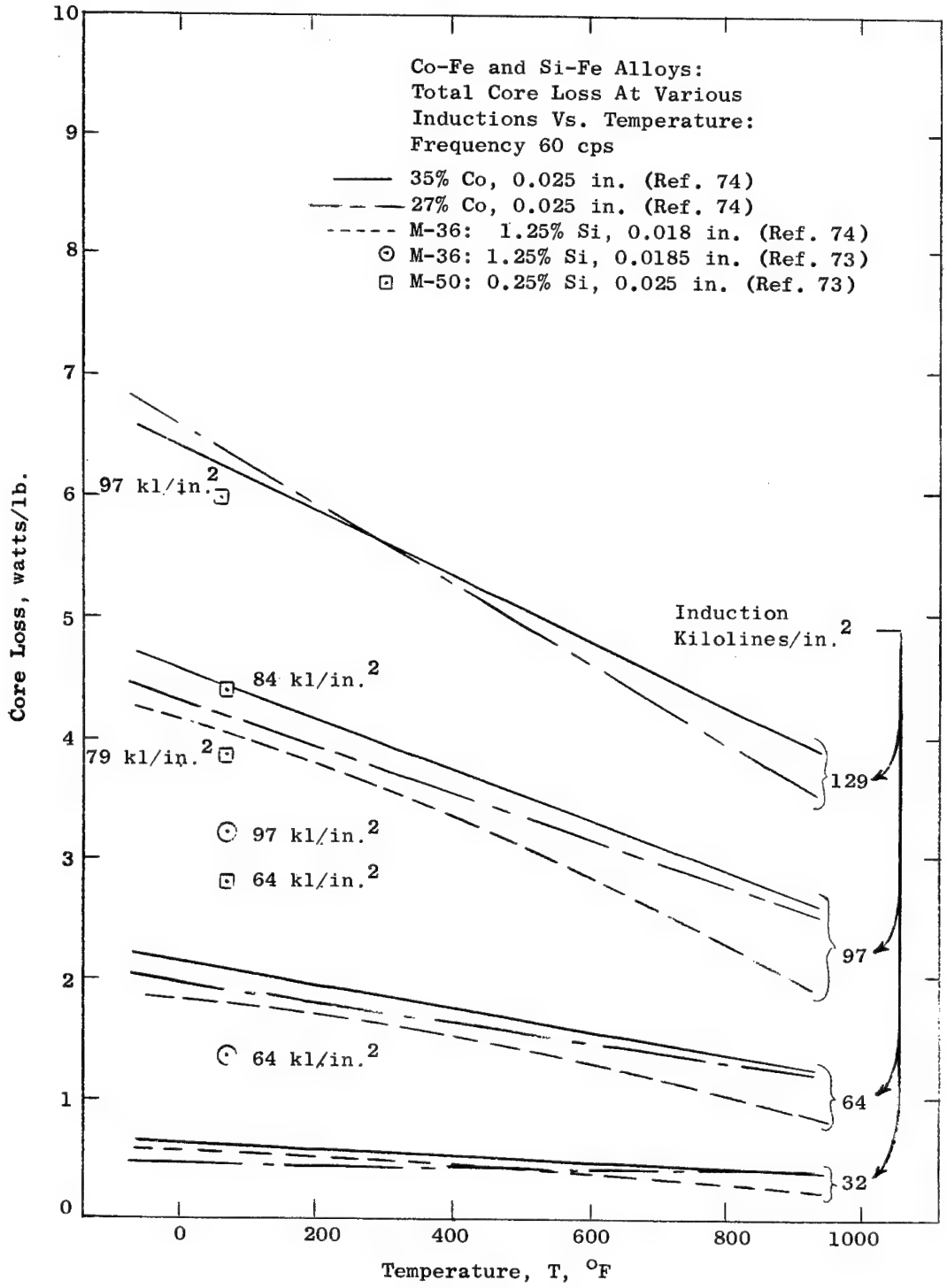

Figure 58. Total Core Loss of Some Magnetic Materials.

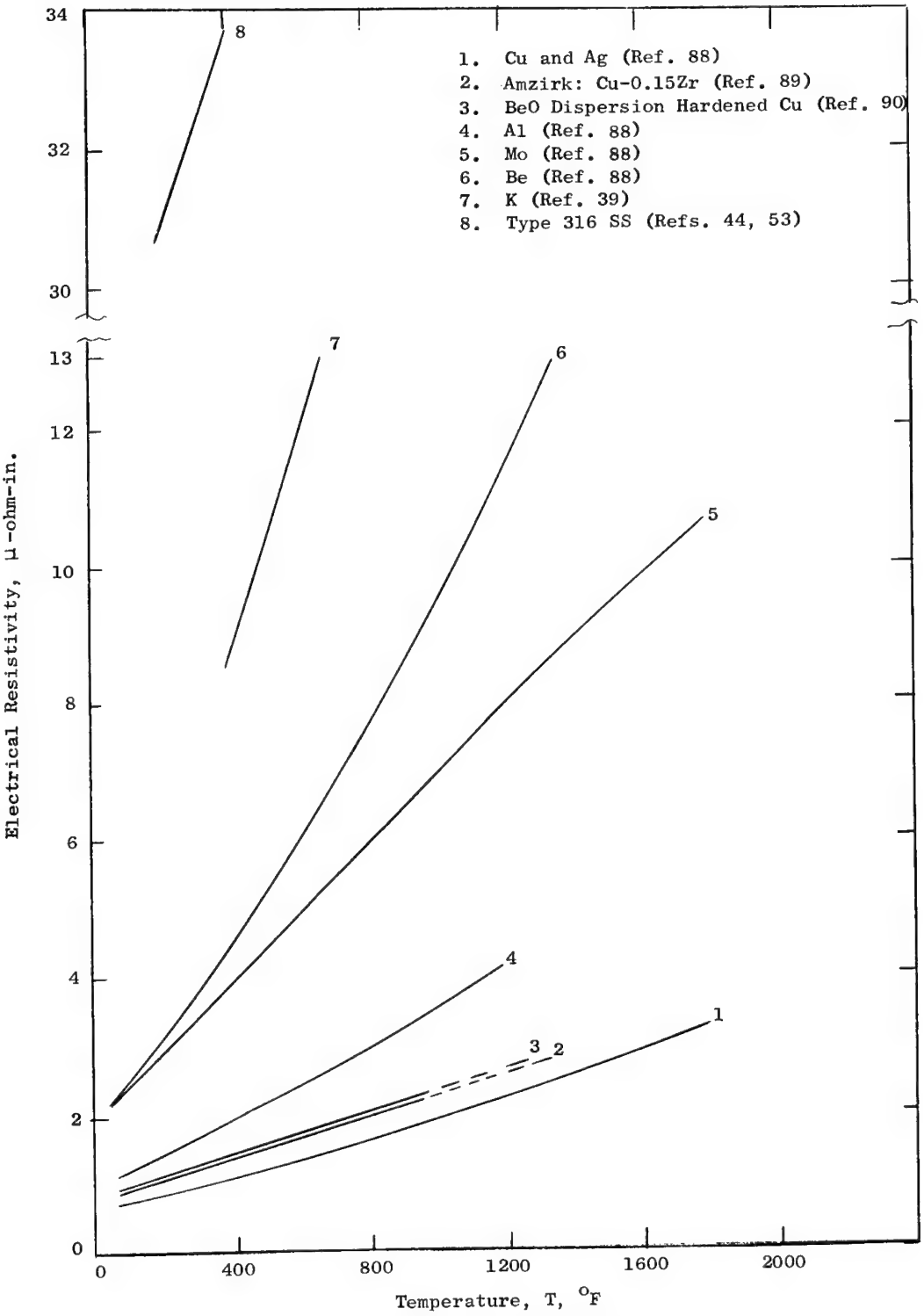

Figure 59. Resistivity of Conductor Materials.

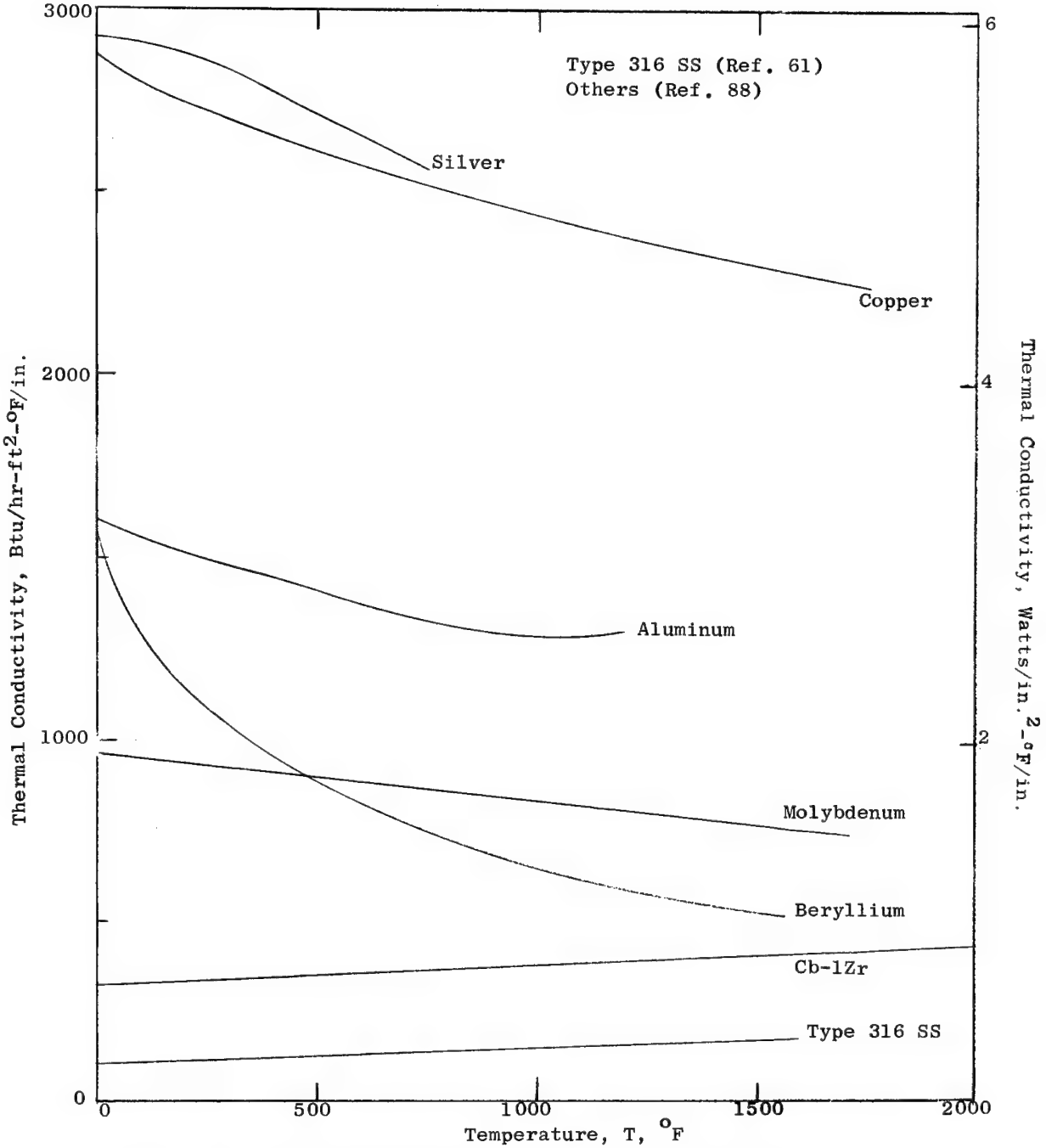

Figure 60. Thermal Conductivity of Conductor Materials.

1. Mo (Ref. 59)
2. BeO Dispersion Hardened Cu, UTS (Ref. 90)
3. Amzirk: Cu-0.15Zr, 84% CW, 842° Faged (Ref. 89)
4. Be, 8-in. Wire (Ref. 91)
5. Al, SAP: Sintered Al Powder (Ref. 92)
6. Cu-0.1 Ag (Ref. 93)
7. 99+% Al, 1/2 Hard (Ref. 94)

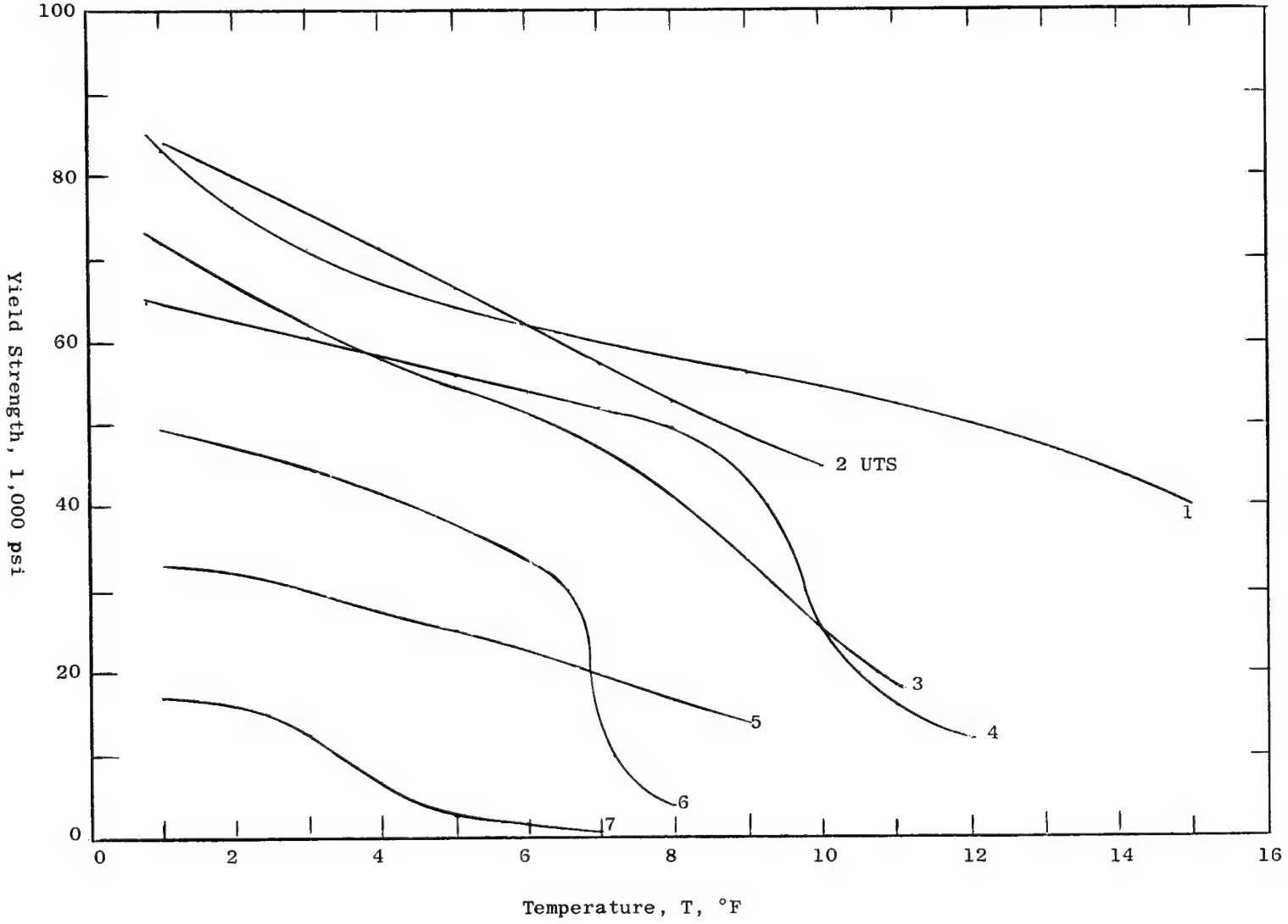

Figure 61. Yield Strength, 0.2% Offset, of Typical Conductor Materials.

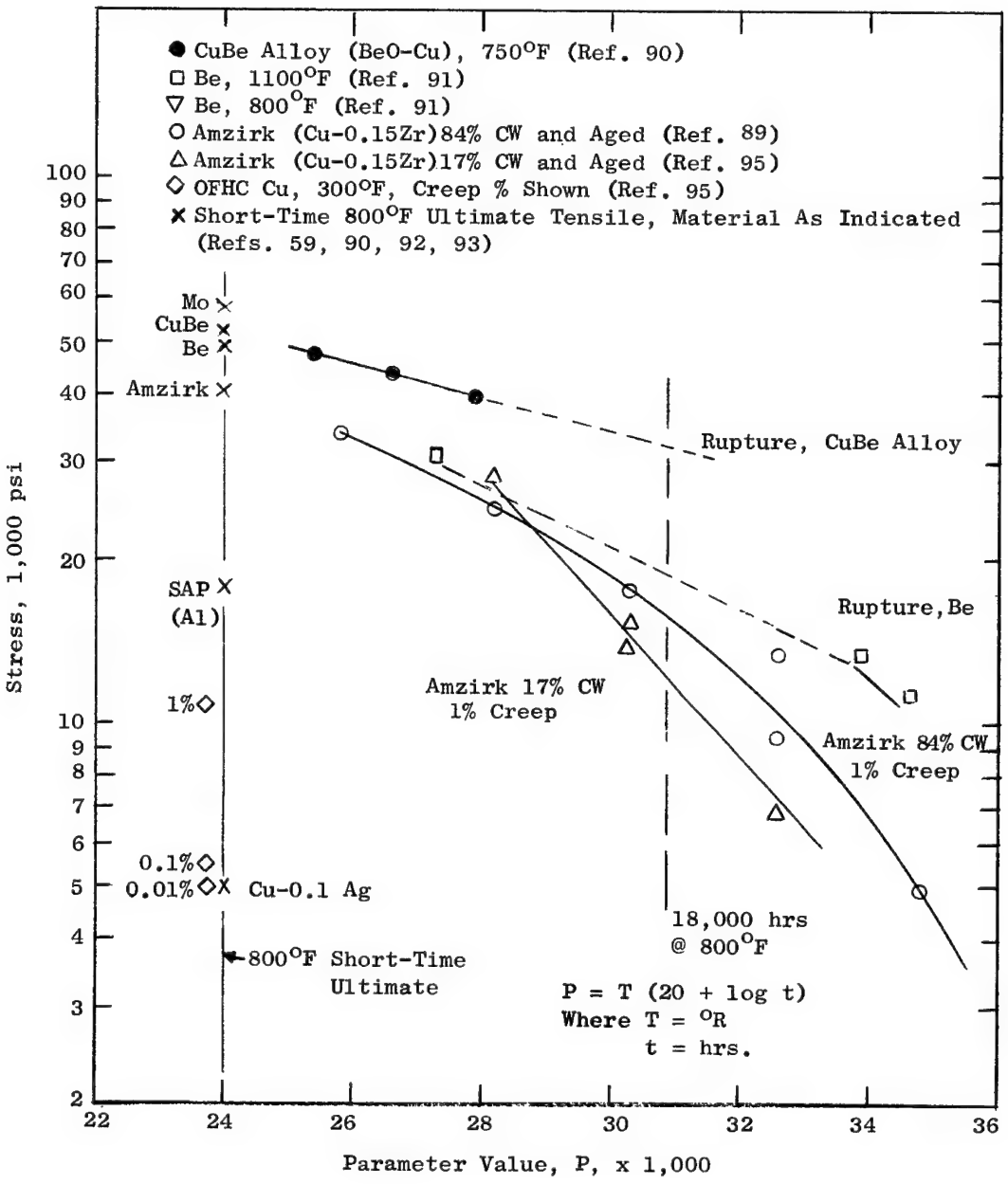

Figure 62. Creep and Rupture Strengths of Selected Conductor Materials.

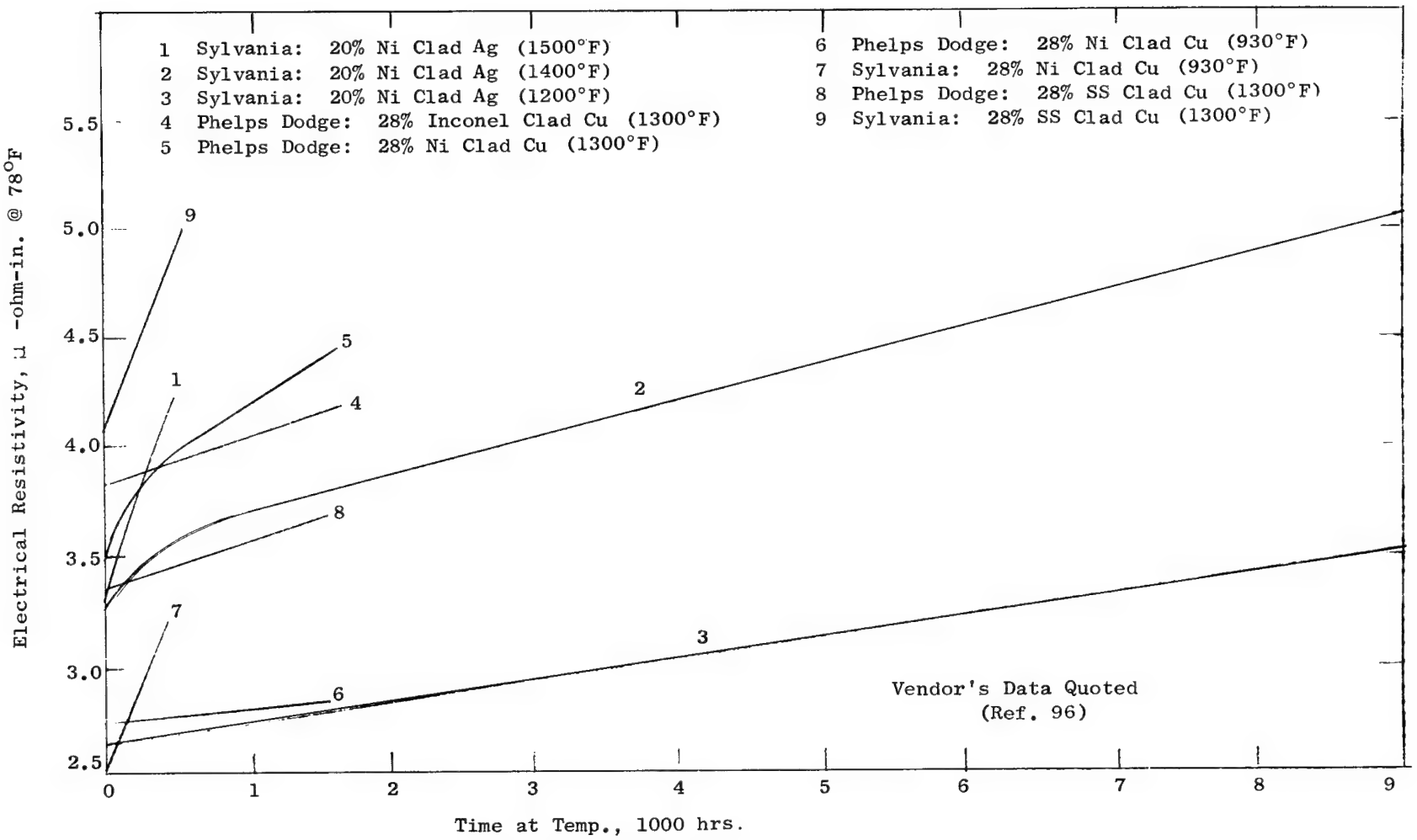

Figure 63. Conductor Resistivity Change with Time at Temperature.

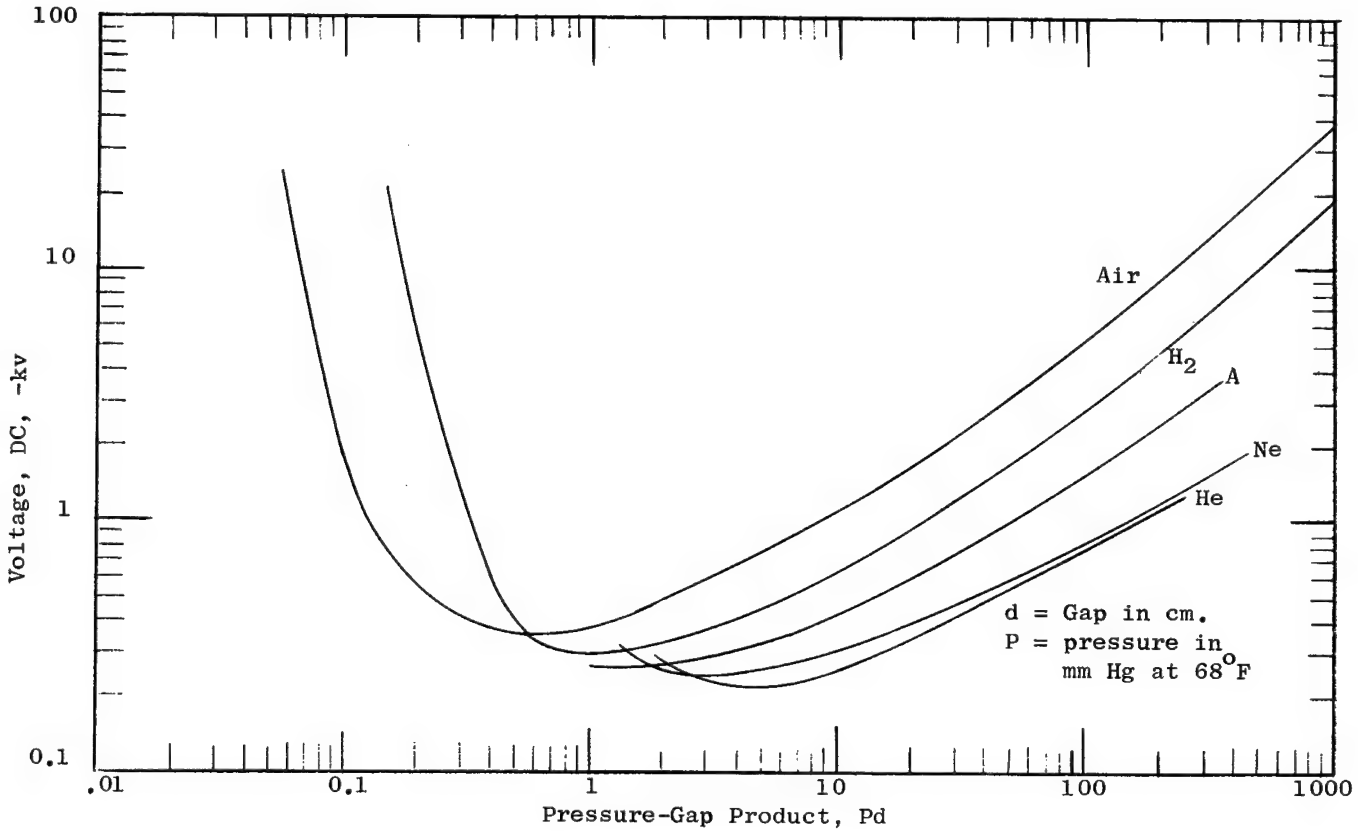

Figure 64. Paschen Curves (Ref. 99).

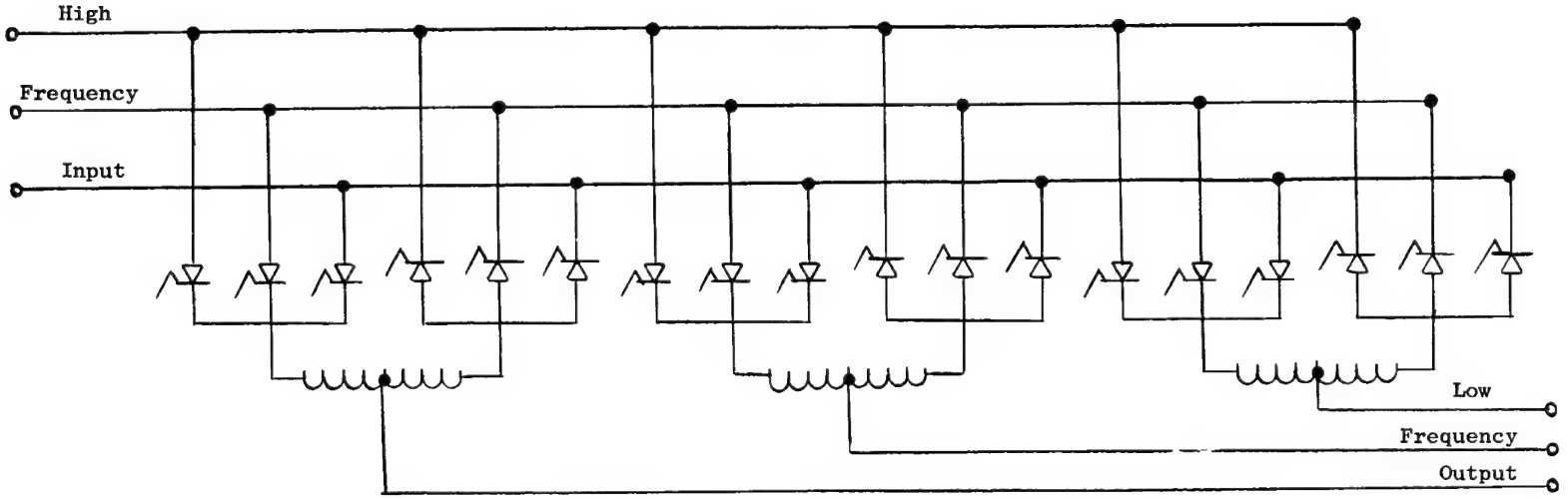

Figure 65. Cycloconverter Type Frequency Converter (Controlled Rectifier Triggering Circuits Not Shown).

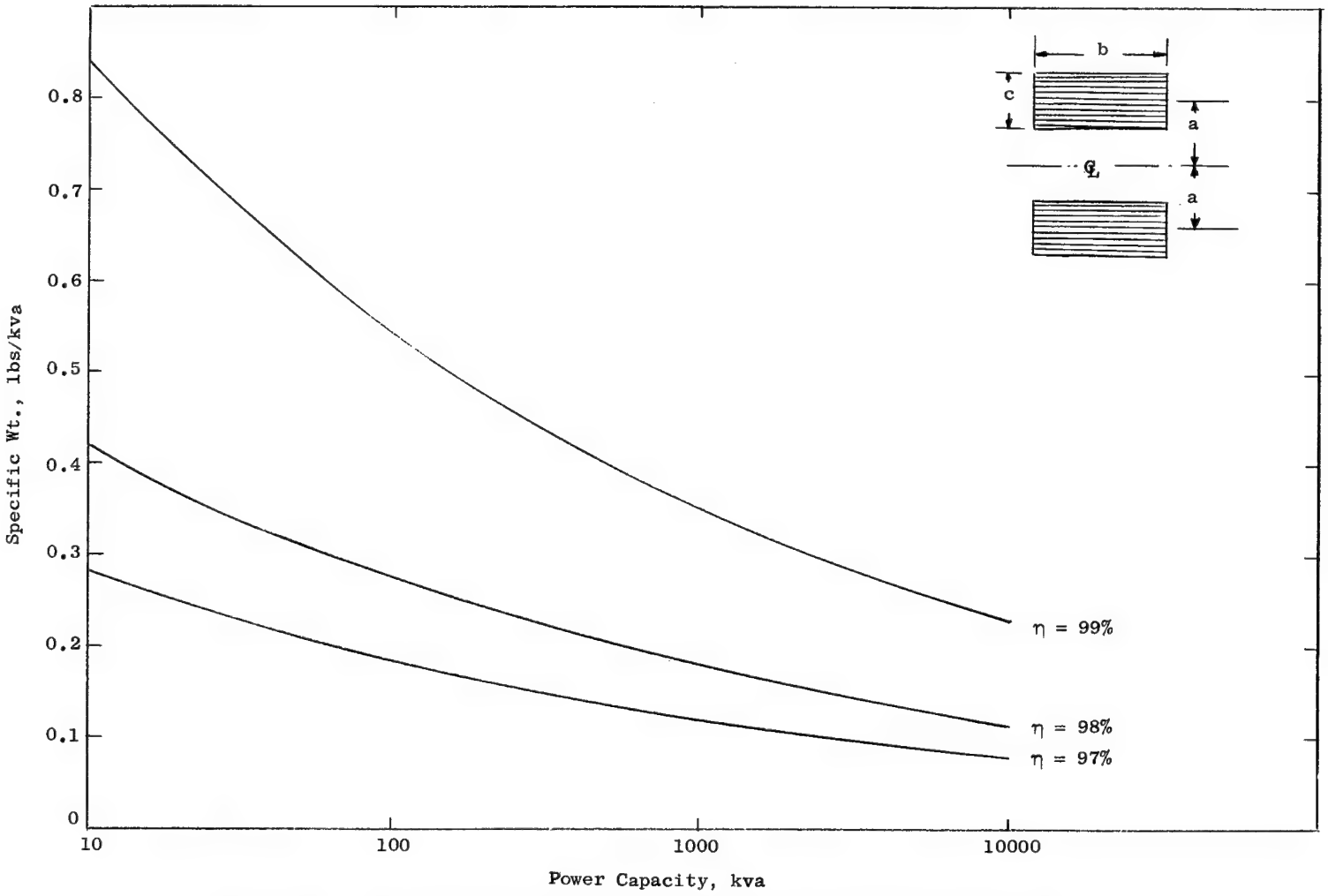

Figure 66. Weight of Frequency Converter Inductors Vs. Kilovolt - Ampere.

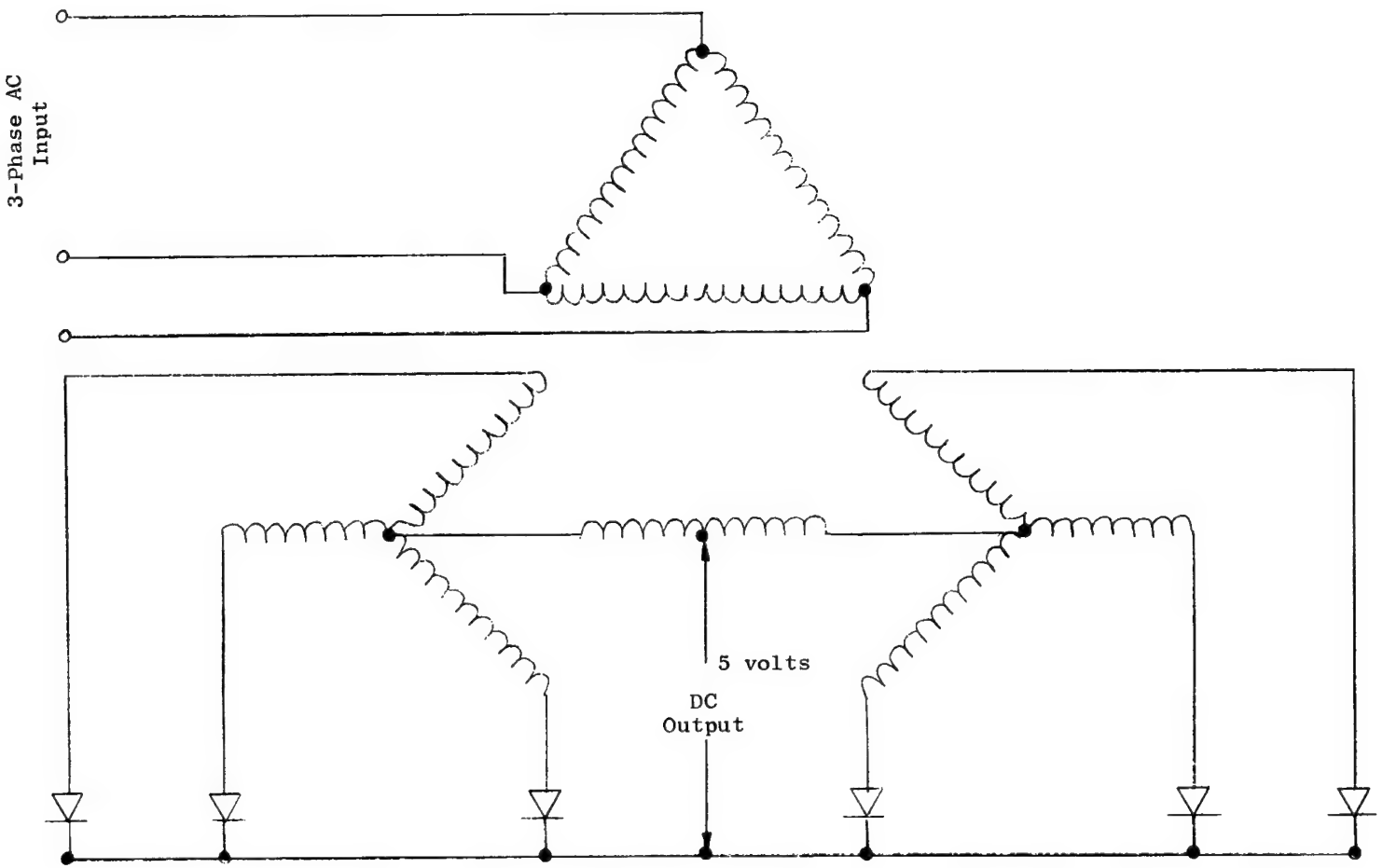

Figure 67. Six-Phase Rectifier Circuit for AC to Low Voltage DC Power Conversion

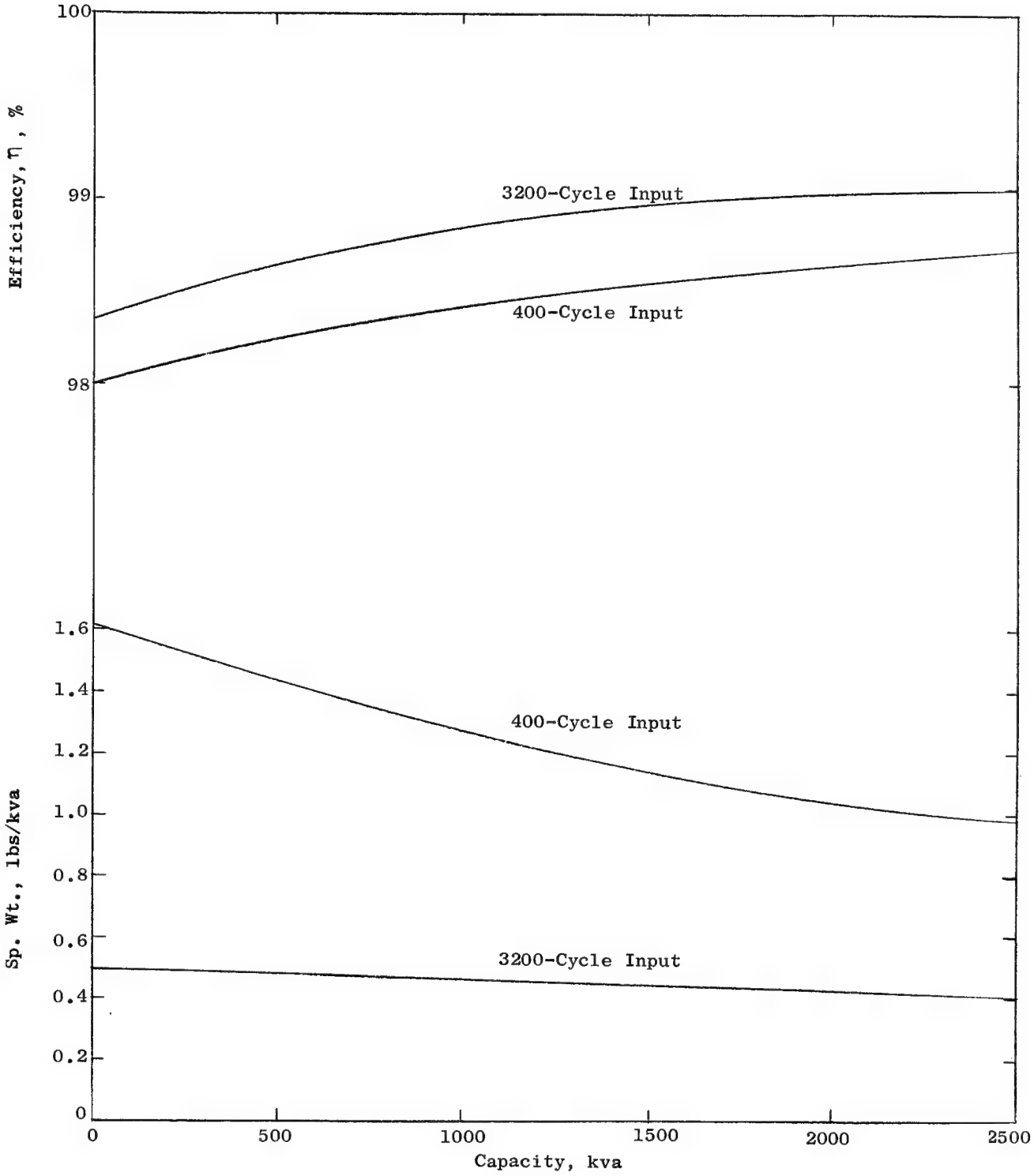

Figure 68. Specific Weight and Efficiency of High Temperature, 3-Phase Transformers Vs. Capacity.

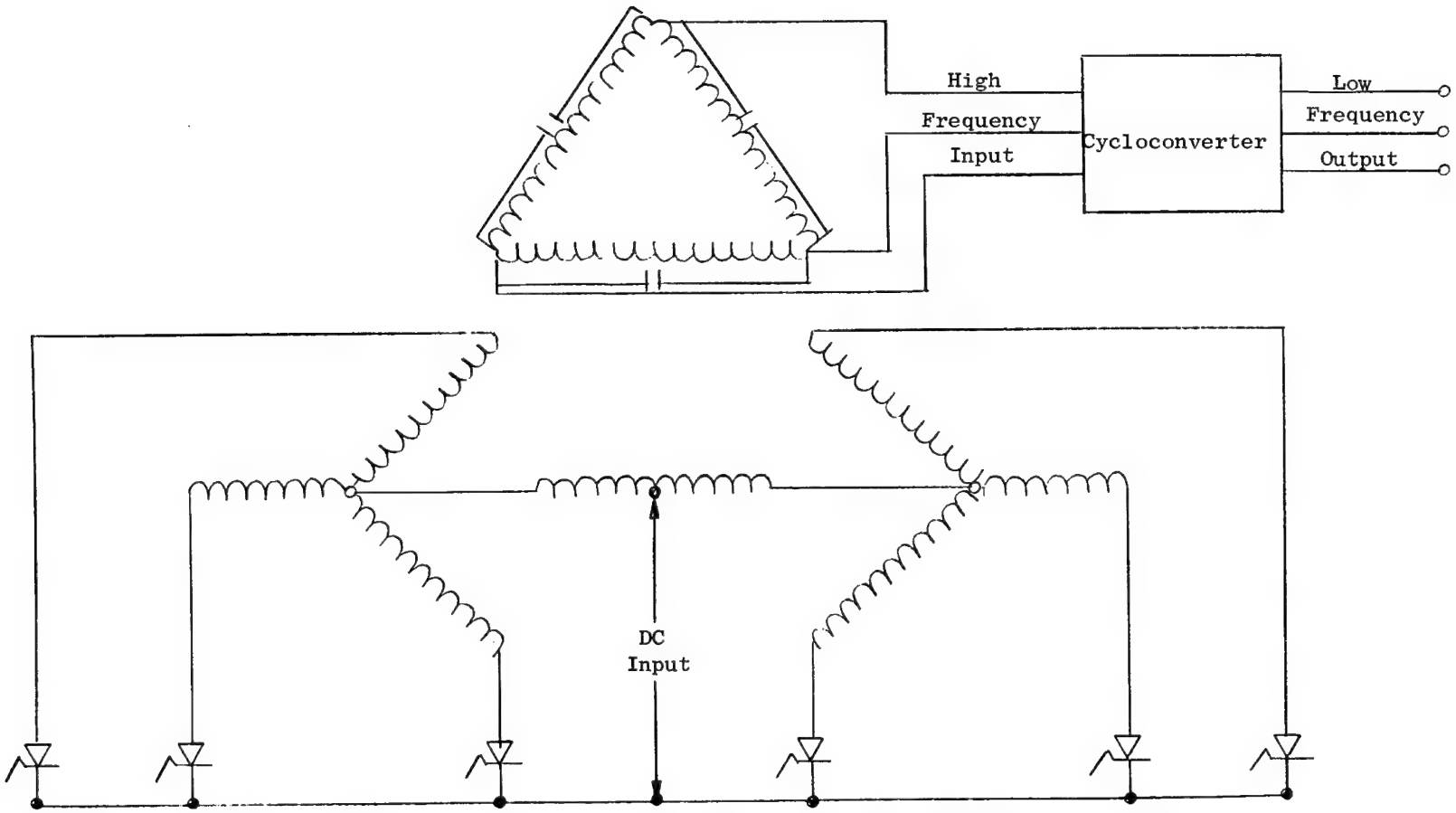

Figure 69. DC to AC Power Conversion System (Controlled Rectifier Triggering Circuits Not Shown).

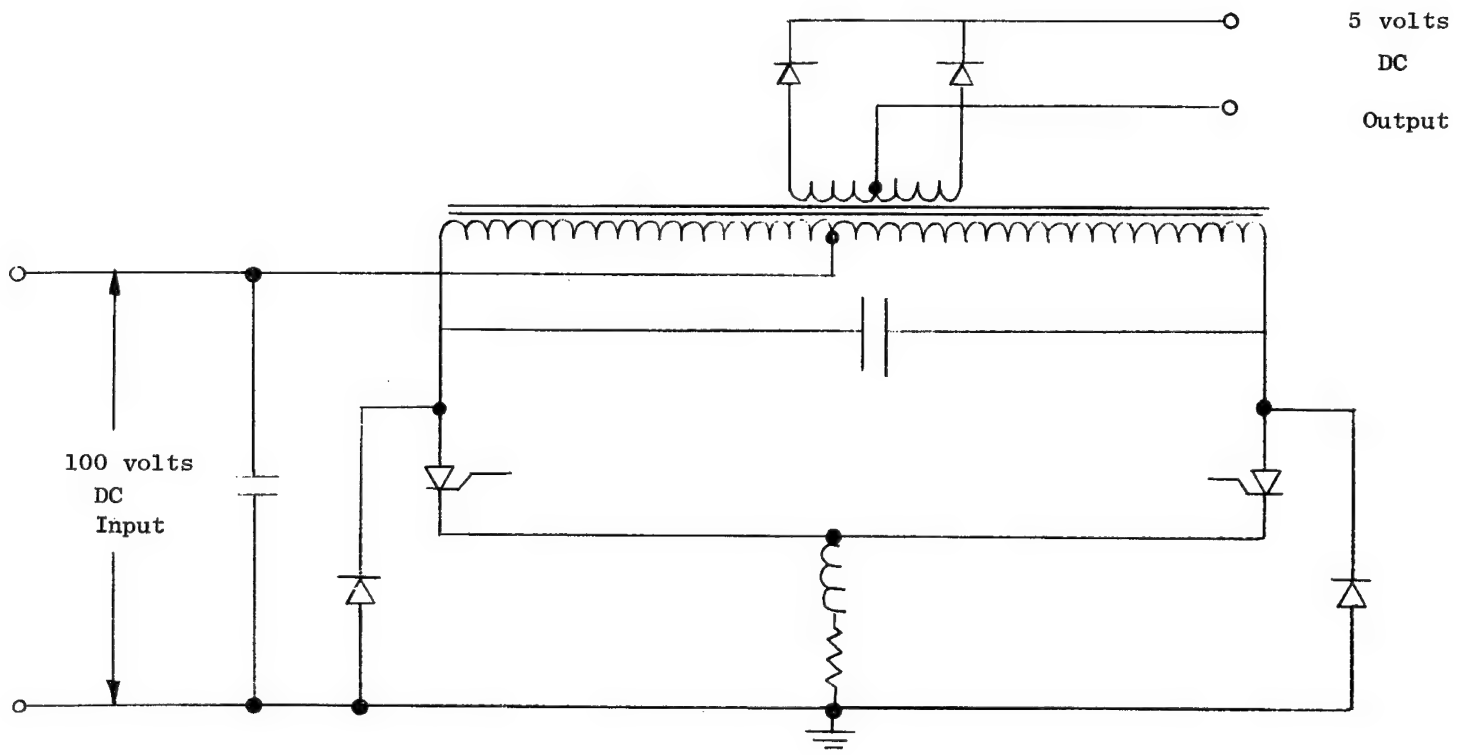

Figure 70. Inverter-Rectifier Circuit for High Voltage to Low Voltage DC Power Conversion.

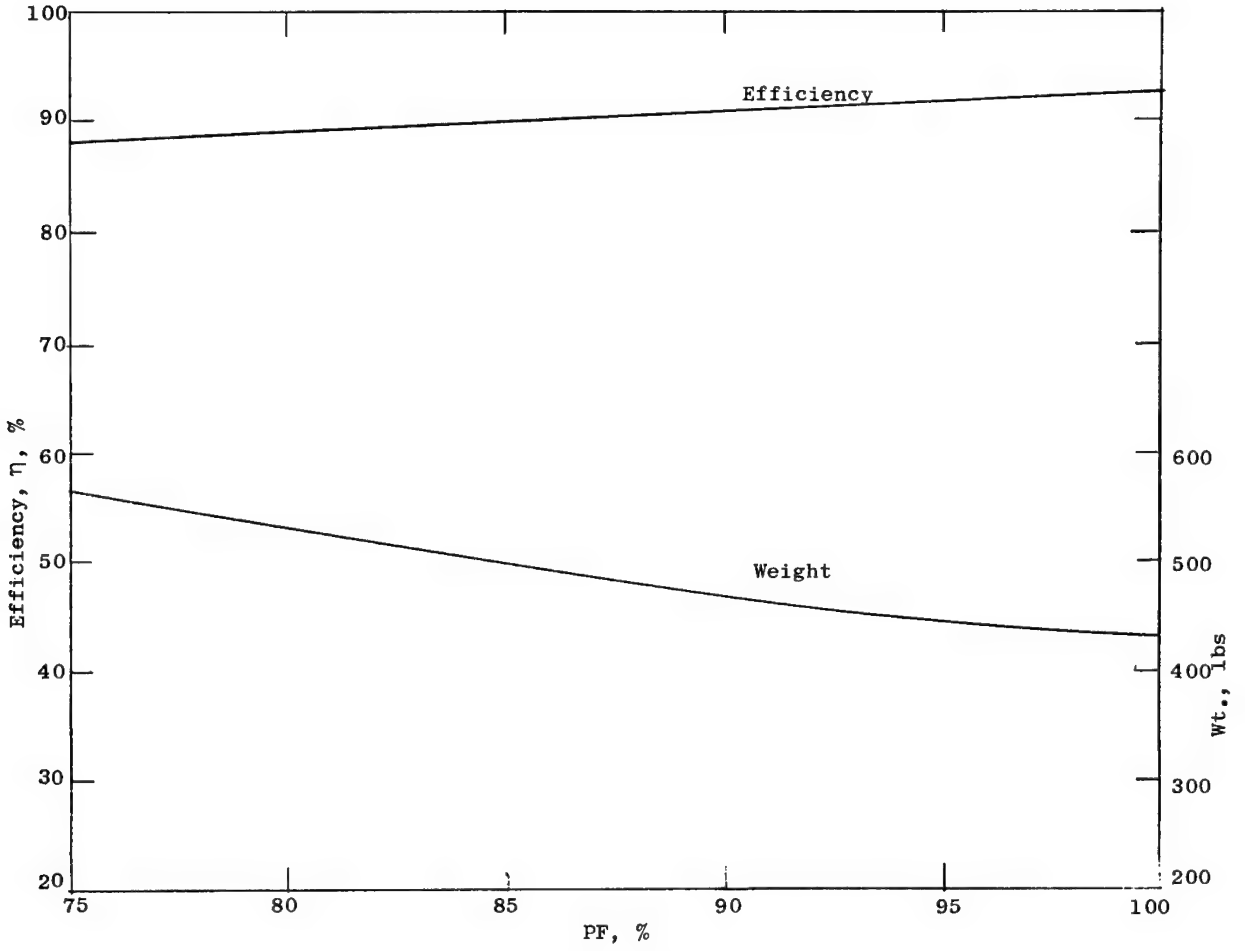

Figure 71. Electromagnetic Weight and Efficiency of 500 KW Inductor Alternator Designs Vs. Machine Power Factor.

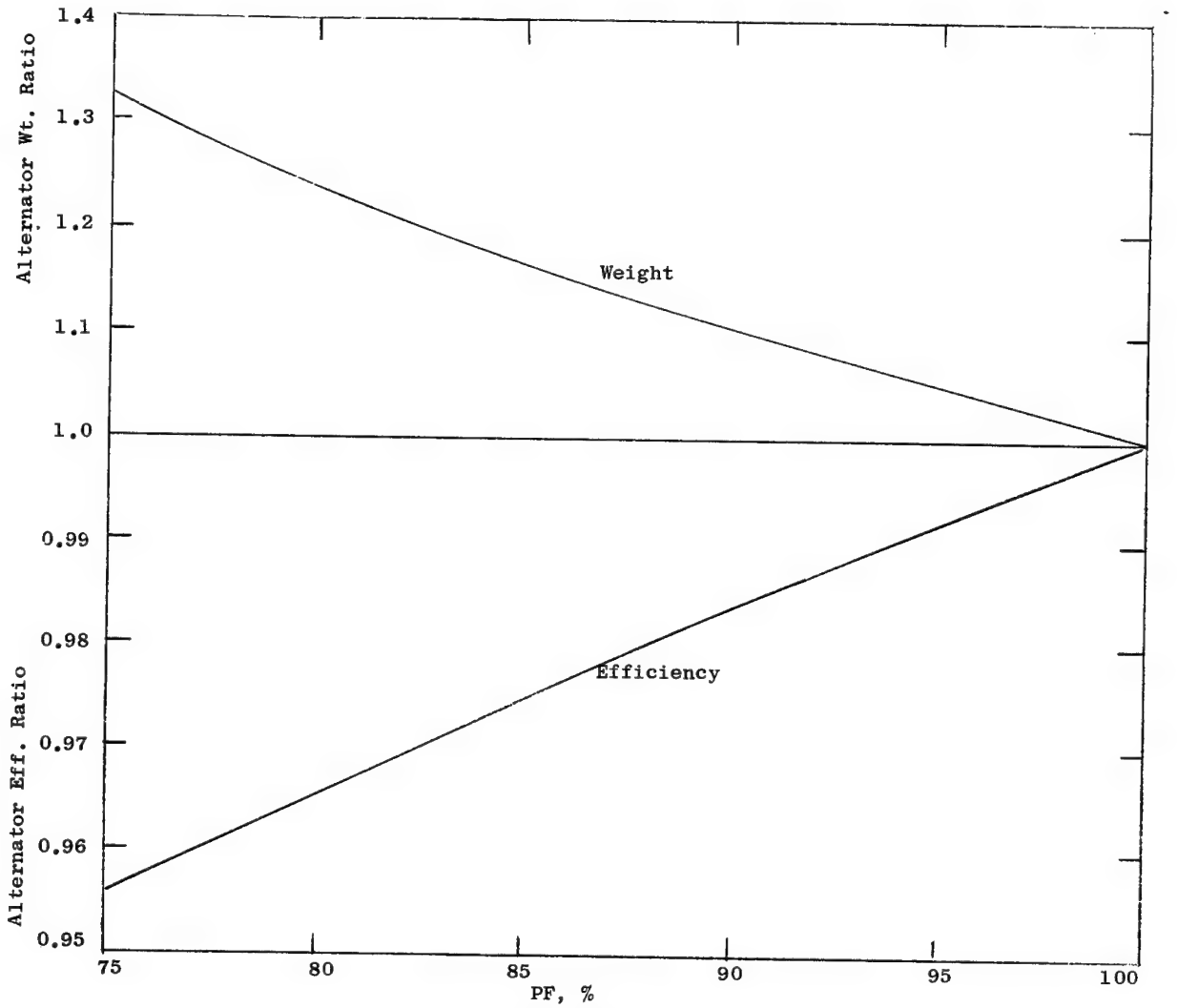

Figure 72. Inductor Alternator Electromagnetic Weight and Efficiency Vs. Power Factor, Referred to Unity Power Factor Design.

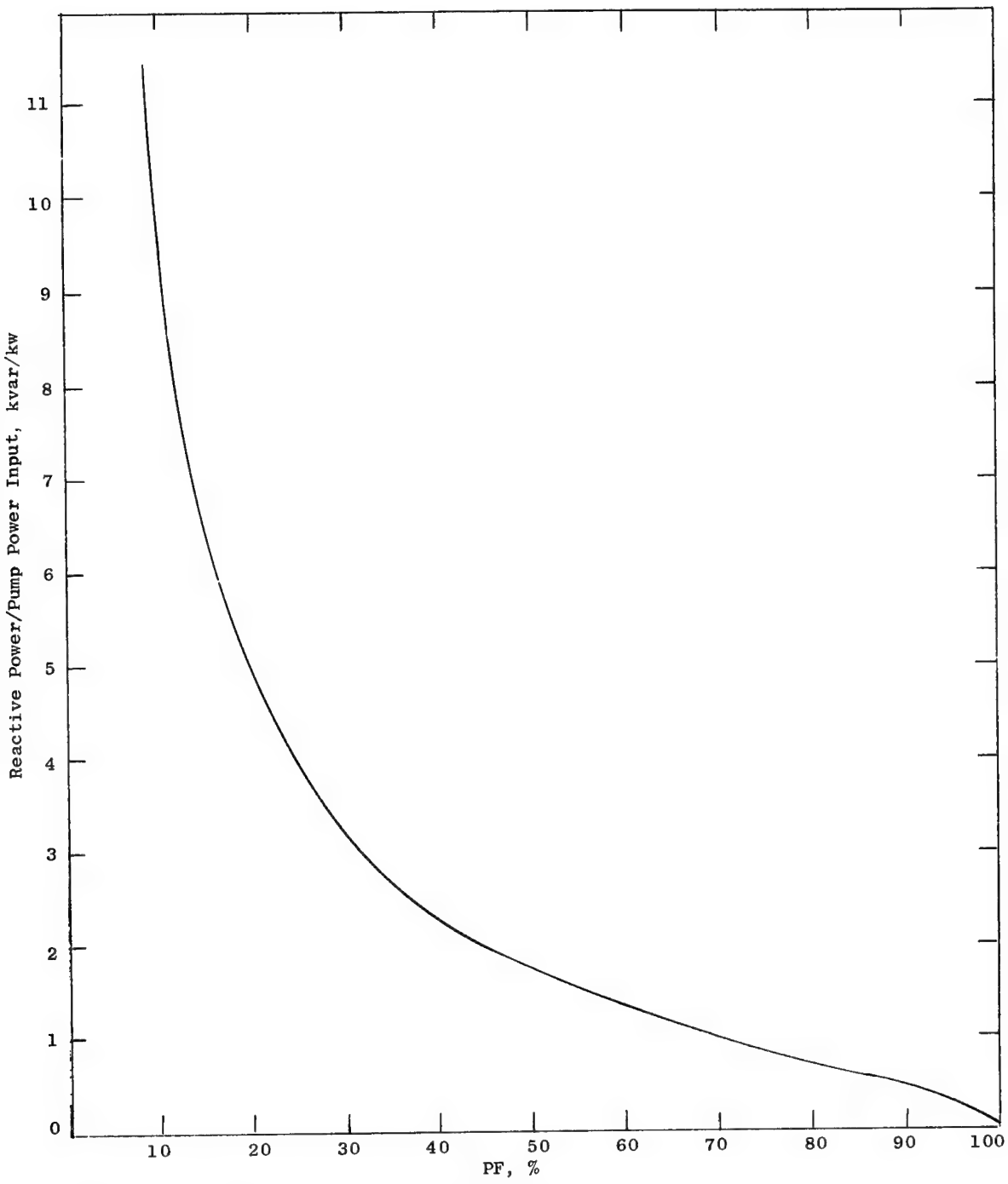

Figure 73. Ratio of Reactive Power/Pump Power Input Vs. Power Factor.

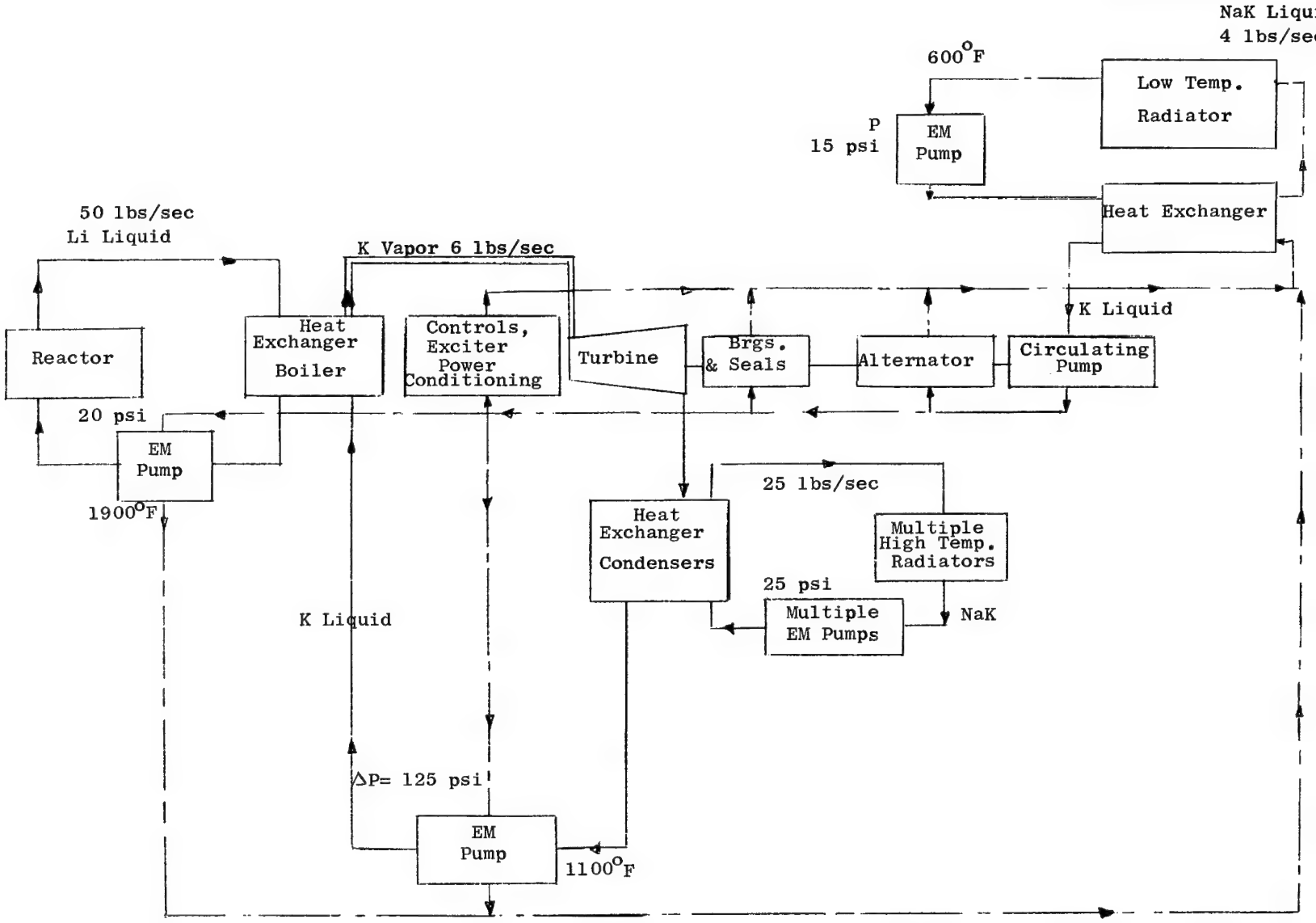

Figure 74. Schematic Flow Diagram Rankine Cycle Turboelectric Space Power System. 1 MW Size.

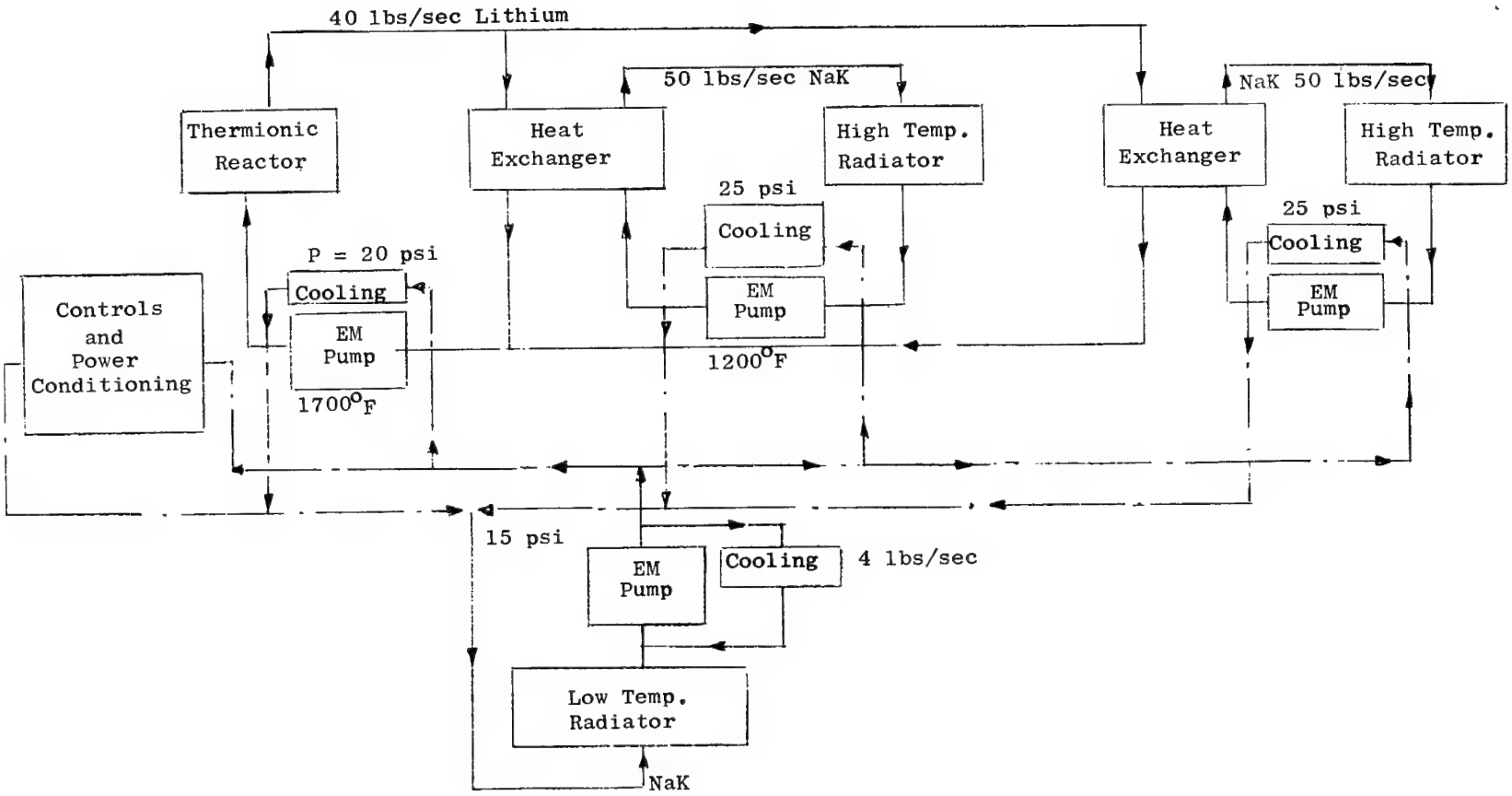

Figure 75. Schematic Flow Circuit Diagram, Thermionic Reactor Space Power System.

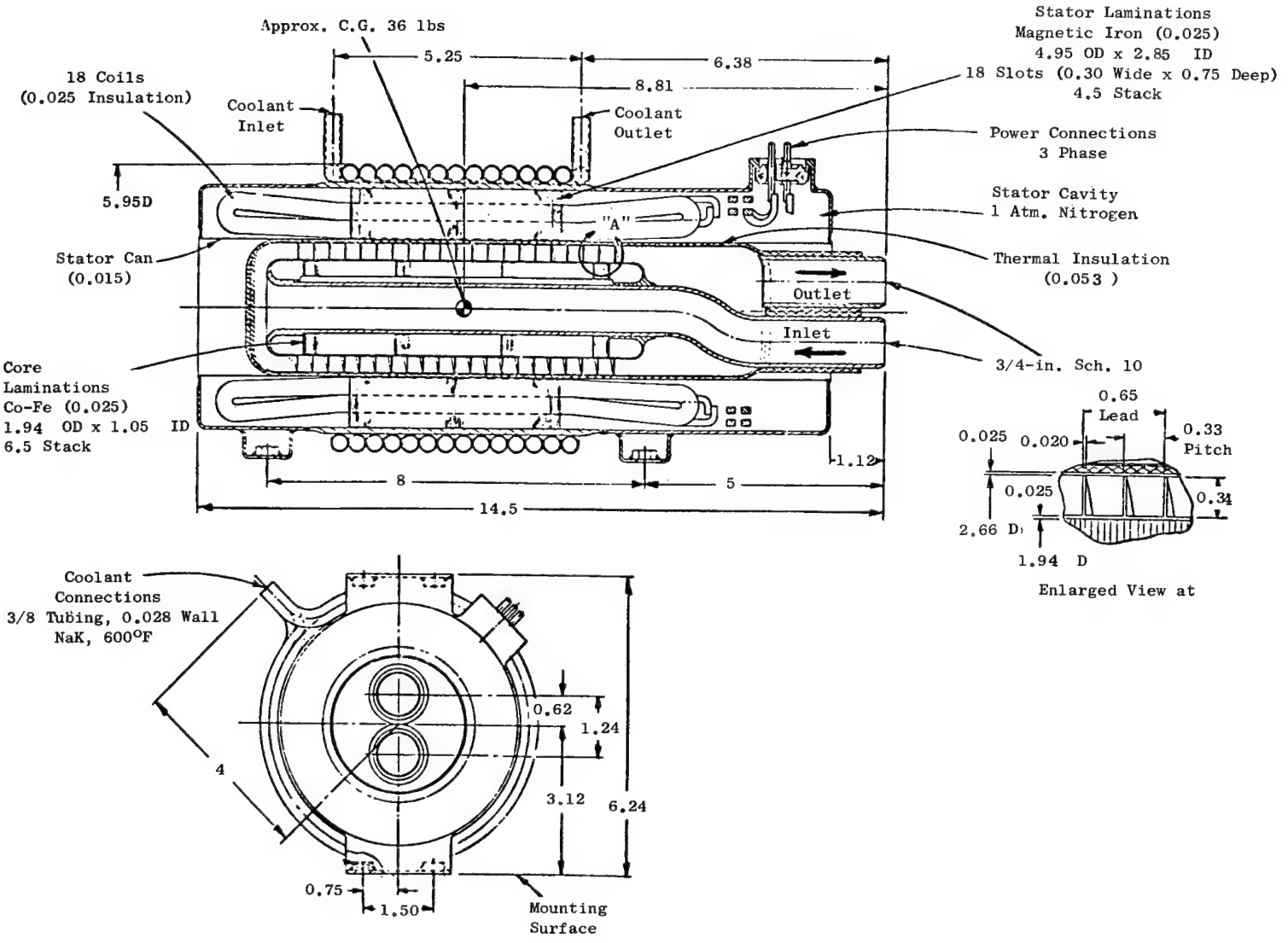

Figure 76. Helical Induction Pump: Center Return.

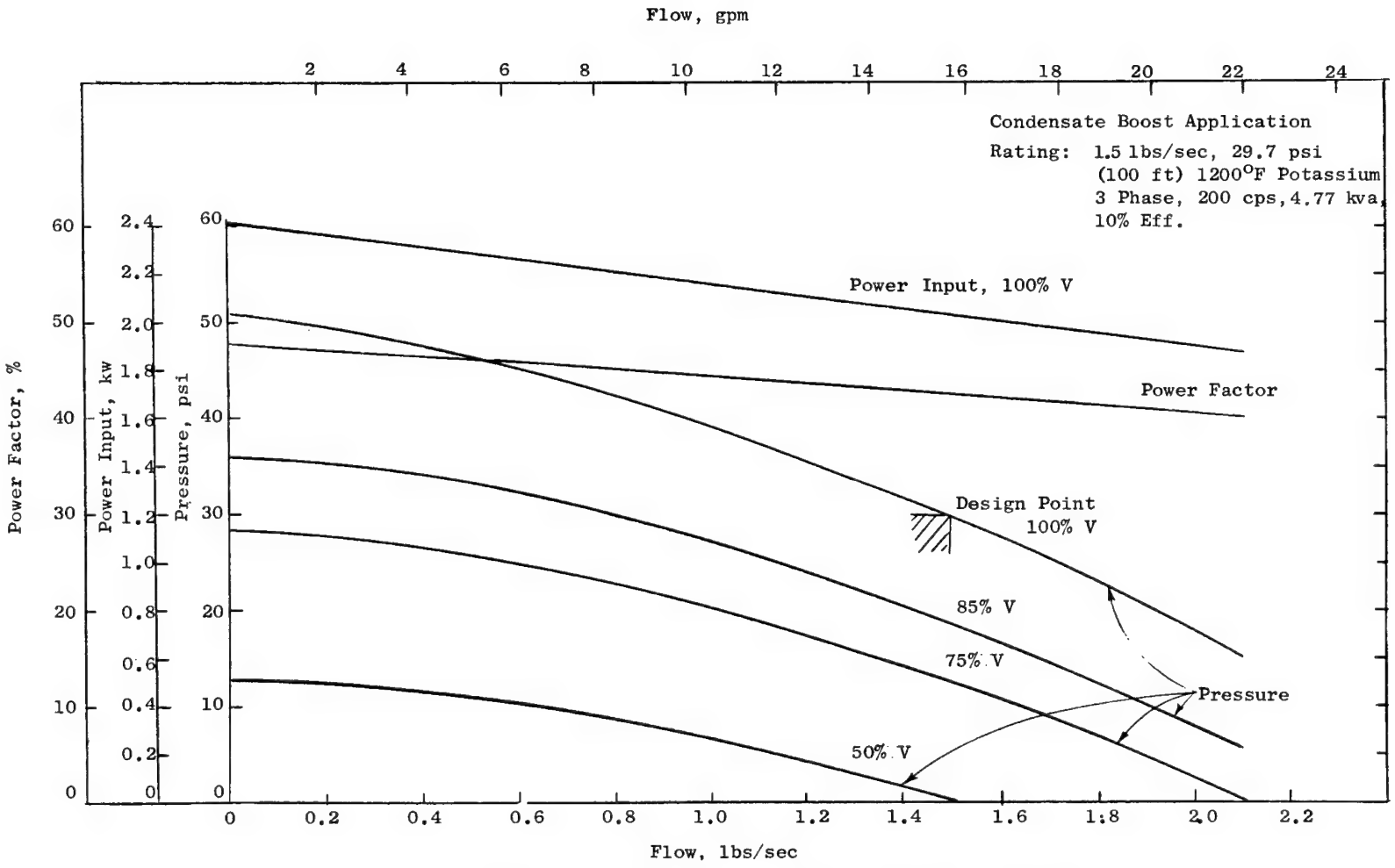

Figure 77. Performance of Helical Induction EM Pump.

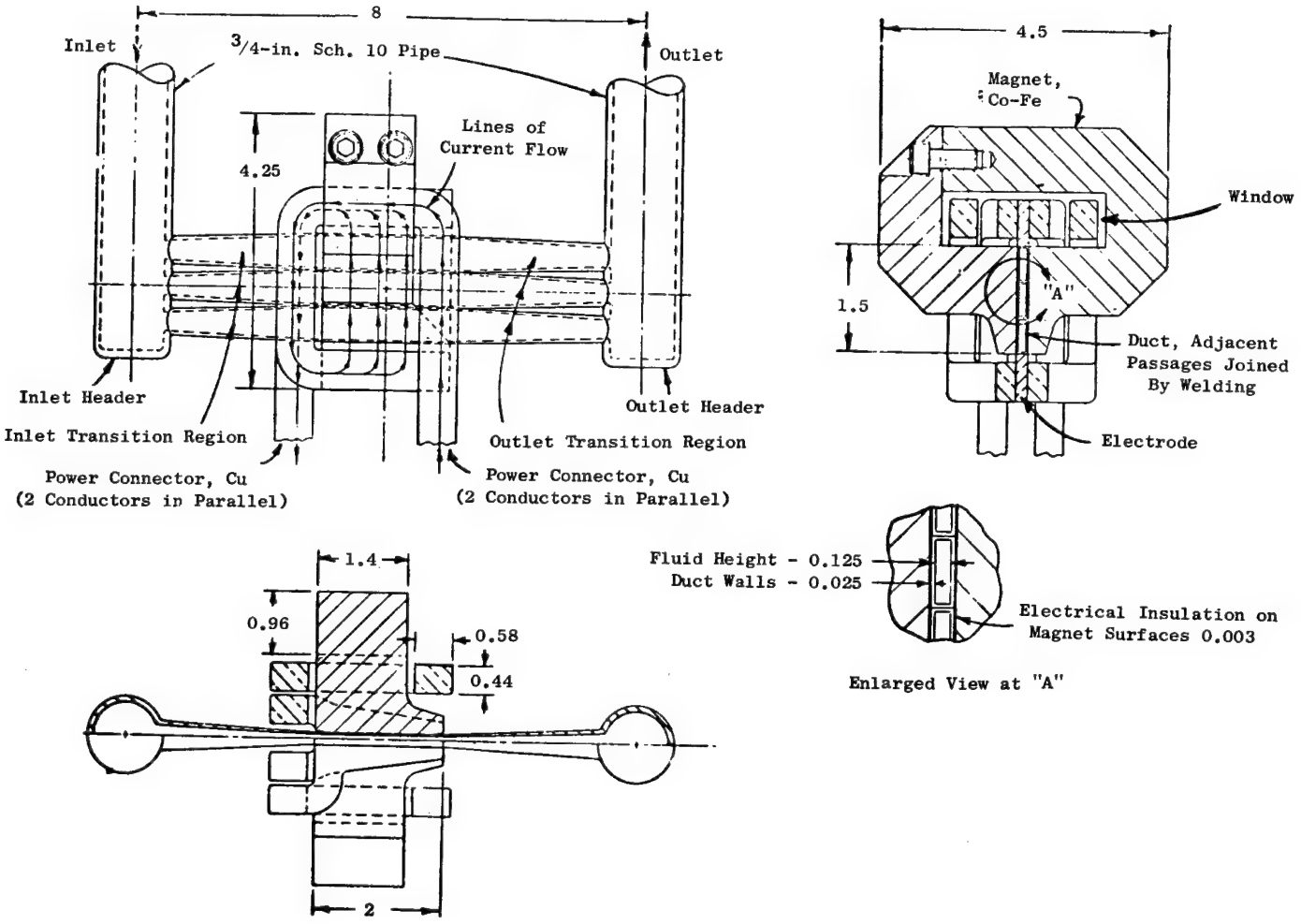

Figure 78. DC Conduction Pump.

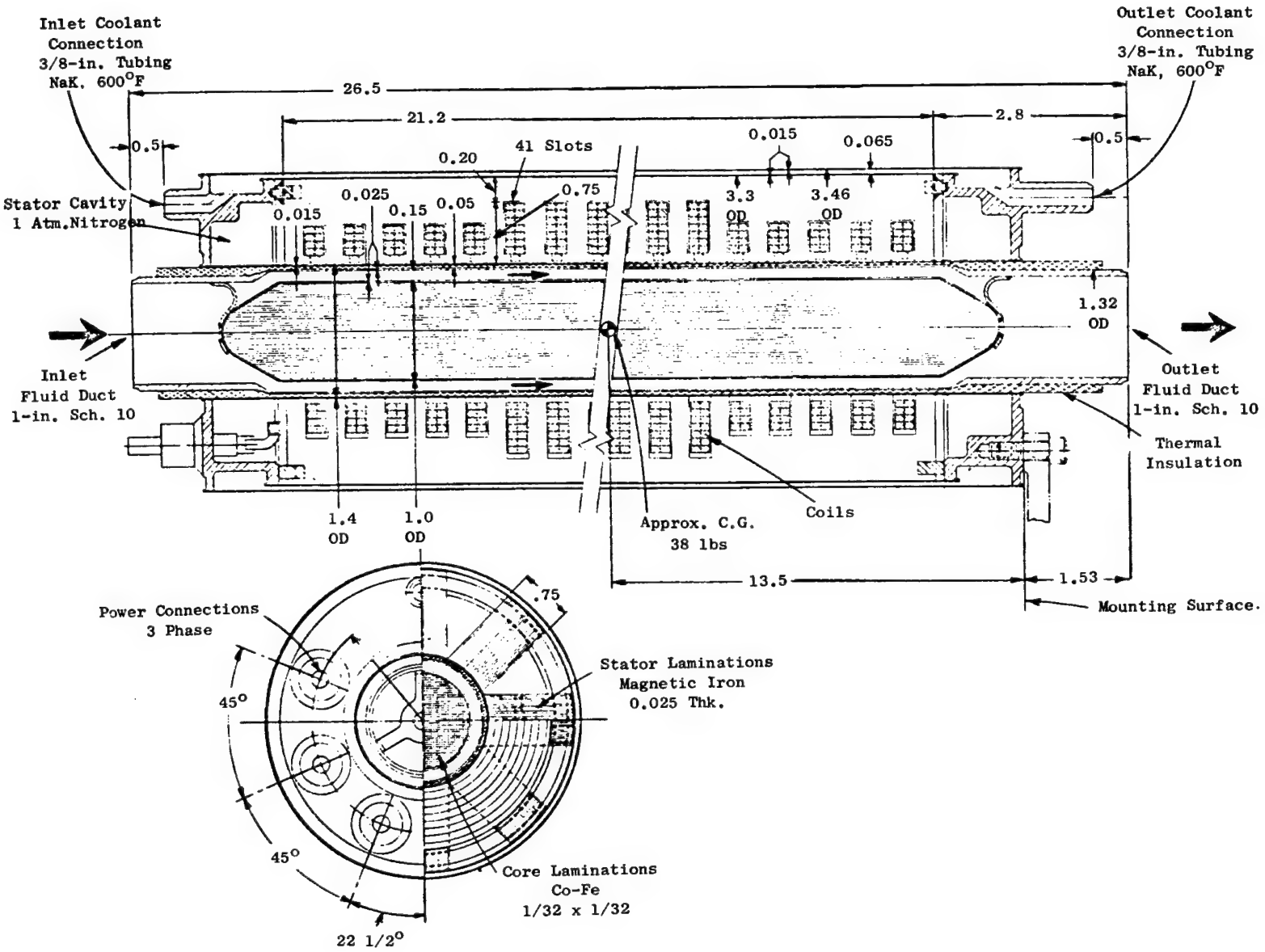

Figure 79. Annular Induction Pump

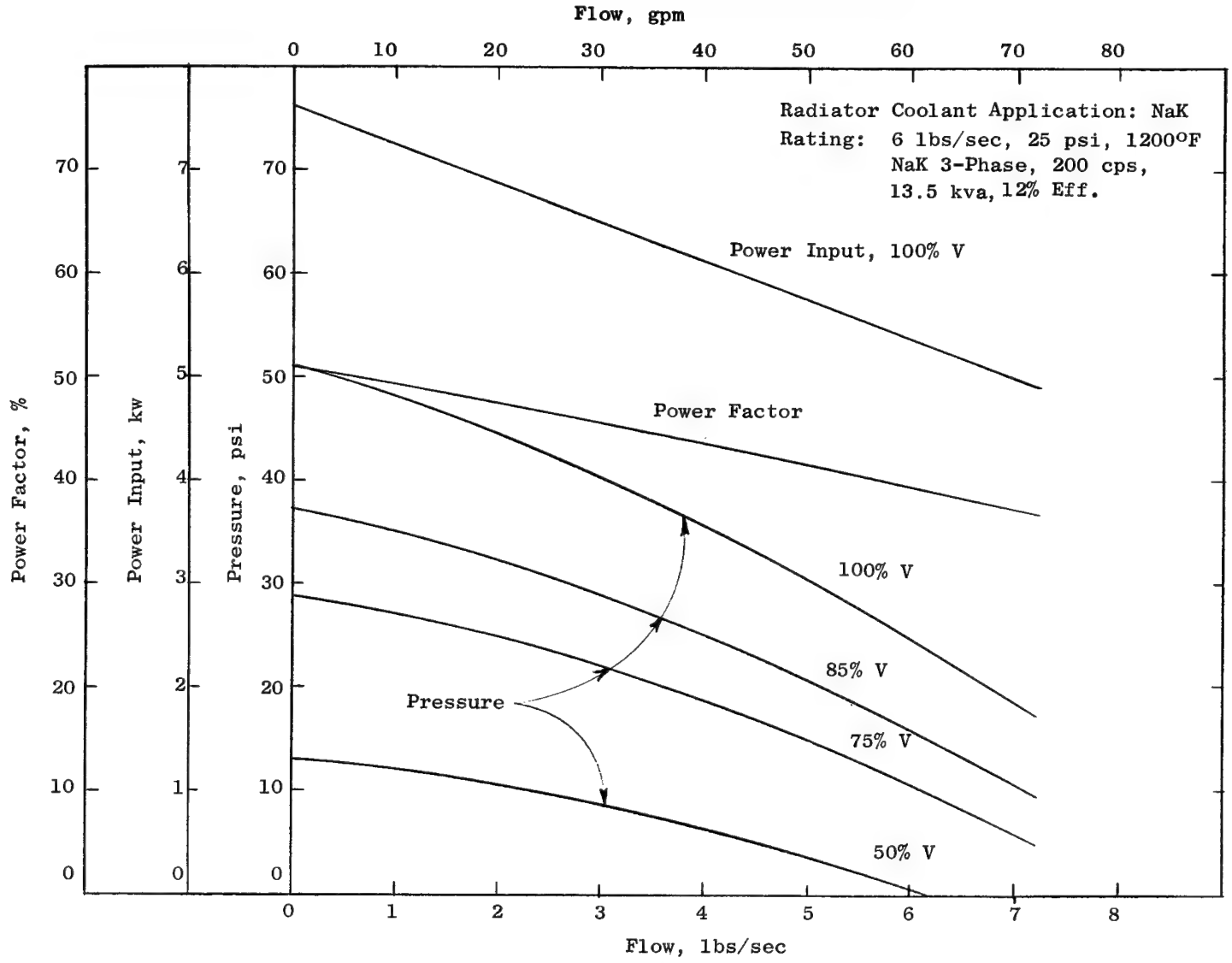

Figure 80. Performance Annular Induction Pump.

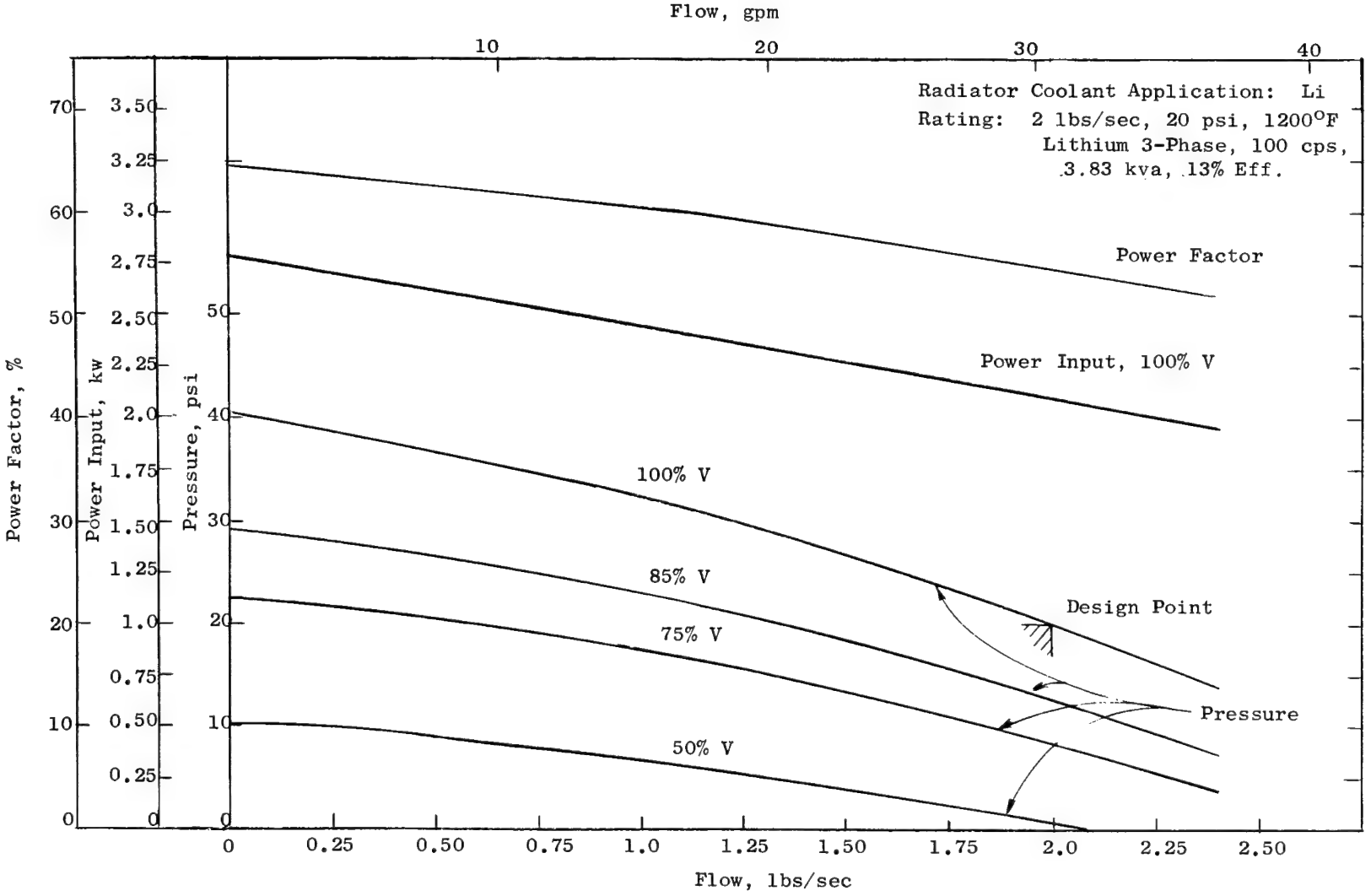

Figure 81. Performance Helical Induction EM Pump.

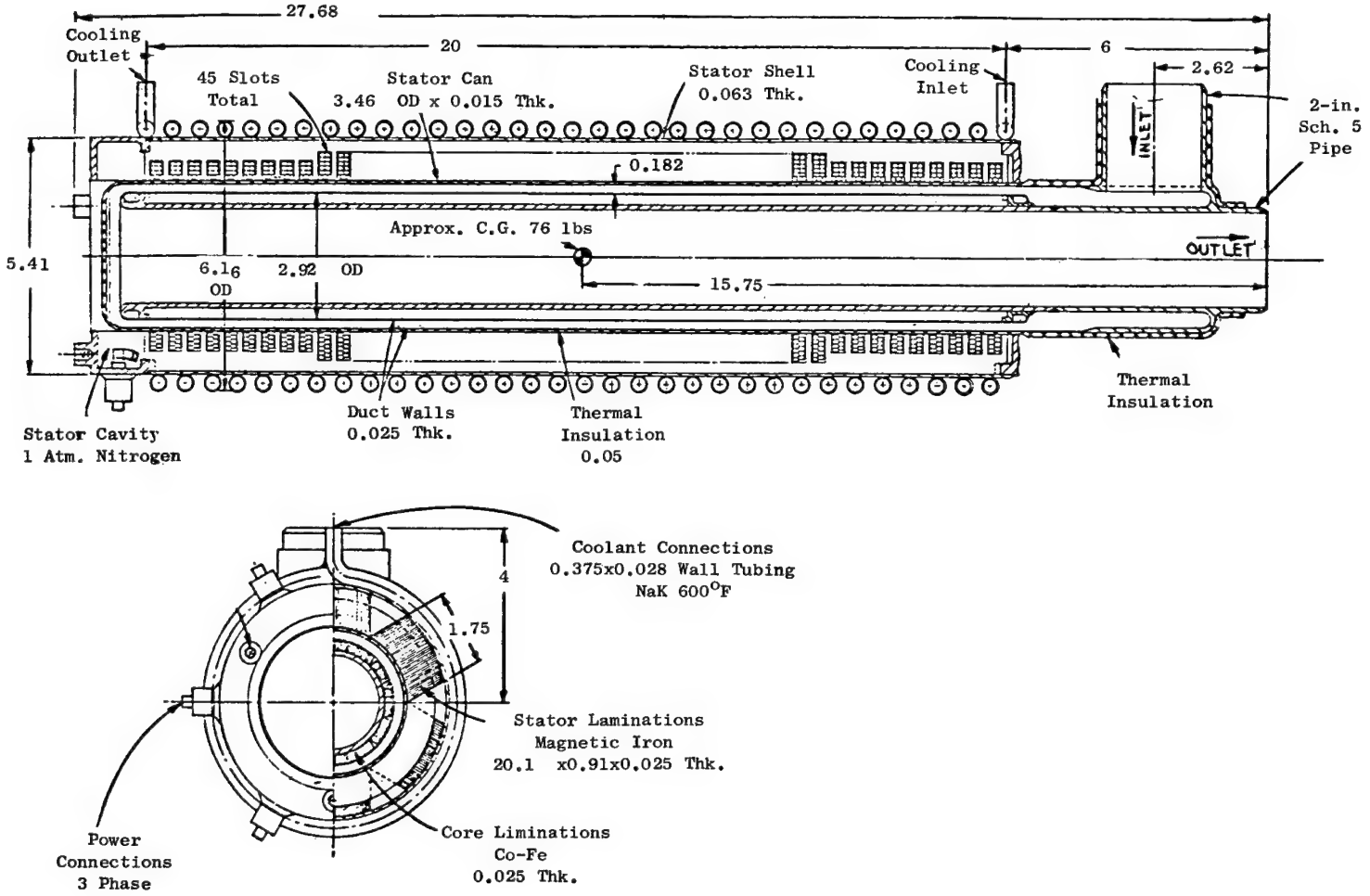

Figure 82. Annular Induction Pump: Center Return.

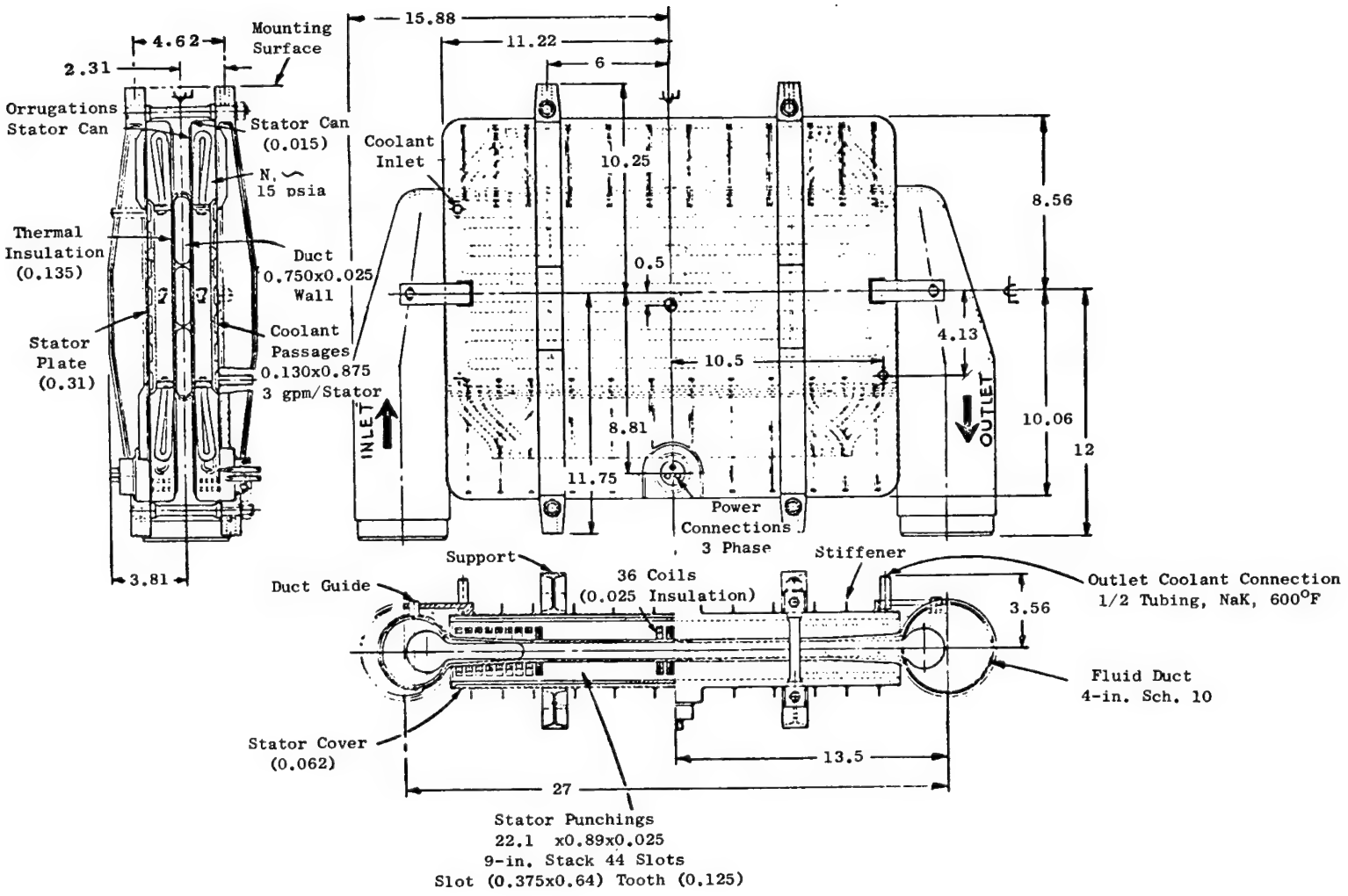

Figure 83. Flat Linear Induction Pump.

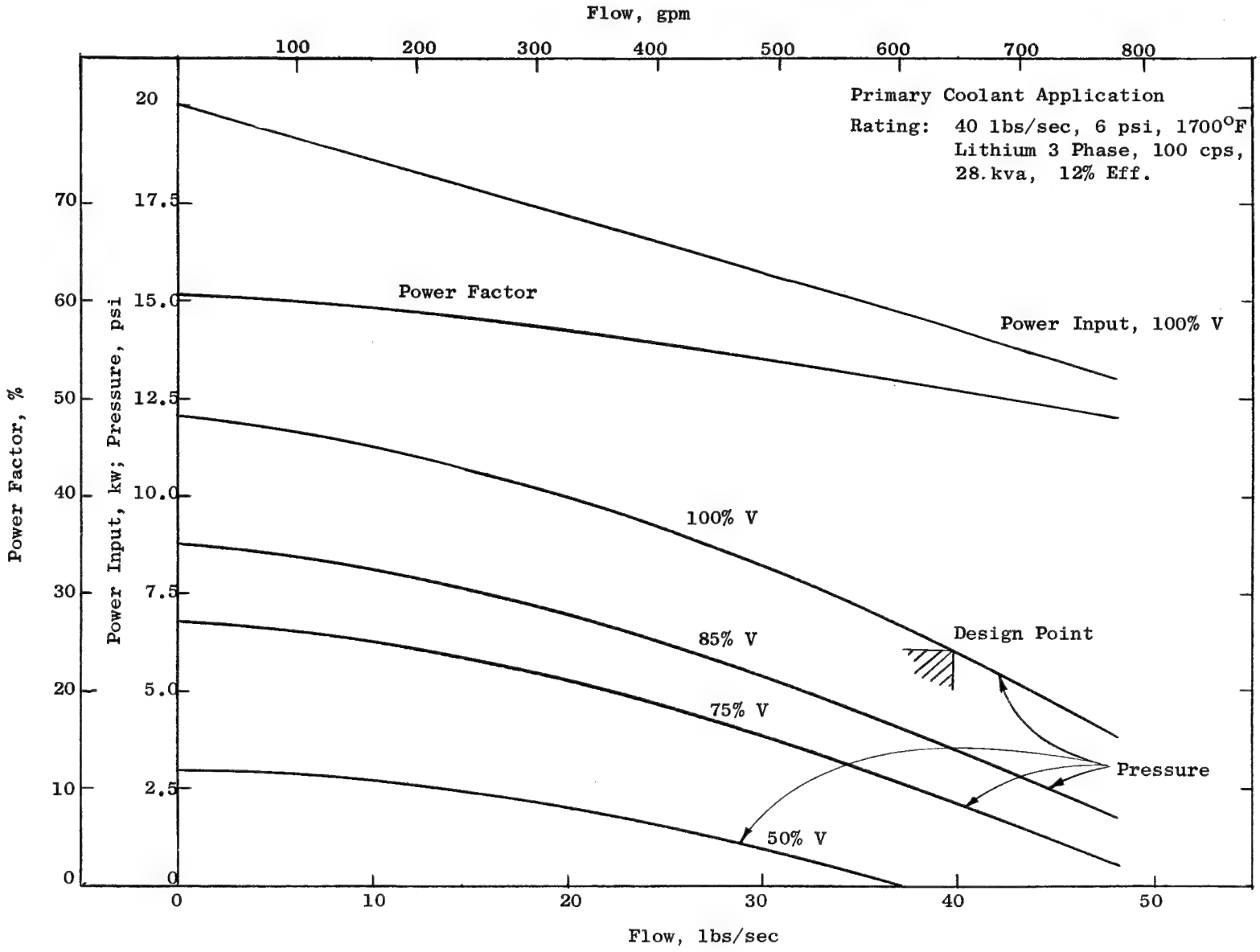

Figure 84. Performance Flat Induction Pump.

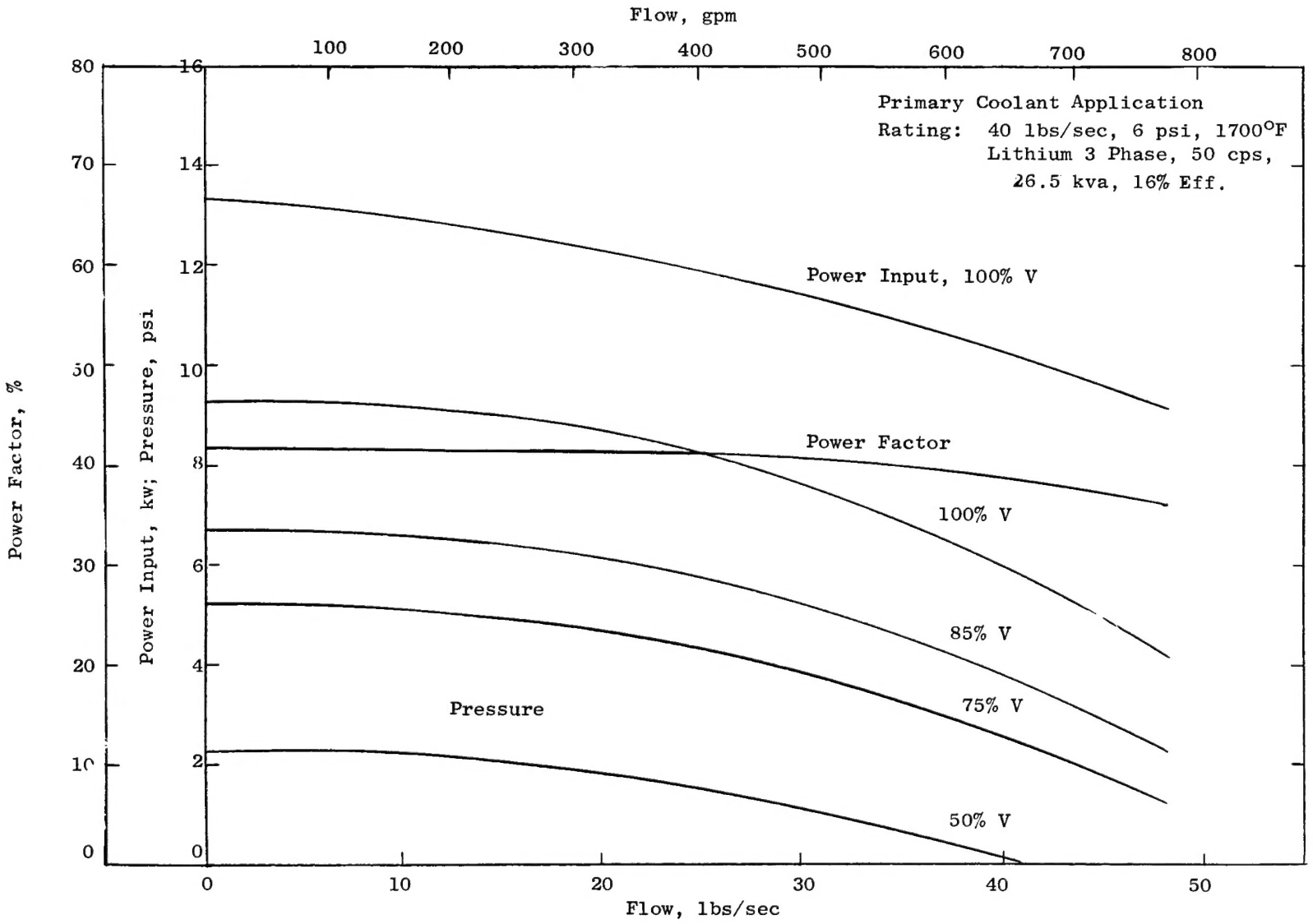

Figure 85. Performance Annular Induction Pump.

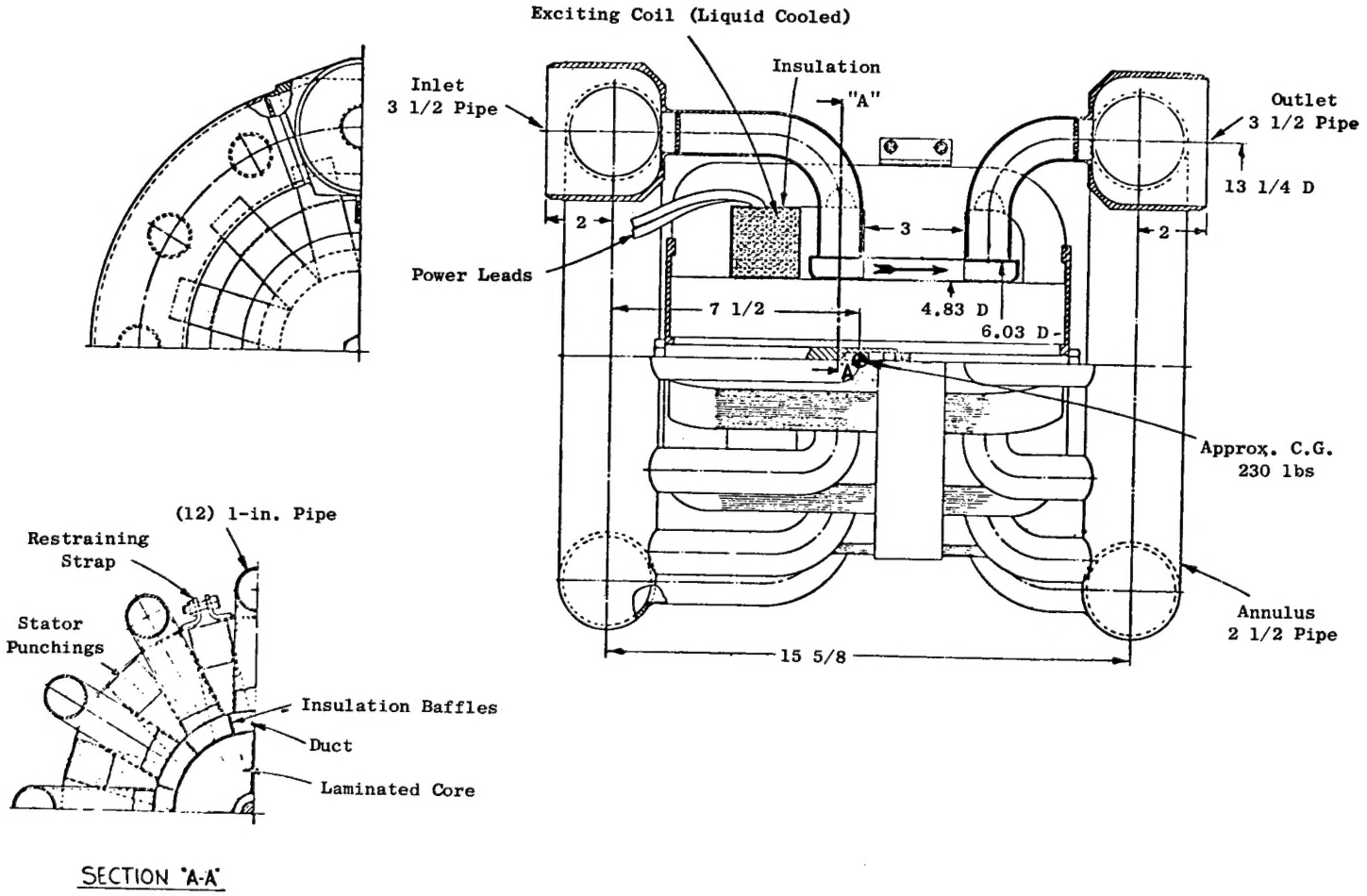

Figure 86. Single Phase Induction Pump.

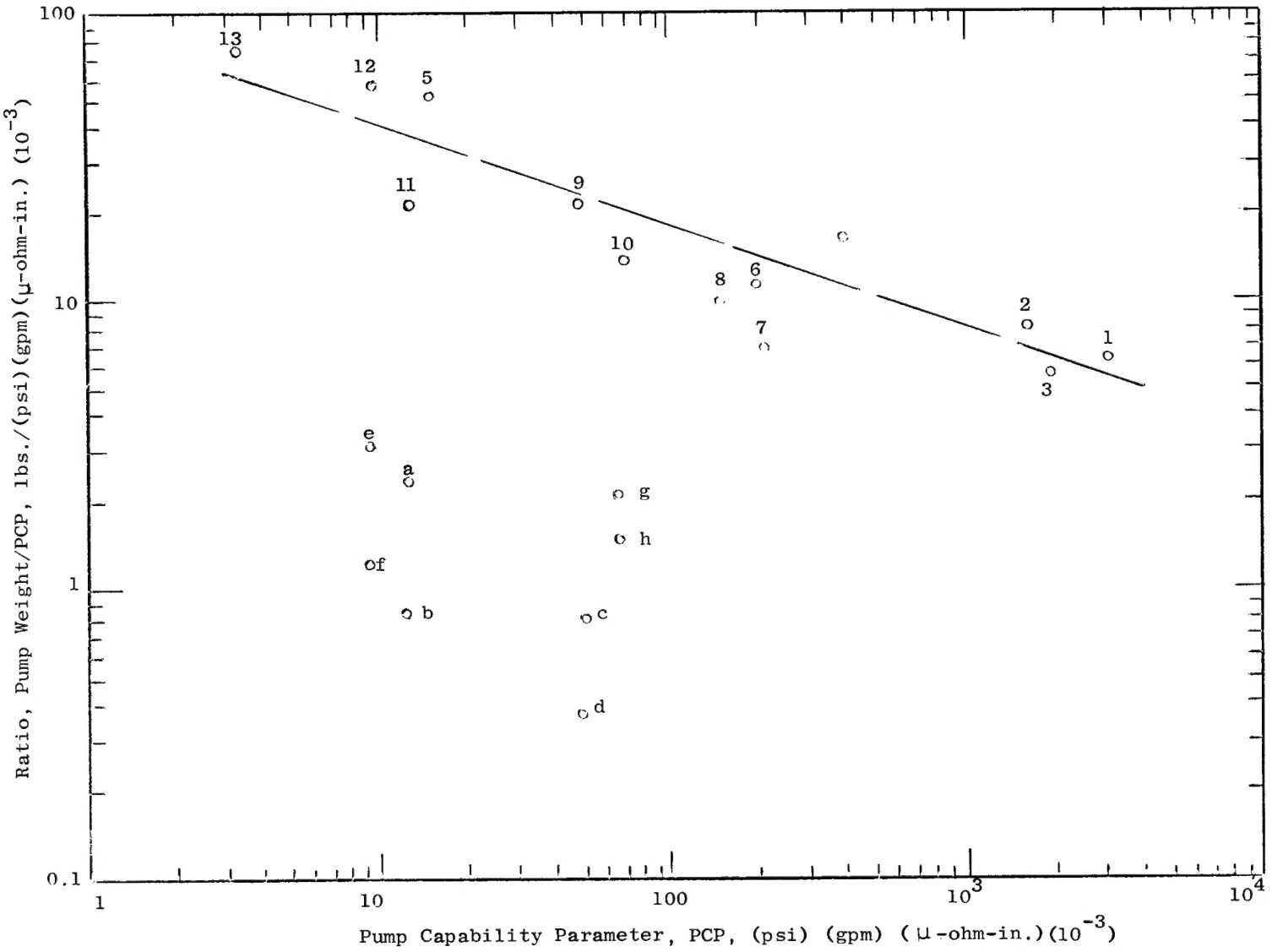

Figure 87. Specific Weight Relationship EM Pumps.

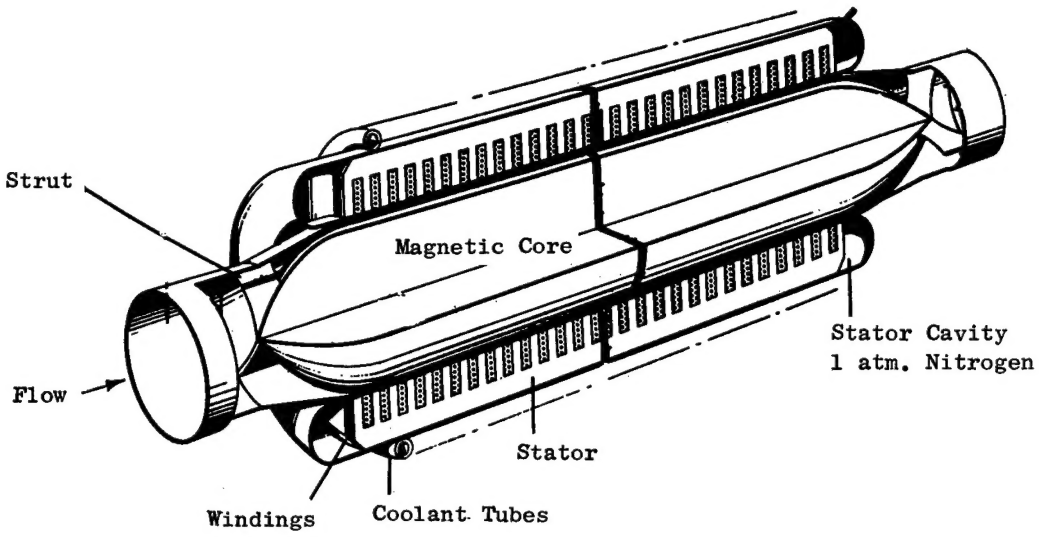

Annular Induction Pump

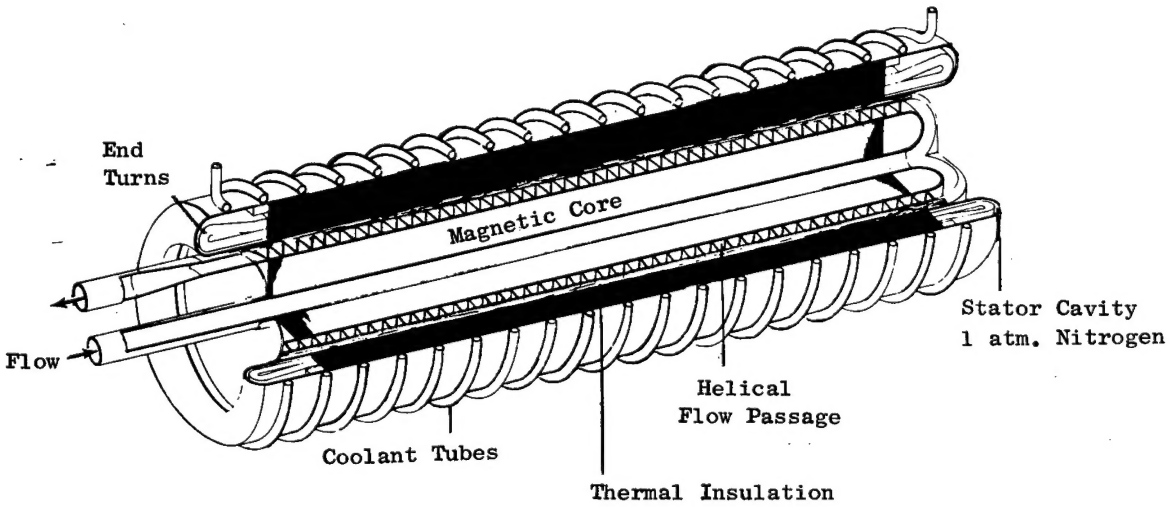

Helical Induction Pump

Figure 88. Induction Pumps for Flight Applications.

NASA-Langley, 1966 E-3193